Advanced Spatial Modulation Schemes: Performance Analysis and Applications

A Thesis

submitted for the award of the degree of

Doctor of Philosophy

by

Anirban Bhowal

Department of Electronics and Electrical Engineering

INDIAN INSTITUTE OF TECHNOLOGY GUWAHATI

GUWAHATI - 781 039, INDIA

July 2020

To my supervisor

and

parents

भारतीय प्रौद्योगिकी संस्थान गुवाहाटी
Indian Institute of Technology Guwahati

Certificate

This is to certify that the thesis entitled "**ADVANCED SPATIAL MODULATION SCHEMES: PERFORMANCE ANALYSIS AND APPLICATIONS**", submitted by **Anirban Bhowal** (156102008), a research scholar in the *Department of Electronics and Electrical Engineering, Indian Institute of Technology Guwahati*, for the award of the degree of **Doctor of Philosophy**, is a record of an original research work carried out by him under my supervision and guidance. I consider it worthy of consideration for the award of the degree of Doctor of Philosophy of the Institute. The results embodied in this thesis have not been submitted to any other University or Institute for the award of any degree or diploma.

Date:
Place: Guwahati.

Prof. Rakhesh Singh Kshetrimayum
Professor
Dept. of Electronics and Electrical Engineering.
Indian Institute of Technology Guwahati
Guwahati - 781 039, Assam, India.

भारतीय प्रौद्योगिकी संस्थान गुवाहाटी
Indian Institute of Technology Guwahati

Declaration

I certify that

a. The work contained in this thesis is original and has been done by me under the guidance of my supervisor.

b. The work has not been submitted to any other Institute for any degree or diploma.

c. I have followed the guidelines provided by the Institute in preparing the thesis.

d. I have conformed to the norms and guidelines given in the Ethical Code of Conduct of the Institute.

e. Whenever I have used materials (data, theoretical analysis, figures, and text) from other sources, I have given due credit to them by citing them in the text of the thesis and giving their details in the references. Further, I have taken permission from the copyright owners of the sources, whenever necessary.

Date:
Place: Guwahati

Anirban Bhowal
Research Scholar
Dept. of Electronics and Electrical Engineering
Indian Institute of Technology Guwahati
Guwahati - 781039, Assam, India.

भारतीय प्रौद्योगिकी संस्थान गुवाहाटी
Indian Institute of Technology Guwahati

Acknowledgement

First and foremost I would like to express my sincere gratitude to my supervisor, Prof. Rakhesh Singh Kshetrimayum of the Department of Electronics and Electrical Engineering for introducing me to this area of research. His invaluable inputs and encouraging discussions at every stage of the work helped me immensely in writing this thesis. He inculcated in me the concept of research and motivated me to work in various fields (FSO communication, D2D communication, spatial modulation etc.) which have contributed to my thesis. I have learnt the art of research paper writing and reviewing from him. His behaviour, eagerness to help, quick response time to any of my doubts has always pushed me to work harder in my research. He has always been there for me with his guidance and support even in the most gloomy phases of my research. He has provided me a good mental space and work environment which plays an important role in research work. He has helped me in making several decisions regarding my career and also provided recommendations wherever necessary. I would like to thank him for his invaluable time and efforts wasted in corrections of all my paper and other research oriented documents. I will always be indebted to him for his role in my career.

I am grateful to the Head of the Department of Electronics and Electrical Engineering for providing me all the facilities to carry out my research work. I would also like to express my sincere gratitude to the members of doctoral committee (Dr. A. Rajesh, Dr. Smarajit Das and Dr. Aryabartta Sahu) and all the faculty members of the department. My sincere thanks to all staffs, deans and faculties of the institute for providing guidance and help at various stages of my career. I would also like to acknowledge all my lab mates of Communication Engineering Lab I (Arijit, Sumantra, Aditya, Ashim) and all other research scholars of Electronics and Electrical Engineering Department. I would like to mention Aditi and Ronak specially for their academic collaborations with me. I would like to thank other friends of my campus- Mohit, Pyarimohan, Upasana, Shivani, Bikash, Darpan, Chandan, Rahul, Pralay, Satyajit, Atanu, Samarjeet, Tilendra, Debajit, Manoranjan, Arijit, Ganji Sreeram, Sanjib Mog, Parth. I would like to take this opportunity to thank some of my seniors- Ramanand, Anand, Niladri, Kaushik, Vimal for providing me guidance throughout my stay in the campus. I would like to thank my Dibang HMC, Gymkhana members and RSF-EEE members for working with me and providing me full cooperation as and when required. I would like to specially mention some of them- Anirban Das, Mayank Kumar, Parul, Pushya, Namrata, Sarath, Nishant, Kaila, Abhijit, Birjit, Sibasis, Anindya, Samarth, Suhas, Samar, Avishek Banik for their support in any administrative work. I would also like to thank my badminton and other team mates in various sports for making my stay in IIT Guwahati comfortable. I would like to specially thank Shikha, Shubh Lakshmi (Shubhi), Sheel, Sukanya and Vivek

for motivating me to overcome the struggles of my PhD tenure and helping me at all stages of my life (academic, non academic or any personal issues). I would like to take this opportunity to thank my friends from different stages of my life specially, Rahul, Ojaswi, Mayank, Nidhi, Deepanshu, Sonam Jain, Komal, Sumouli, Ritika, Arghya, Priyadarshi, Sabyasachi, Souptik, Arnab, Saptarshi for providing moral support throughout my PhD career. I extend my earnest gratitude and thanks to my family members who have supported this endeavor through their deeds and prayers. Their unconditional love and affection are always sources of inspiration for my future life. My heartiest gratitude to my brother, Avirup for his love and support. I would like to extend my utmost thanks to my parents for giving me the freedom of what I wanted to be. Finally, I would like to dedicate this thesis to my family.

Abstract

Spatial Modulation (SM) and its advanced versions are investigated for various applications in this thesis. Performance analysis of advanced spatial modulation (ASM) are carried out in terms of bit error rate (BER) and outage probability (OP). The ASMs considered are enhanced spatial modulation (ESM), spatial media based modulation (SMBM), optical ESM (OESM), optical generalized spatial modulation (OGSM), optical improved quadrature spatial modulation (OIQSM), transmit laser selection (TLS) combined with optical SM (TLS-OSM), hybrid SM (HSM) and transmit source selection (TSS) combined with HSM (TSS-HSM).

Firstly, SM along with physical layer network coding (PLNC) is proposed for full-duplex wireless radio frequency (RF) communication. Closed form expressions of OP of such systems are provided in this thesis. Cascaded $\alpha - \mu$ channel model is considered for such communication. It is observed that such systems can achieve signal-to-noise ratio (SNR) gain of 8 dB over PLNC scheme.

Secondly, ESM and SMBM are proposed for body area network (BAN) communication especially for sporting activities such as running and cycling. Performance analysis is carried out for both single-input-single-output (SISO) system as well as multiple-input-multiple-output (MIMO) system employing the above mentioned ASM schemes in terms of BER and OP. Lognormal-4 (LN-4) channel is considered for BAN communication. It is observed that SMBM outperforms SM and ESM schemes. Another observation is that cycling has better BER and OP than running due to less body shadowing effects.

Thirdly, optical SM (OSM) along with PLNC is proposed for full-duplex free-space optical (FSO) cooperative system. Bounds of OP are calculated for such systems. Further, in order to achieve higher spectral efficiencies in FSO communication, ASM techniques such as OESM, OGSM and OIQSM are proposed. BER, cost and power consumption analysis of the above mentioned ASM techniques are provided in the thesis. Gamma-Gamma (G-G) channel model with pointing error is considered for FSO communication. It is observed that OESM, OGSM, OIQSM and TLS-OSM gives better BER than the conventional OSM.

Fourthly, SISO one-way and two-way relay based underwater optical wireless communication (UOWC) is proposed and performance analysis is carried out in terms of OP. OIQSM and TLS-OSM are proposed for UOWC cooperative communication. Performance analysis of such schemes are carried out in terms of OP and average symbol error probability (ASEP). Lognormal channel is assumed for UOWC. It is observed that OIQSM and TLS-OSM also outperform OSM for UOWC.

Lastly, HSM and TSS are proposed for hybrid FSO/RF cellular communication. In this cellular system, base station (BS) to access points (APs) are assumed to be connected with FSO links and AP to

mobile users are connected using RF links. FSO links are modelled as G-G channel whereas RF links are modelled as Rayleigh fading channel. Performance analysis is carried out in terms of OP. It is observed that TSS-HSM outperforms HSM and TSS based hybrid FSO/RF systems.

Contents

भारतीय प्रौद्योगिकी संस्थान गुवाहाटी
Indian Institute of Technology Guwahati

List of Figures

भारतीय प्रौद्योगिकी संस्थान गुवाहाटी
Indian Institute of Technology Guwahati

List of Tables

भारतीय प्रौद्योगिकी संस्थान गुवाहाटी
Indian Institute of Technology Guwahati

List of Acronyms

RF	Radio Frequency
BAN	Body Area Network
LAN	Local Area Network
MAN	Metropolitan Area Network
WAN	Wide Area Network
FSO	Free Space Optics
UOWC	Underwater Optical Wireless Communication
ROV	Remotely Operated Vehicles
AUV	Autonomous Underwater Vehicles
MU	Mobile User
AP	Access Point
BS	Base Station
MIMO	Multiple-Input-Multiple-Output
SM	Spatial Modulation
ASM	Advanced Spatial Modulation
PLNC	Physical Layer Network Coding
OSM	Optical Spatial Modulation
TLS	Transmit Laser Selection
OGSM	Optical Generalized Spatial Modulation
OESM	Optical Enhanced Spatial Modulation
OIQSM	Optical Improved Quadrature Spatial Modulation
HSM	Hybrid Spatial Modulation
TSS	Transmit Source Selection
D2D	Device-to-Device
AF	Amplify-and-Forward

DF	Decode-and-Forward
CF	Compress-and-Forward
PDF	Probability Density Function
CDF	Cumulative Distribution Function
RV	Random Variable
MGF	Moment Generating Function
SNR	Signal-to-Noise Ratio
SINR	Signal-to-Interference-plus-Noise Ratio
CSI	Channel State Information
BPSK	Binary Phase Shift Keying
DFTWR	Decode-and-Forward Two-Way Relaying
AFOWR	Amplify-and-Forward One-Way Relay
AFTWR	Amplify-and-Forward Two-Way Relay
LOS	Line-of-Sight
NLOS	Non-Line-of-Sight
SISO	Single-Input-Single-Output
ASEP	Average Symbol Error Probability
ESM	Enhanced Spatial Modulation
SMBM	Spatial Media Based Modulation
MG	Mixture of Gamma
BMI	Body Mass Index
QAM	Quadrature Amplitude Modulation
QPSK	Quadrature Phase Shift Keying
MAP	Mirror Activation Pattern
PEP	Pairwise Error Probability
BER	Bit Error Rate
LN-4	Lognormal 4 Distribution
LED	Light Emitting Diode
OOK	On-Off Keying
AT	Atmospheric Turbulence
G-G	Gamma-Gamma
LSB	Least Significant Bit
MSB	Most Significant Bit

SMFD	Spatially Modulated Full Duplex
SOA	Semiconductor Optical Amplifier
MZI	Mach-Zehnder Interferometer
ML	Maximum Likelihood
MRC	Maximal Ratio Combining
TLI	Transmit Laser Index
DCSK	Differential Chaos Shift Keying
OAMSK	Orbital Angular Momentum Shift Keying

भारतीय प्रौद्योगिकी संस्थान गुवाहाटी
Indian Institute of Technology Guwahati

List of Symbols

N_A	Number of Antenna
N_L	Number of Laser
M	M-ary Modulation Scheme
R_d	Target data rate
$\alpha - \mu$	Non linearity of the Medium is denoted by α while μ is the number of Multipath Clusters
η_K	Source Node SNR
η_R	Relay Node SNR
γ_{th}	Threshold SNR
m_f	Number of RF Mirrors
C_n^2	Constant of Refractive Structure
λ	Wavelength
L	Link Distance
R_e	Photodetector Responsivity
γ_{loss}	SNR Loss Factor in dB at the Optical/RF Nodes due to self-interference.
h_p	Fraction of power lost due to Pointing Error
σ_s	Pointing Error Displacement Standard Deviation
$w_{z_{eq}}$	Equivalent Beam Radius at the Receiver
$h_l(z)$	Power Loss due to Attenuation over a Distance z
σ_{att}	Attenuation coefficient
N_D	Number of photodetectors
σ_t	Thermal Noise
σ_s	Shot Noise
σ_d	Dark Current Noise
R_L	Load Resistance
F_n	Noise Figure

I_{DC}	Dark Current
B_w	Bandwidth
k_B	Boltzmann's constant
T	Number of Laser Sources selected out of N_L sources in TLS-OSM.
σ_n	Standard Deviation of Noise
w_z	Corresponding Beam Radius at 1Km
ζ	Jitter ratio for pointing error
θ	Divergence Angle
N_L^S	Number of Laser Sources at Source Node
N_L^R	Number of Laser Sources at Relay Node
α_G	Effective number of large scale cells in FSO scattering process
β_G	Effective number of small scale cells in FSO scattering process
P_o	Power Consumption of each Optical Chain
P_{RF}	Power Consumption of each RF Chain
C_o	Cost of each Optical Chain
C_{RF}	Cost of each RF Chain
P_{tr}	Total Transmitted Optical Power
P_{sw}	Power Consumption of each optical switch
P_{swrf}	Power Consumption of each RF switch
C_{sw}	Cost of each optical switch
C_{swrf}	Cost of each RF switch
$C_{S/P}$	Cost of each Serial to Parallel Converter
L_{min}^2	Minimum Euclidean Distance between two Symbol Vectors
$\mathbf{s}$	Transmitted signal vector
$a(\lambda)$	Absorption Coefficient
$b(\lambda)$	Scattering Coefficient
σ_I^2	Scintillation Index
ϵ	Rate of Dissipation of Turbulent Kinteic Energy per unit Mass of Fluid
ω_{wat}	Relative Strength of Temperature and Salinity Fluctuations
η_{km}	Kolmogorov microscale
κ_f	Scalar spatial frequency
χ_T	Rate of Dissipation of Mean-Square Temperature
μ^{lg}	Mean of lognormal distribution

σ^2	Variance of lognormal distribution
α^{MG}, β^{MG}	Shape and scale parameters of MG distribution
τ	Path Loss Coefficient
$G_{S,R}$	Relative Gain of the Source to Relay Link
$G_{R,D}$	Relative Gain of the Relay to Destination Link
$G_{S_1,R}$	Relative Gain of the Source S_1 to Relay Link
$G_{S_2,R}$	Relative Gain of the Source S_2 to Relay Link
κ_{rg}	Relative geometrical gain factor
Γ	Gamma Function
$G_{p,q}^{m,n}(\cdot\cdot \mid z)$	MeijerG Function

भारतीय प्रौद्योगिकी संस्थान गुवाहाटी
Indian Institute of Technology Guwahati

1. Introduction

The need of the future generation of wireless communications is higher data rates at low cost with good quality of service (QoS). Therefore, new technologies or devices need to be deployed in order to achieve high data rates with good efficiency. In normal cellular communication, two mobile devices interact by means of a base station. However if the devices are located nearby, then it is a complete wastage of resources, power, time and cost by rerouting the information through base station. Instead the devices can directly interact with each other by means of radio frequency (RF) waves. This is called device-to-device (D2D) RF based communication [1], which is a recent topic of research and can be deployed in wireless communication networks like mobile ad-hoc networks [2]. Direct interaction between devices forms an integral part of Internet of Things (IoT) and future 5G and 6G communication networks. Various technologies are available to implement interaction between devices. In the subsequent sections, a brief overview of some of the available technologies to implement point-to-point communication between two nodes, will be presented.

1.1 Body Area Network Communication

RF communication between wearable devices attached to the body of persons can take place and this technology is termed as body area network (BAN) communication. It is a short range wireless network composed of devices situated in, on and around the body. BAN communication [3, 4] has its potential in various fields like sports, health, entertainment, military and other applications [5]. Data transmission takes place from a wearable device on the body of a person to another device fitted on the body of another person either nearby or separated by some distance. BAN communication can be used for health monitoring purpose like monitoring patients remotely, cardiovascular disease detection, sleep monitoring, etc. Real time monitoring of an athlete can also be achieved, thereby preventing any major injuries. Feedback can also be provided back to an athlete in case of any emergency. It can be also beneficial in military applications to monitor the status of a soldier in battlefield and to exchange critical information among soldiers. Exact location and fatigue details can be tracked through such devices resulting in better management of soldiers on warfront [5].

1.2 Free-Space Optical Communication

Due to limited bandwidths and data rates in RF communication, optical wireless communication has come to the forefront and has the potential to overcome the limitations of RF communication. Optical wireless communication can be broadly classified into two categories- outdoor and indoor. The outdoor systems are conventionally called as free-space optical systems. They are of two types- space/laser links and terrestrial links. Indoor communication is carried out mostly using light emitting diode (LED) operating in infrared (IR) wavelength region of 780 nm-950 nm.

In space link optical wireless communication, links can be air-to-ground, air-to-air, aircraft-to-ground or to other spacecraft or deep space, links between different earth orbits to ground, ground to other planets links, etc. In all these links, laser is used because of its narrow beamwidth, more bandwidth than RF devices, smaller size. Free-space optical links can be used as terrestrial links for distances ranging over several kilometres provided there is good line-of-sight (LOS) between the two devices. In the current scenario, high bandwidth connections are required between the local area network (LAN) and metropolitan area network (MAN) or wide area network (WAN). To make sure that end users are receiving high speed gigabit Ethernet connectivity, high bandwidth connectivity between LAN and WAN is necessary which can be achieved by using free-space optical (FSO) links. FSO link deployment and maintenance are cheaper than RF links.

FSO communication offers benefits like ultra-wide bandwidth, inherent security and ease of installation. It exceeds the data rates of traditional RF communication [6, 7, 8, 9]. However, FSO is affected by fluctuations in the atmosphere. FSO is mainly used for LOS communication and hence is not a good option for long distance communication. Cooperative communication is a necessity for effective long distance FSO communication. The light propagation in FSO communication is different from signal propagation in RF communication. Hence some new phenomenon needs to be studied to understand the concepts of FSO communication. The propagation of laser beam in free-space is affected by beam divergence, atmospheric losses, atmospheric turbulence and ambient light.

1.2.1 Beam Divergence

The diffraction of light around the aperture at the sharp edges of the telescope causes beam divergence. The amount of useful signal energy to be collected at the receiver is determined by the amount of divergence. It is independent of the propagation medium. The divergence angle of the beam spread is given by [10]:

$$\theta = \frac{\lambda}{D} , \tag{1.1}$$

where D is the aperture diameter and λ is the propagating wavelength.

1.2.2 Ambient Light

Sun light and moon light which are natural sources of light also have spectral lines in the visible and infrared region. Hence noise is induced in the FSO channels due to the presence of light sources. The peak intensity of noise caused due to solar radiations is generally observed at 480 nm and decreases gradually with increase in wavelength.

1.2.3 Atmospheric Losses

The optical beam while propagating through the atmosphere undergo losses or attenuation due to absorption and scattering. Absorption occurs due to the absorption of photons meaning that energy of photons in the optical beam is transferred to the internal energy of the absorbing particle. Scattering occurs due to collision of light beam with scatterers or some particles, thereby causing change in direction of optical signal. Attenuation of light beam propagating through the atmosphere can be described by Beer Lambert's Law. It states that at a distance x, the transmission coefficient of laser radiation $T(x)$ in the atmosphere is given by [11]:

$$T(x) = \frac{I_x}{I_0} = e^{-\sigma_{att}x} \ , \tag{1.2}$$

where I_x is the intensity of light at a distance of x whereas I_0 is the original light intensity transmitted, σ_{att} is the attenuation coefficient. Attenuation coefficient is the summation of four individual parameters-molecular and aerosol absorption coefficients denoted by α_m and α_a respectively, and molecular and aerosol scattering coefficients denoted by β_m and β_a respectively. These are all functions of wavelengths. Therefore, attenuation coefficient can be evaluated as:

$$\sigma_{att} = \alpha_m + \alpha_a + \beta_m + \beta_a \ . \tag{1.3}$$

1.2.4 Absorption

Absorption particles can be divided into molecular and aerosol absorbers. When the laser beam interacts with the gaseous molecules in the medium like O_2 (oxygen), N_2 (nitrogen), H_2 (hydrogen), etc., then molecular absorption occurs. The particles are distinguished by their refractive index. The imaginary part of refractive index n_m is involved in molecular absorption by the following equation [11]:

$$\alpha_m = \frac{4\pi n_m}{\lambda} = A_{abs} N_{abs} \ , \tag{1.4}$$

where A_{abs} is the cross-section of absorption area and N_{abs} represents the concentration of absorption particles. Thus molecular absorption is a function of wavelength λ. Low absorption losses take place in the spectral wavelength regions of 850 nm, 1300 nm, and 1550 nm. There are suspended solid or

liquid particles present in the atmosphere in the form of fog, mist, etc. which are called liquid aerosols while suspended particles in the form of dust, volcanic debris, and dust particles are called solid aerosols. Aerosols can be formed as a part of industrial waste by man-made conversion of gaseous particles to solid or liquid particles. The size of the particles varies from 0.01 μm to 10 μm.

1.2.5 Scattering

Scattering can be classified into Rayleigh and Mie scattering depending on the size of the particles. The size parameter ω_{sc} is given by:

$$\omega_{sc} = \frac{2\pi r_a}{\lambda} \ , \tag{1.5}$$

where the particle radius is given by r_a and λ is the wavelength. When ω_{sc} <<1, the scattering is said to be of Rayleigh type whereas when ω_{sc} is of the order 1, scattering is said to be of Mie type. If ω_{sc} >>1, then scattering is independent of wavelength and is of non-selective type.

When particle size is very small in comparison to the wavelength of the medium, then Rayleigh scattering dominates. The scattering is inversely proportional to λ^4 meaning shorter wavelengths cause more scattering. Thus longer wavelength infrared region has less prominent Rayleigh scattering effect. In case of Mie scattering, the scattering is inversely proportional to λ^q where q varies from 1.6 to 0. q denotes the size of scattering particle and its value is given as [12]:

$$q = \begin{cases} 1.6 \text{ for high visibility } (V > 50Km) \\ 1.3 \text{ for average visibility } (6Km < V < 50Km) \\ 0.585V^{1/3} \text{ for low visibility } (V < 6Km) \ , \end{cases} \tag{1.6}$$

where V denotes the visibility in Km. Mie scattering process is mainly caused due to the presence of aerosols like fog, mist, haze, etc.

1.2.6 Atmospheric turbulence

Atmospheric turbulence is a random phenomenon caused by change in refractive index of air with time. According to Kolmogorov theory, atmospheric turbulence is characterized by the measure of eddy size and by the atmospheric structure constant C_n^2. The C_n^2 parameter varies with wind velocity and altitude and can be written with the help of Hufnagel Valley formula as [12]:

$$C_n^2(h_{alt}) = 0.00594 \left(\frac{\vartheta}{27}\right)^2 (10^{-5}h_{alt})^{10} \exp\left(\frac{h_{alt}}{100}\right) + 2.7 \times 10^{-16} \exp\left(\frac{-h_{alt}}{1500}\right) + A \exp\left(\frac{-h_{alt}}{100}\right) \ , \tag{1.7}$$

where ϑ is the rms wind speed in m/s, h_{alt} denotes the altitude in metres and A is a nominal value of $C_n^2(0)$ at the ground in $m^{-2/3}$. For atmospheric channels near the ground (for terrestrial links when

h_{alt} <18.5m), C_n^2 varies from $10^{-13}m^{-2/3}$ to $10^{-17}m^{-2/3}$ for strong to weak turbulences.

According to Rytov theory, a propagating optical wave at a distance of L from the source, will have the field equation as:

$$U(r, L) = U_0(r, L) \exp[-\psi(r, L)] \ , \tag{1.8}$$

where $U_0(r, L)$ is the optical field in the absence of turbulence, r is the observation point in the transverse plane at a distance of L, $\psi(r, L)$ is the complex phase perturbations resulting due to random inhomogoneneities along the propagation path. However, this equation is limited to single scattering phenomenon only as it does not take into account the role of decreasing transverse spatial coherence radius of the propagating wave. Hence for multiple scattering regime, the modified Rytov theory can be written as:

$$U(r, L) = U_0(r, L) \exp[\psi_x(r, L) + \psi_y(r, L)] \ , \tag{1.9}$$

where the terms $\psi_x(r, L)$ and $\psi_y(r, L)$ denote complex phase perturbations that are statistically independent and are caused due to large scale and small scale fluctuations respectively. Therefore, the modified irradiance of an optical field can be written as the product of two random processes.

$$I = I_x I_y \ . \tag{1.10}$$

Thus the modified Rytov theory states that the large scale turbulence eddies caused by refraction modulate the small scale turbulence eddies caused by scattering. These turbulence effects can be considered as random processes which are independent of each other. The multiplicative effect of random processes to create a new random process should be considered while designing the FSO channel model.

1.3 Underwater Optical Wireless Communication

Another application of optical wireless communication is in underwater environment and is known as underwater optical wireless communication (UOWC). UOWC offers the best solution for higher data rates, while RF and acoustic carriers have less bandwidth and lower data rates. UOWC has many similarities with atmospheric FSO communication [13], however the environmental conditions are different due to scattering and absorption phenomenon in aquatic environment. UOWC consists of multiple distributed nodes such as seabed sensors, relay buoys, remotely operated underwater vehicles (ROV) and autonomous underwater vehicles (AUV). The ROVs and AUVs perform data exchange with the sensors located at the oceanic beds by means of acoustic or optical transmission modes. The data from these ROVs and AUVs are transferred to submarines and ships, which perform data exchange with the data processing centre located above the marine environment through RF/FSO links. UOWC can be of use

in military applications, environmental monitoring, offshore exploration and disaster precaution.

1.4 Hybrid FSO/RF Communication

A combined version of FSO and RF communication can be used to enhance the efficiency of future generation communication networks. FSO communication is affected by fog and atmospheric turbulences and not by rain, while RF communication is affected by rain but not influenced by atmospheric turbulences [14]. Existing cellular communication systems support only RF communication with no provision for FSO communication. We can incorporate FSO links along with the existing RF based cellular systems to form a hybrid FSO/RF network. In this hybrid system model, the mobile user (MU) can communicate with an access point (AP) through the existing RF links while the APs can exchange data with the base stations (BS) through FSO links. It is difficult to incorporate FSO communication at the mobile user side since the mobile devices do not support FSO communication. Hence it is advantageous and less expensive to incorporate FSO communication at the BS, since BS are few in number. It is also difficult to maintain LOS links for FSO communication between the MU and AP in a crowded and dense urban environment. RF communication can take place in dense crowded places without LOS links. Therefore, the use of RF link is justified for connecting MU with AP. Thus a hybrid FSO/RF system can exploit the benefits of both FSO and RF communication in cellular systems and achieve high data rates.

1.5 Physical Layer Network Coding

An important technology which will be used in further chapters for enhancing the efficiency of bidirectional communication networks is physical layer network coding (PLNC). Suppose there are 2 nodes which can exchange data with the help of relay node as depicted in Fig. 1.1. In the first time slot, source nodes 1 and 2 send its information simultaneously to the relay node (R). In the second time slot, the relay node performs mapping operation and retransmits the information to the source nodes simultaneously. It is not required for the relay node to decode the exact bit values. The source nodes are designated by node i where $i \in (1, 2)$. Let the real part of the signal transmitted by node i is $Re[(a_i + jb_i)e^{j\omega t}]$, where ω is the RF signal frequency. Then the real part of the signal received by the relay, which is a superposition of the signals transmitted by both the source nodes, is $y_R(t) = (a_1 + a_2)\cos(\omega t) - (b_1 + b_2)\sin(\omega t)$. Here the QPSK modulated bits a_i and b_i can take the values of -1 and +1 as given by $a_i \epsilon \{-1, 1\}$, $b_i \epsilon \{-1, 1\}$ where -1 symbol is bit mapped to 1 and 1 symbol is bit mapped to 0. Now the coding operation is simplified according to the mapping table given in Table 1.1. One can observe that if we convert symbol 1 to bit 0 and symbol -1 to bit 1, then the mapping table for a_R is giving exactly bit level exclusive OR of a_1 and a_2. The in-phase (y_R^I) and quadrature phase (y_R^Q) components of the signal received by the relay can be separated as $y_R^I = a_1 + a_2$, $y_R^Q = b_1 + b_2$. Now the relay does not have to decode the bit

values, instead it has to find the values of $a_1 + a_2$ and $b_1 + b_2$ and then find a_R and b_R using the following mapping function. $a_R = a_1 a_2$ can be calculated from y_R^I as follows:

$$a_R = \begin{cases} -1 \;\; if \; y_R^I = 0, \\ 1 \;\; if \; y_R^I = -2 \; or \; 2. \end{cases}$$

Similarly, $b_R = b_1 b_2$ can be evaluated from y_R^Q as follows:

$$b_R = \begin{cases} -1 \;\; if \; y_R^Q = 0, \\ 1 \;\; if \; y_R^Q = -2 \; or \; 2. \end{cases}$$

. In the second time slot, relay transmits signal to nodes 1 and 2 as: $s_R(t) = Re[(a_R + jb_R)e^{j\omega t}] = a_R cos(\omega t) - b_R sin(\omega t)$. Thus only the values of a_R and b_R are required and not the exact values of a_i and b_i. Thus for exchange of two packets, one in each direction, PLNC [15] requires 2 time slots. It is because of the network coding operation automatically performed in the superimposed electromagnetic waves for RF communication and superimposed optical waves for FSO communication.

Table 1.1: Physical layer network coding mapping table

Symbol from node 1, a_1	Symbol from node 2, a_2	Signal received at relay, $y_R^I = a_1 + a_2$	Mapped symbol to be transmitted by relay, a_R
1	1	2	1
1	-1	0	-1
-1	1	0	-1
-1	-1	-2	1

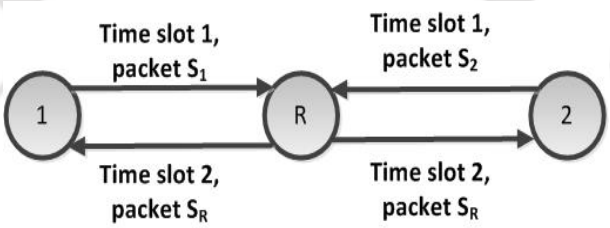

Figure 1.1: Physical layer network coding scheme

1.6 Spatial Modulation

Before going into the concept of spatial modulation (SM) let us have a look at multiple-input-multiple-output (MIMO) technology and the motivation behind proposal of SM technique. MIMO technology can be used in RF and optical domain to increase the data rate by deploying multiple transmit and receive sources. But the drawback of MIMO technique is that multiple RF/optical chains are required in

RF/optical domain leading to excessive power consumption and escalated cost. Multiple antenna/lasers operating simultaneously also leads to inter-antenna/inter-optical interference in MIMO. These problems can be mitigated by a technique called SM which uses only one RF/optical chain. SM can be mixed with physical layer network coding (PLNC) for better efficiency in RF and FSO systems. Power consumption and system cost is escalated considerably by the simultaneous usage of multiple transmit RF/optical chains in PLNC system. Due to the use of multiple antenna/lasers simultaneously, inter-antenna/inter-optical interference also increases in PLNC. This is the motivation for the proposal of SM in RF and FSO communication systems. For RF medium, a single antenna is activated in SM thereby eliminating the inter-antenna interference. From the incoming series of bits, a chunk of bits $(\log_2(N_A) + \log_2(M))$ are taken at a time for spatial modulation, where N_A denotes the number of antenna and M represents the M-ary modulation scheme. The transmit antenna activation is implemented by $\log_2(N_A)$ number of bits starting from LSB part of the information bits, while the remaining $\log_2(M)$ bits are mapped to a symbol using a particular constellation scheme. Similarly for optical medium, a single laser is activated and the technique is known as optical spatial modulation (OSM). From the incoming series of bits, a chunk of bits $(\log_2(N_L) + \log_2(M))$ are taken at a time for OSM, where N_L denotes the number of lasers. The transmit laser activation is implemented by $\log_2(N_L)$ number of bits starting from LSB part of the information bits, while the remaining $\log_2(M)$ bits are mapped to a symbol using a particular constellation scheme. Power consumption and overall cost in SM and OSM are reduced because of the presence of single RF and optical chain in SM and OSM respectively.

1.7 Advanced Spatial Modulation

In spatial modulation we have seen that only one source is activated out of the multiple sources. Hence from the cost perspective, unnecessary money is incurred in buying and deploying the extra sources. To mitigate this issue, advanced spatial modulation (ASM) techniques are introduced in which more than one sources are activated to compensate for the extra cost of the other sources. These techniques also have a capability of achieving higher spectral efficiencies than conventional spatial modulation. These schemes use multiple RF/optical chains, thereby incurring extra cost of the optical/RF chains. Hence there must be a compromise between cost and spectral efficiency. Activating too many sources would negate the benefits of spatial modulation such as less power, less cost and less inter-antenna/laser interference. Some advanced spatial modulation schemes which are described later in the thesis are enhanced spatial modulation (ESM), spatial media based modulation (SMBM), optical ESM (OESM), optical generalized spatial modulation (OGSM), optical improved quadrature spatial modulation (OIQSM), transmit laser selection (TLS) combined with optical SM (TLS-OSM), hybrid SM (HSM) and transmit source selection

(TSS) combined with HSM (TSS-HSM). Advanced spatial modulation schemes can be used both in RF and optical domain.

1.8 Performance Analysis-Main Metrics and Applications

Performance analysis of communication system is done in terms of bit error rate, symbol error rate, outage probability, channel capacity, etc. Bit error rate (BER) is defined as the ratio of number of erroneous bits detected at the receiver to the total number of bits transferred during a given time interval. Symbol error rate (SER) is defined as the ratio of number of erroneous symbols detected to the total number of symbols transferred during a given time interval. A particular BER or SER value is defined as the acceptable BER or SER for a particular communication system below which the system performance is deemed to be unacceptable. Outage probability indicates the probability that the system can be in outage, i.e., the probability that the system cannot successfully decode the transmitted symbols. A communication system is in outage as soon as it transmits at a data rate which is higher than the channel capacity. Channel capacity gives the maximum data rate at which information can be transferred over a given communication channel with minimal probability of error. In this thesis, performance analysis of spectrally efficient advanced spatial modulation based systems is carried out in terms of outage probability, bit error rate and symbol error rate.

1.9 Organization of the Thesis

Chapter 1 gives a brief idea about the various technologies for which SM and ASM schemes can be applied. The rest of the thesis is organized as follows- Chapter 2 proposes SM along with PLNC for RF cooperative communication. Performance analysis of such system is investigated and compared with other techniques available in literature. Chapter 3 investigates performance of BAN communication for SISO and MIMO scenarios for sporting activities like running and cycling. Advanced techniques for SM are also proposed for MIMO BAN communication. Chapter 4 deals with the study of OSM based bidirectional FSO cooperative communication. It also proposes advanced techniques for FSO cooperative communication like transmit laser selection (TLS) and other advanced forms of OSM schemes. Chapter 5 investigates the performance of various types of ASM schemes for UOWC communication. Chapter 6 combines the benefits of RF and FSO communication to propose a hybrid FSO/RF cooperative communication system. Spatial modulation schemes for such a hybrid system are proposed in this chapter. Chapter 7 concludes the thesis and discusses future scope of the thesis.

1.10 Contribution of the Thesis

The primary motivation of our work is to achieve higher spectral efficiencies for various applications at lower error and cost, and also to avoid the inter-optical/inter-antenna interference resulting from simultaneous data transfer as in case of MIMO. Due to the varying nature of the environments and applications for which spatial modulation is being applied, different channel models need to be selected which will be discussed further in the respective chapters. The thesis is broadly classified into five chapters and propose advanced spatial modulation schemes for RF, BAN, FSO, UOWC and hybrid FSO/RF systems. Chapter 2 deals with SM for RF cooperative systems which can be implemented in a D2D scattering environment. The performance analysis of such systems is carried out in terms of lower and upper bounds of outage probability. The novelty of the work is highlighted by the fact that SM along with PLNC is proposed for the first time for two-way relay based decode-and-forward RF cooperative system, over cascaded $\alpha - \mu$ fading channels. The asymptotic analysis gives valuable insights regarding coding and diversity gain of the proposed system, which highlights the contribution of our work.

In Chapter 3, performance analysis of BAN communication in RF domain is performed in terms of outage probability and ASEP. But mixture of lognormal distribution (which is considered as BAN channel) contains certain intractable integrals, hence the closed form expressions cannot be derived. For this purpose, mixture of Gamma (MG) distribution is used to estimate the lognormal mixture distribution [16]. The novelty of this work lies in the fact that MG distribution is applied for performance analysis of BAN communication systems and achieve closed form expressions of ASEP and outage probability. BAN communication is first analyzed for SISO scenario and then the analysis is extended to MIMO scenario, where advanced concepts of SM called enhanced spatial modulation (ESM) and spatial media based modulation (SMBM) are introduced to improve the efficiency of BAN communication. The closed form BER expressions using 5-MG distribution are also derived for ESM and SMBM in this chapter and are novel in nature. The performance analysis of ESM and SMBM are carried out using these novel expressions. Asymptotic analysis is also carried out for these schemes using tractable closed form expressions. The detailed analysis is carried out for running and cycling activities under different scenarios and catering to a diverse set of people, highlighting the importance of our work. Some interesting inferences are deduced which may be helpful in sports industry for monitoring the performance of an athlete and prevent casualties. Such sensor-based communication is proposed for BAN communication for the first time, thereby highlighting our novelty.

Optical spatial modulation (OSM) for two-way decode-and-forward relay based FSO systems are proposed in the next chapter (Chapter 4). The lower and upper bounds of outage probability for full-

duplex OSM based relay system are evaluated in terms of closed form expressions and compared with other techniques available in literature. Monte Carlo simulations are performed under different channel conditions to confirm the correctness of the analytical technique. The effect of varying various parameters of the channel is studied and the results are reported in this chapter. OSM system performance can be impacted if the channel link is down. The transmit laser is selected depending on the value of the message bit, irrespective of the channel conditions. This drawback of OSM can be mitigated by the proposal of a new technique called transmit laser selection (TLS) described in the later part of Chapter 4. We can either use only TLS or TLS combined with OSM to improve the throughput. TLS is used to select the best set of laser sources out of the available multiple laser sources depending on the channel condition. The novelty of our work lies in the fact that TLS and TLS-OSM transmit schemes are proposed for the first time for FSO cooperative system to increase the error performance and spectral efficiency of FSO systems. Performance analysis of TLS and TLS-OSM schemes are studied in terms of closed form expressions of outage probability and ASEP, which highlights the contribution of our work. Some advanced forms of OSM schemes for FSO communication like optical generalized spatial modulation (OGSM), optical enhanced spatial modulation (OESM) and optical improved quadrature spatial modulation (OIQSM) are proposed for the first time. Performance analysis of such schemes are studied for FSO systems in terms of BER for the first time. Error involved in laser index detection is also considered, which highlights a major contribution of our work. The detailed analysis of the proposed schemes in terms of power consumption and cost is also presented in this chapter.

UOWC spatial modulation schemes are analyzed in the next chapter (Chapter 5). Performance analysis of UOWC cooperative systems with amplify-and-forward (AF) technique at the relay is carried out in terms of outage probability and ASEP. The concept of OSM and other advanced forms of OSM like optical improved quadrature spatial modulation (OIQSM) for UOWC cooperative systems are proposed in this chapter and performance analysis in terms of BER is done. The closed form BER expressions for such systems are completely novel in nature. Depending on the value of message bits, transmit laser is selected in OSM, which can impact the system performance if that particular channel link is down. Therefore, TLS and TLS-OSM for UOWC systems are proposed, similar to TLS in FSO communication. The novelty of this work lies in the fact that TLS and TLS-OSM schemes are proposed for UOWC cooperative systems for the first time. The performance analysis of such systems is carried out in terms of ASEP and the corresponding expressions for UOWC system analysis are provided. TLS for UOWC systems has not yet been investigated in literature, highlighting the importance of our work. Such TLS based UOWC systems can be beneficial in military application, offshore sea explorations, disaster precaution and other related activities.

In the subsequent chapter (Chapter 6), hybrid FSO/RF systems are proposed for future cellular communication which exploits both the benefits of FSO and RF communication. The novelty of our work pertains to the fact that hybrid spatial modulation (HSM) and transmit source selection (TSS) schemes are proposed and analyzed for the first time in hybrid FSO/RF systems. The performance of a relay based hybrid FSO/RF system for FSO channel incorporating pointing errors is investigated for HSM, TSS and a combination of both TSS and HSM, employing DF protocol at the relay. The closed form outage probability expressions for cooperative HSM and TSS based hybrid FSO/RF systems are provided. The proposed system model incorporating these technologies can be used in future cellular systems. Detailed power consumption and cost analysis of the RF and optical components for the proposed methods are also illustrated in this chapter. Asymptotic analysis provides valuable information regarding coding and diversity gain of the various methods. The motivation of our work is as follows:

1. Achieving high spectral efficiencies at a reduced cost and power consumption than multiple sources based hybrid FSO/RF system. This motivates the use of TSS and HSM.

2. Proper channel path may not be selected in HSM unlike TSS, while TSS has lesser spectral efficiency than HSM. This is the motivation for combining both the benefits of HSM and TSS into a single technique called TSS-HSM.

The overall contribution of the thesis can thus be summarized as:

- Investigating spatial modulation with PLNC for RF cooperative communication with bidirectional relays in a D2D scattering environment.
- Investigating SISO and MIMO BAN communication for sporting activities, proposing advanced spatial modulation schemes for BAN RF based communication.
- Investigating various advanced forms of optical spatial modulation schemes for FSO communication.
- Investigating advanced versions of optical spatial modulation schemes for UOWC.
- Investigating hybrid spatial modulation schemes for hybrid FSO/RF communication.

2. Spatial Modulation for RF Cooperative Communication

In this chapter, spatial modulation along with PLNC is proposed for bidirectional RF cooperative systems. In this cooperative system, the nodes having low height antennas can interact with each other individually in a high scattering envrionment, which is similar to a D2D communication environment. Therefore, the concepts of D2D communication can be used to explore such a RF cooperative system. D2D communication comprises of low height antennas, almost at the street level, at both the transmitting and receiving ends. Relative motion exists between the transmitter and receiver also. This does not occur in cellular communication where base station is fixed and its antenna is located at a much higher elevation, while only the mobile is in motion and has an antenna at a lower height. In D2D communication, scatterers are located at both ends- transmitter as well as receiver, while in cellular communication, base station is free from local scatterers due to its greater elevation. Due to the presence of multiple scattering groups, conventional channel models fail for D2D communication [17]. Therefore, different channel models are required for D2D communication as explained later in this chapter.

Let us understand some basic concepts related to this chapter first. Mutual information can be defined as the amount of information obtained about one random variable by observation of the other random variable. Thus it represents the decrement in uncertainty about a random variable, provided knowledge of another random variable is given. If mutual information value is high, then it denotes a large decrement in uncertainty. Whereas if mutual information is low, then it indicates a lesser decrement in uncertainty. If mutual information is nil, then it means that the variables are independent. Entropy in communication system refers to the quantity of uncertainty related with one particular outcome or event of a random variable.

The concepts of SM and PLNC have already been introduced in Chapter 1. By utilizing SM and PLNC in this chapter, data rate and bandwidth efficiency of RF cooperative system can be enhanced. Cooperative communication holds the promise for better connectivity, increased coverage area, diversity and multiplexing gains. In cooperative communication, data is exchanged between two devices with the

help of an intermediate device called relay. Cooperative relaying can increase the reliability of wireless communication especially in mobile ad-hoc networks and sensor networks [18], [19]. Amplify-and-forward (AF), decode-and-forward (DF) and compress-and-forward (CF) relaying are some examples of relaying protocols. In AF protocol, the received signal at the relay is simply amplified to compensate for the power loss and then forwarded to the destination nodes. In DF protocol, the relay first decodes the signal, encodes it again and then sends it to the destination nodes. The relays can be unidirectional or bidirectional in nature. Again the relays can have fixed or variable gain. Cooperative communication can be of single hop or multi-hop. Relays can be arranged in parallel or in series. Thus in this chapter, we are going to include the concept of cooperative communication in RF systems in a D2D scattering environment to provide enhanced performance. Before going into further details, related literature is investigated.

The literature survey is presented sequentially starting with a survey of various channel models, then moving on to survey of SM technique, followed by survey of PLNC technique, and concluded by a survey of SM combined with PLNC applications for various channel models. Many channel models for mobile-to-mobile communication are available in the literature ranging from 2D models to 3D models [20, 21, 22, 23, 24, 25, 26]. But a majority of them consider only a single or double scattering group, whereas in reality multiple scattering groups exist for D2D communication. Cascaded channel models are the products of multiple channels, each of which can model a scattering group accurately. Hence cascaded model is more suitable for such D2D communication scenarios. In literature, cascaded Rayleigh fading channel models [27] and N-Nakagami channel model [28], [18] have been reported. Weibull channel generates much deeper fades than conventional Rayleigh and Nakagami channels, hence it is more appropriate for D2D communication. A generalized version of the Weibull and N-Nakagami channel model called cascaded $\alpha - \mu$ channel model has been proposed in [29], [30]. In literature, a cascaded $\alpha - \mu$ model has been modelled by Fox H function [31]. But for computational simplicity, Meijer G function can be used which is readily available in software packages like Matlab and Mathematica. To evaluate the probability density function (PDF) and cumulative distribution function (CDF) for cascaded models, moment generating function (MGF) has been utilized in literature. But the technique has high computational complexity due to the nature of expressions and mathematical calculations involved.

Outage probability for spatial modulation (SM) systems with antenna selection for RF communication has been evaluated in [32]. Using an adaptive mapping scheme, BER for SM in RF communication has been reported in [33]. SM for a bidirectional network coded channel using space shift keying (SSK) has been proposed along with BER analysis in [34]. A differential SM scheme using a denoise-and-forward protocol has been studied for bidirectional relay networks in [35]. A generalized joint 3-D optimized

constellation diagram has been proposed in [36] which increases the transmission reliability of SM. PLNC has been used effectively for classical channel models in [37, 38, 39]. In [37], techniques like transmit and receive beamforming, and transmit and receive antenna selection have been used for relay based PLNC system. Bounds for outage probability and diversity order have been calculated for independent but not necessarily identical Nakagami distribution. The authors in [38] have applied PLNC over K relays with 2 antennas in each relay. Evaluation of outage probability, moment generating function and symbol error probability have been carried out over iid Nakagami fading channels. Transmit and receive antenna selection have been reported in [39] with maximization of sum rate and minimization of overall outage probability being the criteria. PLNC with a fixed gain amplify-and-forward relay over cascaded Nakagami-m fading channels has been studied for vehicular communications in [40]. Performance analysis of PLNC over double Nakagami-m [41] and double Rayleigh [42] fading channels have been done in terms of symbol error rate for cooperative vehicular networks. Full-duplex communication has been implemented by applying SM along with PLNC in [43]. SM along with PLNC for bidirectional relay network with transmit antenna selection over Nakagami-m fading channels have been proposed in [44]. A set of antennas are selected depending on the order of statistics of the channel power. SM along with PLNC has been proposed for a bidirectional cognitive cross network in [45], where optimal power allocation is proposed for sources and the relay.

To the best of the author's knowledge, SM along with PLNC has not yet been proposed for bidirectional RF cooperative communication over cascaded $\alpha - \mu$ channel. Outage probability for such SM-PLNC based systems has not been evaluated for a D2D scenario where cascaded $\alpha - \mu$ fading channel can be used. Coding and diversity gain analysis of such systems are missing in the literature too. Based on these research gaps, the following contributions of the chapter are proposed. In this chapter, multiplication of random variables is used to compute the PDF and CDF for cascaded $\alpha - \mu$ distribution. The performance of proposed bidirectional RF cooperative system over cascaded α-μ fading channels using SM and PLNC technique is evaluated in the further sections. Closed form tractable expressions for lower and upper bounds of outage probability are derived for such systems, which highlights the novelty of our work. Asymptotic expressions are derived in tractable form which helps in the evaluation of coding and diversity gain of our proposed system. There are some challenges in analyzing SM along with PLNC over cascaded $\alpha - \mu$ channel. There is no exact expression available for analyzing outage probability of such system. The PDF and CDF expressions for the channel model are complicated in nature and it is quite challenging to solve the summation and product of CDF equation (due to presence of product of Meijer G function terms) of cascaded $\alpha - \mu$ model. Moreover, due to PLNC, the source nodes are transmitting simultaneously leading to a self-interference effect at the relay. Hence instead of

conventional signal-to-noise ratio (SNR) expressions, signal-to-interference-plus-noise ratio (SINR) must be considered while doing the performance analysis of our proposed system.

2.1 Cascaded α-μ Channel Model

The $\alpha - \mu$ fading model is a generalized physical fading model comprising of multipath clusters which propagate in a non-homogeneous environment [18]-[20]. The channel model comprises of two parameters- α and μ. The non-linearity factor of the propagation medium is depicted by α whereas the number of multipath clusters is represented by μ. Gamma, Rayleigh and Nakagami distributions are some specialized versions of cascaded $\alpha - \mu$ model. Cascaded α-μ model is a cascaded combination of multiple α-μ channel models.

The suitability of using different generalized fading models for such a high scattering environment is explored. $\kappa - \mu$ model comprises of multiple clusters where each cluster comprises of some dominant components called line-of-sight (LOS) components. Such LOS components are not present in D2D communication because of the low height of the antennas and the presence of a dense urban environment causing more obstacles. Therefore $\kappa - \mu$ model is not valid for such scenarios. $\eta - \mu$ model can be used in 2 formats- one where the in-phase and quadrature phase components of the resultant signal in each cluster are independent and have different powers and another where the in-phase and quadrature phase components of the resultant signal in each cluster are correlated and have equal powers. Whereas $\alpha - \mu$ model is used for scenarios having no dominant LOS components and the in-phase and quadrature phase components of the resulting signal in each cluster are independent and have equal powers. We are considering the environment in D2D communication where the scattering clusters have no dominant LOS component and the in-phase and quadrature phase components of the resulting signal in each cluster are independent and have equal powers. Hence we are applying cascaded $\alpha - \mu$ model. $\eta - \mu$ format I may also be used for such models if $\alpha = 2$ is considered for the scattering environment.

Now we will do a brief analysis of cascaded $\alpha - \mu$ channel model to prove how other channel models can be deduced. We will consider a $\alpha - \mu$ channel model to derive various channel models and the corresponding cascaded models can be easily obtained by the multiplicative effect of any individual channel models. In $\alpha - \mu$ channel model, the fading amplitude can be defined as the α^{th} root of the received power in the faded signal. Thus fading amplitude can be written as:

$$X^{\alpha} = \sum_{i=1}^{\mu} \left(I_i^2 + Q_i^2 \right) \ , \tag{2.1}$$

where the number of clusters is represented by μ and the i^{th} cluster in the received signal has resultant in-phase and quadrature phase components denoted by I_i and Q_i respectively. The model consists of

multiple clusters with each cluster having scattered multipath components. I_i and Q_i are the resultant of multipath components of a particular cluster and can be modelled as Gaussian distribution having zero mean and equal variances. Now if a single cluster is considered i.e. $\mu = 1$, then the fading amplitude can be written as:

$$X = \sqrt[\alpha]{I_i^2 + Q_i^2} \ . \tag{2.2}$$

This equation corresponds to the fading amplitude equation of a Weibull channel model. Further if $\alpha = 1$ for Weibull model, then the fading amplitude can be written as:

$$X = I_i^2 + Q_i^2 \ . \tag{2.3}$$

This represents exponential distribution. Thus by putting $\alpha = 1$ and $\mu = 1$ in $\alpha - \mu$ model, we can derive exponential model. Now by considering $\alpha = 2$ and $\mu = 1$ in $\alpha - \mu$ fading amplitude expression, we can write the new fading amplitude as:

$$X = \sqrt{I_i^2 + Q_i^2} \ . \tag{2.4}$$

This corresponds to the fading amplitude expression of a Rayleigh distribution. By considering $\alpha = 2$ and $\mu = 0.5$ in $\alpha - \mu$ fading amplitude expression, we can obtain a one-sided Gaussian distribution. Similarly, Nakagami model can be deduced from $\alpha - \mu$ fading model by putting $\alpha = 2$ and $\mu = m$ in the fading amplitude expression for $\alpha - \mu$ model. Thus the fading amplitude of Nakagami distribution can be written as:

$$X = \sqrt{\sum_{i=1}^{m} (I_i^2 + Q_i^2)} \ . \tag{2.5}$$

Therefore, it can be said that cascaded $\alpha - \mu$ channel is a generalized cascaded fading model as other classical fading models can be derived from it.

2.1.1 PDF and CDF of Cascaded $\alpha - \mu$ Channel

For system performance analysis, PDF and CDF of the channel model are required. To obtain the PDF and CDF of cascaded α-μ fading channels, we have to start from the PDF of a α-μ fading channel and use concepts of probability as shown below in details. Let the random variable (RV), $R \geq 0$ be the signal envelope following α-μ distribution. The PDF $f_R(r)$ of R can be written as [29], [30]:

$$f_R(r) = \frac{\alpha \mu^{\mu} r^{(\alpha\mu - 1)}}{\Gamma(\mu) \hat{r}^{\alpha\mu}} \exp\left[-\mu \left(\frac{r}{\hat{r}}\right)^{\alpha}\right] \ , \tag{2.6}$$

where $\hat{r} = \sqrt[\alpha]{\mathbb{E}(R^{\alpha})}$, $\mathbb{E}$ is the expectation operator and $\exp(\cdot)$ is the exponential function. Let R_1, $R_2, .., R_n$ be n ≥ 2 statistically independent positive RVs and $Z_n = \prod_{i=1}^{n} R_i$ be the product of n RVs. The objective is to evaluate the PDF $f_{Z_n}(z)$ of Z_n. Initially we start with the product of two RVs and then use a recursive approach to find a generalized formula for the PDF of the product of n RVs. From probability, we know:

$$f_{Z_m}(z) = \int_0^{\infty} \frac{1}{t} f_{Z_{m-1}}(\frac{z}{t}) f_{R_m}(t) dt \ , \tag{2.7}$$

where $f_{R_m}(\cdot)$ represents the PDF of R_m random variable and $f_{Z_{m-1}}(\cdot)$ represents the PDF of the partial product $Z_{m-1} = \prod_{i=1}^{m-1} R_i$ in which 2 $\leq$m $\leq$ n. Then the CDF can be computed as $F_{Z_n}(z) = \int_0^z f_{Z_n}(z) dz$. Beginning with the partial product $Z_2 = R_1 R_2$ and taking help of Eq. (2.7), PDF of Z_2 can be written as:

$$f_{Z_2}(z) = \int_0^{\infty} \frac{1}{t} \frac{\alpha_1 \mu_1^{\mu_1} \left(\frac{z}{t}\right)^{(\alpha_1\mu_1 - 1)}}{\Gamma(\mu_1) \hat{r_1}^{\alpha_1\mu_1}} \exp\left[-\mu_1 \left(\frac{\frac{z}{t}}{\hat{r_1}}\right)^{\alpha_1}\right] \times \frac{\alpha_2 \mu_2^{\mu_2} t^{(\alpha_2\mu_2 - 1)}}{\Gamma(\mu_2) \hat{r_2}^{\alpha_2\mu_2}} \exp\left[-\mu_2 \left(\frac{t}{\hat{r_2}}\right)^{\alpha_2}\right] dt \ . \tag{2.8}$$

Now let $h_1 = \frac{\mu_1^{\frac{1}{\alpha_1}}}{\hat{r_1}}$ and $h_2 = \frac{\mu_2^{\frac{1}{\alpha_2}}}{\hat{r_2}}$. Then Eq. (2.8) can be simplified as:

$$f_{Z_2}(z) = \frac{\alpha_1 \alpha_2}{\Gamma(\mu_1)\Gamma(\mu_2)} h_1^{\alpha_1\mu_1} h_2^{\alpha_2\mu_2} z^{\alpha_1\mu_1 - 1} \int_0^{\infty} t^{-\alpha_1\mu_1 + \alpha_2\mu_2 - 1} \exp\left[-\left(\frac{h_1 z}{t}\right)^{\alpha_1} - (h_2 t)^{\alpha_2}\right] dt \ . \tag{2.9}$$

The variables are defined later in this section. This integral has no exact solution, hence certain assumptions are taken. The ratio of $\frac{\alpha_1}{\alpha_2} = \frac{p_2}{q_2}$ is considered where $p_2 \geq 1$ and $q_2 \geq 1$ are co-prime integers. Some variable transformations are done like $x = t^{\alpha_2}$. Now Eq. (2.9) can be written as:

$$f_{Z_2}(z) = \frac{\alpha_1 \alpha_2}{\Gamma(\mu_1)\Gamma(\mu_2)} h_1^{\alpha_1\mu_1} h_2^{\alpha_2\mu_2} z^{\alpha_1\mu_1 - 1} \int_0^{\infty} x^{-\frac{\alpha_1}{\alpha_2}\mu_1 + \mu_2 - \frac{1}{\alpha_2}} \exp\left[-(h_1 z)^{\alpha_1} x^{-\frac{\alpha_1}{\alpha_2}}\right] - \exp\left[h_2^{\alpha_2} x\right] \alpha_2 x^{\left(1 - \frac{1}{\alpha_2}\right)} dx \ . \tag{2.10}$$

Certain formulae are used for the integration and are given as [46]:

$$\exp(-s\gamma) = G_{0,1}^{1,0}\left(\begin{matrix} - \\ 0 \end{matrix} \middle| s\gamma\right) \ . \tag{2.11}$$

$$\int_0^{\infty} x^{\alpha-1} G_{u,v}^{s,t}\left(\begin{matrix} c_1,...,c_t,c_{t+1},...,c_u \\ d_1,...,d_s,d_{s+1},..,d_v \end{matrix} \middle| \sigma x\right) G_{g,h}^{e,f}\left(\begin{matrix} a_1,...,a_f,a_{f+1},..,a_g \\ b_1,...,b_e,b_{e+1},...,b_h \end{matrix} \middle| \mu x^{l/k}\right) dx$$
$$= \frac{k^{\mu} l^{g+\alpha(v-u)-1} \sigma^{-\alpha}}{(2\pi)^{b_\delta(l-1)+c_\delta(k-1)}} G_{kg+lv,kh+lu}^{ke+lt,kf+ls}\left(\begin{matrix} \Delta(k,a_1),...,\Delta(k,a_f),\Delta(l,1-\alpha-d_1),...,\Delta(l,1-\alpha-d_v),\Delta(k,a_{f+1}),...,\Delta(k,a_g) \\ \Delta(k,b_1),...,\Delta(k,b_e),\Delta(l,1-\alpha-c_1),....,\Delta(1-\alpha-c_u),\Delta(k,b_{e+1}),...,\Delta(k,b_h) \end{matrix} \middle| \frac{\mu^k k^{k(g-h)}}{\sigma^l l^{l(u-v)}}\right)$$

where $b_\delta = s+t-\frac{u+v}{2}$, $c_\delta = e+f-\frac{g+h}{2}$, l and k are co-prime integers, $\Delta(k,a) = \frac{a}{k}, \frac{a+1}{k}, .., \frac{a+k-1}{k}$. (2.12)

$$G_{p,q}^{m,n}\left(\begin{matrix}a_p\\b_q\end{matrix}\middle|\, z\right) = G_{q,p}^{n,m}\left(\begin{matrix}1-b_q\\1-a_p\end{matrix}\middle|\, z^{-1}\right) . \tag{2.13}$$

Therefore PDF of Z_2 turns out to be (with help of Eq. (9.31.2) and (9.31.5) in [47]):

$$f_{Z_2}(z) = \frac{\alpha_1 q_2^{\mu_1+\frac{3}{2}} p_2^{\mu_2+\frac{\alpha_1}{\alpha_2}-\frac{1}{2}}}{(2\pi)^{\frac{p_2+q_2-2}{2}}\Gamma(\mu_1)\Gamma(\mu_2)}(h_1h_2)^{-\alpha_1} z^{-\alpha_1-1} G_{0,p_2+q_2}^{p_2+q_2,0}\left(\begin{matrix}-\\ \Delta(q_2,\mu_1+1),\Delta(p_2,\mu_2+\frac{\alpha_1}{\alpha_2})\end{matrix}\middle|\, \frac{(h_1h_2z)^{\alpha_1 q_2}}{p_2^{p_2} q_2^{q_2}}\right) , \tag{2.14}$$

where $G_{p,q}^{m,n}(:|\, z)$ is the Meijer G function [47], [48]. An iterative approach is taken to obtain the PDF for the next random variable $Z_3 = Z_2R_3$. The results are given in [30]. Thus with the help of Eq. (2.14), (2.7) and (2.6), we can write the PDF of Z_3 as:

$$f_{Z_3}(z) = \int_0^\infty \frac{1}{t}\frac{\alpha_1 q_2^{\mu_1+\frac{3}{2}} p_2^{\mu_2+\frac{\alpha_1}{\alpha_2}-\frac{1}{2}}}{(2\pi)^{\frac{p_2+q_2-2}{2}}\Gamma(\mu_1)\Gamma(\mu_2)}(h_1h_2)^{-\alpha_1}\left(\frac{z}{t}\right)^{-\alpha_1-1}$$
$$\times G_{0,p_2+q_2}^{p_2+q_2,0}\left(\begin{matrix}-\\ \Delta(q_2,\mu_1+1),\Delta(p_2,\mu_2+\frac{\alpha_1}{\alpha_2})\end{matrix}\middle|\, \frac{(h_1h_2z/t)^{\alpha_1 q_2}}{p_2^{p_2} q_2^{q_2}}\right) \times \frac{\alpha_3\mu_3^{\mu_3} t^{(\alpha_3\mu_3-1)}}{\Gamma(\mu_3)\hat{r_3}^{\alpha_3\mu_3}} \exp\left[-\mu_3\left(\frac{t}{\hat{r_3}}\right)^{\alpha_3}\right] dt . \tag{2.15}$$

Again we assume $h_3 = \frac{\mu_1^{\frac{1}{\alpha_1}}}{\hat{r_1}}$. Consider $x = t^{\alpha_3}$ and $\frac{\alpha_1}{\alpha_3} = \frac{p_3}{q_3}$ such that $p_3 \geq 1$ and $q_3 \geq 1$ are co-prime integers. With the help of reference formulas given in Eq. (2.11), (2.12) and (2.13), we can obtain the PDF of Z_3 (with the help of Eq. (2.24.3.1) in [48]) as [30]:

$$f_{Z_3}(z) = \frac{\alpha_1 q_2^{\mu_1+\frac{3}{2}} q_2^{\mu_3+\frac{\alpha_1}{\alpha_3}-\frac{1}{2}} p_2^{\mu_2+\frac{\alpha_1}{\alpha_2}-\frac{1}{2}} p_3^{\mu_3+\frac{\alpha_1}{\alpha_3}-\frac{1}{2}} q_3^{\mu_2+\frac{\alpha_1}{\alpha_2}-\frac{1}{2}} q_3^{\mu_1+\frac{3}{2}}}{(2\pi)^{\frac{q_2q_3+p_2q_3+p_3q_2-3}{2}}\Gamma(\mu_1)\Gamma(\mu_2)\Gamma(\mu_3)}(h_1h_2h_3)^{-\alpha_1} z^{-\alpha_1-1}$$
$$\times G_{0,q_2q_3+p_2q_3+p_3q_2}^{q_2q_3+p_2q_3+p_3q_2,0}\left(\begin{matrix}-\\ \Delta(q_2q_3,\mu_1+1),\Delta(p_2q_3,\mu_2+\frac{\alpha_1}{\alpha_2}),\Delta(p_3q_2,\mu_3+\frac{\alpha_1}{\alpha_3})\end{matrix}\middle|\, \frac{(h_1h_2h_3z)^{\alpha_1 q_2q_3}}{(q_2q_3)^{q_2q_3}\,(p_2q_3)^{p_2q_3}\,(p_3q_2)^{p_3q_2}}\right) . \tag{2.16}$$

If we follow this recursive approach (like $Z_4 = Z_3R_4$, $Z_5 = Z_4R_5$ and so on), then we obtain the PDF of Z_n. Certain assumptions are taken to evaluate the integral. The ratio of $\frac{\alpha_1}{\alpha_j} = \frac{p_j}{q_j}$ is considered where $p_j \geq 1$ and $q_j \geq 1$ are co-prime integers, $j = 2, ..., n$. From the PDF of Z_2 and Z_3, we can observe a similar pattern in the final expressions and hence the PDF of Z_n can be written as [29, 49]:

$$f_{Z_n}(z) = \frac{(2\pi)^{\frac{n-v_s}{2}} u v_p}{\Gamma(\mu) h_p^{\alpha_1} z^{\alpha_1+1}} G_{0,v_s}^{v_s,0}\left(\begin{matrix}-\\ b\end{matrix}\middle|\, \frac{(h_pz)^u}{v_e}\right) . \tag{2.17}$$

The variables are defined as:

$$h_i = \frac{\mu_i^{\frac{1}{\alpha_i}}}{\hat{r_i}} , \quad h_p = \prod_{i=1}^{n} h_i , \quad v_1 = \prod_{l=2}^{n} q_l , \quad v_j = \frac{p_j}{q_j} v_1 , \tag{2.18}$$

$$v_s = \sum_{l=1}^{n} v_l , \quad v_e = \prod_{l=1}^{n} v_l^{v_l} , \quad v_p = \prod_{l=1}^{n} v_l^{\mu_l+\frac{\alpha_1}{\alpha_l}-\frac{1}{2}} , \quad \Gamma_u = \prod_{l=1}^{n} \Gamma(\mu_l) , \tag{2.19}$$

$$u = \alpha_1 v_1 = ... = \alpha_n v_n \ , \tag{2.20}$$

$$b^{(i)} = \Delta(v_i, \mu_i + \frac{\alpha_1}{\alpha_i}), b = b^{(1)}, b^{(2)}, ..., b^{(n)} \ and \ \Delta(k,a) = \frac{a}{k}, \frac{a+1}{k}, ..., \frac{a+k-1}{k} \ . \tag{2.21}$$

Here h_p represents the product of h_i variables, v_1 denotes the product of q_l variables, v_j denotes the ratio of co-prime integers multiplied with v_1, v_s denotes the summation of all v_l variables, v_e represents the product of power of v_l variables raised to itself. Γ_u denotes the product of $\Gamma(\mu_l)$ variables (μ_l representing the fading parameter of each component of the cascaded channel), while u is the product of each α and v variables. $b^{(i)}$ represents a triangular function, Δ which is denoted as $\Delta(k,a)$. The number of cascaded components should be an integer.

If $\alpha_1 = \alpha_2 = ... = \alpha_n = \alpha$, resulting in $p_j = q_j = 1$, where j=2, 3, ..., n, v_p =1, v_1 =1, v_s =n, the above PDF simplifies to:

$$f_{Z_n}(z) = \frac{\alpha}{\Gamma(\mu) z} G_{0,n}^{n,0}\left({}^{-}_{\mu_1,\mu_2,...,\mu_n} \middle| (h_p z)^{\alpha} \right) \ . \tag{2.22}$$

Certain steps for this simplification are:

$$(h_p z)^{\alpha} / v_e = t \ . \tag{2.23}$$

$$G_{s,t}^{u,v}\left({}^{\alpha+a_1,...,\alpha+a_v,\alpha+a_{v+1},....,\alpha+a_s}_{\alpha+b_1,...,\alpha+b_u,\alpha+b_{u+1},....,\alpha+b_t} \middle| z \right) = z^{\alpha} G_{s,t}^{u,v}\left({}^{a_1,...,a_v,a_{v+1},....,a_s}_{b_1,...,b_u,b_{u+1},....,b_t} \middle| z \right) \ . \tag{2.24}$$

The CDF is obtained by integrating Eq. (2.17) and can be expressed as:

$$F_{Z_n}(z) = \frac{(2\pi)^{\frac{n-v_s}{2}} v_p}{\Gamma(\mu)(h_p z)^{\alpha_1}} G_{1,v_s+1}^{v_s,1}\left({}^{\frac{1}{v_1}+1}_{b,\frac{1}{v_1}} \middle| \frac{(h_p z)^u}{v_e} \right) \ , \tag{2.25}$$

where the ratios and the other terms have been defined earlier. Formula used for integration is [46]:

$$\int z^{\alpha-1} G_{s,t}^{u,v}\left({}^{a_1,...,a_v,a_{v+1},....,a_s}_{b_1,...,b_u,b_{u+1},....,b_t} \middle| zw \right) dz = z^{\alpha} G_{s+1,t+1}^{u,v+1}\left({}^{1-\alpha,a_1,...,a_v,a_{v+1},....,a_s}_{b_1,...,b_u,b_{u+1},....,b_t,-\alpha} \middle| zw \right) \ . \tag{2.26}$$

Similarly if $\alpha_1 = \alpha_2 = ... = \alpha_n = \alpha$, resulting in $p_j = q_j = 1$, where $j = 2, 3, ..., n$, v_p =1, v_1 =1, v_s =n, the CDF can be written in simplified form as (considering Eq. (2.23) and Eq. (2.24)):

$$F_{Z_n}(z) = \frac{1}{\Gamma(\mu)} G_{1,n+1}^{n,1}\left({}^{1}_{\mu_1,\mu_2,....,\mu_n,0} \middle| (h_p z)^{\alpha} \right) \ . \tag{2.27}$$

The derivations of these PDF and CDF expressions are necessary to achieve tractable closed form expressions. These expressions will enable to achieve performance analysis of our proposed system in terms of closed form expressions. Without these tractable expressions, further analysis of the proposed system would be difficult. One may argue that numerical analysis can be done for obtaining results but it takes lot of time in simulation due to high computational complexity. If closed form expressions are used, then

the nature of the results can be predicted by observing the expressions. For example, on observing the variations of Meijer G function, one can predict whether the system performance will improve or degrade with increase in signal-to-noise ratio value. The closed form tractable expressions will also help us in performing asymptotic analysis and calculating diversity and coding gain. Such concepts will be later explained in the chapter. Thus closed form expression analysis can be helpful to the wireless networking engineers for planning and optimizing a communication network without going into the tedious work of computing exact results for all cases.

2.2 Proposed System Model

Cascaded $\alpha - \mu$ channel model is used for further analysis. Fig. 2.1 depicts a simple 3 node bidirectional cooperative model, where the two mobile source nodes (MS1 and MS2) exchange information through a mobile relay node (MR) located in between the two source nodes. This is the proposed system model [50] for which further analysis is performed. All the nodes are spatially modulated full-duplex (SMFD) nodes. Let MS1 node has N_{S1} antennas while MS2 has N_{S2} antennas. The relay is equipped with N_R antennas. To combat the effect of self-interference, it is assumed that the nodes have independent RF chains for transmission and reception purpose. For this proposed system, data bits are exchanged among the two source nodes using PLNC at the relay employing DF technique. The relative gains [51, 52] of the corresponding links are expressed as $G_{S_1,R} = (\frac{d_{SD}}{d_{SR}})^{\tau}$, $G_{S_2,R} = (\frac{d_{SD}}{d_{RD}})^{\tau}$ where the relative gain of MS1 to MR link is denoted by $G_{S_1,R}$ while the relative gain of MR to MS2 link is denoted by $G_{S_2,R}$, τ is the coefficient of path loss, d_{SD}, d_{SR} and d_{RD} are the distances between MS1 and MS2, MS1 and MR, and MR and MS2 links respectively. Relative geometrical gain factor $\kappa_{rg} = \frac{G_{S_1,R}}{G_{S_2,R}}$ indicates the position of MR node as compared to the locations of MS1 and MS2 nodes. κ_{rg}, when expressed in dB, is negative if $d_{RD} < d_{SR}$ whereas κ_{rg} is positive in dB if $d_{RD} > d_{SR}$ and if both distances are equal, then κ_{rg} is 0 dB.

Let us assume for simplicity that there are 2 antennas at each source node. Thus $N_{S1} = N_{S2} = N_A = 2$. N_A is just a variable used for equal number of antennas at the source nodes. Analysis for different number of antennas at the nodes can also be done, as illustrated later. The transmit antenna which is made active for $N_A = 2$ is chosen as:

$$j_k = \begin{cases} 2, & \text{if } c_k^{LSB}[n] = 1 \\ 1, & \text{if } c_k^{LSB}[n] = 0 \end{cases}, \tag{2.28}$$

where n represents the n^{th} time slot and k indicates the source node which may be 1 or 2 in this case. $c_k[n]$ represents the bits which may be 0 or 1 for BPSK (Binary phase shift keying). The value of j_1

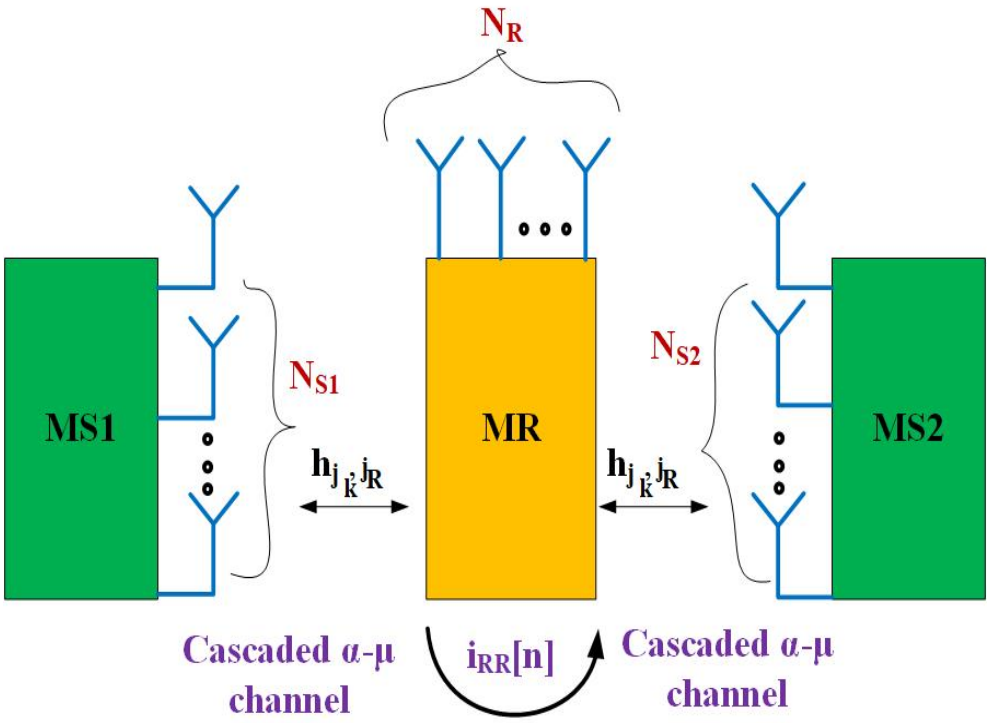

Figure 2.1: Proposed system model

basically indicates antenna index of MS1 while the value of j_2 denotes antenna index of MS2 node. If $N_A > 2$, then $\log_2 N_A$ number of bits (from LSB side) will be used for transmit antenna activation and remaining $\log_2 M$ message bits will be used for M-ary modulation scheme. Note that $N_A = 2^n$ where n is any integer and $n = 1, 2, 3, ..\infty$. It is pertinent to note that if number of antennas are variable at the source nodes, then the corresponding $\log_2(N_{S1})$ or $\log_2(N_{S2})$ number of bits from LSB side are chosen for antenna activation. BPSK modulation scheme is considered for our case. Both the sources transmit data to relay node simultaneously using BPSK as:

$$x_k^{MSB}[n] = 2c_k^{MSB}[n] - 1 \ , \tag{2.29}$$

where $k = 1,\ 2$. At the relay node, the signal received in n^{th} time slot at the j_R antenna is computed as:

$$y_R^{j_R}[n] = \sum_{k=1}^{2} \sqrt{P_k G_{S_k,R}}\ h_{j_k,j_R} x_k^{MSB}[n] + i_{RR}[n] + w_R[n] \ . \tag{2.30}$$

Suppose j_k is the selected transmit antenna from which message would be transmitted at the source node and j_R is the selected receive antenna at the relay node. Then h_{j_k,j_R} represents cascaded α-μ channel coefficients between the selected transmit and receive antenna at the source and relay nodes respectively. P_k indicates the power of transmission at the source nodes, k=1, 2. $w_R[n]$ represents complex Gaussian random noise with variance N_0 and a mean of zero at relay node MR. As the relay

node receives message from both the source nodes simultaneously, hence it suffers from self-interference indicated by $i_{RR}[n]$. The term is described as Gaussian random variable with zero mean and power $I_R = N_0[10^{\gamma_{loss}/10} - 1],\ \gamma_{loss} \geq 0$ where the SNR loss factor in dB is denoted by γ_{loss} [53]. The readers may note that interference effect at the relay can be mitigated by many interference mitigation techniques which is out of scope of this thesis, but can be considered in future research works. The parameters j_1, j_2, $x_1^{MSB}[n]$, and $x_2^{MSB}[n]$ are obtained by applying the principle of maximum likelihood (ML) detection [54], and can be estimated as $\hat{j_1}$, $\hat{j_2}$, $\hat{x}_1^{MSB}[n]$ and $\hat{x}_2^{MSB}[n]$ respectively, as shown below:

$$(\hat{j_1}, \hat{j_2}, \hat{x}_1^{MSB}[n], \hat{x}_2^{MSB}[n]) = \underset{(j_1, j_2, x_1^{MSB}[n], x_2^{MSB}[n])}{min} \left| y_R^{j_R}[n] - \sum_{k=1}^{2} \sqrt{P_k G_{S_k,R}} h_{j_k,j_R} x_k^{MSB}[n] \right|^2 . \quad (2.31)$$

The transmit antenna selection is done according to the formula $j_R = \hat{j_1} \oplus \hat{j_2}$. For bitwise XOR operation, the antenna index would be coded, for example in case of $N_A = 2$, antenna index 1 would be denoted by 0 and antenna index 2 would be denoted by 1. The encoded symbol forwarded by the relay to the source nodes is given by:

$$x_R^{MSB}[n] = \hat{x}_1^{MSB}[n] \oplus \hat{x}_2^{MSB}[n] \ . \quad (2.32)$$

The j_k antenna at k^{th} source node receives the signal given by:

$$y_k^{j_k}[n] = \sqrt{P_R G_{S_k,R}}\ h_{j_k,j_R} x_R^{MSB}[n] + i_{kk}[n] + w_k[n], \quad k = 1, 2 \ . \quad (2.33)$$

$w_k[n]$ represents complex Gaussian random noise with variance N_0 and a mean of zero at source node MS1 or MS2. The value of k determines the source node- if $k = 1$ then MS1 node is the source node, whereas if $k = 2$, then MS2 is the source node. The particular source node because of its full-duplex nature undergoes self-interference which is indicated by $i_{kk}[n]$. This term is described as Gaussian random variable with zero mean and power $I_k = N_0[10^{\gamma_{loss}/10} - 1],\ \gamma_{loss} \geq 0$ where the SNR loss factor in dB is denoted by γ_{loss}, as described earlier. It is assumed that the source nodes have knowledge about channel state information (CSI). Perfect channel state information is assumed in the analysis. But in practice, it may not be true. In general, pilot signals are transmitted to estimate the channels. A discussion on the channel estimation is out of the scope of the thesis. The parameters j_R, $x_R^{MSB}[n]$ are detected at the source nodes using ML method and can be estimated as $\hat{j}_R$ and $\hat{x}_R^{MSB}$ respectively.

$$(\hat{j_R}, \hat{x}_R^{MSB}[n]) = \underset{(j_R, x_R^{MSB}[n])}{min} \left| y_k^{j_k}[n] - \sqrt{P_R G_{S_k,R}} h_{j_k,j_R} x_R^{MSB}[n] \right|^2 . \quad (2.34)$$

The source nodes already have the values of j_k and $x_k^{MSB}[n]$ as they transmit the respective bits. Hence

the bits estimated at the k^{th} source node are denoted by $\hat{x}_k^{MSB}$ and $\hat{x}_k^{LSB}$. The estimated bits are obtained by the following equations:

$$\hat{x}_k^{LSB}[n] = \hat{j_R} \oplus j_k \quad k = 1, 2 \ , \tag{2.35}$$

$$\hat{x}_k^{MSB}[n] = \hat{x}_R^{MSB}[n] \oplus x_k^{MSB}[n], \quad k = 1, 2 \ . \tag{2.36}$$

2.3 Performance Analysis

The proposed system uses SM along with PLNC making exact outage probability analysis all the more difficult. The end-to-end PDF and CDF needs to be evaluated for exact analysis which is not tractable for cascaded $\alpha - \mu$ channel. Numerically the results can be obtained, but the absence of closed form expressions defeats the motive of mathematical analysis in understanding the system performance. This however can be considered as a scope for future work. Hence instead of exact expressions, analytical expressions of outage probability bounds will be derived in this section.

2.3.1 Lower Bound of Outage Probability

Assume $\eta_k = \frac{P_k}{N_0}$ (k=1, 2) be the source node SNR while $\eta_R = \frac{P_R}{N_0}$, be the SNR at mobile relay node. The j_R antenna of MR node will possess a signal-to-interference-plus-noise ratio (SINR) which can be evaluated as:

$$\gamma_{S_k,R}^{j_R} = \frac{\eta_k G_{S_k,R} \left(h_{j_k,j_R}\right)^2}{\frac{I_R}{N_0} + 1}, \quad k = 1, 2 \ . \tag{2.37}$$

The source node S_k will have a SINR at j_k antenna, which can be evaluated as:

$$\gamma_{R,S_k}^{j_k} = \frac{\eta_R G_{S_k,R} \left(h_{j_k,j_R}\right)^2}{\frac{I_R}{N_0} + 1}, \quad k = 1, 2 \ . \tag{2.38}$$

The outage probability of the SM based decode-and-forward two-way relay (DFTWR) system will be bounded at a lower level for a data rate of R_d bits/s which can be defined as:

$$\begin{aligned} P_{out}^{R\_LB}(R_d) \geq P[&\log_2(N_{S1}) + \log_2(N_{S2}) \\ &+ \log_2(1 + \min(\max(\gamma_{S_1,R}^1, \gamma_{S_1,R}^2, ..., \gamma_{S_1,R}^{N_{S1}}), \max(\gamma_{S_2,R}^1, \gamma_{S_2,R}^2, ..., \gamma_{S_2,R}^{N_{S2}}))) < R_d] \ , \end{aligned} \tag{2.39}$$

where $P(\cdot)$ represents the probability function. For simplifying the expression, we can assume $N_{S1} = N_{S2} = N_A$. Then the expression can be simplified as:

$$P_{out}^{R\_LB}(R_d) \geq P[2\log_2(N_A) + \log_2(1 + \min(\max(\gamma_{S_1,R}^1, \gamma_{S_1,R}^2, ..., \gamma_{S_1,R}^{N_A}), \max(\gamma_{S_2,R}^1, \gamma_{S_2,R}^2, ..., \gamma_{S_2,R}^{N_A}))) < R_d] \ . \tag{2.40}$$

The term $2\log_2(N_A)$ is used because of the capacity generated due to the spatial domain part [55]. Assuming there is no error in estimating the transmitting antenna, $\log_2(N_A)$ bits are used for activating the antenna and since the system is bidirectional the term is multiplied by 2. The detailed explanation for the inclusion of this term is given below.

We can write the mutual information of the system as [55]:

$$I(X, X_{ch}; Y) = I(X; Y|X_{ch}) + I(X_{ch}; Y) \ , \tag{2.41}$$

where $I(X; Y|X_{ch})$ denotes the mutual information between the modulation domain space and the output space, and $I(X_{ch}; Y)$ denotes the mutual information between the spatial domain space and the output space. Here one transmit source is activated which is determined by the source antenna symbol x_{ch}. x is the symbol emitted from the transmitted antenna and modulated by a conventional modulation scheme and y is the output. Thus $I(X; Y|X_{ch})$ is determined by the channel model and modulation scheme which is being used. To calculate the mutual information between spatial domain and output space, we take the help of upper bound as closed form expression is not available.

$$I(X_{ch}; Y) = H(Y) - H(Y|X_{ch}) \ , \tag{2.42}$$

where the entropy of the received signal, denoted by H(Y), has a tight upper bound as:

$$H(Y) \leq \frac{1}{N_A} \sum_{i=1}^{N_A} [\log_2 N_A + \log_2(\pi e \sigma_i^2)] \tag{2.43}$$

and the conditional entropy of the received signal, $H(Y|X_{ch})$ can be written as:

$$H(Y|X_{ch}) = -\frac{1}{N_A} \sum_{i=1}^{N_A} \int_0^\infty \frac{1}{\pi\sigma_i^2} \exp\left[-\frac{|y|^2}{\sigma_i^2}\right] \log_2 \left[\frac{1}{\pi\sigma_i^2} \exp\left[-\frac{|y|^2}{\sigma_i^2}\right]\right] dy = \frac{1}{N_A} \sum_{i=1}^{N_A} \log_2[\pi e \sigma_i^2] \ . \tag{2.44}$$

Putting Eq. (2.43) and Eq. (2.44) in Eq. (2.42), we obtain the upper bound of the spatial domain mutual information as:

$$I(X_{ch}; Y) \leq \log_2 N_A \ . \tag{2.45}$$

Capacity is the maximum amount of mutual information that can be transmitted over a given channel bandwidth. Thus the maximum value of mutual information (or capacity) is $\log_2 N_A$ as shown in the equation. This extra term generated from spatial domain capacity calculation has to be added to the capacity expression. Since our system operates in full-duplex bidirectional mode, twice of $\log_2 N_A$ i.e. $2\log_2 N_A$ will be added to the capacity expression as the value of spatial domain capacity. The SM

capacity is computed as the capacity of conventional modulation plus the capacity of the spatial domain [56, 57, 58]. The max-min criteria is used for selecting the optimum SINR for lower bound in this case [59, 60]. There are two broad techniques available in literature for selecting the optimum antenna or SNR for bidirectional multi-antenna relay system. These are transmit beamforming and max-min criteria [59]. However transmit beamforming requires exact knowledge of CSI to estimate the best beamforming. On the other hand, max-min technique does not require exact knowledge of CSI. Therefore, max-min technique is used in our analysis.

Thus for evaluating lower bound of outage probability at relay node, both the source-to-relay links have to be considered for first stage of transmission. Outage probability will be least when either of the source-to-relay link fails. Even if one link is working, then relay node will be able to receive information from one of the source nodes. Any of the link failure can be satisfied by the criteria of minimum of random variables. Now each source node has multiple antennas. Outage probability will only occur for a particular source-to-relay link when all the links from the antenna at a source node to the antenna at relay node fails. Even if one antenna at a source node is working, then message can be transmitted to the relay node. Hence when all the antennas fail, then outage probability occurs. The all link failure condition is satisfied by the maximum of multiple random variables criteria. Thus the max-min criteria is used in this case.

From Eq. (2.39), let us assume $\psi_R = \min(\max(\gamma^0_{S_1,R}, \gamma^1_{S_1,R}, ..., \gamma^{N_{S1}}_{S_1,R}), \max(\gamma^1_{S_2,R}, \gamma^2_{S_2,R}, ..., \gamma^{N_{S2}}_{S_2,R}))$ and $\gamma_{th} = 2^{R_d - \log_2(N_{S1}) - \log_2(N_{S2})} - 1$. Hence the lower bound of outage probability at the relay node can rewritten as:

$$P^{R\_LB}_{out}(\gamma_{th}) \geq P[\psi_R \leq \gamma_{th}] \ . \tag{2.46}$$

The CDF of ψ_R is written as:

$$F_{\psi_R}(\gamma_{th}) = P\left\{\min\left[\max(\gamma^1_{S_1,R}, \gamma^2_{S_1,R}, ..., \gamma^{N_{S1}}_{S_1,R}), \max(\gamma^1_{S_2,R}, \gamma^2_{S_2,R}, ..., \gamma^{N_{S2}}_{S_2,R})\right] \leq \gamma_{th}\right\} \ . \tag{2.47}$$

Before solving this expression further, let us understand two basic formulas given in Eq. (2.48) and (2.49). Let $Z = \min(X, Y)$ where X and Y are independent random variables. The CDF of random variable Z needs to be evaluated such that $P(Z \leq z)$. Thus $P(Z \leq z)$ is evaluated as:

$$\begin{aligned} P(\min\{X, Y\} \leq z) &= 1 - P(\min\{X, Y\} > z) \\ &= 1 - P(\{X > z\} \cap \{Y > z\}) \\ &= 1 - P(X > z) \cdot P(Y > z) \end{aligned}$$

$$= 1 - (1 - P(X \leq z))(1 - P(Y \leq z))$$
$$= 1 - (1 - F_X(z))(1 - F_Y(z)). \tag{2.48}$$

Now let $Z = \max(X, Y)$. Then the CDF of Z such that $P(Z \leq z)$ is calculated as:

$$\begin{aligned}
P(\max\{X, Y\} \leq z) &= P(X < Y \leq z) + P(Y < X \leq z) \\
&= \int_{x=-\infty}^{z} \int_{y=x}^{z} f_Y(y) f_X(x) dy dx + \int_{y=-\infty}^{z} \int_{x=y}^{z} f_Y(y) f_X(x) dx dy \\
&= \int_{y=-\infty}^{z} \int_{x=-\infty}^{y} f_Y(y) f_X(x) dx dy + \int_{y=-\infty}^{z} \int_{x=y}^{z} f_Y(y) f_X(x) dx dy \\
&= \int_{y=-\infty}^{z} f_Y(y) \left(\int_{x=-\infty}^{y} f_X(x) dx dy + \int_{x=y}^{z} f_X(x) dx \right) dy \\
&= \int_{y=-\infty}^{z} f_Y(y) \left(\int_{x=-\infty}^{z} f_X(x) dx dy \right) dy \\
&= F_Y(z) F_X(z).
\end{aligned} \tag{2.49}$$

The logic behind the minimum case is that $Z \leq z$ can be true when either $X \leq z$ and $Y \leq z$ holds valid. For maximum case, $Z \leq z$ holds true when both $X \leq z$ and $Y \leq z$ are true. This can be explained by the following equation:

$$F_{\min\{X,Y\}}(z) = P(X \leq z \ \cup \ Y \leq z) = F_X(x) + F_Y(z) - F_X(z) \cdot F_Y(z)$$
$$F_{\max\{X,Y\}}(z) = P(X \leq z \ \cap \ Y \leq z) = F_X(z) \cdot F_Y(z) \ . \tag{2.50}$$

We can write $P(Z \leq z) = F(z)$. Now using the relations given in Eq. (2.48) and (2.49), Eq. (2.47) can be simplified as:

$$\begin{aligned}
F_{\psi_R}(\gamma_{th}) &= 1 - P\left\{ \min\left[\max(\gamma^1_{S_1,R}, \gamma^2_{S_1,R}, ..., \gamma^{N_{S1}}_{S_1,R}), \max(\gamma^1_{S_2,R}, \gamma^2_{S_2,R}, ..., \gamma^{N_{S2}}_{S_2,R}) \right] > \gamma_{th} \right\} \\
&= 1 - P(\max(\gamma^1_{S_1,R}, \gamma^2_{S_1,R}, ..., \gamma^{N_{S1}}_{S_1,R}) > \gamma_{th}) P(\max(\gamma^1_{S_2,R}, \gamma^2_{S_2,R}, ..., \gamma^{N_{S2}}_{S_2,R}) > \gamma_{th}) \\
&= 1 - \left[\left\{ 1 - P(\max(\gamma^1_{S_1,R}, \gamma^2_{S_1,R}, ..., \gamma^{N_{S1}}_{S_1,R}) \leq \gamma_{th}) \right\} \left\{ 1 - P(\max(\gamma^1_{S_2,R}, \gamma^2_{S_2,R}, ..., \gamma^{N_{S2}}_{S_2,R}) \leq \gamma_{th}) \right\} \right] \\
&= 1 - \Big[\Big\{ 1 - P(\gamma^1_{S_1,R} \leq \gamma_{th}) P(\gamma^2_{S_1,R} \leq \gamma_{th}) ... P(\gamma^{N_{S1}}_{S_1,R} \leq \gamma_{th}) \Big\} \\
&\quad \Big\{ 1 - P(\gamma^1_{S_2,R} \leq \gamma_{th}) P(\gamma^2_{S_2,R} \leq \gamma_{th}) ... P(\gamma^{N_{S2}}_{S_2,R} \leq \gamma_{th}) \Big\} \Big] \\
&= 1 - (1 - F_{\gamma^1_{S_1,R}}(\gamma_{th}) F_{\gamma^2_{S_1,R}}(\gamma_{th}), ..., F_{\gamma^{N_{S1}}_{S_1,R}}(\gamma_{th}))(1 - F_{\gamma^1_{S_2,R}}(\gamma_{th}) F_{\gamma^2_{S_2,R}}(\gamma_{th}), ..., F_{\gamma^{N_{S2}}_{S_2,R}}(\gamma_{th})) \ .
\end{aligned} \tag{2.51}$$

Considering equal number of antennas at the source nodes, $N_{S1} = N_{S2} = N_A$, Eq. (2.51) can be further

simplified as:

$$F_{\psi_R}(\gamma_{th}) = 1 - \prod_{k=1}^{2}(1 - F_{\gamma^1_{S_k,R}}(\gamma_{th})F_{\gamma^2_{S_k,R}}(\gamma_{th}), ..., F_{\gamma^{N_A}_{S_k,R}}(\gamma_{th})) \ . \tag{2.52}$$

By referring to Eq. (2.37), the CDF of SINR can be computed as:

$$F_{\gamma^{j_R}_{S_k,R}}(\gamma_{th}) = P\left[\frac{\eta_k G_{S_k,R}(h_{j_k,j_R})^2}{\frac{I_R}{N_0}+1} \leq \gamma_{th}\right], \ j_R = 1, 2, ...N_R, \ k = 1, 2. \tag{2.53}$$

(h_{j_k,j_R}) follows cascaded α-μ distribution, as given in Eq. (2.17). Let $y = (h_{j_k,j_R})^2$. After taking into consideration the change of random variable (RV), the PDF of y is evaluated as [61]:

$$f_Y(y) = \frac{(2\pi)^{(\frac{N-v_s}{2})}uv_p}{2\Gamma(\mu){h_p}^{\alpha_1}y^{\frac{\alpha_1}{2}+1}}G^{v_s,0}_{0,v_s}\left(\begin{matrix}-\\ b\end{matrix}\middle|\frac{h_p^u y^{u/2}}{v_e}\right) . \tag{2.54}$$

The PDF is integrated to obtain the corresponding CDF which can be written as [61]:

$$F_Y(y) = \frac{(2\pi)^{(\frac{N-v_s}{2})}v_p}{\Gamma(\mu){h_p}^{\alpha_1}y^{\frac{\alpha_1}{2}}}G^{v_s,1}_{1,v_s+1}\left(\begin{matrix}\frac{1}{v_1}+1\\ b,\frac{1}{v_1}\end{matrix}\middle|\frac{h_p^u y^{u/2}}{v_e}\right) . \tag{2.55}$$

Using Eq. (2.37), Eq. (2.53) and Eq. (2.55) we can write:

$$F_{\gamma^{j_R}_{S_k,R}}(\gamma_{th}) = \frac{(2\pi)^{(\frac{N-v_s}{2})}v_p}{\Gamma(\mu){h_p}^{\alpha_1}(\gamma_{th}\gamma_{abs}/(\eta_k G_{S_k,R}))^{\frac{\alpha_1}{2}}}G^{v_s,1}_{1,v_s+1}\left(\begin{matrix}\frac{1}{v_1}+1\\ b,\frac{1}{v_1}\end{matrix}\middle|\frac{h_p^u(\gamma_{th}\gamma_{abs}/(\eta_k G_{S_k,R}))^{u/2}}{v_e}\right) , \tag{2.56}$$

where $\gamma_{abs} = 10^{\gamma_{loss}/10}$. The values obtained from Eq. (2.56) is put into Eq. (2.51) to compute $F_{\psi_R}(\gamma_{th})$. The next step is to evaluate the lower bound of outage probability at the source node for message transmission in the second time slot. Outage probability is the least when any of the antenna at relay node fails to transmit to the antenna at the source node. Any one of the link failure is satisfied by the minimum of random variables condition. Thus the source node S_k (k=1, 2) will have a lower bound of outage probability that can be computed as [60]:

$$P^{S_k}_{out}(R_d) \geq P[2\log_2(N_R) + \log_2(1 + \min(\gamma^1_{R,S_k}, \gamma^2_{R,S_k}, ..., \gamma^{N_R}_{R,S_k})) < R_d], \quad k = 1, 2 \ . \tag{2.57}$$

The $2\log_2(N_R)$ term is used due to spatial domain capacity calculation as explained earlier in Eq. (2.40). It is assumed that there is no error in estimating the transmitting antenna of relay node. Such an assumption is taken to achieve tractable closed form expressions. Assume $\psi_{S_k} = \min(\gamma^1_{R,S_k}, \gamma^2_{R,S_k}, ..., \gamma^{N_R}_{R,S_k})$. Thus the outage probability lower bound at the source node S_k can be expressed as:

$$P^{S_k}_{out}(\gamma_{th}) \geq P[\psi_{S_k} \leq \gamma_{th}], \quad k = 1, 2 \ , \tag{2.58}$$

where $\gamma_{th} = 2^{R_d - 2\log_2 N_R}$. The lower bound of outage probability at the source node is written as (with the help of the relation given in Eq. (2.48)):

$$\begin{aligned} F_{\psi_{S_k}}(\gamma_{th}) &= P\left\{\min(\gamma^1_{R,S_k}, \gamma^2_{R,S_k}, ..., \gamma^{N_R}_{R,S_k}) \leq \gamma_{th}\right\} \\ &= 1 - P\left\{\min(\gamma^1_{R,S_k}, \gamma^2_{R,S_k}, ..., \gamma^{N_R}_{R,S_k}) > \gamma_{th}\right\} \\ &= 1 - P(\gamma^1_{R,S_k} > \gamma_{th})P(\gamma^2_{R,S_k} > \gamma_{th})...P(\gamma^{N_R}_{R,S_k} > \gamma_{th}) \\ = 1 - \left[(1 - P\left\{\gamma^1_{R,S_k} \leq \gamma_{th}\right\})(1 - P\left\{\gamma^2_{R,S_k} \leq \gamma_{th}\right\})....(1 - P\left\{\gamma^{N_R}_{R,S_k} \leq \gamma_{th}\right\})\right] \\ &= 1 - \textstyle\prod_{j_k=1}^{N_R}(1 - F_{\gamma^{j_k}_{R,S_k}}(\gamma_{th})), \quad k = 1, 2\ . \end{aligned} \tag{2.59}$$

By referring to Eq. (2.38), the CDF of SINR can be computed as:

$$F_{\gamma^{j_k}_{R,S_k}}(\gamma_{th}) = P\left[\frac{\eta_R G_{S_k,R}(h_{j_k,j_R})^2}{\frac{I_R}{N_0} + 1} \leq \gamma_{th}\right],\ k = 1, 2, j_k = 0, 1, ..., N_{S1} \text{ or } N_{S2}\ . \tag{2.60}$$

(h_{j_k,j_R}) follows cascaded α-μ distribution, as given in Eq. (2.17). Let $y = (h_{j_k,j_R})^2$. After taking into consideration the change of random variable (RV), the PDF of y, can be written as shown in Eq. (2.54). Again using Eq. (2.38) and Eq. (2.55) we can write CDF of SINR as:

$$F_{\gamma^{j_k}_{R,S_k}}(\gamma_{th}) = \frac{(2\pi)^{(\frac{N-vs}{2})} v_p}{\Gamma(\mu) {h_p}^{\alpha_1} (\gamma_{th}\gamma_{abs}/(\eta_R G_{S_k,R}))^{\frac{\alpha_1}{2}}} G^{v_s,1}_{1,v_s+1}\left(\begin{matrix}\frac{1}{v_1}+1 \\ b, \frac{1}{v_1}\end{matrix}\middle| \frac{h_p^u(\gamma_{th}\gamma_{abs}/(\eta_R G_{S_k,R}))^{u/2}}{v_e}\right), \tag{2.61}$$

where depending upon the value of k, $G_{S_1,R}$ or $G_{S_2,R}$ is chosen. The values obtained from Eq. (2.61) is put into Eq. (2.59) to obtain $F_{\psi_{S_k}}(\gamma_{th})$. The total system outage probability can be computed by taking into account, the outage probabilities at the source and relay nodes. The terms obtained from Eq. (2.51) and Eq. (2.59) are used and the final lower bound of outage probability is expressed as:

$$\begin{aligned} P^{LB}_{out}(\gamma_{th}) &= P^{R\_LB}_{out}(\gamma_{th}) + (1 - P^{R\_LB}_{out}(\gamma_{th}))P^{S_k}_{out}(\gamma_{th}) \\ \geq 1 - (1 - F_{\gamma^1_{S_1,R}}(\gamma_{th})F_{\gamma^2_{S_1,R}}(\gamma_{th}), ..., F_{\gamma^{N_{S1}}_{S_1,R}}(\gamma_{th}))(1 - F_{\gamma^1_{S_2,R}}(\gamma_{th})F_{\gamma^2_{S_2,R}}(\gamma_{th}), ..., F_{\gamma^{N_{S2}}_{S_2,R}}(\gamma_{th})) \\ + \left[(1 - F_{\gamma^1_{S_1,R}}(\gamma_{th})F_{\gamma^2_{S_1,R}}(\gamma_{th}), ..., F_{\gamma^{N_{S1}}_{S_1,R}}(\gamma_{th}))(1 - F_{\gamma^1_{S_2,R}}(\gamma_{th})F_{\gamma^2_{S_2,R}}(\gamma_{th}), ..., F_{\gamma^{N_{S2}}_{S_2,R}}(\gamma_{th}))\right] \\ \times \left[1 - \textstyle\prod_{j_k=1}^{N_R}(1 - F_{\gamma^{j_k}_{R,S_k}}(\gamma_{th}))\right]\ . \end{aligned} \tag{2.62}$$

Now to simplify the expression for easier analysis, let us assume that $N_{S1} = N_{S2} = N_R = N_A$. After this assumption, the overall lower bound of outage probability can be simplified as:

$$P^{LB}_{out}(\gamma_{th}) \geq 1 - \left[\prod_{k=1}^{2}(1 - F_{\gamma^1_{S_k,R}}(\gamma_{th})F_{\gamma^2_{S_k,R}}(\gamma_{th}), ..., F_{\gamma^{N_A}_{S_k,R}}(\gamma_{th}))\right] \times \left[\prod_{j_k=1}^{N_A}(1 - F_{\gamma^{j_k}_{R,S_k}}(\gamma_{th}))\right]\ . \tag{2.63}$$

The total transmission includes two phases. The source nodes transmit message to the relay in the

first phase, for which the term $P_{out}^{R\_LB}(\gamma_{th})$ defines the outage probability of the first phase. The relay broadcasts the message to both the source nodes in the second phase. The second term in Eq. (2.62) given by $(1 - P_{out}^{R\_LB}(\gamma_{th}))P_{out}^{S_k}(\gamma_{th})$ yields the outage probability for this phase. The individual outage probability terms need to be studied to understand the nature of the system.

In Eq. (2.63), we can observe that the term $F_{\gamma_{R,S_k}^{j_k}}(\gamma_{th})$ does not vary with SNR if η_R is kept fixed. If η_R is varied, then the Meijer G term decreases with an increase in η_R and the resultant term when subtracted from 1 causes an increment in the value. The outage probability mainly depends on the term $F_{\gamma_{S_k,R}^{j_R}}(\gamma_{th})$. This term contains the Meijer G function, as can be seen from Eq. (2.56), which depends on the SNR η_k. As SNR increases, the Meijer G function decreases resulting in a decrease in value of the overall term $F_{\gamma_{S_k,R}^{j_R}}(\gamma_{th})$. Hence the product of such terms also decreases. The subtraction of the resulting product term from 1 gives an increase in the result and the overall incremented term is again subtracted from 1, thereby causing an overall decrease in the outage probability value with increase in SNR. Thus this variation of outage probability with respect to SNR can be easily studied from the closed form expressions, which highlights the importance of derivation of closed form expressions.

2.3.2 Upper Bound of Outage Probability

The upper bound of outage probability is also derived in two steps by calculating the upper bounds of outage probability at the relay and source nodes. Now for the first stage, the SM based DFTWR system will have its outage probability bounded at an upper level for a data rate of R_d bit/s which can be defined as:

$$P_{out}^{R\_UB}(R_d) \leq P[\log_2(N_{S1})+\log_2(N_{S2})+\log_2(1+\min(\gamma_{S_1,R}^1, \gamma_{S_1,R}^2, ..., \gamma_{S_1,R}^{N_{S1}}, \gamma_{S_2,R}^1, \gamma_{S_2,R}^2, ..., \gamma_{S_2,R}^{N_{S2}})) < R_d] \,. \tag{2.64}$$

The other steps would remain the same as that of lower bound computation. It is considered that $\log_2(N_{S1})$ and $\log_2(N_{S2})$ bits are required for activating a particular antenna at the two source nodes. For upper bound, the error has to be maximum meaning the weakest link has to be chosen. Therefore, the weakest link and the weakest SINR at each source node is chosen by computing the minimum SINR. When either of the source-to-relay node link fails or when any one of the links between any antenna at the source node and an antenna at the relay node fails, outage probability is maximum. Hence this condition is satisfied by minimum of all random variables. The minimum SINR among all the SINRs of the available source-to-relay links for both MS1 and MS2 source nodes is selected.
Assume $\psi_{S_k} = \min(\gamma_{S_1,R}^1, \gamma_{S_1,R}^2, ..., \gamma_{S_1,R}^{N_{S1}}, \gamma_{S_2,R}^1, \gamma_{S_2,R}^2, ..., \gamma_{S_2,R}^{N_{S2}})$ and $\gamma_{th} = 2^{R_d - \log_2(N_{S1}) - \log_2(N_{S2})} - 1$. The

upper bound of outage probability at the relay node is given by (using the relation in Eq. (2.48)):

$$\begin{aligned}
P_{out}^{R_UB}(\gamma_{th}) &\leq F_{\psi_{S_k}}(\gamma_{th}) \\
&= P\left\{\min(\gamma_{S_1,R}^1, \gamma_{S_1,R}^2, ..., \gamma_{S_1,R}^{N_{S1}}, \gamma_{S_2,R}^1, \gamma_{S_2,R}^2, ..., \gamma_{S_2,R}^{N_{S2}}) \leq \gamma_{th}\right\} \\
&= 1 - P\left\{\min(\gamma_{S_1,R}^1, \gamma_{S_1,R}^2, ..., \gamma_{S_1,R}^{N_{S1}}, \gamma_{S_2,R}^1, \gamma_{S_2,R}^2, ..., \gamma_{S_2,R}^{N_{S2}}) > \gamma_{th}\right\} \\
&= 1 - P(\gamma_{S_1,R}^1 > \gamma_{th})P(\gamma_{S_1,R}^2 > \gamma_{th})...P(\gamma_{S_1,R}^{N_{S1}} > \gamma_{th})P(\gamma_{S_2,R}^1 > \gamma_{th})P(\gamma_{S_2,R}^2 > \gamma_{th})...P(\gamma_{S_2,R}^{N_{S2}} > \gamma_{th}) \\
&= 1 - \left(\left(1 - P(\gamma_{S_1,R}^1 \leq \gamma_{th})\right)\left(1 - P(\gamma_{S_1,R}^2 \leq \gamma_{th})\right)...\left(1 - P(\gamma_{S_1,R}^{N_{S1}} \leq \gamma_{th})\right)\right. \\
&\quad \left.\times \left(1 - P(\gamma_{S_2,R}^1 \leq \gamma_{th})\right)\left(1 - P(\gamma_{S_2,R}^2 \leq \gamma_{th})\right)...\left(1 - P(\gamma_{S_2,R}^{N_{S2}} \leq \gamma_{th})\right)\right) \\
&= 1 - (\prod_{j_k=1}^{N_{S1}}(1 - F_{\gamma_{S_1,R}^{j_k}}(\gamma_{th})))(\prod_{j_k=1}^{N_{S2}}(1 - F_{\gamma_{S_2,R}^{j_k}}(\gamma_{th}))) \ ,
\end{aligned} \tag{2.65}$$

where $F_{\gamma_{S_k,R}^{j_k}}(\gamma_{th})$ is defined earlier. Therefore the total outage probability upper bound, after using the terms from Eq. (2.65) and Eq. (2.59), can be defined as:

$$\begin{aligned}
P_{out}^{UB}(\gamma_{th}) &= P_{out}^{R_UB}(\gamma_{th}) + (1 - P_{out}^{R_UB}(\gamma_{th}))P_{out}^{S_k}(\gamma_{th}) \\
&\leq 1 - (\prod_{j=1}^{N_{S1}}(1 - F_{\gamma_{S_1,R}^{j}}(\gamma_{th})))(\prod_{j=1}^{N_{S2}}(1 - F_{\gamma_{S_2,R}^{j}}(\gamma_{th}))) \\
&+ \left[(\prod_{j_k=1}^{N_{S1}}(1 - F_{\gamma_{S_1,R}^{j_k}}(\gamma_{th})))(\prod_{j_k=1}^{N_{S2}}(1 - F_{\gamma_{S_2,R}^{j_k}}(\gamma_{th})))\right]\left[1 - \prod_{j_R=1}^{N_R}(1 - F_{\gamma_{R,S_k}^{j_R}}(\gamma_{th}))\right] \ ,
\end{aligned} \tag{2.66}$$

where the term $F_{\gamma_{R,S_k}^{j_R}}(\gamma_{th})$ has been derived earlier. Again to simplify the above equation, let us assume $N_{S1} = N_{S2} = N_A$ i.e. equal number of antennas at the source nodes. Thus the simplified equation can be written as:

$$P_{out}^{UB}(\gamma_{th}) \leq 1 - \left[\prod_{k=1}^{2}(\prod_{j_k=1}^{N_A}(1 - F_{\gamma_{S_k,R}^{j_k}}(\gamma_{th})))\right]\left[\prod_{j_R=1}^{N_A}(1 - F_{\gamma_{R,S_k}^{j_R}}(\gamma_{th}))\right] \ . \tag{2.67}$$

During the first phase, message is transmitted by the source nodes to the relay and the term $P_{out}^{R\_UB}(\gamma_{th})$ defines the outage probability for this phase. The second phase is the broadcasting stage from the relay. The second term in Eq. (2.66) given by $(1 - P_{out}^{R\_UB}(\gamma_{th}))P_{out}^{S_k}(\gamma_{th})$ yields the outage probability for this phase. In Eq. (2.67), we can observe that the term $F_{\gamma_{R,S_k}^{j_R}}(\gamma_{th})$ does not vary with SNR as η_R is generally kept fixed. However if η_R is varied, the Meijer G component decreases with increase in SNR resulting in increment in value when the CDF term is subtracted from 1 and multiplied. The term $F_{\gamma_{S_k,R}^{j_k}}(\gamma_{th})$ contains the Meijer G function, as can be seen from Eq. (2.56), which depends on the SNR η_k. As SNR increases, the Meijer G function decreases resulting in a decrease in value of the overall term $F_{\gamma_{S_k,R}^{j_k}}(\gamma_{th})$. The subtraction of this CDF term from 1 will result in an increment and the product of such (1- CDF) terms will result in more increment. However, the final product value is subtracted from 1 to give a large

decrement. Thus it causes an overall decrease in the outage probability value with increase in SNR.

2.3.3 Asymptotic Analysis of Outage Probability Bounds

First we perform asymptotic analysis for lower bounds on outage probability. For this the Meijer G function terms needs to be analyzed. Considering lower bounds on outage probability, the argument in Meijer G function in Eq. (2.56) is first inverted using Eq. (6.2.2) in [62] and the expression is written as:

$$F_{S_k,R}^{asym}(\gamma_{th}) \approx \frac{(2\pi)^{(\frac{N-v_s}{2})} v_p}{\Gamma(\mu) {h_p}^{\alpha_1} (\gamma_{th}\gamma_{abs}/(\eta_k G_{S_k,R}))^{\frac{\alpha_1}{2}}} G_{v_s+1,1}^{1,v_s}\left(\begin{matrix} 1-b, 1-\frac{1}{v_1} \\ -\frac{1}{v_1} \end{matrix} \middle| \frac{v_e}{h_p^u(\gamma_{th}\gamma_{abs}/(\eta_k G_{S_k,R}))^{u/2}} \right). \quad (2.68)$$

Let $z = \frac{v_e}{h_p^u(\gamma_{th}\gamma_{abs}/(\eta_k G_{S_k,R}))^{u/2}}$. Then the Meijer G function at very high values of its argument can be written (with the help of Eq. (41) in [63]) as:

$$\lim_{z\to\infty^+} G_{p,q}^{m,n}\left(\begin{matrix} a_1,....,a_n,...a_p \\ b_1,...,b_m,...b_q \end{matrix} \middle| z \right) = \sum_{k=1}^{n} z^{a_k-1} \times \frac{\prod_{l=1;l\neq k}^{n} \Gamma(a_k-a_l) \prod_{l=1}^{m} \Gamma(1+b_l-a_k)}{\prod_{l=n+1}^{p} \Gamma(1+a_l-a_k) \prod_{l=m+1}^{q} \Gamma(a_k-b_l)}, \quad (2.69)$$

where $a_k - a_l \neq 0, \pm 1, \pm 2, ...; (k, l = 1, ..., n; k \neq l)$ and $a_k - b_l \neq 1, 2, 3, ...; (k = 1, ..., n; l = 1, ..., m)$. Thus the overall asymptotic expression for our CDF function can be written as:

$$F_{S_k,R}^{asym}(\gamma_{th}) \approx \frac{(2\pi)^{(\frac{N-v_s}{2})} v_p}{\Gamma(\mu) {h_p}^{\alpha_1} (\gamma_{th}\gamma_{abs}/(\eta_k G_{S_k,R}))^{\frac{\alpha_1}{2}}} \sum_{m=1}^{v_s} z^{c_m-1} \frac{\prod_{l=1,l\neq m}^{v_s} \Gamma(c_m - c_l) \prod_{l=1}^{1} \Gamma(1 + d_l - c_m)}{\prod_{l=v_s+1}^{v_s+1} \Gamma(1 + c_l - c_m)}, \quad (2.70)$$

where $c = [1-b, 1-\frac{1}{v_1}]$ and $d = [-\frac{1}{v_1}]$. Next the Meijer G argument in Eq. (2.61) is inverted to obtain:

$$F_{R,S_k}^{asym}(\gamma_{th}) \approx \frac{(2\pi)^{(\frac{N-vs}{2})} v_p}{\Gamma(\mu) {h_p}^{\alpha_1} (\gamma_{th}\gamma_{abs}/(\eta_R G_{S_k,R}))^{\frac{\alpha_1}{2}}} G_{v_s+1,1}^{1,v_s}\left(\begin{matrix} 1-b, 1-\frac{1}{v_1} \\ -\frac{1}{v_1} \end{matrix} \middle| \frac{v_e}{h_p^u(\gamma_{th}\gamma_{abs}/(\eta_R G_{S_k,R}))^{u/2}} \right). \quad (2.71)$$

Let $z = \frac{v_e}{h_p^u(\gamma_{th}\gamma_{abs}/(\eta_R G_{S_k,R}))^{u/2}}$. Then the Meijer G function at very high values of its argument can be written as described in Eq. (41) in [63]. Hence the overall asymptotic expression is written as:

$$F_{R,S_k}^{asym}(\gamma_{th}) \approx \frac{(2\pi)^{(\frac{N-v_s}{2})} v_p}{\Gamma(\mu) {h_p}^{\alpha_1} (\gamma_{th}\gamma_{abs}/(\eta_R G_{S_k,R}))^{\frac{\alpha_1}{2}}} \sum_{m=1}^{v_s} z^{c_m-1} \frac{\prod_{l=1,l\neq m}^{v_s} \Gamma(c_m - c_l) \prod_{l=1}^{1} \Gamma(1 + d_l - c_m)}{\prod_{l=v_s+1}^{v_s+1} \Gamma(1 + c_l - c_m)}, \quad (2.72)$$

where $c = [1-b, 1-\frac{1}{v_1}]$ and $d = [-\frac{1}{v_1}]$. The asymptotic CDF values from Eq. (2.70) and (2.72) are inserted into Eq. (2.62) to obtain the final asymptotic value for lower bound of outage probability. A similar analysis is conducted for asymptotic analysis of upper bound of outage probability. The asymptotic CDF values from Eq. (2.70) and (2.72) are inserted into Eq. (2.66) to obtain the final asymptotic value for upper bound of outage probability.

Now coding gain and diversity gain can be calculated from asymptotic expressions and graphs. In the graph, coding gain is defined as the horizontal shift between the two curves while diversity gain is

defined as the slope of the outage probability curve with respect to SNR at very high values of SNR on a log-log scale. The coding and diversity gain can be analytically calculated as:

$$\lim_{SNR\to\infty} P_{out}(SNR) \approx (C_g SNR)^{-D_g} \ , \tag{2.73}$$

where C_g and D_g are the coding and diversity gains respectively. $P_{out}(\cdot)$ is the outage probability expression. The calculation of coding and diversity gain of our system is a tricky one because of the presence of multiple Meijer G functions. This is where the asymptotic expressions in tractable form comes into play. The outage probability expression of our proposed system is a complex one, hence we will analyze the diversity and coding gain of a single Meijer G function initially and then expand it for the entire expression. From Eq. (2.70) and (2.72), the SNR term variation is studied which is basically variation of η_k and η_R. On writing those two equations in the form of Eq. (2.73), diversity gain is $D_g = -\left(\frac{u}{2}(\min(c)-1)+\frac{\alpha_1}{2}\right)$. It is pertinent to note that the diversity gain will be determined by the negative component of the highest exponent of SNR. Hence the minimum value of c vector is considered. It is interesting to note that the diversity gain depends on the channel parameters. The variables for channel parameters have already been defined earlier. Let us calculate the diversity gain for a cascaded $\alpha-\mu$ channel where only two components are present i.e. $N=2$ and the remaining parameter values are $\mu_1=\mu_2=1, \alpha_1=2, p_1=p_2=q_1=q_2=1, u=\alpha_1 v_1=2, c=[-1,-1,0], N_{S1}=N_{S2}=N_R=2, \eta_k=\eta_R$. Then diversity gain will be 1.

The coding gain will be a complex expression also due to the nature of the Meijer G product terms. Using Eq. (2.70), (2.72) and (2.73), the coding gain of a single Meijer G term can be written as:

$$C_g^{part} = \left(\frac{(2\pi)^{\left(\frac{N-v_s}{2}\right)} v_p}{\Gamma(\mu) {h_p}^{\alpha_1} \left(\frac{\gamma_{th}\gamma_{abs}}{(G_{S_k,R})}\right)^{\frac{\alpha_1}{2}}} \sum_{m=1}^{v_s} \left(\frac{v_e}{h_p^u (\gamma_{th}\gamma_{abs}/(G_{S_k,R}))^{u/2}} \right)^{c_m-1} \times \frac{\prod_{l=1,l\neq m}^{v_s} \Gamma(c_m-c_l) \prod_{l=1}^{1} \Gamma(1+d_l-c_m)}{\prod_{l=v_s+1}^{v_s+1} \Gamma(1+c_l-c_m)} \right)^{\frac{1}{\left(\frac{u}{2}(\min(c)-1)+\frac{\alpha_1}{2}\right)}} . \tag{2.74}$$

Due to the product of Meijer G terms in the final lower bound outage probability expression, the corresponding coding gains will be raised to the power equivalent to the number of antennas and the resultant coding gain can be written as:

$$C_g^{low} = (C_g^{part})^{N_{S1}} (C_g^{part})^{N_{S2}} (C_g^{part})^{N_R} \ . \tag{2.75}$$

Please note that both lower and upper bounds of outage probability will have same diversity gains and coding gains. This is because the maximum exponent of SNR is considered while calculating the gains.

The exact expression is irrelevant, the nature of the expressions suggest that both the lower and upper bounds contain the same number of product of Meijer G terms.

2.3.4 Average Data Rate

The average data rate for this proposed system is computed and compared with other existing models. Amplify-and-forward two-way relaying (AFTWR), amplify-and-forward one-way relaying (AFOWR) and PLNC are the methods available in literature. Average data rate of the proposed system deploying DF relaying technique can be written as:

$$\bar{R} = \mathbb{E}[\log_2(N_{S1}) + \log_2(N_{S2}) + \log_2(1 + \min(\max(\gamma^1_{S_1,R}, \gamma^2_{S_1,R}, ..., \gamma^{N_{S1}}_{S_1,R}), \max(\gamma^1_{S_2,R}, \gamma^2_{S_2,R}, ..., \gamma^{N_{S2}}_{S_2,R})))] \ , \tag{2.76}$$

where $\mathbb{E}[\cdot]$ denotes expectation. All the terms have been explained while deriving lower bound expression.

In AFTWR, the system performance is worse than AFOWR due to the presence of self-interference because in AFTWR, the source and relay nodes transmit and receive messages simultaneously, but in case of AFOWR, only the relay operates in full-duplex mode. The average date rates of the systems are defined in [64].

2.4 Results and Discussion

In this section, bounds on outage probability are analytically calculated for various system parameters and the results are validated by Monte Carlo simulations. All the nodes are assumed to have 2 antennas i.e. $N_{S1} = N_{S2} = N_R = N_A = 2$. This assumption is just for the sake of easier analysis. All the analysis holds true for variable number of antennas as well. We will investigate the possibility of variable number of antennas in the later part of this section as well. The parameters considered are $\gamma_{loss} = 0\ dB$, number of cascaded components ($N = 2$), ratio of p and q is 1, and $\kappa_{rg} = 0\ dB$ for all cases unless explicitly specified. Please note that the ratio of p and q integers are part of the channel parameters as defined earlier while explaining cascaded $\alpha - \mu$ channel.

The proposed system is investigated according to performance metric of outage probability and comparison is done with the methods existing in literature by evaluating all the lower bounds. It is evident from Fig. 2.2 that outage probability value is least for SM based DFTWR (SM-DFTWR) followed by AFOWR, PLNC and AFTWR. It is clearly evident that the simulation results follow a tight lower bound for the proposed method, thereby validating our analysis. The parameters used for comparison are $\gamma_{loss} = 0\ dB$ and $N = 2$ while $\eta_R = \eta_k$ (implying SNR at all nodes are equal).

The different SNR values required to achieve certain target outage probability values for different methods are tabulated in Table 2.1. Three different target outage probability values are chosen as 0.1,

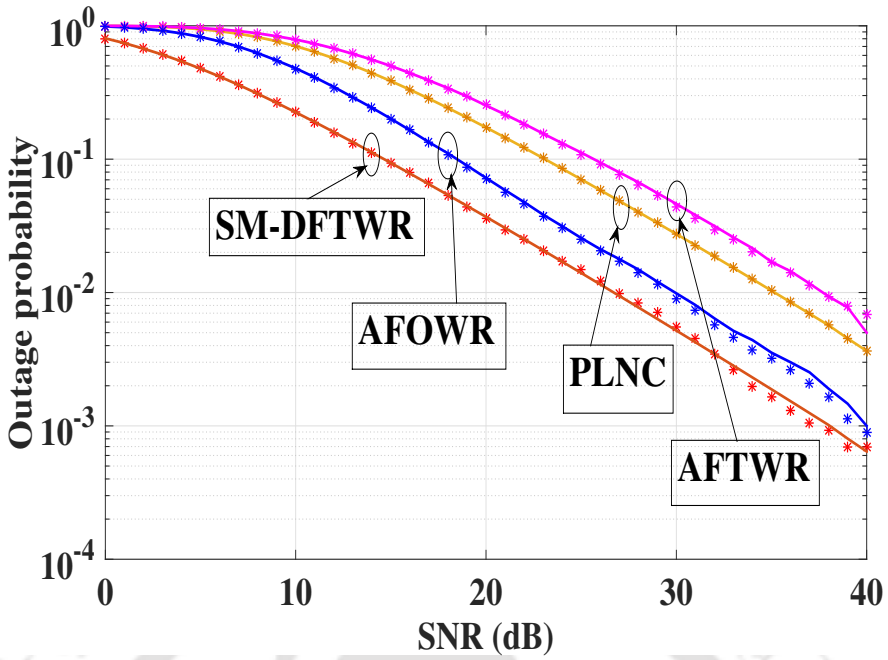

Figure 2.2: Outage probability analysis of the proposed and existing systems
(Solid line represents analytical results while $*$ sign indicates simulation results).

0.05 and 0.03. It is evident from the table that least SNR value is required to achieve the target outage value for our proposed method (SM based DFTWR). For example in case of 0.1 outage value, SM based DFTWR requires 14 dB of SNR while PLNC requires 23 dB. As the outage value decreases, the gain in SNR for our proposed method is much more which is beneficial. This is due to the fact that extra bits are used for activating the transmitting antenna thereby causing only one antenna to be active at a time which reduces the inter-antenna interference. The SNR gain over PLNC is 8 dB, while it is 3 dB over AFOWR for outage probability value of 0.03. Another interpretation of the result is that PLNC operates with simultaneous functioning of all antennas, while SM based DFTWR activates only one antenna. The operation of multiple antennas in PLNC leads to more inter-antenna interference causing degradation of system performance.

Table 2.1: Comparison of lower bounds of outage probability of different techniques.

P_{out}	SNR for various techniques (in dB)			
	SM-DFTWR	AFOWR	PLNC	AFTWR
0.1	14	18	23	25
0.05	18	21	26	29
0.03	21	24	29	32

The upper bounds on outage probability of the new method and PLNC are compared in Fig. 2.3 analytically. For both γ_{loss}=0 dB and γ_{loss}=3 dB, the SM based DFTWR system shows improvement

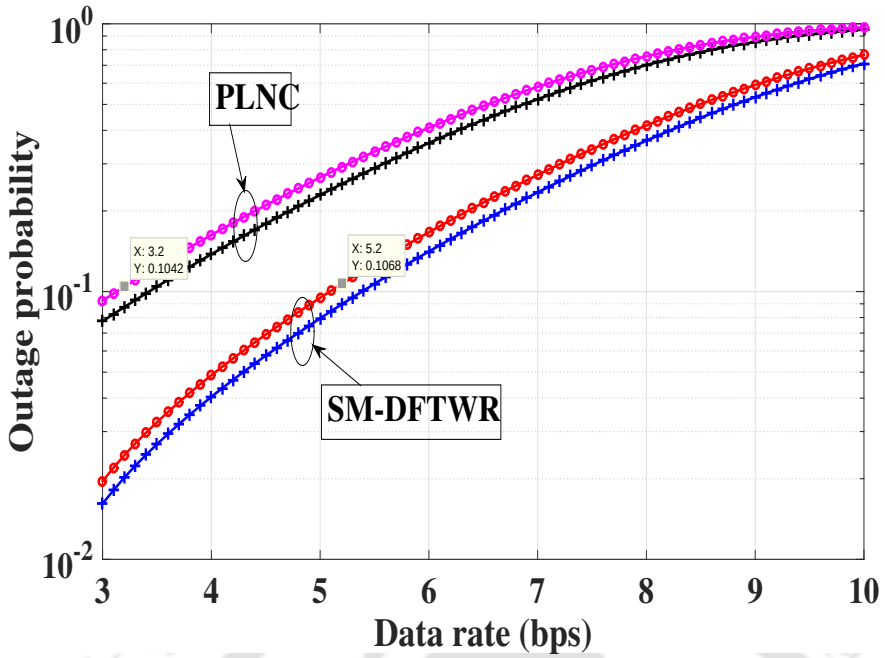

Figure 2.3: Upper bound on outage performance comparison between the proposed system and the existing PLNC system in terms of data rate
(+ sign indicates γ_{loss}=0 dB while • sign indicates γ_{loss}=3 dB).

in performance. $N = 2$ and $\eta_R = 40\ dB$ are considered for this case. The data rate of PLNC is exceeded by the data rate of the proposed system by a value of 2. This is attributed to the extra bits which are required for antenna activation, which in our case is 1. The increment factor will be 2 since communication is full-duplex in nature. This can be illustrated with an example. For γ_{loss}=3 dB and outage probability value of 0.1, PLNC has a data rate of 3.2 bps while SM based DFTWR has a data rate of 5.2 bps.

For different SNR loss factors, γ_{loss}=0 dB, γ_{loss}=3 dB and $\gamma_{loss} = 7dB$, the lower bounds on outage probabilities are shown in Fig. 2.4. The target data rate is 3 bps and the SNR at relay node and source nodes are assumed to be equal. $N = 2$ is considered for this case. The SNR loss factor increment causes the system performance to degrade due to the enhancement in inter-antenna interference, as is evident from the graph. For example, for $\gamma_{loss} = 0\ dB$ and outage probability value of 0.01, SNR required is 26 dB while, for $\gamma_{loss} = 3\ dB$, SNR required is 27 dB and for $\gamma_{loss} = 7\ dB$, SNR required is 30 dB. We can notice that outage probability value increases with an increment in SNR loss factor. As SNR loss factor increases, the relay is unable to decode message properly in the first time slot. Hence in the second time slot, the relay node is incapable of effective transmission of message to the source nodes. The performance of relay node in second time slot mainly governs the system performance, hence the overall performance is affected if relay node is unable to function properly due to presence of high amount of self-interference.

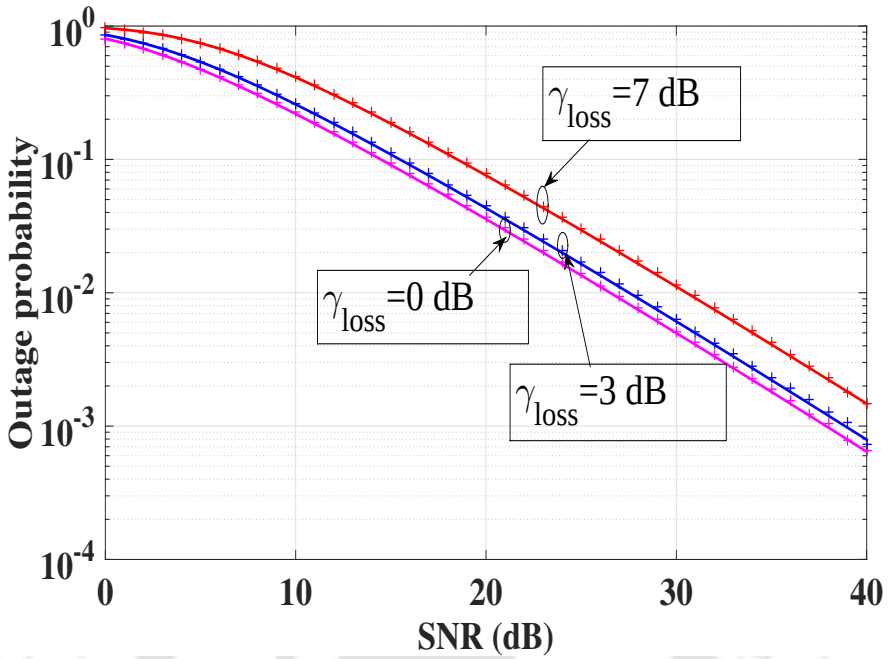

Figure 2.4: Lower bound of outage performance of the system with γ_{loss}=0 dB, γ_{loss}=3 dB and γ_{loss}=7 dB
(Solid line represents analytical results while + sign indicates simulation results).

The lower bounds on outage probability are plotted for various channel parameters like N, μ, κ_{rg} and α where the parameters have been defined earlier. The impact on lower bounds of outage probability by varying N, μ and α is depicted in Fig. 2.5, Fig. 2.6 and Fig. 2.7 respectively. Relative geometrical gain (κ_{rg}) also influences the system performance, as is illustrated in Fig. 2.8. All the nodes are assumed to have same SNR values, while $\gamma_{loss} = 0\ dB$ and r=1 values are considered for all the cases. For Fig. 2.5 the parameters are taken as data rate (R_d)=3 bps, α_1=2, μ=1 and κ_{rg}=0 dB for all links. For Fig. 2.6, where variation of fading parameter (μ) is analyzed, the values are taken as R_d=3 bps, α_1=2, N=2 and κ_{rg}=0 dB. For comparison of κ_{rg} values, the remaining parameters are taken as R_d=3 bps, μ=1, N=2 and α_1=2. In Fig. 2.7, the parameters are R_d=3 bps, μ=1, κ_{rg}=0 dB and N=2. It can be noticed from Fig. 2.5 that with an increment in the value of number of cascaded components (N), there is an increment in lower bound on outage probability value resulting in degradation of system performance. This is attributed to the fact that increment of N factor results in more fading. The system performance is improved by an increment in μ value as illustrated in Fig. 2.6. Increment in value of α_1 also improves the system performance, as can be visualized in Fig. 2.7. Impact of variation in relay position is illustrated in Fig. 2.8. From the graph it is evident that κ_{rg}=0 dB provides the optimum performance. κ_{rg} is varied between 0 dB to 30 dB with increments of 10 dB i.e. relay is brought much closer to MS1. Performance gradually worsens with increase in κ_{rg} value. This is because as the relay node is brought closer to MS1, it is not able to receive message properly from MS2 leading to degradation

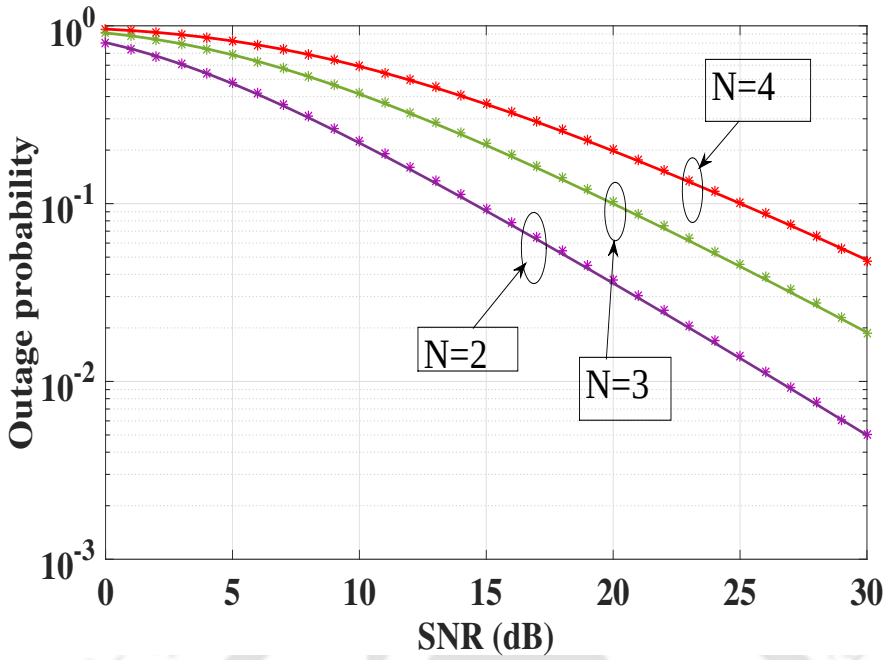

Figure 2.5: The impact of N on lower bound of outage performance
(Solid line represents analytical results while $*$ sign indicates simulation results).

of system performance. From the results, it can be inferred that the system can yield good performance even when the number of multipath clusters and non-linearity factor are quite high. This validates that the channel model used is suitable for such communication in a high scattering environment. It is to be noted that asymptotic analysis has been included in Fig. 2.6 and 2.7. The asymptotic values in both the figures for different values of μ and α_1 converge to the analytical and simulation results at higher values of SNR, thereby validating our analysis. The asymptotic analysis can be obtained in a similar manner for other graphs also, but has not been included to avoid the graphs from getting too clumsy.

The outage probability lower bound is compared for different values of data rates in Fig. 2.9. The values are taken as α_1=2, N=2, κ_{rg}=0 dB, $\eta_R = 40\ dB$, $\gamma_{loss} = 0\ dB$ and μ=1 for all links. As the target data rate value increases, the system performance worsens with the increment in outage probability value. This is due to the fact that it is difficult to achieve higher target data rates and may cause more errors.

The influence of different number of antennas at source and relay node is explored in Fig. 2.10. It is to be noted that number of antenna at any node can only be a power of 2 for SM. Five configurations of antenna are considered in this figure. It is evident that when the equal number of antennas is increased from 2 to 4 and 8, the system performance degrades. This is due to the fact that more antenna gives rise to more interference thereby causing poorer performance. It is also noted that when number of antennas at source node are 4 and only 2 antennas are present at the relay node, then the system performance is almost similar to that of a system having 2 antennas at all the source nodes. Again it can be observed that the performance of a system having 4 antennas at the relay node and 2 antennas at each source

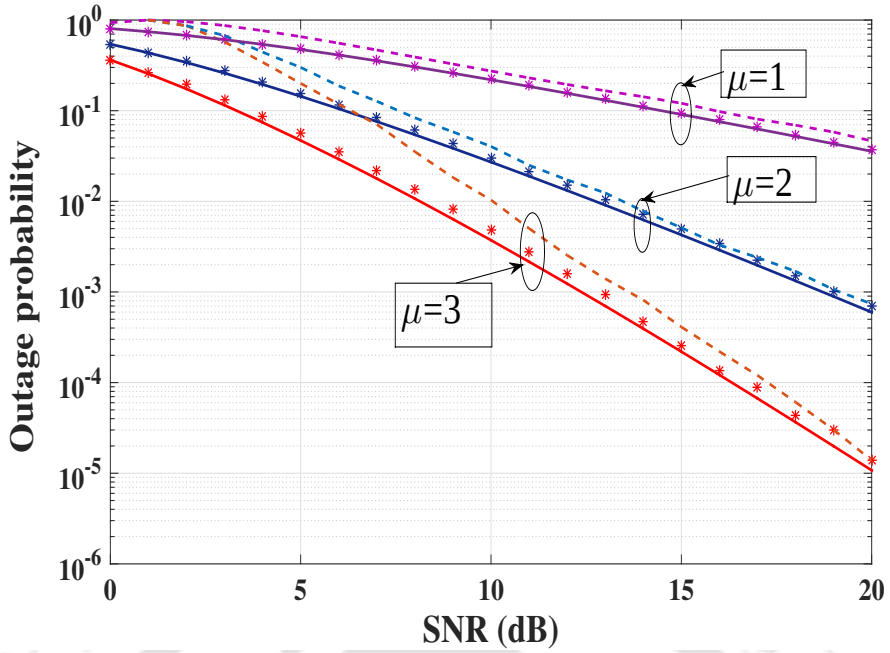

Figure 2.6: The impact of fading factor μ on lower bound of outage performance
(Solid line represents analytical results, $*$ sign indicates simulation results and dashed line represents asymptotic results).

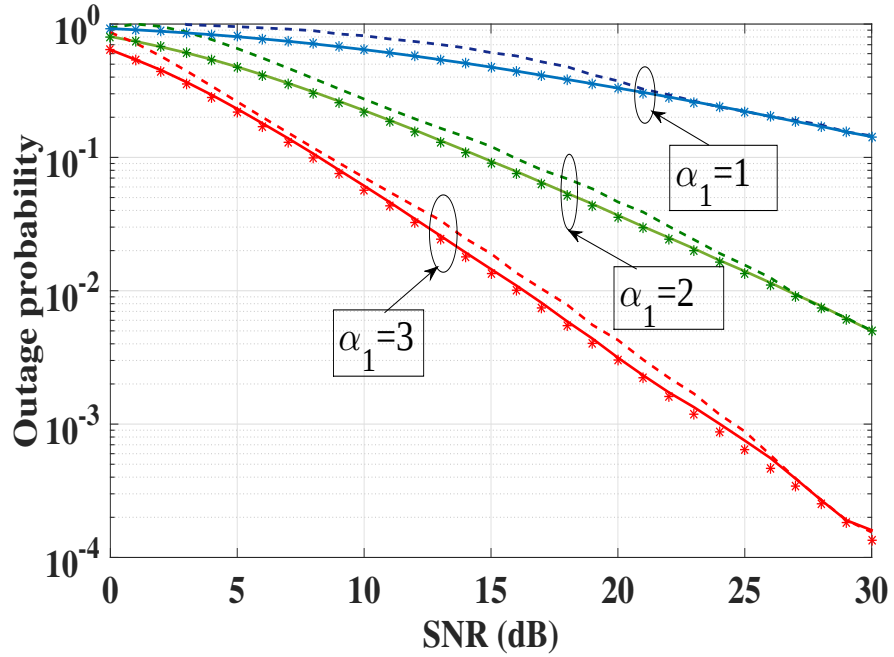

Figure 2.7: The effect of α_1 on lower bound of outage performance
(Solid line represents analytical results, $*$ sign indicates simulation results and dashed line represents asymptotic results).

node, is similar to that of a system having 4 antennas at each of the 3 nodes. From this it can be inferred that the number of antennas at the relay node basically governs the system performance. This is because in the second stage of the two stage operation, the relay node transmits message. Therefore relay can

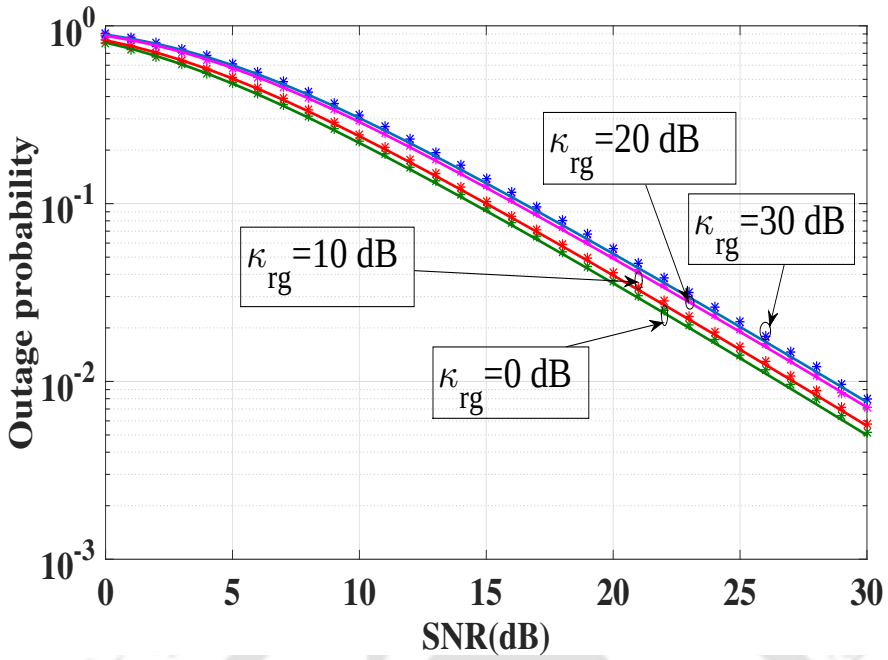

Figure 2.8: The impact of relative geometrical gain κ_{rg} on lower bound of outage performance (Solid line represents analytical results while $*$ sign indicates simulation results).

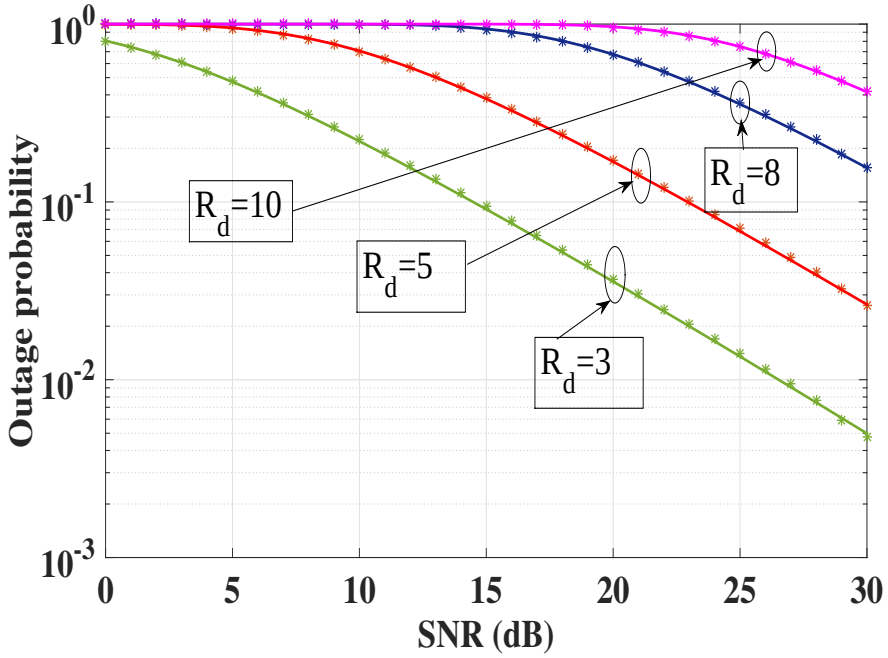

Figure 2.9: The impact of data rate R_d on outage performance (Solid line represents analytical results while $*$ sign indicates simulation results).

overcome the drawbacks of error or interference caused during transmission from source nodes in the first stage. The dominant factor in system performance is the amount of interference at the relay node which is directly influenced by the number of antennas at the relay node.

Comparison of the average data rate of the proposed system is performed with other algorithms. The Monte Carlo simulation results are plotted in Fig. 2.11. It is deduced from the graph that the proposed

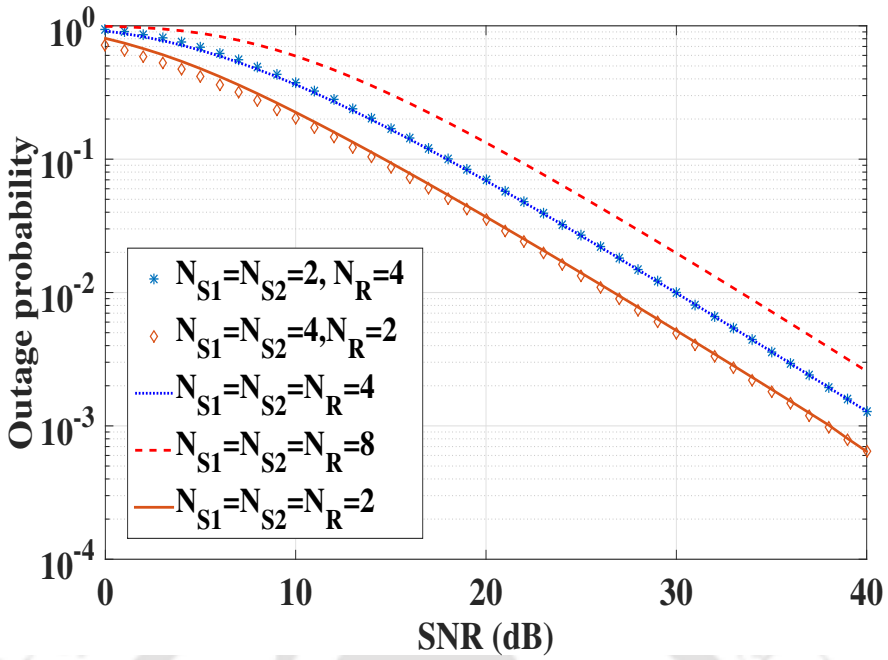

Figure 2.10: The impact of different number of antennas at source and relay nodes.

model outperforms PLNC. AFOWR performs the worst followed by PLNC. SM based DFTWR has higher average data rate than AFTWR in case of lower SNR values where our proposed system is able to suppress the inter-antenna interference. However, on crossing a certain threshold SNR point, the inter-antenna interference dominates in case of SM based DFTWR and hence AFTWR gives better average data rate than our proposed system.

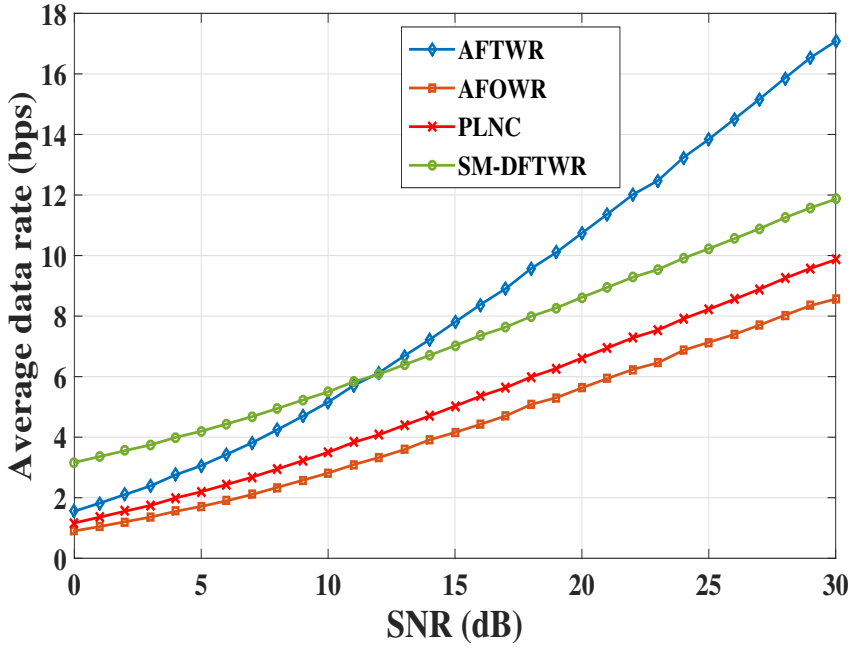

Figure 2.11: Simulation results for comparison of average data rate of various systems.

2.5 Conclusion

The derivation of analytical expressions for outage probability of SM based DFTWR system has been done and the analytical results have been validated by implementing Monte Carlo simulations. The cascaded α-μ channel model has been utilized for this purpose. This system can be implemented for D2D communication, where two devices located far away from each other can interact through a relay. The SM based DFTWR system outperforms the systems available in literature. It doubles the efficiency of a conventional AF/DF system as only two time slots are consumed to perform the SM based DFTWR operation. The performance improvement in outage probability and data rate compensates the increase in system complexity for this method. In this research field, future works can be done by exploring the possibility of applying generalized fading models like $\kappa - \mu$ and $\eta - \mu$ channels for RF cooperative system in high scattering environment.

3. Spatial Modulations for Body Area Network-Based Communication

3.1 Introduction

In this chapter, body area network (BAN) communication is explored both for SISO and MIMO scenarios for sporting activities like running and cycling. In sports activities, some critical parameters like heart rate, breath rate, blood glucose level, position and movement of body parts, etc. need to be monitored at regular intervals to generate the optimum output. Hence different wearable sensors are attached to the arms of athletes. Sensors can be accelerometer/gyroscope, blood glucose sensor, blood pressure sensor, ECG/EEG/EMG sensor, humidity and temperature sensor, etc. Each type of sensor detects a particular physiological parameter and provides data for further processing. All these data are transferred in a cooperative manner from each sensor to another sensor till it reaches a fixed central server for monitoring. If individual sensors on the body of an athlete transfer data directly to the central server then there will be network congestion and unnecessary wastage of spectral bandwidth. It will also require more transmit power and costlier equipment. To save bandwidth and make efficient resource utilization, sensors interact with each other thereby transferring its own data. This data is relayed to the central server. For this, communication between two sensors needs to be investigated such that effective BAN can be established in a particular area [65].

Different types of sensors function differently and transmit a particular parameter. In running, some parameters like gait position, periodic hip movement, amount of strides taken, oscillatory hand movement are critical to yield optimum performance from the runner. These data can be stored and studied to rectify the errors and enhance the performance of athletes in future events. Sometimes it has been seen that many players have died during sporting events due to malfunctioning of heart, lungs, livers or kidneys [66]. While performing any physical activities, some organs like heart, lungs work at an enhanced rate thereby increasing the risk of fatalities. If the heart and respiratory rates can be monitored live during events and if these rates cross a certain threshold, then a warning signal can be sent from the

monitoring server back to the particular sensor through a relay system of other sensors. This warning will provide an indication to the athlete that all activities must be stopped immediately to prevent any fatality. This will help in reducing casualties during sporting events. A block diagram of the proposed sensor model for sporting activities is illustrated pictorially in Fig. 3.1.

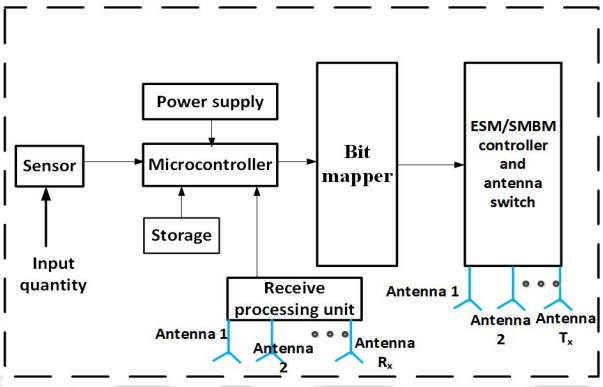

Figure 3.1: Block diagram of the proposed sensor for sporting activities.

In BAN, shadowing effects are caused due to body movements and impacts the data transmission at both ends. Thus both the transmitter and receiver are influenced by the existence of scatterers, thereby affecting the communication channels. Relative motion exists between the two bodies, thereby resulting in time varying shadowing effects. BAN channels cannot be modelled by means of a normal indoor channel because of mobility of human beings and different location of the antenna in different parts of the body thereby yielding different channel gains. BAN communication differs from device-to-device (D2D) communication in certain aspects. The body shadowing effects caused due to the movement of various body parts are not present in D2D communication. The relative height of the different body parts also plays an important role in time varying shadowing effects. Therefore, a different channel model is required as discussed in the subsequent sections. Before going into further details, a brief literature review is presented.

BAN communication has been used for various communication scenarios depending on the nature of application. BAN based communication can be line-of-sight (LOS) or non-line-of-sight (NLOS) type. In [67], the authors have shown that $\kappa - \mu$ channel is more suitable model than other channel models like Weibull, Rayleigh, Rice, Nakagami and lognormal for indoor BAN communication. The authors in [68] have stated that lognormal, Gamma and Weibull are suitable for BAN communication irrespective of environmental conditions. Shadowing effects in BAN communication have been appropriately modelled by lognormal channel model [69]. Large scale and small scale fading effects have been explored for various BAN scenarios in [70, 71]. BAN communication has been explored for various scenarios- indoor, outdoor, healthcare systems, etc. In [70], effect on the BAN communication has been studied by placing

the antenna in 3 different positions- head, belt and wrist. The BAN communication channel is designed depending on the large and small scale fading effects for three different locations of the antenna. The authors in [72] have investigated channel for abnormal gestures of patients suffering from Parkinson's disease. The effect of different types/sizes of bodies on BAN channel model has been studied in [73]. S band sensing has been used to study amplitude and phase of channel data for abnormal positions of patients suffering from dementia [74] and cerebellar abnormalities [75]. In [74], phase and amplitude data of the channel is classified for 3 different wandering patterns- random, pacing and lapping. Using support vector machine (SVM) algorithm, the features of the patients suffering from dementia has been classified. In [75], gait abnormality and hand tremors are used as features for amplitude and phase data classification for patients suffering from cerebellar abnormalities. An energy efficient BAN communication system has been proposed in [76] to exchange data between the patients and fixed access points through clouds. Semantic web technology for data and processing interface between humans and computers has been discussed in [77].

The shadowing effect is more prominent in sporting activities like running and cycling, hence the performance analysis of BAN communication needs to be explored. The authors in [3] have claimed that the histograms of measured data for various sporting activities like running and cycling show mixture and skewed distribution curves. This justifies the existence of distinct scattering clusters for BAN communication channels which can be appropriately characterized by a mixture distribution. Thus scattering is more as compared to normal environmental scattering effect because of body shadowing. Therefore, the shadowing effects can be modelled by a different channel model. A lognormal mixture shadowing model has been used in [3] to model the BAN channels for various sporting activities and the mixture model matches closely with the original data than the unimodal distributions. The weighted related mean difference (WRMD) parameter has been considered in [3] to compare the fitting of experimental data with the PDF of a particular distribution. It can be observed that lognormal mixture distribution has the least WRMD indicating best fitting of data. Hence this channel model is utilized for the performance analysis of our proposed system.

After doing the literature survey, it is observed that the performance analysis of sporting activities like running and cycling has not been analyzed for BAN communication. Such an analysis can help us in developing better sensors which can communicate with better data rates and lower error rate. Valuable information can be exchanged between such sensors and data can be recorded regarding physical parameters of the athletes during live events or training which can help in avoiding fatalities. If some parameter exceeds a certain threshold, then a warning can be raised and the event can be stopped. For such sensors to work effectively, first we have to understand the intricacies of such communication

and the effect of environment on BAN communication. Hence both SISO and MIMO methods with new SM based schemes need to be explored which can increase the spectral efficiency of such BAN communication and negate the effects of body shadowing and clusters. The contribution of our work lies in the performance analysis of BAN communication in terms of outage probability and ASEP for sporting activities like running and cycling under two different scenarios. First the analysis is conducted for SISO scenario, then it is extended to MIMO scenario. Methods like SM, enhanced spatial modulation (ESM) and spatial media based modulation (SMBM) are proposed for MIMO based BAN communication and the performance analysis is studied in terms of BER which is completely novel in nature. However, performance analysis of these methods is a challenging task as the channel model contains intractable integrals which prevents us from getting closed form expressions of BER. The error analysis can be achieved numerically, but valuable insights regarding the system performance cannot be gained without the availability of closed form expressions. Numerical simulation takes up time and leads to computational complexities. Asymptotic analysis can also be done if closed form expressions are available, leading to calculations of coding and diversity gain. Thus closed form expressions need to be derived for error analysis of BAN communication for all schemes. This challenging task can be solved by introduction of a new distribution called mixture of Gamma (MG) distribution. The approximation of the channel model with MG distribution and deriving closed form expressions of BER is carried out in this chapter. Thus the key contributions of this chapter are as follows:

- An accurate approximation of mixture of lognormal distribution is proposed in terms of mixture of Gamma distribution for BAN communication.

- Performance analysis in terms of BER for BAN communication, especially sporting activities such as cycling and running is carried out for both SISO and MIMO systems.

- Closed form expressions of BER for SISO as well as MIMO systems employing ASMs such as ESM and SMBM are provided.

- All the analytical results are validated by Monte Carlo simulation results and they are found to be in close agreement with each other.

- It is observed that cycling activities have better BER than running activities because of less body shadowing effect. It is found out that SMBM outperforms SISO as well as MIMO systems employing ESM for such sporting activities.

3.2 System Model

For measuring data, transmitting and receiving nodes (a small strip of Velcro) are used [3]. Two different situations are considered- running (average speed of 3.3m/s) and cycling (average speed of 5m/s). The experiments were conducted under two different scenarios- one where the test subjects were behind one another and the other where the test subjects were beside each other. Distance of separation was maintained as 1 m for all cases. The test subjects considered were adult males of height 1.80 m and weight 80 Kg, and height 1.85 m and weight 75 Kg, as mentioned by the authors in [3]. All the results were obtained in an outdoor environment. A programmable radio transceiver (CC2500) from Texas Instruments was programmed to transmit a packet every 4 ms with constant transmission power of 1 dBm at a carrier frequency of 2.425 GHz [78]. Horizontal polarized Wurth Electronik 7488910245 chip antenna were used at the nodes and the received information (packet number along with the received signal strength indicator) were stored on a MicroSD memory card. The experiment was conducted over an outdoor stretch of 500 m with collection of 25 kilo samples for each scenario. The stretch was bounded by industrial buildings on one side and a road on the other side. The data sets collected for two scenarios each for two different activities, were normalized to their corresponding mean values before processing. The scenarios are illustrated by means of self-explanatory diagrams, Fig. 3.2 and 3.3. In Fig. 3.2, the test subjects are running and cycling behind one another. In Fig. 3.3, the test subjects are running and cycling beside one another. Henceforth in the chapter, the two scenarios will be referred as Scenario I and Scenario II respectively.

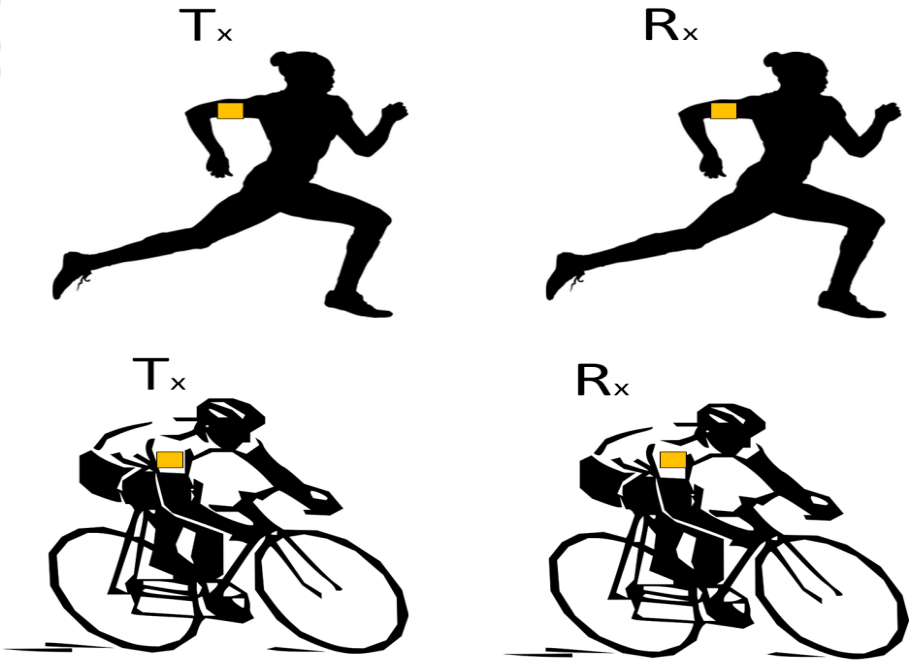

Figure 3.2: Scenario I where the test subjects are running and cycling behind one another.

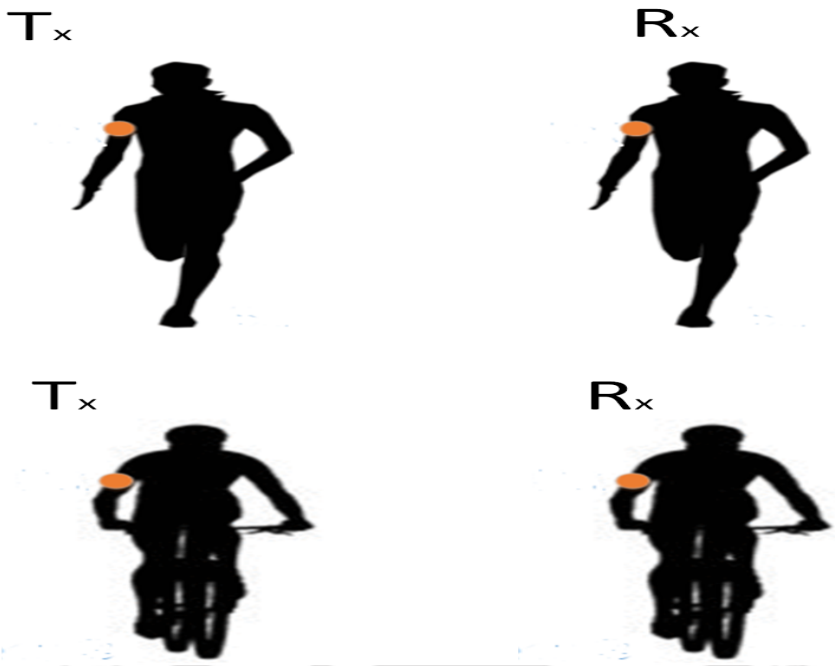

Figure 3.3: Scenario II where the test subjects are running and cycling beside one another.

The BAN channels vary according to body mass index (BMI) as shown in [73]. BMI value depends on height and weight of an individual. Depending on the BMI value, classification is done- normal, overweight and obese as shown in Table 3.1. Since the experimental setup and diverse kinds of test subjects are not available with us presently to conduct the experiment, thereby we are providing the analytical results. To perform the analysis, we have taken the help of datasets available in [73]. The test subjects considered earlier fall under the category of BMI1.

Table 3.1: Classification of BMI

Category	BMI value	Classification
1	18.5-24.9	Normal
2	25-29.5	Overweight
3	≥30	Obese

3.3 Channel Model

In this work, lognormal mixture distribution [16] is used which is a weighted mixture of several lognormal distributions having different mean and variance values. To achieve performance analysis in terms of outage probability and ASEP, the CDF and PDF of the channel model are required. Hence the first objective is to evaluate the PDF and CDF of the lognormal mixture distribution. The PDF of lognormal mixture distribution ($f_Y(y)$) can be expressed as [16]:

$$f_Y(y) = \sum_{k=1}^{\infty} w_k f_H(h) \ , \tag{3.1}$$

where $f_H(h) \varepsilon\ LN(\mu_k^{lg}, \sigma_k^2)$ (LN representing lognormal distribution), μ_k^{lg} and σ_k^2 are the mean and variance parameters of the k^{th} mixture component (k=1,2,...), w_k is the weight factor of the k^{th} component such that $\sum_{k=1}^{\infty} w_k = 1$. The mixture distribution is made up of multiple components, thereby making it clear that the PDF of a single lognormal distribution needs to be evaluated first. The lognormal PDF of the k^{th} component can be written as given in Eq. (4) of [16].

$$f_H(h) = \frac{1}{h\sqrt{2\pi\sigma_k^2}} \exp\left[\frac{-(\ln\ h - \mu_k^{lg})^2}{2\sigma_k^2}\right] . \tag{3.2}$$

Let $\gamma = h^2 E/N_0$ where $\bar{\gamma} = E/N_0$ is the source node SNR. Thus by applying the concept of change of random variable in PDF, we can obtain the PDF of received SNR. Hence the PDF of received SNR, γ for the k^{th} component can be expressed as [79]:

$$f_\gamma(\gamma) = \frac{\bar{\gamma}}{2\gamma\sqrt{2\pi\sigma_k^2}} \exp\left[\frac{-(\ln\ (\frac{\gamma}{\bar{\gamma}}) - 2\mu_k^{lg})^2}{8\sigma_k^2}\right] . \tag{3.3}$$

For derivation of the CDF of lognormal mixture distribution, we can assume $t = \frac{(\ln\ (\frac{\gamma}{\bar{\gamma}}) - 2\mu_k^{lg})}{\sqrt{8\sigma_k^2}}$. Then the integration of PDF equation will take the form of $\frac{1}{\sqrt{\pi}} \int_0^x e^{-t^2} dt$ which can be denoted in terms of error function $erf(\cdot)$. Please note that $erfc(\cdot)$ is the complementary error function denoted by $erfc(x) = 1 - \frac{2}{\sqrt{\pi}} \int_0^x e^{-t^2} dt$. The CDF of the lognormal mixture distribution after integrating the PDF and applying proper weights, can be expressed as [79]:

$$F_\gamma(\gamma) = \sum_{k=1}^{\infty} w_k \left(1 - \frac{1}{2} erfc\left(\frac{\ln\left(\frac{\gamma}{\bar{\gamma}}\right) - 2\mu_k^{lg}}{\sqrt{8}\sigma_k}\right)\right) . \tag{3.4}$$

The outage probability of lognormal mixture distribution for a threshold data rate of R_d bps can be evaluated as (from CDF equation):

$$P_{out}(\gamma_{th}) = \sum_{k=1}^{\infty} w_k \left(1 - \frac{1}{2} erfc\left(\frac{\ln\left(\frac{\gamma_{th}}{\bar{\gamma}}\right) - 2\mu_k^{lg}}{\sqrt{8}\sigma_k}\right)\right) , \tag{3.5}$$

where $\gamma_{th} = 2^{R_d} - 1$. In this work, finite number of K Gaussian kernels are utilized to form a mixture of lognormal distribution and it is evident from the results in [3], that K=4 gives the best estimate of the actual PDF. This indicates that weighted mixture of 4 lognormal components is the most suitable distribution to model BAN channels for sporting activities. Therefore, we have used lognormal-4 distribution for further analysis and it is denoted by LN-4 in our work. Thus by considering 4 components of

lognormal mixture distribution, outage probability of LN-4 can be rewritten as:

$$P_{out}(\gamma_{th}) = \sum_{k=1}^{4} w_k \left(1 - \frac{1}{2} erfc\left(\frac{\ln\left(\frac{\gamma_{th}}{\tilde{\gamma}}\right) - 2\mu_k^{lg}}{\sqrt{8}\sigma_k}\right)\right) , \tag{3.6}$$

where $\gamma_{th} = 2^{R_d} - 1$. For M-ary modulation scheme, the average ASEP for BAN communication is evaluated as [80]:

$$P_e \cong \sum_{k=1}^{4} \int_0^{\infty} w_k a Q(\sqrt{e\gamma}) f_\gamma(\gamma) d\gamma \ . \tag{3.7}$$

The PDF $f_\gamma(\gamma)$ is obtained from Eq. (3.3). The integral is calculated using Mathematica software. In this work, binary phase shift keying (BPSK) modulation scheme is used. The values of a and e depend on the constellation scheme deployed and has been chosen from Eq. (7) of [81]. Due to the presence of intractable integrals, the existence of closed form expressions is impossible. Hence, mixture of gamma (MG) distribution is used to approximate lognormal distributions and achieve closed form expressions of ASEP. This will help us in gaining valuable insights regarding performance of BAN system like diversity gain, coding gain, asymptotic behaviour of the system for high SNR values. The approximation of lognormal distribution by MG distribution is the next challenging part of this chapter, where the process of obtaining closed form error expressions is illustrated.

3.4 Mixture of Gamma Distribution

To evaluate error using MG distribution, we need the PDF of MG distribution. So the first step is to approximate lognormal PDF using the PDF of MG distribution. The PDF of MG distribution [82] can be written as in Eq. (22) of [79]:

$$f_{MG}(x) = \sum_{i=1}^{n} P_i \frac{x^{(\alpha_i^{MG}-1)}\left(\beta_i^{MG}\right)^{\alpha_i^{MG}}}{\Gamma(\alpha_i^{MG})} e^{-x\beta_i^{MG}} , \tag{3.8}$$

where P_i is the mixing coefficient of the i^{th} Gamma distribution and the shape and scale parameters of the i^{th} Gamma distribution are α_i^{MG} and β_i^{MG} respectively. CDF of MG distribution can be obtained by integrating the PDF and can be written as in Eq. (23) of [79].

$$F_{MG}(x) = \sum_{i=1}^{n} P_i \left(1 - \frac{1}{\Gamma(\alpha_i^{MG})} G_{1,2}^{2,0}\left(_{0,\alpha_i^{MG}}^{1} \middle| \beta_i^{MG} x\right)\right) \ . \tag{3.9}$$

We can observe that the integration of PDF function can be written in terms of Gamma function ($\Gamma(\alpha_i^{MG}, \beta_i^{MG} x)$). Gamma function can be represented in terms of Meijer G function. After some algebraic manipulations, the final CDF formula can be derived as in Eq. (3.9). The formula required is

[46, 47, 48]:

$$\Gamma(\rho, x) = G_{1,2}^{2,0}\left(\begin{smallmatrix}1\\ \rho,0\end{smallmatrix}\middle| x\right) . \tag{3.10}$$

Outage probability of MG distribution can be written after replacing the x term in Eq. (3.9) with threshold SNR value i.e. γ_{th} [79]. Now in our BAN system, we are considering mixture of lognormal distribution, hence the approximation by MG distribution has to be extended for multiple components now. The PDF and CDF equations of MG distribution when summed up over 4 components gives us the PDF and CDF of LN-4 channel. The outage probability of the BAN system after approximating LN-4 with MG distribution, can be evaluated as:

$$P_{out} \cong \sum_{k=1}^{4} w_k \sum_{i=1}^{n} P_{k,i}\left(1 - \frac{1}{\Gamma(\alpha_{k,i}^{MG})} G_{1,2}^{2,0}\left(\begin{smallmatrix}1\\ 0,\alpha_{k,i}^{MG}\end{smallmatrix}\middle| \frac{\beta_{k,i}^{MG}\gamma_{th}}{\bar{\gamma}}\right)\right) , \tag{3.11}$$

where $G_{p,q}^{m,n}(:|\, z)$ denotes the Meijer G function [47, 62], $\gamma_{th} = 2^{R_d} - 1$, R_d is the target data rate. Number of mixing coefficients is denoted by n, Γ denotes the Gamma function, $P_{k,i}$ is the mixing coefficient of the i^{th} Gamma distribution and k^{th} component of LN-4, having properties like $P_{k,i} > 0$ and $\sum_{i=1}^{n} P_{k,i} = 1$. The shape and scale parameters of the i^{th} Gamma distribution and k^{th} component are $\alpha_{k,i}^{MG}$ and $\beta_{k,i}^{MG}$ respectively. The ASEP of the system can be computed as (with the help of Eq. (3.8)):

$$\begin{aligned}
P_e &\cong \sum_{k=1}^{4} w_k \int_0^{\infty} f_{MG}(\gamma) a Q(\sqrt{e\gamma}) d\gamma \\
&= \sum_{k=1}^{4} w_k \int_0^{\infty} \sum_{i=1}^{n} \frac{P_{k,i}(\beta_{k,i}^{MG})^{\alpha_{k,i}^{MG}} (\frac{\gamma}{\bar{\gamma}})^{\alpha_{k,i}^{MG}-1} e^{-\beta_{k,i}^{MG}\frac{\gamma}{\bar{\gamma}}}}{\Gamma(\alpha_{k,i}^{MG})} a Q(\sqrt{e\gamma}) d\gamma \\
&= \sum_{k=1}^{4} w_k \sum_{i=1}^{n} \int_0^{\infty} \frac{P_{k,i}(\beta_{k,i}^{MG})^{\alpha_{k,i}^{MG}} (\frac{\gamma}{\bar{\gamma}})^{\alpha_{k,i}^{MG}-1}}{\Gamma(\alpha_{k,i}^{MG})\sqrt{\pi}} G_{0,1}^{1,0}\left(\begin{smallmatrix}-\\ 0\end{smallmatrix}\middle| \frac{(\beta_{k,i}^{MG})\gamma}{\bar{\gamma}}\right) a G_{1,2}^{2,0}\left(\begin{smallmatrix}1\\ 0,1/2\end{smallmatrix}\middle| e\gamma\right) \\
&= \sum_{k=1}^{4} w_k \sum_{i=1}^{n} \frac{a P_{k,i}\bar{\gamma}}{\Gamma(\alpha_{k,i^{MG}})\sqrt{\pi}} G_{2,2}^{2,1}\left(\begin{smallmatrix}1-\alpha_{k,i}^{MG},1\\ 0,1/2\end{smallmatrix}\middle| \frac{e\bar{\gamma}}{\beta_{k,i}^{MG}}\right) .
\end{aligned} \tag{3.12}$$

$Q(x)$ function denotes the probability that a standard normal random variable takes a value larger than x. $Q(x) = \frac{1}{\sqrt{2\pi}} \int_x^{\infty} \exp(-u^2/2) du$. For deriving Eq. (3.12), the following formulae are used [46, 47, 48]:

$$\begin{aligned}
&\int_0^{\infty} \tau^{\alpha-1} G_{u,v}^{s,t}\left(\begin{smallmatrix}c_1,\ldots,c_t,c_{t+1},\ldots,c_u\\ d_1,\ldots,d_s,d_{s+1},..d_v\end{smallmatrix}\middle| \tau w\right) G_{p,q}^{m,n}\left(\begin{smallmatrix}a_1,\ldots,a_n,a_{n+1},\ldots,a_p\\ b_1,\ldots,b_m,b_{m+1},\ldots,b_q\end{smallmatrix}\middle| \tau z\right) d\tau \\
&\qquad = w^{-\alpha} G_{v+p,u+q}^{m+t,n+s}\left(\begin{smallmatrix}a_1,.,a_n,1-\alpha-d_1,..,1-\alpha-d_s,a_{n+1},.,a_p\\ b_1,.,b_m,1-\alpha-c_1,\ldots,1-\alpha-c_t,b_{m+1},..,b_q\end{smallmatrix}\middle| \frac{z}{w}\right) .
\end{aligned} \tag{3.13}$$

$$Q(x) = \frac{1}{2} erfc(\frac{x}{\sqrt{2}}), erfc(\sqrt{z}) = \frac{1}{\sqrt{\pi}} G_{1,2}^{2,0}\left(\begin{smallmatrix}1\\ 0,1/2\end{smallmatrix}\middle| z\right) . \tag{3.14}$$

$$e^{-z} = G_{0,1}^{1,0}\left(\begin{smallmatrix}-\\ 0\end{smallmatrix}\middle| z\right) . \tag{3.15}$$

The complexity of the expectation maximization (EM) algorithm (comprising of E-step and M-step) for calculation of MG distribution coefficients is analyzed. In general, the algorithm complexity depends on the number of iterations, stopping criteria and initial values of model parameters provided. Good initial values mean the values converge to a local solution in less number of iterations. The complexity for one particular iteration is analyzed. In E-step, the complexity is given by $O(m*k^2)$ where k is the number of mixing coefficients and m is the number of model parameter points. In M-step, the complexity is given by $O(m*k)$. If k increases, the complexity of E-step increases by square of that value which tends to be quite large for higher values of k.

3.5 Asymptotic Analysis of SISO BAN Communication

To analyze the ASEP expression for asymptotic behaviour, the Meijer G component has to be written in a different form. As stated in the earlier chapter, the Meijer G function at very high values of its argument can be written as described in Eq. (41) in [63]. Therefore Eq. (3.12) at very high values of SNR can be written as:

$$P_e^{asym} \approx \sum_{k=1}^{4} w_k \sum_{i=1}^{n} \frac{aP_{k,i}\bar{\gamma}}{\Gamma(\alpha_{k,i}^{MG})\sqrt{\pi}} \sum_{m=1}^{1} \left(\frac{e\bar{\gamma}}{\beta_{k,i}^{MG}}\right)^{c_m-1} \frac{\prod_{l=1}^{2}\Gamma(1+d_l-c_k)}{\prod_{l=2}^{2}\Gamma(1+c_l-c_m)}\,, \tag{3.16}$$

where $c = [1-\alpha_{k,i}^{MG}, 1]$ and $d = [0, 1/2]$. For diversity analysis the highest exponent of SNR is required only. The exponent will be highest for maximum value of $\max(\alpha_{k,i}^{MG})$. In this case the highest exponent of SNR is $1-1-\max(\alpha_{k,i}^{MG})+1 = 1-\max(\alpha_{k,i}^{MG})$. The coding and diversity gain can be analytically calculated as:

$$\lim_{SNR\to\infty} P_e^{asym} \approx (C_g SNR)^{-D_g}\,, \tag{3.17}$$

where C_g and D_g are the coding and diversity gains respectively. Hence after taking the negative exponent of SNR, we can write diversity gain of SISO BAN system as $D_g = \max(\alpha_{k,i}^{MG}) - 1$. It is pertinent to note that the diversity gain is dependent on the parameter of 5-MG distribution. The coding gain can be written as:

$$C_g = \left(\sum_{k=1}^{4} w_k \sum_{i=1}^{n} \frac{aP_{k,i}}{\Gamma(\alpha_{k,i}^{MG})\sqrt{\pi}} \left(\frac{e}{\beta_{k,i}^{MG}}\right)^{-\alpha_{k,i}^{MG}} \frac{\prod_{l=1}^{2}\Gamma(d_l+\alpha_{k,i}^{MG})}{\prod_{l=2}^{2}\Gamma(c_l+\alpha_{k,i}^{MG})}\right)^{\frac{1}{1-\alpha_{k,i}^{MG}}}\,. \tag{3.18}$$

3.6 Results

The parameters (μ_k^{lg}, σ_k^2 and w_k) of LN-4 distribution for running and cycling activities under two different scenarios of BMI1 category are listed in Table 3.2 and 3.3 [3]. It can be observed from [73] that the mean and variance parameters of the channel vary for inter BMI categories. The mean varies

Table 3.2: Scenario 1 parameters for BMI1

Activity	Model	Parameters		
Running	LN-4	μ_1^{lg} =-0.0769	σ_1^2 =0.0537	w_1 =0.3531
		μ_2^{lg} =-1.3645	σ_2^2 =0.1563	w_2 =0.2245
		μ_3^{lg} =0.6879	σ_3^2 =0.092	w_3 =0.2921
		μ_4^{lg} =-0.6476	σ_4^2 =0.0793	w_4 =0.1303
Cycling	LN-4	μ_1^{lg} =-0.3353	σ_1^2 =0.0663	w_1 =0.3485
		μ_2^{lg} =-0.6487	σ_2^2 =0.2319	w_2 =0.1273
		μ_3^{lg} = 0.0372	σ_3^2 =0.0300	w_3 =0.3690
		μ_4^{lg} = 0.3266	σ_4^2 =0.0350	w_4 =0.1551

Table 3.3: Scenario 2 parameters for BMI1

Activity	Model	Parameters		
Running	LN-4	μ_1^{lg} =-1.5353	σ_1^2 =0.1391	w_1 =0.2063
		μ_2^{lg} =-0.9126	σ_2^2 =0.1086	w_2 =0.3216
		μ_3^{lg} =0.4865	σ_3^2 =0.1337	w_3 =0.1964
		μ_4^{lg} =-0.1630	σ_4^2 =0.1129	w_4 =0.2757
Cycling	LN-4	μ_1^{lg} =0.4655	σ_1^2 =0.0452	w_1 =0.1297
		μ_2^{lg} =-0.8142	σ_2^2 =0.118	w_2 =0.2189
		μ_3^{lg} = 0.0993	σ_3^2 =0.0356	w_3 =0.2914
		μ_4^{lg} = -0.3385	σ_4^2 =0.0552	w_4 =0.3600

by around 0.3 dB between BMI1 and BMI2, while it varies by around 0.7 dB between BMI2 and BMI3 categories. Similarly, the standard deviation (σ) varies by around 1 dB between each BMI category. Accordingly, we have also varied our mean and standard deviation parameters for lognormal channels by the same amount to perform approximate analysis for each BMI category. After the variation of mean and standard deviation parameters for lognormal channels, we have obtained the μ_k^{lg} and σ_k parameters for LN-4 channel for running and cycling activities under different scenarios by applying EM algorithm. The parameters for Scenario I and II of BMI2 are listed in Table 3.4 and 3.5 respectively while the parameters for Scenario I and II of BMI3 are listed in Table 3.6 and 3.7 respectively.

Table 3.4: Scenario 1 parameters for BMI2

Activity	Model	Parameters		
Running	LN-4	μ_1^{lg} =-0.0824	σ_1^2 =0.0676	w_1 =0.3531
		μ_2^{lg} =-1.4621	σ_2^2 =0.1968	w_2 =0.2245
		μ_3^{lg} =0.7371	σ_3^2 =0.1158	w_3 =0.2921
		μ_4^{lg} =-0.6939	σ_4^2 =0.0998	w_4 =0.1303
Cycling	LN-4	μ_1^{lg} =-0.3593	σ_1^2 =0.0835	w_1 =0.3485
		μ_2^{lg} =-0.6951	σ_2^2 =0.2919	w_2 =0.1273
		μ_3^{lg} = 0.0399	σ_3^2 =0.0378	w_3 =0.3690
		μ_4^{lg} = 0.35	σ_4^2 =0.0441	w_4 =0.1551

Lognormal distribution can be best approximated by MG distribution as portrayed by simulation

Table 3.5: Scenario 2 parameters for BMI2

Activity	Model	Parameters		
Running	LN-4	μ_1^{lg} =-1.64	σ_1^2 =0.1751	w_1 =0.2063
		μ_2^{lg} =-0.9751	σ_2^2 =0.1367	w_2 =0.3216
		μ_3^{lg} =0.5213	σ_3^2 =0.1683	w_3 =0.1964
		μ_4^{lg} =-0.1747	σ_4^2 =0.1421	w_4 =0.2757
Cycling	LN-4	μ_1^{lg} =0.4988	σ_1^2 =0.0569	w_1 =0.1297
		μ_2^{lg} =-0.8724	σ_2^2 =0.1486	w_2 =0.2189
		μ_3^{lg} = 0.1064	σ_3^2 =0.0448	w_3 =0.2914
		μ_4^{lg} = -0.3627	σ_4^2 =0.0695	w_4 =0.3600

Table 3.6: Scenario 1 parameters for BMI3

Activity	Model	Parameters		
Running	LN-4	μ_1^{lg} =-0.0968	σ_1^2 =0.0851	w_1 =0.3531
		μ_2^{lg} =-1.7178	σ_2^2 =0.2477	w_2 =0.2245
		μ_3^{lg} =0.8660	σ_3^2 =0.1458	w_3 =0.2921
		μ_4^{lg} =-0.8153	σ_4^2 =0.1257	w_4 =0.1303
Cycling	LN-4	μ_1^{lg} =-0.4221	σ_1^2 =0.1051	w_1 =0.3485
		μ_2^{lg} =-0.8167	σ_2^2 =0.3675	w_2 =0.1273
		μ_3^{lg} = 0.0468	σ_3^2 =0.0475	w_3 =0.3690
		μ_4^{lg} = 0.4122	σ_4^2 =0.0555	w_4 =0.1551

Table 3.7: Scenario 2 parameters for BMI3

Activity	Model	Parameters		
Running	LN-4	μ_1^{lg} =-1.9238	σ_1^2 =0.2205	w_1 =0.2063
		μ_2^{lg} =-1.1489	σ_2^2 =0.1721	w_2 =0.3216
		μ_3^{lg} =0.6125	σ_3^2 =0.2119	w_3 =0.1964
		μ_4^{lg} =-0.2052	σ_4^2 =0.1789	w_4 =0.2757
Cycling	LN-4	μ_1^{lg} =0.586	σ_1^2 =0.716	w_1 =0.1297
		μ_2^{lg} =-1.025	σ_2^2 =0.187	w_2 =0.2189
		μ_3^{lg} = 0.1250	σ_3^2 =0.0564	w_3 =0.2914
		μ_4^{lg} = -0.4261	σ_4^2 =0.0875	w_4 =0.3600

results in Fig. 3.4. The analysis is done for values of $\mu_k^{lg} = -0.0769$ and $\sigma_k^2 = 0.0537$. It is observed in [79], that higher components of MG distributions closely match with that of lognormal curve but keeping a trade-off between error and computational complexity, 5-MG distribution shows almost perfect match with lognormal distribution and hence is considered for further system analysis. For performance analysis, 1 bps is taken as the target data rate (R_d). Values of $P_{k,i}$, $\alpha_{k,i}^{MG}$ and $\beta_{k,i}^{MG}$ for each set of μ_k^{lg}, σ_k^2 and w_k values are obtained using EM algorithm [82].

The outage probability results for the proposed system under Scenario I are evaluated analytically and verified by means of Monte Carlo simulations. The results obtained using LN-4 distribution are verified by results which are evaluated using 5-MG distribution, as depicted from Fig. 3.5. The analytical

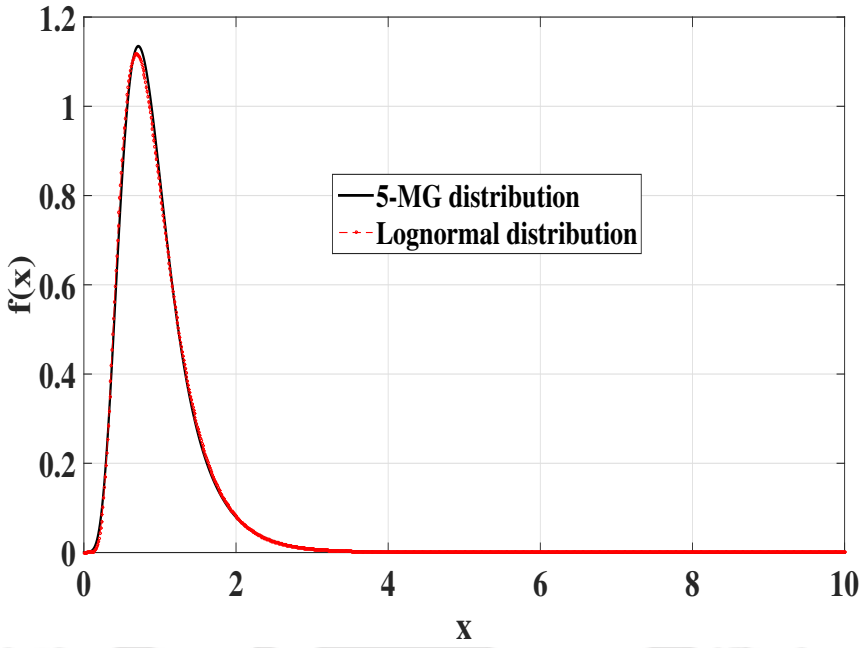

Figure 3.4: Lognormal distribution approximation for n=5.

results are obtained using Eq. (3.6), while the approximate outage probability is evaluated using 5-MG distribution by using Eq. (3.11). The results are in close agreement to each other, thereby justifying our analysis. The analysis is conducted for two different activities-running and cycling. Similar analysis is conducted for Scenario II as shown in Fig. 3.6. The results for a particular activity like running does not vary by a significant amount for different scenarios. Thus the location of the test subjects does not have significant influence on the system performance. This is because in case of cycling, the arms are outstretched and are relatively constant. Therefore, a LOS path can exist between the two arms for side-by-side and back-to-back cycling. In case of running, the arms are in oscillatory motion, but the body shadowing effect impacts the communication in a similar manner for both the scenarios. This leads to similar results for running in both scenarios.

The following figures illustrate the outage probability analysis for running and cycling activities according to different BMI and different scenarios. It is observed from Fig. 3.7 that cycling activity outperforms running activity for each BMI category in case of Scenario I (where test subjects are situated behind one another). In Fig. 3.8, cycling activity also outperforms running activity for each BMI category in case of Scenario II (where test subjects are situated beside one another). Hence it can be deduced from the analysis that irrespective of height, weight and age of the test subjects, outage probability results for cycling are better than that of running. It is to be noted that performance degrades due to increment in BMI category. This is because the body shadowing effect increases with increase in BMI category. As the body height or weight increases with BMI category, the body hinders signal transmission, thereby

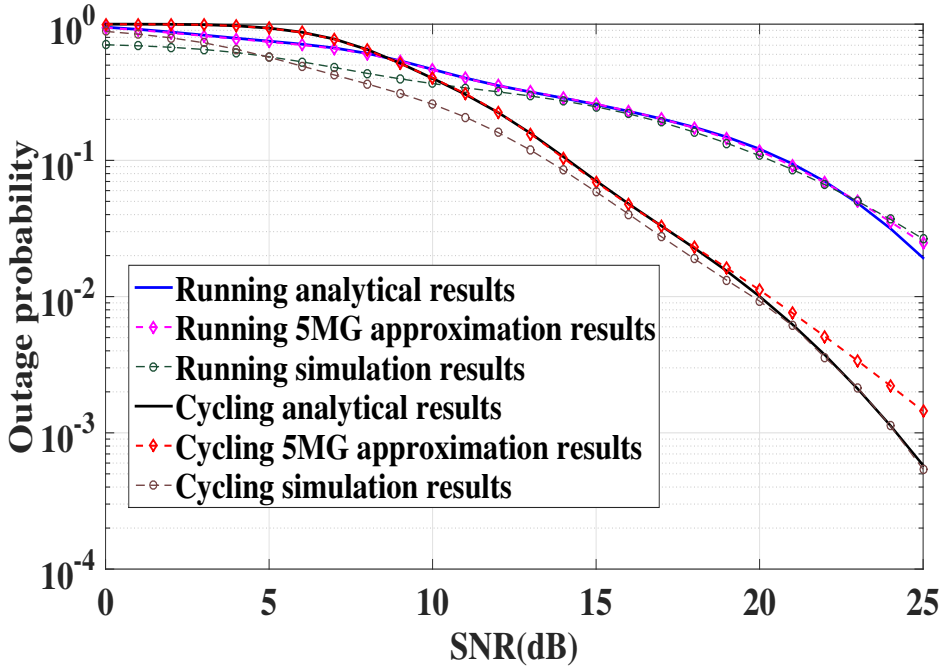

Figure 3.5: Outage probability results for running and cycling activities under Scenario I of BMI1 category.

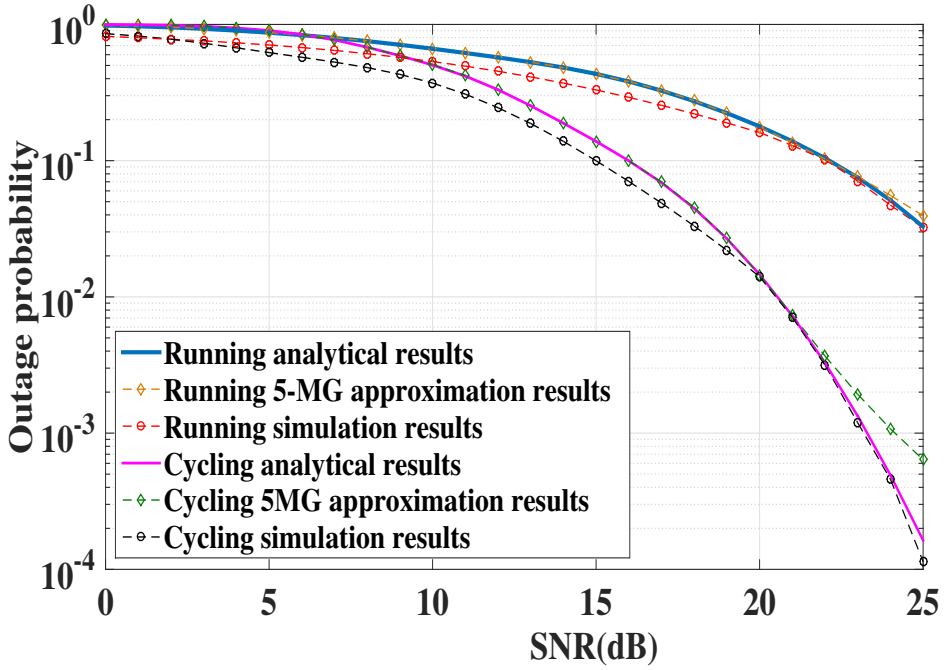

Figure 3.6: Outage probability results for running and cycling activities under Scenario II of BMI1 category.

leading to poorer performance.

The outage probability results for running and cycling activities under Scenario I and II for BMI2 category are evaluated analytically and verified by 5-MG approximation results, as can be seen from Fig. 3.9. Cycling outperforms running for all scenarios in BMI2 category also. The physical interpretation of the results is done in the later paragraphs of this section. It is evident from all analysis, that for any BMI

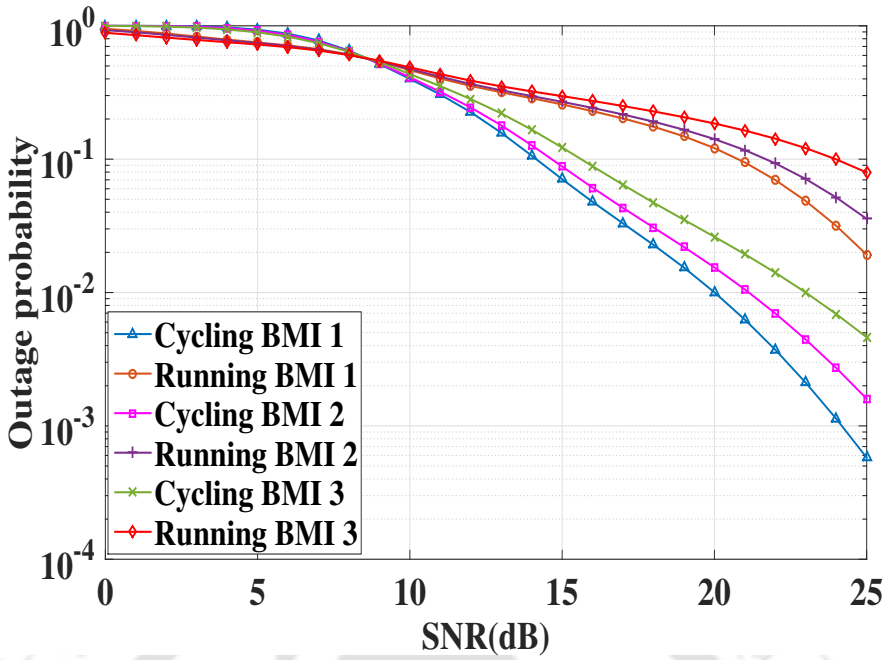

Figure 3.7: Outage probability results for different activities and different BMI under Scenario I.

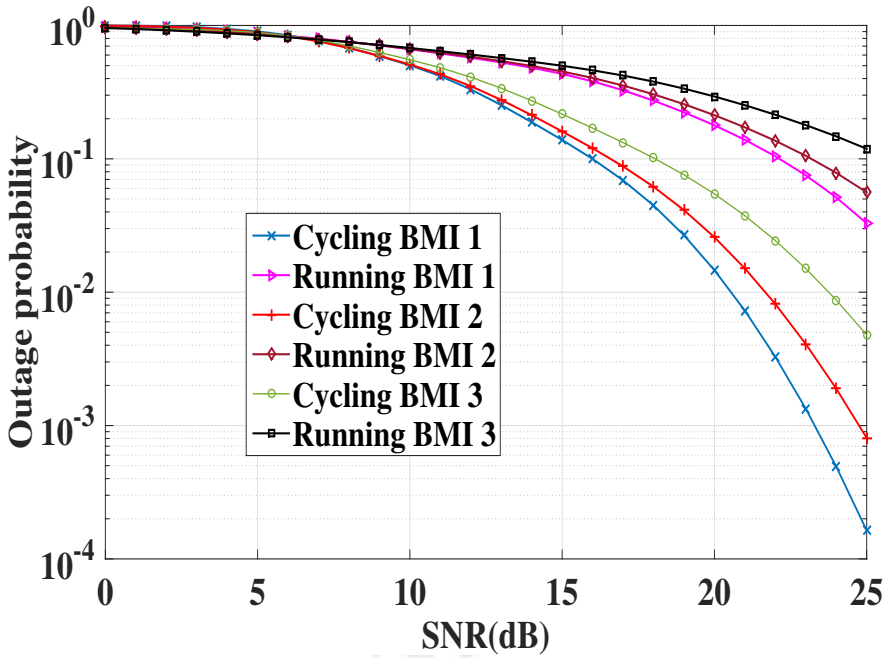

Figure 3.8: Outage probability results for different activities and different BMI under Scenario II.

value and for any μ_k^{lg} and σ_k^2 values, the cycling activity performs better than running. The same analysis would hold true for ASEP analysis also. The expressions of outage probability and ASEP depend only on μ_k^{lg} and σ_k^2 parameters, thereby the ASEP and outage probability results also shift by a certain amount according to different BMI categories. But for each BMI category and particular scenario, the nature of results remains the same as cycling outperforms running.

The ASEP results for the proposed system under Scenario I and Scenario II of BMI1 category

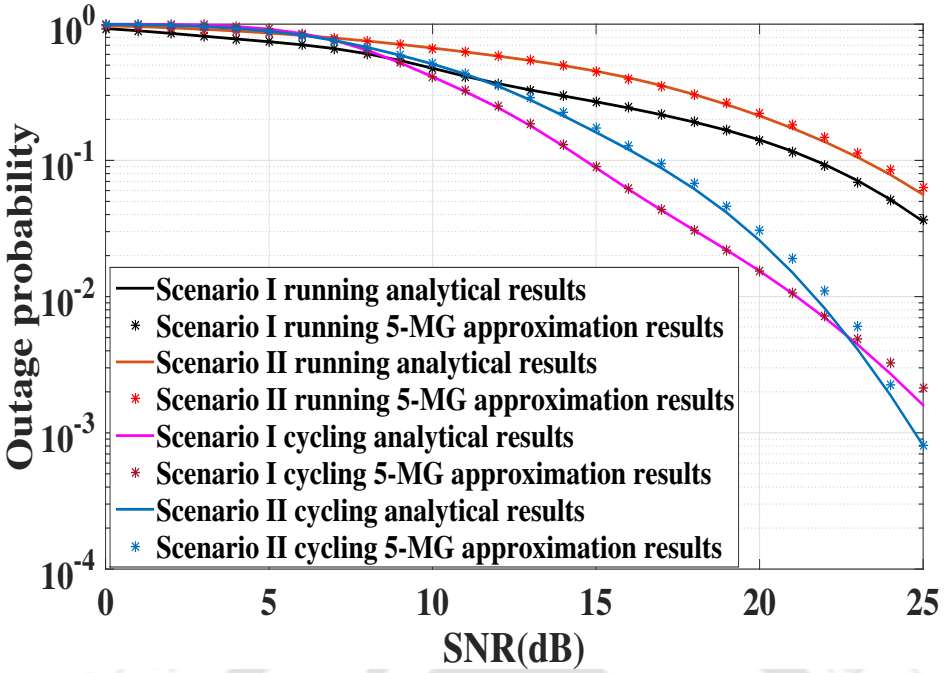

Figure 3.9: Outage probability results for different activities under different scenarios of BMI2 category.

are similarly shown in Fig. 3.10 and Fig. 3.11 respectively. The analytical results obtained using LN-4 distribution (by using Eq. (3.7)) are verified by means of Monte Carlo simulations and 5-MG distribution results (by using Eq. (3.12)). The results are in close agreement to each other, thereby justifying the use of 5-MG distribution. Asymptotic analysis is also performed for Scenario I and II results. It can be noticed from the graphs that at high values of SNR, the asymptotic results converge with the analytical and simulation values, thereby validating our analysis. Let us calculate the diversity gain for cycling Scenario II BMI1 category. Considering a SNR range of 15-25 dB, the slope is given by $10\log_{10}(0.0005/0.00000012)/10 \approx 3.62$. This is nearly equal to the theoretical value of 3.5 considering the maximum value of $\alpha_{k,i}^{MG}$ to be 4.5 (as obtained using EM algorithm for this scenario). The coding gain of cycling over running can be calculated for a particular scenario by measuring the horizontal shift between the two curves. It is noticed that cycling activity for Scenario II yields a coding gain of more than 5 dB over running activity at SNR values of more than 10 dB. The coding gain of cycling over running for Scenario I is also around 5 dB for SNR values of more than 10 dB.

It is visible both from the outage probability and ASEP results that cycling activities outperforms the running activities in both scenarios. In running there is oscillatory movement of the arms to which the devices are attached, while in case of cycling the arms are relatively stationary, and leaning and tilting of the body takes place [78]. However, the movement due to body tilting in cycling is much less as compared to the oscillatory arm movement in running. As a consequence, the distinction between clusters are less pronounced in case of cycling activities, while the scatterers are more distinct in case

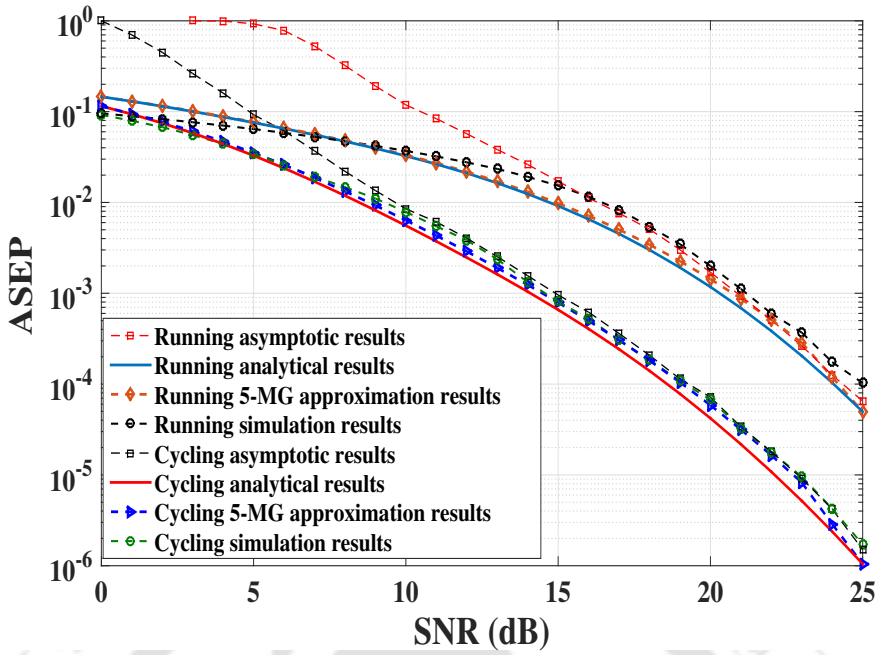

Figure 3.10: ASEP results for different activities under Scenario I of BMI1 category.

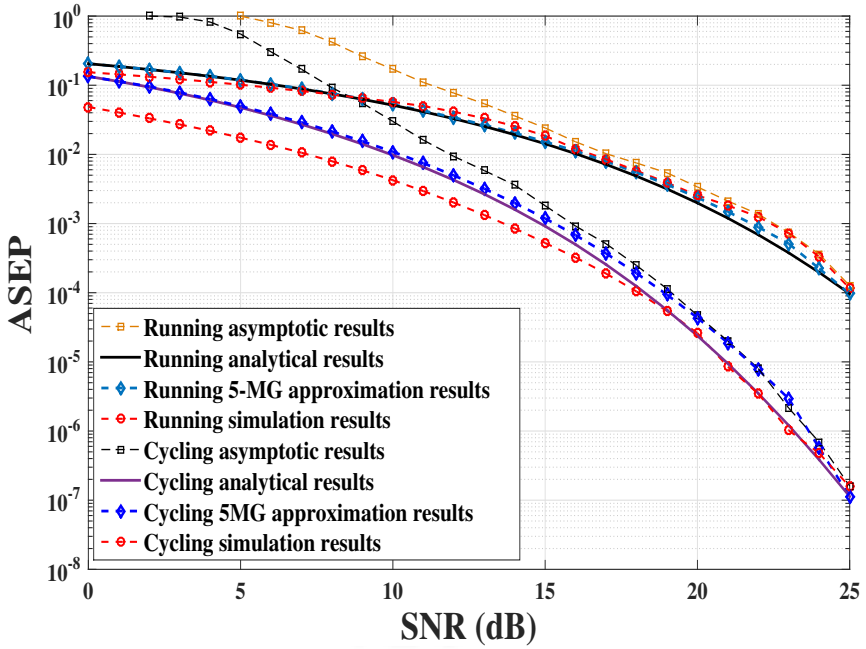

Figure 3.11: ASEP results for different activities under Scenario II of BMI1 category.

of running activities. This is evident from Fig. 3 and Fig. 5 in [3] where the measured PDF curves for running exhibit mixture and skewed distribution curves. When the test subjects are behind one another (Scenario I), other factors such as environmental changes and relative locations of the subjects dominate the scattering effect and outperforms the scattering effect caused by body motion in cycling. This leads to more scattering effect in cycling Scenario I activity as compared to cycling Scenario II activity. Since the PDFs are skewed for running activities, the curve deviates from the standard lognormal distribution

yielding mean which is different from the usual value. Due to the presence of more scattering groups in running activities, the running scenario gives poor performance as compared to cycling activities. We can conclude from the results that body shadowing effect dominates in running due to greater movement of body parts.

3.7 Need for MIMO BAN Communication

To support higher data rates with better reliability, MIMO technology needs to be implemented for BAN communication. However, there are drawbacks of MIMO systems which leads to the introduction of SM [83, 84], as already discussed in the first chapter. To achieve more higher spectral efficiencies, advanced spatial modulation schemes need to be explored for BAN communication. The next few sections will deal with the challenges of applying ASM schemes in BAN communication. The closed form expressions of BER need to be derived for these schemes in order to gain valuable insights regarding asymptotic behaviour of the system. We will also analyze how the running and cycling activities behave under these new schemes and the reasons for such behaviour. Such analysis is missing in the literature and will benefit the sports industry in implementing SM based schemes in sensors to monitor the performance of the players. ESM [85] and SMBM are two such advanced schemes which are proposed for BAN communication.

3.8 ESM for BAN Communication

In ESM, one primary constellation and two secondary constellations are used. In case of single transmit antenna activation, a symbol is transmitted from the primary constellation. In case of double antenna activation, two symbols are transmitted from one of the secondary constellations. If size of primary constellation is considered to be M, and $m = \log_2(M)$, then size of each of the secondary constellations is $\sqrt{M}$. M denotes the M-ary modulation scheme and T_x denotes the number of transmit antenna. T_x^2 number of active antenna and modulation combinations in ESM are available [85]. To select any one combination out of T_x^2 combinations, $2\log_2(T_x)$ bits are required. $\log_2(M)$ bits are used for constellation mapping of symbols. Either one symbol of m bits is transmitted from primary constellation, or two symbols, each of $m/2$ bits, are transmitted from a secondary constellation. Thus, spectral efficiency of ESM is $(m + 2\log_2(T_x))$ bpcu which is higher than that of SM for a fixed value of m and T_x.

For example if $T_x = 4$ and M=4, then primary constellation will be quadrature phase shift keying (QPSK) and secondary constellation will be BPSK. QPSK constellation scheme can take symbols from the value $\{\pm 1 \pm j\}$. $BPSK_0$ and $BPSK_1$ are the secondary constellation schemes given by $BPSK_0 = \{\pm 1\}$ and $BPSK_1 = \{\pm j\}$. In this version of ESM there are 16 total combinations, where the first 4 combinations are same as that of SM where one antenna is active. There are 6 cases where double antennas are

activated at a time and symbols are transmitted according to one of the secondary constellation scheme $BPSK_0$ while the next 6 cases correspond to the secondary constellation scheme $BPSK_1$. The detailed combination is described by means of Table 3.8. T_1, T_2, T_3 and T_4 denote the four antenna and the different combinations of active antenna are denoted by P_n where $n = 1, 2, ..., T_x^2$. Thus this version of ESM can yield a spectral efficiency of 6 bpcu.

Table 3.8: ESM with $T_x = 4$ and $\eta_{ESM} = 6$ *bpcu*

	T_1	T_2	T_3	T_4
P_1	QPSK	0	0	0
P_2	0	QPSK	0	0
P_3	0	0	QPSK	0
P_4	0	0	0	QPSK
P_5	$BPSK_0$	$BPSK_0$	0	0
P_6	$BPSK_0$	0	$BPSK_0$	0
P_7	$BPSK_0$	0	0	$BPSK_0$
P_8	0	$BPSK_0$	$BPSK_0$	0
P_{10}	0	0	$BPSK_0$	$BPSK_0$
P_{11}	$BPSK_1$	$BPSK_1$	0	0
P_{12}	$BPSK_1$	0	$BPSK_1$	0
P_{13}	$BPSK_1$	0	0	$BPSK_1$
P_{14}	0	$BPSK_1$	$BPSK_1$	0
P_{15}	0	$BPSK_1$	0	$BPSK_1$
P_{16}	0	0	$BPSK_1$	$BPSK_1$

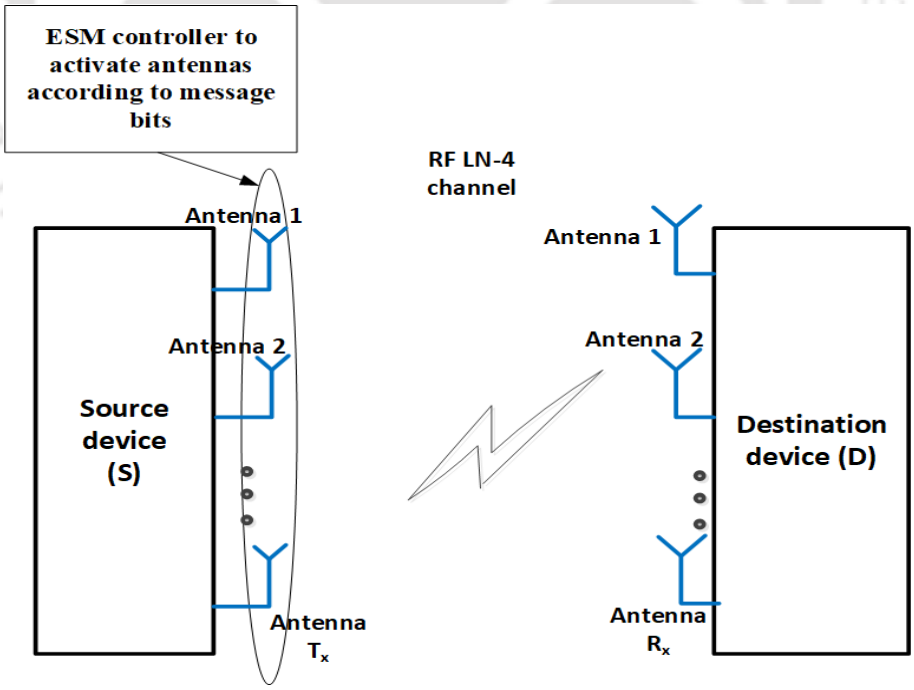

Figure 3.12: Proposed system model for ESM

In ESM, the single RF chain constraint of SM is relaxed because depending on the message bits, double antenna may be activated. The single antenna activation process is same as that of SM with a

single RF chain being activated. The RF chain comprises of source encoders and modulators. In case of double antenna activation, the source data is split and RF signal is modulated by source data according to the secondary constellation schemes for each antenna. A switch is used to connect the RF chains with the corresponding antenna to be activated. Similarly at the receiver, the antenna is used for reception and the receive RF chain comprises of demodulators to retrieve the initial data. Maximum likelihood (ML) decoding is used at the receiver to estimate the antenna index used for transmission. A MIMO system operating over BAN channels is considered for analysis in Fig. 3.12. Let there be T_x antennas at the transmitting node, and R_x antennas at the receiving node. The received symbol vector may be written as:

$$\mathbf{y} = \sqrt{\gamma}\mathbf{H}\mathbf{s} + \mathbf{n} \ , \tag{3.19}$$

where $\mathbf{H}$ is the R_x x T_x channel matrix, γ represents SNR at receiver. Elements of $\mathbf{H}$ are independent and identically distributed (i.i.d.) random variables. Envelope of each element follows LN-4 distribution as in Eq. (3.1). $\mathbf{s}$ is the T_x x 1 transmit symbol vector having unit energy, i.e., $\mathbb{E}[\mathbf{s}^H\mathbf{s}] = 1$, $\mathbf{s} = \mathbf{x}/\sqrt{E}$ and $\mathbb{E}[\mathbf{x}^H\mathbf{x}] = E$. $\mathbf{n}$ is the R_x x 1 noise vector. E denotes symbol vector energy. $\mathbb{E}$ is the expectation operator. Noise is modelled as additive white Gaussian noise (AWGN) which follows i.i.d. Gaussian distribution, having zero mean and variance N_0. In ESM, either single or double transmit antennas are active at a time, which means that $\mathbf{x}$ contains 1 or 2 non-zero entries.

3.9 SMBM for BAN Communication

SM can be mixed with other techniques like Media Based Modulation (MBM) [86, 87, 88, 89, 90] to enhance the spectral efficiency of BAN communication. SMBM is a comparatively new technique which involves changing of RF properties near the transmitting antenna for creating different channel perturbations. These perturbations can be achieved by changing extrinsic properties such as permeability, resistivity or permittivity near the transmitting antenna. RF mirrors [87] are used to create distinct channel perturbations called Mirror Activation Patterns (MAP). However, the number of RF mirrors that can be used for single antenna is limited because of the excess use of pilot signals for training which requires excessive use of resources and system becomes prone to channel time variation [91].

SMBM system model as shown in Fig. 3.13 has m_f RF mirrors at each transmit antenna. $T_x \times R_x$ MIMO system is analysed for M-ary Quadrature Amplitude Modulation (M-QAM) scheme. The information bits in SMBM are divided into bit-stream of size η_{SMBM} where $\eta_{SMBM} = \log_2 MT_x + m_f$. The information is divided into three units i.e. m_f, T_x and M. m_f bits are used for m^{th} MAP, $m \in [1 : M_f]$ where $M_f = 2^{m_f}$. $\log_2 T_x$ bits are used for antenna activation with index j where $j \in [1 : T_x]$. $\log_2 M$ bits are used for selection of a symbol x_l from signal constellation where $l \in [1 : M]$.

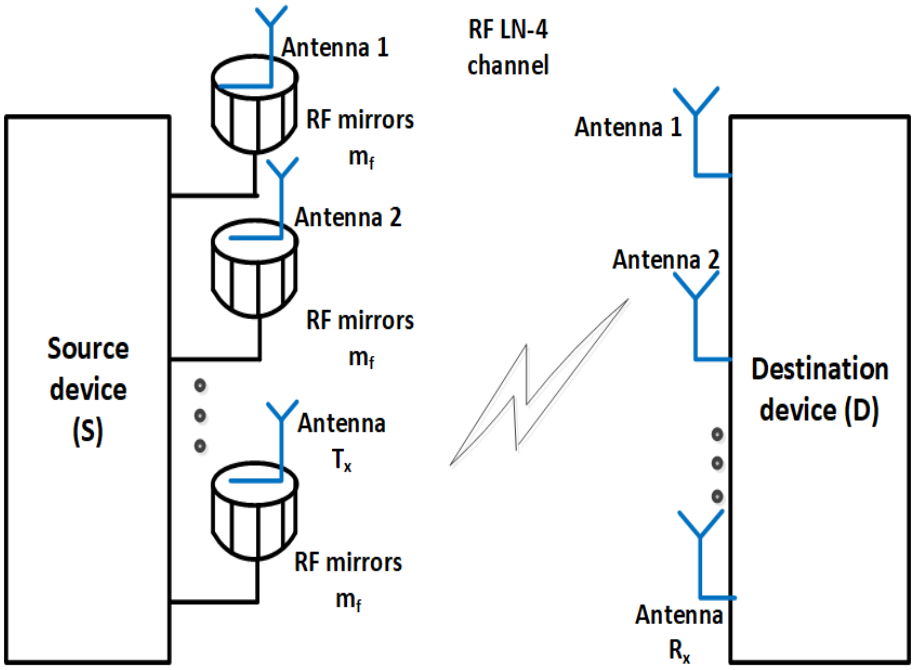

Figure 3.13: Proposed system model for SMBM

The SMBM system's channel matrix $\mathbf{H}$ has elements which are i.i.d. random variable (RV), where the envelope of each element follows LN-4 mixture distribution. The received signal vector $(R_x \times 1)$, $\mathbf{y} = [y_1\ y_2\ \ldots\ y_{R_x}]^T$ is given as [86]:

$$\mathbf{y} = \sqrt{\gamma}\,\mathbf{H}_j x_l^j\,\mathbf{e}_m + \mathbf{n}, \tag{3.20}$$

where x_l^j is l^{th} symbol of M-QAM constellation to be transmitted by j^{th} transmit antenna, $\mathbf{e}_m$ is an $M_f \times 1$ vector whose only m^{th} element is 1. Vector $\mathbf{n}$ is an $R_x \times 1$ AWGN vector with entries as i.i.d. Gaussian RV with zero mean and variance N_0.

In SMBM, only one RF chain is used at the transmitter which saves the cost of multiple RF chains being used simultaneously as in other MIMO techniques. The RF chain comprises of modulators, source encoders, etc. The RF signal is modulated with source data which is transmitted into free space by the antenna. A RF switch is used to connect the single RF chain to the particular antenna according to the message bit. The mirror activation pattern activated helps in creating a distinct channel scatterer resulting in transmission of signal through that particular channel. At the receiver, ML algorithm is used to decode the index of the MAP and antenna used. The signal is demodulated to retrieve the initial data. The ML decoding at the receiver is done according to the following equation:

$$[\hat{l}, \hat{j}, \hat{m}] = \underset{\substack{l\in[1:M], j\in[1:T_x] \\ m\in[1:M_f]}}{\operatorname{argmin}} \left(\|\mathbf{y} - \sqrt{\gamma}\mathbf{H}_j \mathbf{x}_l^j e_m\|_F^2 \right), \tag{3.21}$$

where $\hat{l}, \hat{j}, \hat{m}$ are the estimated indices of the transmitted symbol, transmit antenna and activated MAP

respectively. $\|\cdot\|_F^2$ is the Frobenius norm.

MAP, created by RF mirrors, is the status of RF mirrors (ON or OFF) placed near the transmit antenna. These MAPs increase spectral efficiency of MBM linearly against the logarithmic increase in SM as $\eta_{SM}= \log_2 MT_x$. This is one of the key advantages of using RF mirrors. Implementation of a MBM transmit unit consisting of $m_f = 14$ RF mirrors placed in a compact cylindrical structure having dipole transmit antenna placed at centre of the cylindrical structure has been reported in [91]. A single-input multiple-output (SIMO) with RF mirrors was simulated in [88]. The results show SIMO-MBM gives better result compared to that of traditional SIMO system. An example of output pattern of SMBM switch controller is illustrated in Table 3.9 where $T_x = 4, m_f = 2, M = 4$. Depending on the message bit value, the particular mirror surrounding the particular antenna is activated and the symbol is transmitted using M-ary modulation scheme.

Table 3.9: Output of SMBM switch controller

Message bits	Symbol (x_l)	Antenna (j)	MAP (m)
000101	-1-i	2	2
010010	-1+i	1	3
101000	1-i	3	1
111111	1+i	4	4

3.10 Performance Analysis of MIMO BAN Communication using LN-4 Distribution

The LN-4 channel model is used for SM, ESM and SMBM BAN communication. Channel model, measurement procedure and BMI categories are same as defined earlier. The challenging task in the error analysis of MIMO based communication is the channel matrix which is not a scalar quantity anymore like it was in SISO. The BER needs to be evaluated by using the concept of pairwise error probability. The readers may note that achieving closed form expressions for the same is a difficult task due to the nature of LN-4 distribution and the difficulty in finding expectation over the channel PDF (the channel being a matrix now). Let us start the error analysis with pairwise error probability concept first.

At the receiver for SM, ESM and SMBM, an estimate of the transmit symbol vector is computed by using maximum likelihood (ML) detection as follows:

$$\hat{\mathbf{s}} = \arg\min_{\mathbf{s}\in\mathbb{S}} \|\mathbf{y} - \mathbf{Hs}\|^2, \tag{3.22}$$

where $\mathbb{S}$ is the set of normalized transmit symbol vectors. Each scheme - SM, ESM and SMBM - has its own predefined set $\mathbb{S}$, containing all the symbol vectors for that particular scheme. Pairwise error

probability (PEP) is the probability of symbol vector $\mathbf{s}$ being decoded as $\mathbf{s}'$. The union bound for average BER (ABER) is given by [85] :

$$ABER \leq \frac{1}{|\mathbb{S}|\log_2(|\mathbb{S}|)} \sum_{\mathbf{s}\in\mathbb{S}} \sum_{\mathbf{s}'\in\mathbb{S}} n(\mathbf{s}\rightarrow\mathbf{s}')PEP(\mathbf{s}\rightarrow\mathbf{s}'). \tag{3.23}$$

where $n(\mathbf{s}\rightarrow\mathbf{s}')$ is the number of bit errors that occur when $\mathbf{s}$ is decoded as $\mathbf{s}'$. $|\mathbb{S}|= T_xM$ for SM, T_x^2M for ESM and T_xMM_f for SMBM. Therefore to calculate BER of any scheme, the PEP needs to be calculated first. The set of symbol vectors for a particular scheme needs to be known. The challenging aspect of this equation is that it can only be solved when the symbol vector set is known and for that one has to know the working of the particular scheme in order to generate the symbol vector according to a particular modulation scheme. PEP is calculated as:

$$\begin{aligned} PEP(\mathbf{s}\rightarrow\mathbf{s}') &= \mathbb{E}_{\mathbf{H}}\left[\mathcal{Q}\left(\sqrt{\frac{\|\mathbf{Hs}-\mathbf{Hs}'\|^2}{2N_0}}\right)\right] \\ &= \mathbb{E}_{\mathbf{H}}\left[\mathcal{Q}\left(\sqrt{\frac{\gamma_{s-s'}}{2N_0}}\right)\right] \\ &= \sum_{k=1}^{4} w_k \int_0^{\infty} \mathcal{Q}\left(\sqrt{\frac{\gamma_{s-s'}}{2N_0}}\right) f_{\gamma_{s-s'}}(\gamma_{s-s'})d\gamma_{s-s'} \\ &= \sum_{k=1}^{4} w_k \int_0^{\infty} \frac{1}{2\sqrt{\pi}} G_{1,2}^{2,0}\left(\begin{matrix}1\\0,1/2\end{matrix}\middle|\frac{\gamma_{s-s'}}{4N_0}\right) f_{\gamma_{s-s'}}(\gamma_{s-s'})d\gamma_{s-s'} \quad . \end{aligned} \tag{3.24}$$

where $\gamma_{s-s'} = \|\mathbf{Hs}-\mathbf{Hs}'\|^2$, $G_{p,q}^{m,n}(:|\ z)$ denotes the Meijer G function [47]. In the above expression Q function is expressed in terms of Meijer G function as shown earlier. $f_{\gamma_{s-s'}}(\gamma_{s-s'})$ is the PDF following LN-4 distribution. The above expression contains intractable integrals and deriving closed form expressions is not possible. Hence, MG distribution is used to approximate the PDF of the random variable $\gamma_{s-s'}$.

3.11 Performance Analysis of MIMO BAN Communication using MG Distribution

Our goal is to achieve closed form expressions of PEP which will make the expression tractable and make it easier for further analysis. For this purpose, LN-4 distribution can be approximated by MG distribution as described earlier. The parameters (μ_k^{lg}, σ_k^2 and w_k) of LN-4 distribution for running and cycling activities under two different scenarios in case of BMI1 category are listed in Table 3.2 and 3.3. The terms of MG distribution and LN-4 distribution have been defined earlier. The PDF $f_{\gamma_{s-s'}}(\gamma_{s-s'})$ can be approximated by MG distribution. First the lognormal distribution is approximated with Eq. (3.8) and then summed up over the 4 components of LN-4 distribution. The PEP, after this approximation,

is written in closed form as:

$$
\begin{aligned}
&PEP(\mathbf{s}\to\mathbf{s}') \\
&= \sum_{k=1}^{4} w_k \int_0^{\infty} \frac{1}{2\sqrt{\pi}} G_{1,2}^{2,0}\left({}^{1}_{0,1/2} \,\middle|\, \frac{\gamma_{s-s'}}{4N_0}\right) \sum_{i=1}^{n} P_{k,i} \frac{(\gamma_{s-s'})^{\alpha_{k,i}^{MG}-1}(\beta_{k,i}^{MG})^{\alpha_{k,i}^{MG}}}{\Gamma(\alpha_{k,i}^{MG})(\|\mathbf{s}-\mathbf{s}'\|^2)^{\alpha_{k,i}^{MG}-1}} \exp\left(\frac{-\beta_{k,i}^{MG}\gamma_{s-s'}}{\|\mathbf{s}-\mathbf{s}'\|^2}\right) d\gamma_{s-s'} \\
&= \sum_{k=1}^{4} w_k \sum_{i=1}^{n} \frac{P_{k,i}(\beta_{k,i}^{MG})^{\alpha_{k,i}^{MG}}(\|\mathbf{s}-\mathbf{s}'\|^2)^{-\alpha_{k,i}^{MG}+1}}{2\sqrt{\pi}\Gamma(\alpha_{k,i}^{MG})} \\
&\times \int_0^{\infty} (\gamma_{s-s'})^{\alpha_{k,i}^{MG}-1} G_{0,1}^{1,0}\left({}^{-}_{0} \,\middle|\, \frac{\beta_{k,i}^{MG}\gamma_{s-s'}}{\|\mathbf{s}-\mathbf{s}'\|^2}\right) G_{1,2}^{2,0}\left({}^{1}_{0,1/2} \,\middle|\, \frac{\gamma_{s-s'}}{4N_0}\right) d\gamma_{s-s'} \\
&= \sum_{k=1}^{4} w_k \sum_{i=1}^{n} \frac{P_{k,i}(\|\mathbf{s}-\mathbf{s}'\|^2)}{2\sqrt{\pi}\Gamma(\alpha_{k,i}^{MG})} G_{2,2}^{2,1}\left({}^{1-\alpha_{k,i}^{MG},1}_{0,1/2} \,\middle|\, \frac{\|\mathbf{s}-\mathbf{s}'\|^2}{4N_0\beta_{k,i}^{MG}}\right) \qquad (3.25)
\end{aligned}
$$

Some steps should be followed while deriving the above formula. The exponential function needs to be written in terms of Meijer G function. Then on rearranging the terms, and with some algebraic manipulations, the equation can be expressed as the integration of the product of two Meijer G functions and a variable. The following formulae are used [46, 47, 48]:

$$
e^{-z} = G_{0,1}^{1,0}\left({}^{-}_{0} \,\middle|\, z\right) . \qquad (3.26)
$$

$$
\begin{aligned}
&\int_0^{\infty} \tau^{\alpha-1} G_{u,v}^{s,t}\left({}^{c_1,\ldots,c_t,c_{t+1},\ldots,c_u}_{d_1,\ldots,d_s,d_{s+1},..d_v} \,\middle|\, \tau w\right) G_{p,q}^{m,n}\left({}^{a_1,\ldots,a_n,a_{n+1},\ldots,a_p}_{b_1,\ldots,b_m,b_{m+1},\ldots,b_q} \,\middle|\, \tau z\right) d\tau \\
&= w^{-\alpha} G_{v+p,u+q}^{m+t,n+s}\left({}^{a_1,.,a_n,1-\alpha-d_1,..,1-\alpha-d_s,a_{n+1},.,a_p}_{b_1,.,b_m,1-\alpha-c_1,\ldots,1-\alpha-c_t,b_{m+1},..,b_q} \,\middle|\, \frac{z}{w}\right) . \qquad (3.27)
\end{aligned}
$$

Average bit error rate (ABER) is calculated by Eq. (3.23). Thus PEP and ABER can be written in closed form in terms of Meijer G function which was not possible using LN-4 distribution.

3.12 Asymptotic Analysis of MIMO BAN Communication

To calculate the diversity and coding gain of MIMO BAN systems, asymptotic analysis is required. For this purpose, the argument in Meijer G function can be expressed in a different form for high SNR values, as given in Eq. (41) of [63]. Hence the PEP is written as:

$$
P_e^{asym} \approx \sum_{k=1}^{4} w_k \sum_{i=1}^{n} \frac{P_{k,i}(\|\mathbf{s}-\mathbf{s}'\|^2)}{2\sqrt{\pi}\Gamma(\alpha_{k,i}^{MG})} \sum_{m=1}^{1} \left(\frac{\|\mathbf{s}-\mathbf{s}'\|^2}{4N_0\beta_{k,i}^{MG}}\right)^{c_m-1} \frac{\prod_{l=1}^{2}\Gamma(1+d_l-c_k)}{\prod_{l=2}^{2}\Gamma(1+c_l-c_m)} , \qquad (3.28)
$$

where $c = [1-\alpha_{k,i}^{MG}, 1]$ and $d = [0, 1/2]$. In this case let SNR $\bar{\gamma}$ be equal to $(\|\mathbf{s}-\mathbf{s}'\|^2)$. The maximum value of SNR will only be obtained when the highest component of SNR is calculated for maximum value of $\alpha_{k,i}^{MG}$. Thus the highest component of SNR is again given as $1-\max(\alpha_{k,i}^{MG})$. Now using Eq. (3.17),

diversity gain is given by $D_g = \max(\alpha_{k,i}^{MG}) - 1$. For coding gain, highest exponent of SNR is considered. The overall coding gain for ABER is given by:

$$C_g = \frac{1}{|\mathbb{S}|\log_2(|\mathbb{S}|)} n(\mathbf{s} \to \mathbf{s}') \left(\sum_{k=1}^{4} w_k \sum_{i=1}^{n} \frac{P_{k,i}}{2\sqrt{\pi}\Gamma(\alpha_{k,i}^{MG})} \left(\frac{1}{4N_0\beta_{k,i}^{MG}} \right)^{-\alpha_{k,i}^{MG}} \frac{\prod_{l=1}^{2}\Gamma(d_l + \alpha_{k,i}^{MG})}{\prod_{l=2}^{2}\Gamma(c_l + \alpha_{k,i}^{MG})} \right)^{\frac{1}{1-\alpha_{k,i}^{MG}}} . \tag{3.29}$$

3.13 Results

In this section, we will analyze the performance of our proposed methods for BAN communication and highlight how it is influenced by the behaviour of body movements under different situations. The system performance of SM, ESM and SMBM methods for BAN communication is illustrated by means by Fig. 3.14. Running and cycling results are compared for Scenario I BMI1 category in Fig. 3.14. It is evident that ESM performs better than SM while SMBM performs the best irrespective of activity and scenario. Similarly for Scenario II, all the methods- SM, ESM and SMBM are compared in Fig. 3.15 for running and cycling activities in BMI1 category. ESM performs better than SM while SMBM outperforms the other two methods. For SM running and cycling case, the values considered are $T_x = 4, R_x = 4, 16-QAM, \eta_{SE} = 6$. Here η_{SE} denotes spectral efficiency in bpcu (bits per channel use). For ESM running and cycling case, the parameters considered are $T_x = 4, R_x = 4, 4-QAM, \eta_{SE} = 6$ while for SMBM running and cycling case, the parameters considered are $T_x = 4, R_x = 4, 4-QAM, m_f = 2, \eta_{SE} = 6$. These parameters are valid for all figures unless mentioned explicitly. All the analysis is for BMI1 category unless stated explicitly.

It can be observed from both the graphs (Fig. 3.14 and 3.15) that SMBM performs better than SM and ESM. It can be noted that ESM and SMBM require only 4-QAM to achieve the same spectral efficiency as that of SM which uses 16-QAM. Higher modulation schemes mean the symbol vectors are closely packed, hence due to less distance between symbol vectors, probability of error is more. Thus SM performs the worst among the three methods. It can be noted that SMBM uses RF mirrors which creates more channel perturbations, thereby increasing the channel diversity. Another key point is that ESM has 2 RF chains and can activate one or two antennas depending on the message bits. On the other hand, SMBM has only one RF chain. Hence chances of inter-antenna interference is more in ESM, thereby resulting in poorer performance of ESM in comparison to SMBM.

The diversity gain can be calculated from BER vs SNR curve of Fig. 3.17. Assuming the case of ESM cycling in Scenario II and a range of 10 dB SNR (10-20 dB SNR), we get the BER value of 7×10^{-6} at 20 dB SNR and a BER value of 0.01 at 10 dB of SNR. Hence diversity gain is given as $\log_{10}(0.01/(7 \times 10^{-6})) = 3.15$. Similarly for SMBM cycling and considering SNR range of 8-18 dB,

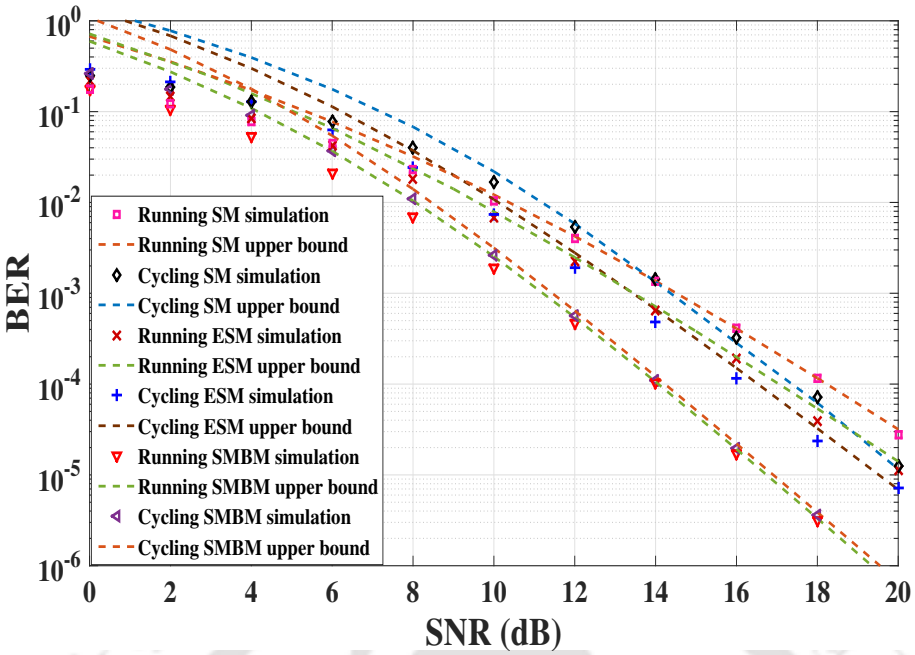

Figure 3.14: Performance analysis of various methods for Scenario I activities in BMI1 category.

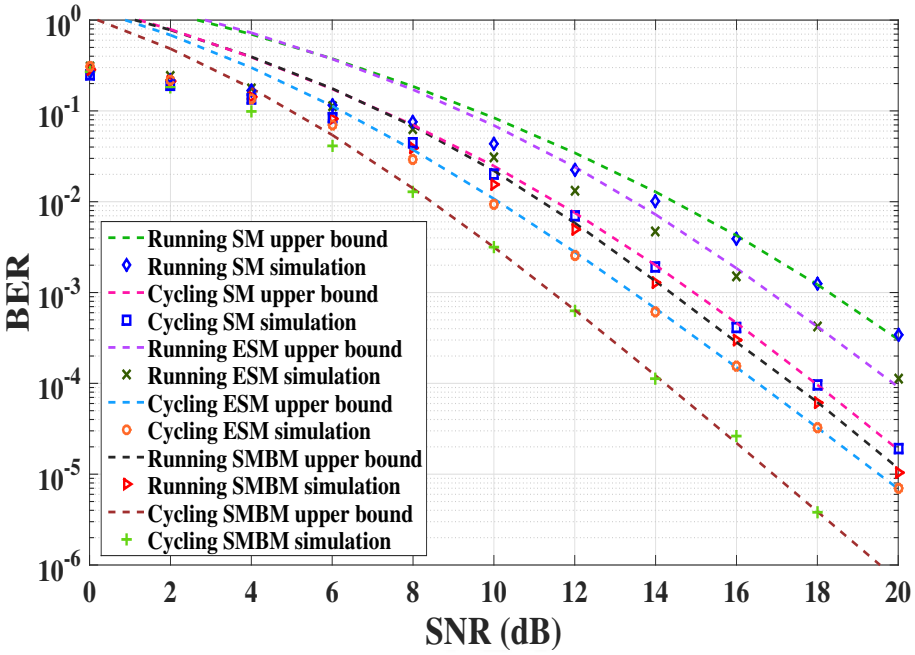

Figure 3.15: Performance analysis of various methods for Scenario II activities in BMI1 category.

diversity gain can be calculated as $\log_{10}(0.012/(4 \times 10^{-6})) = 3.44$. This can be theoretically validated also. The maximum $\alpha_{k,i}^{MG}$ parameter obtained for generating these results is 4.5 (as generated using EM algorithm). Thus theoretical diversity gain is given by $\alpha_{k-1}^{MG} - 1 = 4.5 - 1 = 3.5$. Theoretical and practical diversity gain values are almost same. Now if we observe the horizontal shift between ESM and SMBM cycling curves, we can observe that SMBM has a 2 dB of coding gain over ESM at SNR values of more than 10 dB, which indicates that SMBM has a SNR gain of at least 2 dB over ESM. Similarly

for running activities, if we compare the horizontal shift between ESM and SMBM curves, then we can observe that SMBM has a 2 dB of coding gain over ESM. The asymptotic results for Scenario II activities and different methods like ESM and SMBM, converge with the analytical and simulation results at high SNR values, thereby validating our asymptotic analysis.

Coding gain can be observed for Scenario I activities in Fig. 3.16. In this figure, the asymptotic results for Scenario I activities and different methods like ESM and SMBM, are plotted. It can be noticed that the asymptotic results converge with the analytical and simulation results at high SNR values, thereby justifying our asymptotic analysis. Coding gain of running SMBM over running ESM is computed by considering the horizontal shift between the two curves. The shift is at least 2 dB for any SNR values of more than 10 dB. Similarly cycling SMBM achieves a coding gain of at least 2 dB over cycling ESM at high SNR values of more than 10 dB.

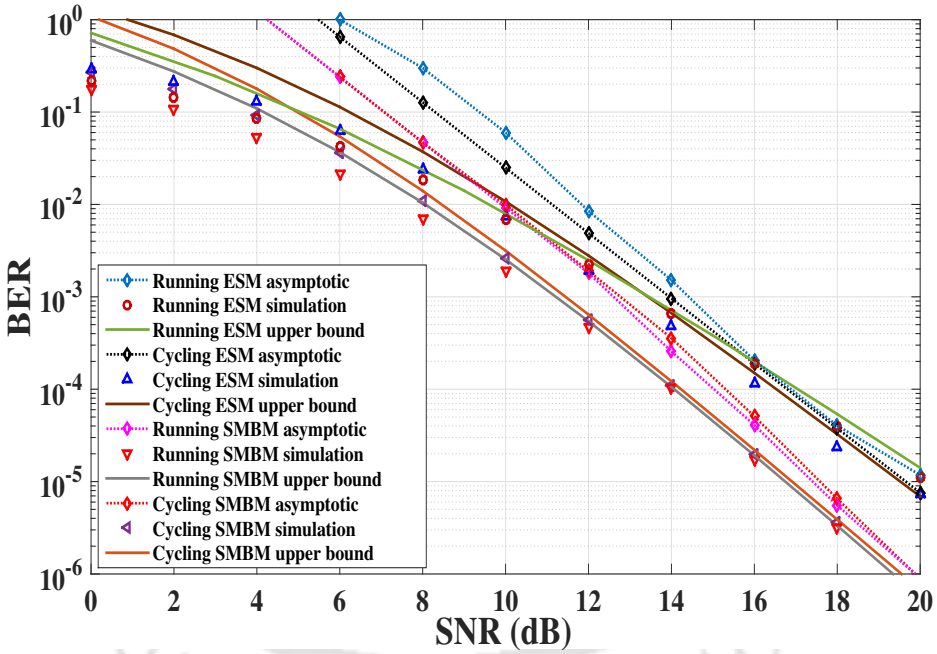

Figure 3.16: Analysis of ESM and SMBM results for Scenario I in BMI1 category.

Since it is evident from BMI1 analysis that Scenario II yields distinct results between running and cycling, hence we have provided figures only for Scenario II activities for other BMI categories. For BMI2 and BMI3 category, running and cycling activities for Scenario II are compared for ESM and SMBM methods. The analytical upper bounds are verified by simulation results in Fig. 3.18 for BMI2 and in Fig. 3.19 for BMI3 [92]. It is observed that SMBM method yields superior results as compared to ESM for any BMI category considering a value of 6 bpcu spectral efficiency with 4 transmit and receive antennas each. This is due to the fact that SMBM uses RF mirrors to create more channel perturbations. To generate the same number of channel perturbations as that of SMBM, ESM will require more number of

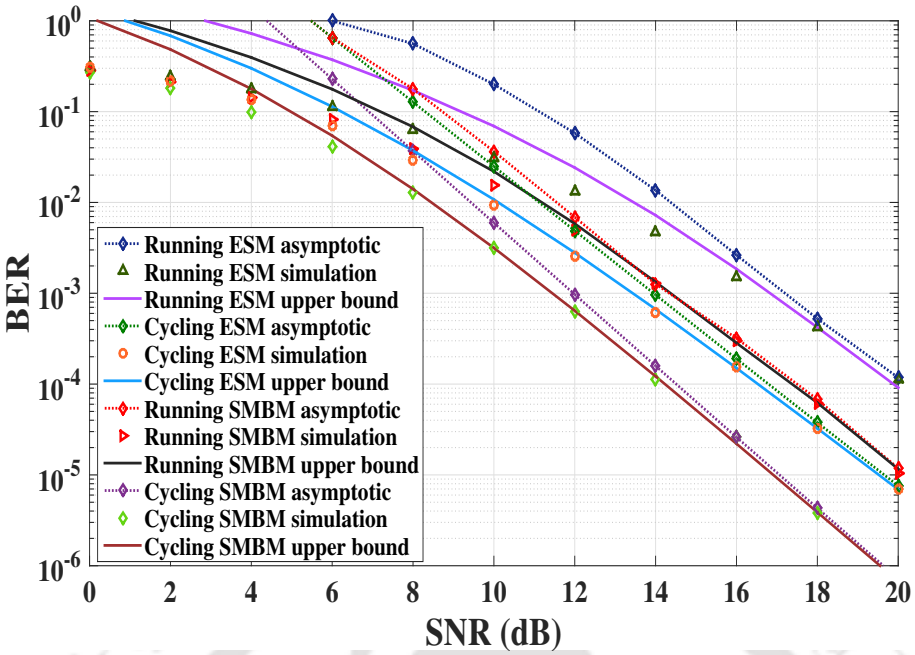

Figure 3.17: Analysis of ESM and SMBM results for Scenario II in BMI1 category.

transmit antennas or higher modulation scheme which will lead to degradation of performance in ESM. Due to presence of more RF chains in ESM as explained earlier, ESM will suffer from more inter-antenna interference than SMBM. SMBM can select the best link out of the multiple channels available depending on value of message bits. All these facts point out to the inference that SMBM can perform better than ESM for any activities under any scenario.

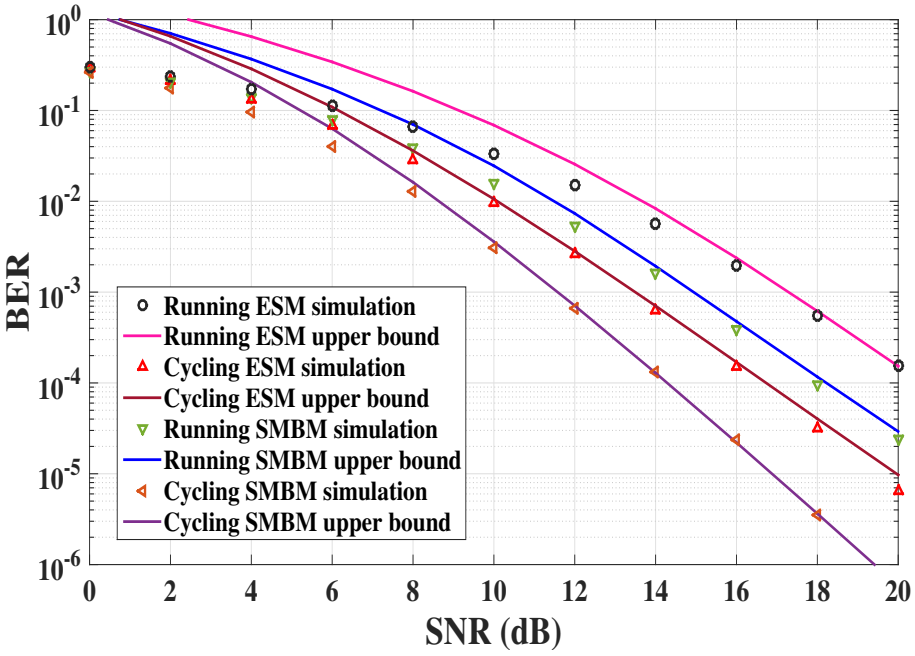

Figure 3.18: BER results of ESM and SMBM for Scenario II BMI2 category.

Now let us analyze the results obtained till now in a physical aspect. The results differ for various

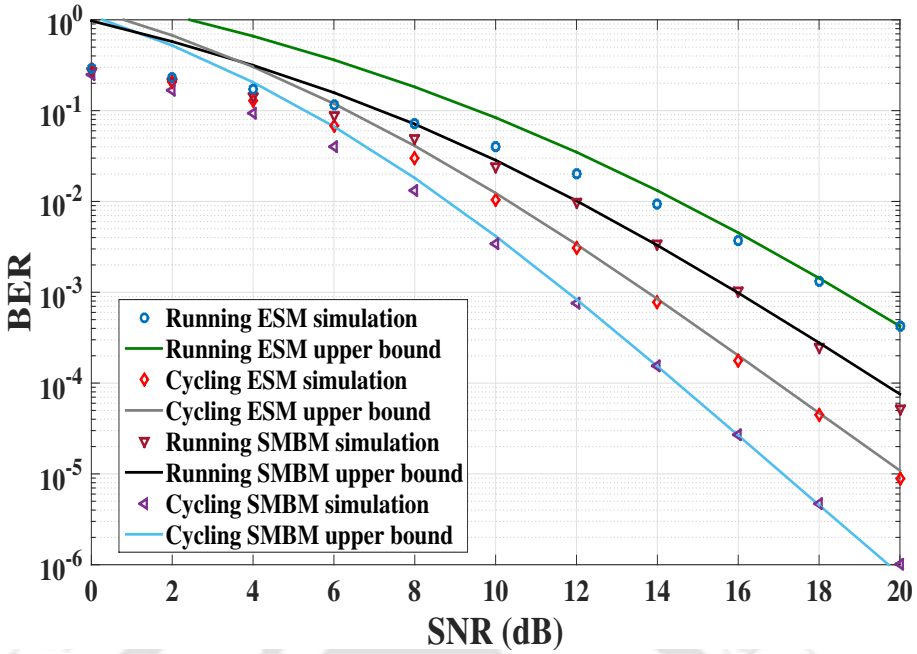

Figure 3.19: BER results of ESM and SMBM for Scenario II BMI3 category.

scenarios and various activities due to different body postures and body movements. As seen in the case of SISO BAN communication, the upper body remains relatively constant for cycling while in case of running, both the upper and lower body parts are in oscillatory motion. Running activity has more body shadowing effect since more scattering clusters are present in running, as a result of which running generates inferior performance than cycling irrespective of BMI category. Out of the two scenarios, Scenario II running performs the worst because in case of side-by-side running, the body comes in the way of signal transmission which results in more body shadowing effect. While in case of Scenario I running, there is no body obstruction for signal transmission as the test subjects are behind one another and the devices are attached to the arms. For cycling Scenario I and II, the upper body remains relatively constant, thereby the body shadowing effect is relatively same for both cases. Since the arms of the test subjects are outstretched in case of cycling for both scenarios, hence the body shadowing effect is same for both scenarios as signal transmission is not hindered by body obstruction. Consequently, the BMI variation does not influence the results in cycling, hence the cycling results across BMI categories are relatively close. This is attributed to the fact that body obstruction does not hinder the signal transmission in case of cycling. Since all cases are MIMO transmission, hence receiver diversity nullifies the channel condition to yield relatively same results for cycling activities across all BMI categories and scenarios. Receiver diversity was absent in SISO case, thereby resulting in distinct results for different BMI categories in cycling. Meanwhile in running Scenario II, body shadowing plays a key role in effective signal transmission. Thus with an increase in BMI value the performance deteriorates. The BMI value

increase means the body is either heavier or larger due to more weight or higher height values. This causes more body shadowing effect, thereby hindering signal propagation. Due to the absence of receiver and transmit diversity in SISO case, the results of running and cycling were distinct across different BMI categories [93]. The overall conclusion from all the results is that SMBM performs the best across all BMI categories, activities and scenarios.

To understand the performance improvement of SMBM over ESM and SM, let us tabulate the results for a particular scenario and BMI category. It is evident from Table 3.10 that SMBM outperforms SM and ESM for running and cycling activities in Scenario II BMI1 case. The SNR values needed to achieve different target BER values are compared for different methods for Scenario II BMI1 case. It can be observed that SMBM has a SNR gain of at least 2.5 dB over ESM and 3.5 dB over SM for running activities, while for cycling activities SMBM has a SNR gain of around 2 dB over ESM and 4 dB over SM.

Table 3.10: Comparison of BER for Scenario II BMI1 activities.

BER	SNR for various methods (in dB)					
	SM running	SM cycling	ESM running	ESM cycling	SMBM running	SMBM cycling
0.001	18	15	17	13	14	11
0.0001	21	18	20	16	17.5	14
0.00001	24.5	21	23	19	20	16

The results of SM, ESM and SMBM are compared with the results of SISO case for BAN communication [93] of Scenario II BMI1 category, using the same LN-4 channel. It can be observed from Fig. 3.20 that our proposed methods ESM and SMBM outperform the SISO results (using BPSK) for running and cycling cases. For SISO, BPSK modulation can offer the best performance. For 4-QAM or 16-QAM, SISO will offer worse BER, hence it is justified that ESM and SMBM convincingly outperform SISO results at higher SNR values. At lower values of SNR, SISO is giving better results than ESM and SMBM in some cases because we are comparing BPSK SISO with 4-QAM ESM and SMBM. From a physical point of view, the reasoning behind SISO BAN communication yielding poorer performance has been explained earlier. An interesting fact to note is that SISO can yield better results than MIMO based BAN communication for lower SNR values. This is because for lower SNR values (where noise power is less), SISO communication is able to perform better as the signal propagation can take place despite the body hindrance while doing side-by-side running and cycling. However as the SNR increases (noise power becomes more), the body hindrance causes performance in SISO communication to become poorer. While in case of MIMO techniques, the receiver diversity is able to continue the communication in a reliable manner, resulting in better results for SM, ESM and SMBM as compared to SISO results.

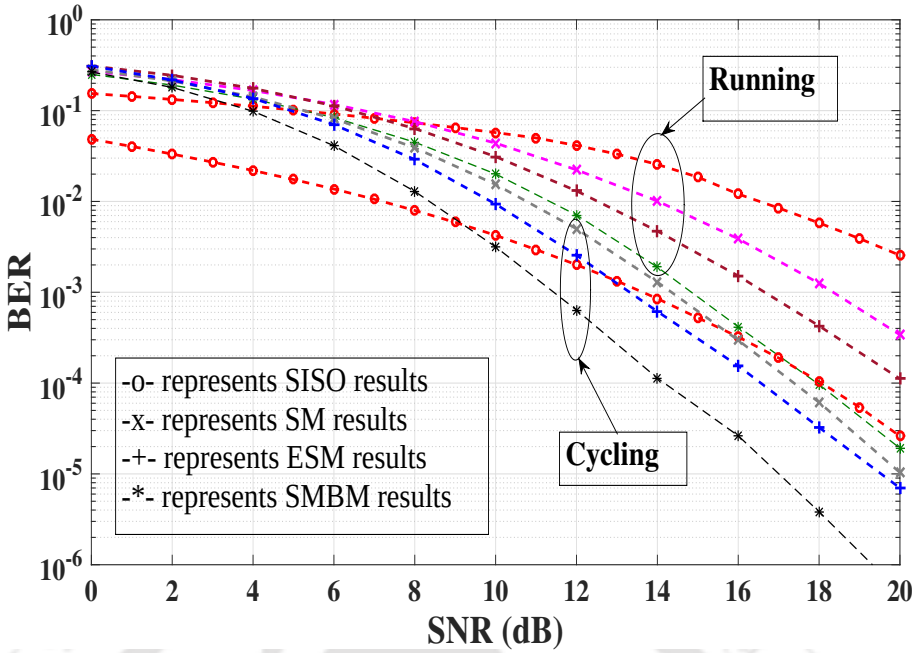

Figure 3.20: BER comparison with existing methods

The variation of various parameters for system performance implementing SMBM is explored in Fig. 3.21. The analysis is conducted for Scenario II cycling as that particular case yields the best results for any BMI category. Parameters like T_x, m_f, QAM and spectral efficiency (η_{SE}) are varied to explore their impact on system performance. The cases are mentioned in the figure only. In the figures, $(T_x, R_x, M, m_f, \eta_{SE})$ and (T_x, R_x, M, η_{SE}) conventions are used to denote the values of parameters for SMBM and ESM respectively. It is observed that as the number of transmit antenna increases, the system performance degrades. This is due to the fact that as the number of antenna increases, there is higher chance of inter-antenna interference resulting in poorer performance. It can be seen that as the number of mirrors increases, the performance degrades as the scattering environment increases with increase in number of RF mirrors. The effect of constellation scheme on system performance is investigated by considering 4-QAM and 16-QAM. With increase in constellation size, system performance degrades. This is due to the fact that the symbol points become closer as constellation size increases leading to more chances of error. All the analytical upper bounds are plotted using 5-MG approximation (Eq. (3.25)). The upper bounds are validated by means of Monte Carlo simulations. The simulation results are in close agreement to the upper bounds at high values of SNR thereby justifying our analysis. All these analyses are conducted for Scenario II cycling for BMI1 category.

Similarly, variation of parameters for system performance implementing ESM is investigated in Fig. 3.22. It is observed that system performance similarly improves with decrease in number of transmit antennas, number of RF mirrors and constellation size. As the constellation size decreases, then symbol

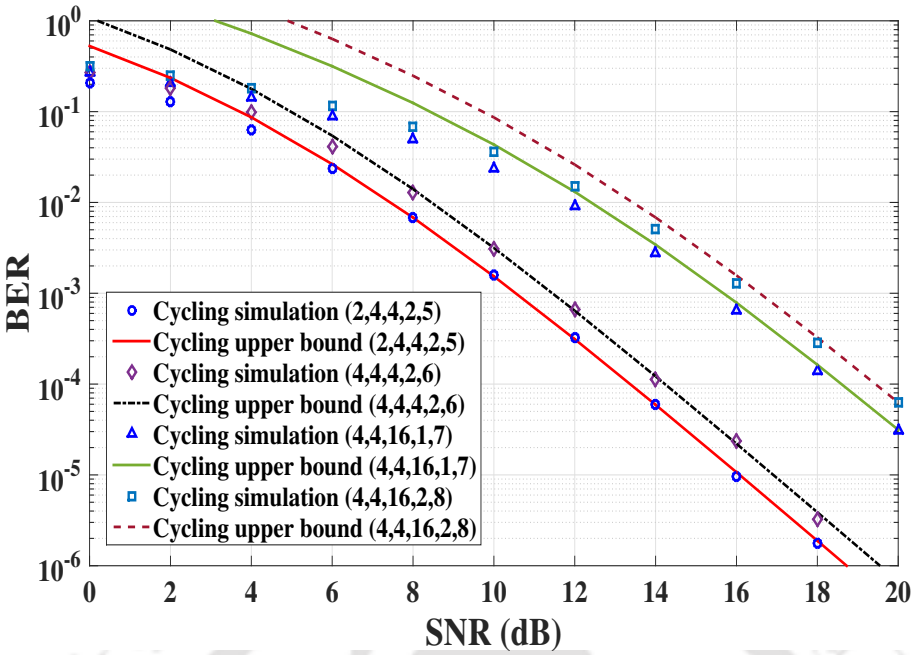

Figure 3.21: Effect of parameters on SMBM performance for cycling Scenario II.

spacing increases leading to lesser chances of error. Lesser number of antenna and RF mirrors means lesser interference, thereby giving better performance. It is also observed that as the spectral efficiency value increases, the system performance degrades. This is attributed to the fact that more bits are required to achieve higher spectral efficiencies. The simulation results are in close agreement to the upper bounds at high values of SNR thereby justifying our analysis. This analysis is conducted for Scenario II cycling for BMI1 category.

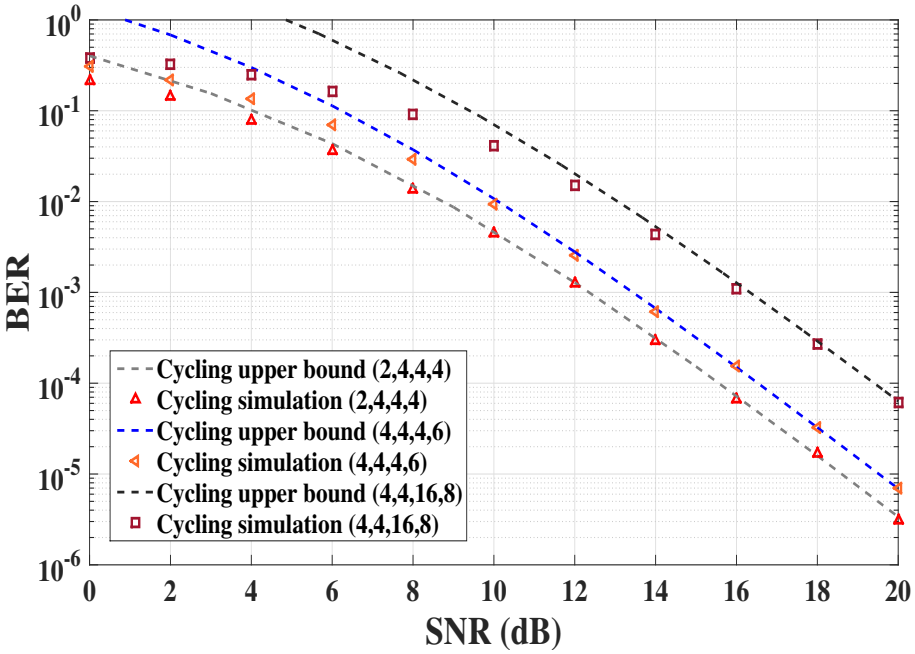

Figure 3.22: Effect of parameters on ESM performance for cycling Scenario II.

3.14 Conclusion

To enhance the spectral efficiency of MIMO based BAN communication, two new methods- ESM and SMBM have been proposed in this chapter. These methods can achieve a higher spectral efficiency than SM by using less number of transmit sources and lower modulation scheme. ESM and SMBM also yield better performance than SISO BAN communication. In this chapter, the performance analysis of SISO and MIMO BAN communication have been analysed for running and cycling activities in various scenarios for different BMI categories of individuals. Cycling performs better than running because of less body shadowing effect. In future, this work can be extended to BAN cooperative communication along with advanced versions of SM.

4. Optical Spatial Modulation for Free-Space Optical Communication

In the last few chapters, we have seen the implementation of SM in RF communication. In this chapter, the concept of spatial modulation in FSO communication is investigated to overcome the limitations of RF communication. The basic concepts of FSO communication have been provided in Chapter 1. Considering the phenomenon occurring in FSO communication, the modulation schemes and channel models in FSO communication are described in Section 4.1 and 4.2 respectively. The remainder of the chapter is broadly divided into three major categories. The first major contribution (Section 4.3) deals with derivation of closed form expressions of outage probability bounds for the system, where OSM along with PLNC is applied for bidirectional FSO cooperative communication. The next part (Section 4.4) tries to resolve the drawbacks of conventional OSM technique by proposing new schemes like transmit laser selection (TLS), and a mixture of TLS and OSM for FSO cooperative communication. Outage probability and ASEP closed form expressions are derived for such ASM schemes. Subsequently, Section 4.5 deals with BER, cost and power consumption analysis of advanced OSM schemes like OGSM, OESM and OIQSM, which aims to increase the spectral efficiency of OSM based FSO systems. It is shown through results that the proposed ASM schemes offer better BER performance than conventional OSM. The chapter ends with a conclusion in Section 4.6, where the key contributions of the chapter along with future work are highlighted.

4.1 Modulation Schemes in FSO Communication

In this section, we will justify the choice of modulation scheme for FSO communication. On-off keying (OOK), generally deployed as the modulation scheme in FSO systems, requires adaptive threshold to adapt to the atmospheric turbulence. Therefore, BPSK is preferred as the modulation scheme in our work for the following reasons [94]. After applying BPSK, the signal distribution remains similar for bits 1 and 0, irrespective of the presence or absence of turbulence. Bit 0 is modulated as -1 and bit 1 is modulated as +1 in BPSK, thereby source is transmitting data for both 0 and 1, whereas in OOK source is switched off in case of 0 bit and switched on for 1 bit. While decoding of bits, a threshold

mark has to be fixed for the signal power, above which the signal will be decoded as 1 and below which the signal will be decoded as 0. Since the signal shape in BPSK is similar for both bits 0 and 1, and are spaced equally on either side of the zero mark, hence the threshold position can be fixed at the zero mark for BPSK based system irrespective of the amount of turbulence. In FSO communication, the data is modulated onto a high frequency RF subcarrier signal by using BPSK modulation scheme, thereby shifting the frequency domain of the signal from the low frequency region to a much higher subcarrier frequency region. Due to the high frequency modulated signal, turbulence effect cannot have much impact, as a small shift in the high frequency regime would not change the signal centre frequency by a huge amount. While in case of OOK, the signal distribution is not distinctly spaced on either side of the zero mark and the signal pattern for both bits 0 and 1 are different. Depending on the nature of turbulence the signal pattern varies. Due to variable and unpredictable signal pattern, the threshold mark has to be decided depending on the value of signal power and the amount of turbulence. Also the signal power in case of OOK is concentrated at lower frequencies which makes it susceptible to be affected by turbulence. In BPSK the distance between the constellation points is also maximum among other M-ary modulation schemes, leading to least chances of error. Therefore, BPSK is more suitable than other M-ary modulation schemes.

4.2 Channel Models for FSO Communication

The channel is the primary obstacle in FSO communication systems. The outdoor environment is dynamic due to the presence of strong atmospheric turbulence (AT) [95]. Negative exponential, lognormal, K distribution, Gamma-Gamma (G-G), etc, are some of the channel models present in literature which consider the AT effect. Negative exponential can appropriately model high turbulence effects while lognormal distribution can model low turbulence effects accurately. Lognormal distribution is mainly valid for single scattering events which are predominantly prevalent in weak turbulence conditions. In strong turbulence conditions, multiple scattering occurs and hence lognormal distribution is not a good option for such conditions. When distance of propagation is less than few kilometers, amplitude variation of lognormal distribution is very small in comparison the phase variations. However over larger distances, when turbulences become more prominent, the amplitude variations can become comparable to the phase variations. FSO communication deals with large distances over several kilometers, thereby rendering lognormal distribution unsuitable. On the other hand, negative exponential fails for low turbulence conditions. G-G channel model on the other hand can model both weak and strong turbulence effects accurately [7].

According to the modified Rytov theory explained earlier in Chapter 1, the multiplicative effect of

two independent random processes can describe the irradiance process [96]. G-G channel model which is formed by the multiplicative effect of two Gamma functions satisfies this condition. Gamma function can suitably model both small-scale and large-scale fluctuations in the atmosphere, hence the product of two Gamma functions can accurately model the optical irradiance process. Generalized Malaga channel model [97] exists in literature, but fails to model all types of turbulence conditions accurately. However, the G-G model can satisfy all the atmospheric turbulence conditions. AT induced fading affects the optical signals, resulting in irradiance fluctuations in the received optical intensity. This phenomenon, known as scintillation is caused due to variations in atmospheric temperature, pressure and humidity, thereby resulting in fluctuations of refractive index. Such fading effects can be effectively modelled by a G-G channel model [98]. Hence G-G channel model is considered as the channel model for further analysis.

4.2.1 G-G Channel Model

To evaluate outage probability or BER, we require the PDF and CDF of the received SNR of the channel. Let the random variable $\varrho \geq 0$ be the signal envelope following G-G distribution as in Eq. (3) of [99], in Eq. (6) of [100] and in Eq. (6) of [101], then the PDF can be written as:

$$f_{\varrho}(\rho) = \frac{(\alpha_G \beta_G)^{(\frac{\alpha_G+\beta_G}{2})} \rho^{(\frac{\alpha_G+\beta G}{2}-1)}}{\Gamma(\alpha_G)\Gamma(\beta_G)} G_{0,2}^{2,0}\Big(\frac{}{\frac{\alpha_G-\beta_G}{2}, \frac{\beta_G-\alpha_G}{2}} \Big| \alpha_G \beta_G \ \rho \Big) \ , \tag{4.1}$$

where α_G and β_G are the effective number of large scale cells and effective number of small scale cells of the scattering process respectively. Γ denotes Gamma function. Meijer G function has been described in [47, 48]. Assuming planar wave propagation, the values of α_G and β_G can be adjusted from experimental data and written as in Eq. (4) of [99].

$$\alpha_G = \exp\left(\frac{0.49\sigma_l^2}{(1+1.11\sigma_l^{12/5})^{7/6}} - 1 \right)^{-1} . \tag{4.2}$$

$$\beta_G = \exp\left(\frac{0.51\sigma_l^2}{(1+0.69\sigma_l^{12/5})^{5/6}} - 1 \right)^{-1} . \tag{4.3}$$

Rytov variance σ_l^2 can be expressed as in Eq. (4) [99].

$$\sigma_l^2 = 1.23 C_n^2 K^{7/6} L^{11/6} \ , \tag{4.4}$$

where L=2, 6, 8 Km, K=$\frac{2\pi}{\lambda}$, λ=1550 nm, C_n^2 varies from 10^{-13} to 10^{-17} $m^{-2/3}$. Greater values of C_n^2 mean stronger turbulence, whereas lower values of C_n^2 mean weaker turbulence. Thus this parameter denotes the amount of turbulence. L represents link distance and λ is the wavelength. The CDF can be

written as:

$$F_{\varrho}(\rho) = \frac{(\alpha_G\beta_G)^{(\frac{\alpha_G+\beta_G}{2})}\rho^{(\frac{\alpha_G+\beta_G}{2})}}{\Gamma(\alpha_G)\Gamma(\beta_G)} \times \; G_{1,3}^{2,1}\left(\begin{matrix} 1-\frac{\alpha_G+\beta_G}{2} \\ \frac{\alpha_G-\beta_G}{2}, \frac{\beta_G-\alpha_G}{2}, -\frac{\alpha_G+\beta_G}{2} \end{matrix} \middle| \alpha_G\beta_G\ \rho \right) . \tag{4.5}$$

The following formula is used [46], (Eq. (26) of [102]):

$$\int_0^{\infty} z^{\alpha-1} G_{p,q}^{m,n}\left(\begin{matrix} a_1,a_2,\ldots,a_p \\ b_1,b_2,\ldots,b_q \end{matrix} \middle| zw \right) = z^{\alpha} G_{p+1,q+1}^{m,n+1}\left(\begin{matrix} 1-\alpha_1,a_1,\ldots,a_p \\ b_1,\ldots,b_q,-\alpha \end{matrix} \middle| zw \right) \tag{4.6}$$

Our objective is to find PDF and CDF of received SNR. Hence assume $\gamma = \rho^2$. Taking into account change in random variables, PDF of received SNR (γ) is calculated which is integrated to calculate the CDF:

$$F_{\gamma}(\gamma) = \frac{(\alpha_G\beta_G)^{(\frac{\alpha_G+\beta_G}{2})}\gamma^{(\frac{\alpha_G+\beta_G}{4})}}{\Gamma(\alpha_G)\Gamma(\beta_G)} \times \; G_{1,3}^{2,1}\left(\begin{matrix} 1-\frac{\alpha_G+\beta_G}{2} \\ \frac{\alpha_G-\beta_G}{2}, \frac{\beta_G-\alpha_G}{2}, -\frac{\alpha_G+\beta_G}{2} \end{matrix} \middle| \alpha_G\beta_G\gamma^{1/2} \right) . \tag{4.7}$$

Table 4.1 presents the value of turbulence parameters under different atmospheric conditions while Table 4.2 lists the value of the turbulence parameters for different link distances.

Table 4.1: Turbulence parameters for various atmospheric conditions

Turbulence region	α_G	β_G	σ_l^2
Strong	4.2	1.4	3.5
Moderate	4.0	1.9	1.6
Weak	11.6	10.1	0.2

Table 4.2: Turbulence parameters for various link distances

Link distance (Km)	α_G	β_G	σ_l^2
2	4.2	1.4	3.5
6	8.24	1.03	26.57
8	10.19	1.01	45.02

4.3 Optical Spatial Modulation for FSO Cooperative Communication

In Chapter 2, we have seen how SM along with PLNC can increase the efficiency of RF cooperative communication. On a similar vein, optical spatial modulation (OSM) for two way relaying in FSO cooperative systems can also enhance the system performance. OSM, the optical version of SM, has been explained earlier along with the benefits of OSM over MIMO and PLNC techniques in Chapter 1. FSO is primarily a LOS communication. Thus cooperative FSO communication is a necessity for long distance communication. Bidirectional relays increase the efficiency of the system as simultaneous data transfer can take place between the nodes. In the next few subsections, OSM along with PLNC [103, 104] is proposed for full-duplex communication in FSO systems. This will result in higher data rate and bandwidth efficiency.

In literature, error rate performance of FSO links over G-G channels has been analyzed in [105]. BER analysis has also been reported for MIMO based FSO systems over G-G channels in [106]. User cooperation diversity has been proposed in [107] for FSO cooperative systems and BER analysis has been done. A relay based FSO system has been studied for AF and DF protocol in terms of outage probability in [108]. A single relay cooperative model has been analyzed for non-coherent FSO communication in [109] by deriving semi-analytical and closed form expressions of bit error rate. Optical preamplification and diversity reception techniques have been proposed for FSO systems in [110] to counter the effects of atmospheric turbulence. MIMO terrestrial FSO system has been investigated in terms of symbol error probability for Q-ary PPM modulation over Rayleigh and lognormal channels in [111]. A partial dual relay selection technique has been studied for two-way relay based FSO communication over G-G channel with pointing error [112]. Parallel relaying in FSO communication with multiple half-duplex AF based relays have been proposed in [113]. The notion of OSM has been proposed for FSO links [84, 114]. In indoor environments, OSM has been investigated for BER performance in [115, 116, 117, 118, 119]. The indoor channel fading is deterministic which makes the analysis a lot easier. However in outdoor FSO communication, the BER analysis becomes all the more difficult due to the varying channel fading. There are some limited works regarding OSM in outdoor FSO communication. In [120], OSM has been implemented for outdoor FSO networks, with a mixture of pulse position and pulse amplitude modulation techniques. This technique has been shown to offer improved power, spectral and performance efficiencies than conventional modulation techniques. OSM for coherent FSO systems has been studied using homodyned-K fading distribution in [121]. MIMO based optical space shift keying known as MIMO-OSSK has been proposed in [122] where only the laser index conveys the information. MIMO-OSSK has been studied over lognormal and negative exponential channels in [122]. MIMO-OSSK has also been studied for Gamma-Gamma channel in terms of BER in [100, 101]. PLNC for two-way relay based FSO system has been analyzed over strong turbulence channels in [103] and Bayesian estimate for bit detection has been used in absence of CSI. Network coding for optical networks has been proposed in [104]. Outage probability and bit error rate for such systems have been evaluated [123, 124, 125]. In [123], outage probability and symbol error rate have been evaluated for PLNC two-way relay FSO systems over G-G channel. In [124], outage probability and BER have been evaluated for PLNC two-way relay system over weak turbulence region. PLNC for two-way relay FSO systems has been studied in terms of BER in [125].

To sum it up, previous works have used OSM and PLNC separately for FSO communication. Optical SSK, which is a special case of OSM, has also been implemented. FSO communication without OSM and PLNC has also been analyzed for SISO and MIMO case both for conventional and cooperative

communication. However, there is a significant research gap in analyzing the combined effect of OSM and PLNC for bidirectional FSO cooperative communication which can increase the efficiency of normal OSM or PLNC coded relay networks. Such study has not yet been performed over any type of channel or turbulence effect. This motivates us to propose a OSM and PLNC based decode-and-forward two-way relaying (DFTWR) system which enables bidirectional FSO cooperative communication with high spectral efficiency.

The novelty of our work lies in the fact that outage probability lower and upper bounds are evaluated for OSM-PLNC based bidirectional FSO cooperative systems for the first time. Closed form expressions for the same are derived which makes the expressions more tractable and the analysis becomes more easier. Coding gain and diversity gain are evaluated to gain more insights about asymptotic behaviour of the system. The influence of various channel parameters on the system performance is studied and key inferences are made about the behaviour of the system. In case of satellite based FSO communication, laser misalignment can cause pointing errors. But in our work, we consider FSO cooperative communication for terrestrial purpose where link distance is less. Therefore, pointing error can be ignored for LOS cooperative FSO communication [96].

In the subsequent sections, the system model will be studied which is similar to that of the RF cooperative system that we studied earlier in Chapter 2. However, in optical domain there are many differences. Firstly, the atmospheric turbulence behaves differently than RF fading. The intensity modulation and direct detection processes are carried out in optical domain. Another issue is the tackling of self-interference at the relay node which occurs due to simultaneous message transfer from both the source nodes. Similar to RF counterparts, SINR analysis needs to be done for outage probability analysis. Closed form expressions are useful to gain valuable insights about the system performance like coding gain, diversity gain. Deriving closed form expressions are challenging because of the complex nature of expressions involving product and summation of multiple Meijer G terms. One may point out that numerical methods may be used to analyze the performance, but such methods take up a lot of time and has high computational complexity. It is cumbersome and time consuming to do numerical analysis everytime to understand the effect of parameters on the system performance. It is convenient for network design engineers to design networks using tractable closed form expressions.

4.3.1 Proposed System Model

The simplest form of 3 node bidirectional cooperation model, comprising of 2 source nodes- Source 1 (S1) and Source 2 (S2), and relay node (RN), is considered, as depicted in Fig. 4.1. There is no direct link between S1 and S2. All the nodes are spatially modulated full-duplex (SMFD) nodes with N_L lasers and N_L photodetectors. It is assumed that the nodes have independent transmit and receive

chains to mitigate self-interference. Source nodes exchange data bits among each other using PLNC at the relay employing DF technique. For transmitting purpose, N_L lasers are used and for receiving side, N_L photodetectors of responsivity R_e are used. The relative gains of the links as described in Section II of [51] and Eq. 3 of [52] are given as: $G_{S_1,R} = (\frac{d_{SD}}{d_{SR}})^\tau$, $G_{S_2,R} = (\frac{d_{SD}}{d_{RD}})^\tau$ where $G_{S_1,R}$ and $G_{S_2,R}$ are the relative gain of the S1 to RN link and RN to S2 links respectively, τ is the path loss coefficient, d_{SD}, d_{SR} and d_{RD} are the distances between S1 and S2, S1 and RN, and RN and S2 links respectively. Relative geometrical gain factor $\kappa_{rg} = \frac{G_{S_1,R}}{G_{S_2,R}}$ denotes the location of RN node with respect to S1 and S2. κ_{rg} is less than 1 if distance between relay node and S2 is lesser whereas κ_{rg} is more than 1 if distance between relay node and S1 is lesser and if both distances are equal then κ_{rg} is 1.

Such a model can be considered for long distance FSO communication. FSO is primarily a LOS based communication. Therefore too many obstacles like high buildings can cause a hindrance in FSO communication. In urban areas specially, the density of obstacles is a matter of huge concern. If two nodes in FSO communication want to exchange information over long distances (like several kilometers), then effective communication may not take place due to blockage in light path. This problem can be resolved if cooperative FSO communication is considered where relay can be placed at short intervals. It is easier to create a LOS link between two short distance nodes rather than creating a LOS link over large distances. Hence our bidirectional cooperative model is designed taking into consideration that data transfer can take place between two long distance nodes with the help of a relay. Such a model can be considered trivial in RF domain because RF signal propagation is not a LOS propagation. It can pass through obstacles and RF signals propagate through reflection, scattering and multipath propagation. Meanwhile optical signals undergo changes in direction and energy due to turbulence effect. This fundamental difference in behaviour of signal propagation in optical domain justifies the reason for choosing such a model for our proposed method.

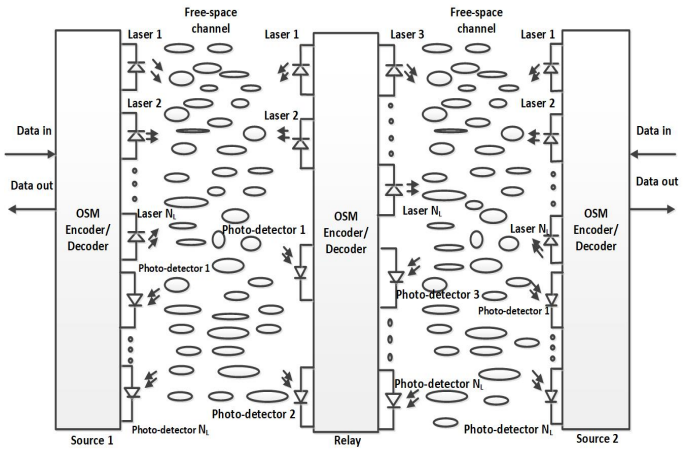

Figure 4.1: System model for OSM based DFTWR.

Optical chain comprises of source encoders, RF modulators, DC bias adders, etc. In OSM, according to the message bit, laser along with aperture is selected and the corresponding laser is connected to the single transmit optical chain through a switch. Thus in case of OSM, only laser with its aperture is present in multiple numbers, while the transmit optical chain requirement is 1 only. Intensity modulation principle is used at the transmitting end where the optical power output is varied according to some characteristic of the modulating signal. Direct detection principle is used at the receiver where the electrical signal is generated by the photodetector according to the intensity of the received optical signal. This process does not require any carrier information at the receiver. In all the nodes, a RF subcarrier signal is modulated by source data and the modulated signal is then used to modulate the intensity of optical source like laser. The sinusoidal nature of the modulated signal in RF domain causes a necessity of addition of DC bias to make the signal positive in order to drive the optical source. The negative part of the BPSK modulated signal is removed by adding a DC bias signal. A chunk of message bits of length $\log_2(N_L)$ is used for selecting the laser index from which the optical signal would be sent. An optical switch (made of silicon waveguide with embedded phase change material) is used for creating the connection between the single transmit chain and the selected laser. The receive chain converts optical signal into electrical signal. Direct detection by a photodetector is performed at the receiver without any local oscillator, to retrieve the electrical signal. The signal subsequently undergoes demodulation by a RF coherent BPSK demodulation scheme to obtain the original data [96]. Semiconductor optical amplifier (SOA) based Mach-Zehnder interferometer (MZI) [126] is used to design an all optical XOR gate. A symmetrical MZI is used with one SOA in each arm located at the same relative position. The input logic signals A and B, are taken as inputs into the two arms of the MZI via two multiplexers. They act as control signals. A clock signal is split into two parts using a coupler, thus forming the probe signals. If both the control signals are identical, output is zero as the SOA-MZI is balanced. But if one is zero and the other is not, then due to the cross phase modulation effect in the SOAs, a differential phase shift is introduced and the output is one.

For $N_L = 2$, the transmit laser source which is made active is chosen as:

$$j_{ktx} = \begin{cases} 2, & \text{if } c_k^{LSB}[n] = 1 \\ 1, & \text{if } c_k^{LSB}[n] = 0 \ , \end{cases} \tag{4.8}$$

where n represents the n^{th} time slot and k indicates the source node which may be 1 or 2 in this case. If $N_L > 2$, then $\log_2 N_L$ number of bits (from LSB side) will be used for transmit laser source activation and $\log_2 M$ message bit will be used for M-ary modulation scheme. We will consider BPSK modulation

scheme for our case. The table of laser source activation depending upon the message bits is listed in Table 4.3 and Table 4.4 for N_L=4 and N_L=8 respectively.

Table 4.3: Optical spatial modulation for N_L=4

Input bits	Laser index	BPSK symbol
000	1	-1
001	2	-1
010	3	-1
011	4	-1
100	1	1
101	2	1
110	3	1
111	4	1

Table 4.4: Optical spatial modulation for N_L=8

Input bits	Laser index	BPSK symbol
0000	1	-1
0001	2	-1
0010	3	-1
0011	4	-1
0100	5	-1
0101	6	-1
0110	7	-1
0111	8	-1
1000	1	1
1001	2	1
1010	3	1
1011	4	1
1100	5	1
1101	6	1
1110	7	1
1111	8	1

$c_k[n]$ represents the bits which may be 0 or 1 in this case. Both the sources transmit data using BPSK to relay node simultaneously. The received signal obtained at the j_{Rrx} photodetector of relay node in n^{th} time slot is expressed as:

$$y_R^{j_{Rrx}}[n] = \sum_{k=1}^{2} \sqrt{R_e P_k G_{S_k,R}}\, h_{j_{ktx},j_{Rrx}} x_k^{MSB}[n] + i_{RR}[n] + w_R[n] \ . \tag{4.9}$$

$h_{j_{ktx},j_{Rrx}}$ represents G-G channels between the selected laser j_{ktx} of S_k source node and photodetector j_{Rrx} of the relay node. j_{Rtx} denotes the laser index at relay node, while j_{Rrx} denotes the photodetector index at relay node. Similarly j_{ktx} denotes the laser index at S_k source node, while j_{krx} denotes the photodetector index at S_k node. P_k indicates the transmit power at the source node S_k, k=1, 2. $w_R[n]$ represents the shot noise from ambient light at the relay node. Shot noise from ambient light is independent of the

signal and can be represented as white Gaussian random noise with zero mean and variance N_0. The self-interference at the relay node is indicated by $i_{RR}[n]$. It is described as Gaussian random variable with zero mean and power $I_R = N_0[10^{\gamma_{loss}/10} - 1],\ \gamma_{loss} \geq 0$ where γ_{loss} denotes the SNR loss factor in dB. Hence the received signal at the relay node can be modelled as a complex Gaussian random variable. $x_k^{MSB}[n]$ represents the message bit from the MSB side which is used for M-ary modulation scheme. The parameters j_1, j_2, $x_1^{MSB}[n]$, and $x_2^{MSB}[n]$ are obtained using maximum likelihood (ML) detection method [54] as shown below:

$$(\hat{j_1}, \hat{j_2}, \hat{x}_1^{MSB}[n], \hat{x}_2^{MSB}[n]) = \underset{(j_1, j_2, x_1^{MSB}[n], x_2^{MSB}[n])}{min} \left| y_R^{j_{Rrx}}[n] - \sum_{k=1}^{2} \sqrt{R_e P_k G_{S_k,R}} h_{j_{ktx}, j_{Rrx}} x_k^{MSB}[n] \right|^2 . \tag{4.10}$$

Here $\hat{j_1}$ is the estimated transmit laser index of S_1, $\hat{j_2}$ is the estimated transmit laser index of S_2. The laser source selection at the relay for the next time slot is done according to the formula $j_R = \hat{j_1} \oplus \hat{j_2}$. The encoded symbol $x_R^{MSB}[n]$, forwarded by the relay to the source nodes is given by:

$$x_R^{MSB}[n] = \hat{x}_1^{MSB}[n] \oplus \hat{x}_2^{MSB}[n] \ , \tag{4.11}$$

where the estimated values of the message bits coming from the two sources, at the relay are $\hat{x}_1^{MSB}[n]$ and $\hat{x}_2^{MSB}[n]$ and $\oplus$ is the bitwise XOR operator. The source nodes receive the signals in the next time slot, which is given by:

$$y_k^{j_{krx}}[n+1] = \sqrt{R_e P_R G_{S_k,R}}\ h_{j_{krx}, j_{Rtx}} x_R^{MSB}[n] + i_{kk}[n] + w_k[n], \quad k = 1, 2 \ , \tag{4.12}$$

where j_{krx} denotes the photodetector of the S_k source node. $w_k[n]$ is the noise at source node S_k which can be represented by zero mean white Gaussian random variable having variance N_0. $i_{kk}[n]$ is the self-interference at the source node S_k due to full-duplex nature of operation of the source nodes. P_R is the transmission power of relay node. An assumption is considered that perfect channel state information (CSI) is available at the source nodes. However considering CSI to be updated at regular intervals, performance analysis for outdated and imperfect CSI can be considered for future work. The channels in FSO communication exhibit a quasi-static nature resulting in a very slowly varying channel, thereby making reliable feedback a possibility. Power adjustment can be done based on CSI to improve the performance. Power imbalance technique along with adaptive optical source labelling in OSSK has been considered in [127], where channel gain ordering has been sent though the feedback link instead of the exact channel gain values, thereby saving valuable feedback overhead bits. Future research can be

conducted in extending a similar type of analysis for outdoor OSM and PLNC based FSO cooperative systems also. Thus considering CSI is available at the source nodes, the parameters j_R, $x_R^{MSB}[n]$ are detected using ML method. The estimated symbols at the source node are $\hat{j}_R$ and $\hat{x}_R^{MSB}$. Using the known bit values, the message bits are calculated at the S_k source node and are denoted by $\hat{x}_k^{MSB}$ and $\hat{x}_k^{LSB}$.

$$\hat{x}_k^{LSB}[n] = \hat{j_R} \oplus j_k \quad k = 1, 2 \ , \tag{4.13}$$

$$\hat{x}_k^{MSB}[n] = \hat{x}_R^{MSB}[n] \oplus x_k^{MSB}[n], \quad k = 1, 2 \ . \tag{4.14}$$

4.3.2 Performance Analysis

Evaluation of exact outage probability expression is difficult for OSM and PLNC based bidirectional cooperative communication. For exact expressions, the end-to-end SNR, PDF and CDF need to be evaluated. This is a challenging task due to the complex intractable nature of the expressions for such a system model. Hence we are opting for lower and upper bound evaluation of outage probability. Future research work may focus on deriving end-to-end SNR, PDF, CDF and outage probability expressions for such a system model. Analytical expressions for lower and upper bounds of outage probability are derived and verified in this section.

4.3.2.1 Lower Bound of Outage Probability

Assume $\eta_k = \frac{P_k}{N_0}$, $\eta_R = \frac{P_R}{N_0}$, k=1, 2 be the SNR at source nodes and relay node respectively. Thus η_k and η_R are the average electrical SNRs at the corresponding nodes. The SINR at relay node and source node S_k are denoted by $\gamma_{S_k,R}^{j_{Rrx}}$ and $\gamma_{R,S_k,}^{j_{krx}}$ respectively. The SINR at a particular photodetector (whose index is given by j_{Rrx}) located at relay node, is given by:

$$\gamma_{S_k,R}^{j_{Rrx}} = \frac{\eta_k R_e G_{S_k,R} \left(h_{j_{ktx},j_{Rrx}}\right)^2}{\frac{I_R}{N_0} + 1}, \quad k = 1, 2 \ . \tag{4.15}$$

The SINR at photodetector (whose index is given by j_{krx}) located at source node S_k, is given by:

$$\gamma_{R,S_k,}^{j_{krx}} = \frac{\eta_R R_e G_{S_k,R} \left(h_{j_{krx},j_{Rtx}}\right)^2}{\frac{I_R}{N_0} + 1}, \quad k = 1, 2 \ . \tag{4.16}$$

The outage probability lower bound of OSM-DFTWR for a data rate of R_d bits/s can be defined as:

$$P_{out}^{R\_LB}(R_d) \geq$$
$$P[2\log_2(N_L) + \log_2(1 + \min(\max(\gamma_{S_1,R}^1, \gamma_{S_1,R}^2, ..., \gamma_{S_1,R}^{N_L}), \max(\gamma_{S_2,R}^1, \gamma_{S_2,R}^2, ..., \gamma_{S_2,R}^{N_L}))) < R_d] \ . \tag{4.17}$$

It is assumed that there is no error in laser selection. This assumption is taken because if laser selection error is considered, then it will be difficult to achieve closed form expressions. Numerical analysis has to be done which defeats our initial motive of obtaining closed form expressions. The PDF of the random variable obtained from the difference of two G-G random variable is unknown. Without the difference PDF, the pairwise error probability, BER and outage probability cannot be evaluated. Research is going on to solve the nature of the difference PDF and this can be a scope for future work. The addition with the $2\log_2(N_L)$ term is due to the fact that $\log_2 N_L$ bits are used for activating a particular laser and since it is full-duplex communication, therefore $2\log_2(N_L)$ bits will be used. The detailed analysis of this term is provided in Appendix of [128] and already provided earlier in Chapter 2 for RF communication. The max-min criteria has been used for selecting the optimum SINR for lower bound in this case [59, 60]. This criteria is used for RF domain also and the logic behind the selection of this criteria has already been explained in Chapter 2. One has to remember that outage probability occurs when either of the two links (relay-to-source 1 or relay-to-source 2) fails. This condition is only satisfied when minimum of random variables is considered as explained in minimum criteria of Eq. (2.50). Again there are multiple lasers at each of the source nodes. Hence for a particular source node-to-relay link, the minimum chance of outage probability is when all the lasers fail to transmit for that particular link. Even when a single laser can transmit the signal properly, then that source-to-relay link can be maintained. Therefore minimum outage probability is possible when maximum of random variables at each source node (all link failure condition) is considered as explained in maximum condition of Eq. (2.50). Hence the laser photodetector link generating the maximum SINR for a particular source-to-relay node is selected, and out of the maximum SINR of each source-to-relay node path, the minimum one is chosen such that lowest outage is generated. Assume $\psi_R = \min(\max(\gamma^1_{S_1,R}, \gamma^2_{S_1,R}, ..., \gamma^{N_L}_{S_1,R}), \max(\gamma^1_{S_2,R}, \gamma^2_{S_2,R}, ..., \gamma^{N_L}_{S_2,R}))$ and $\gamma_{th} = 2^{R_d - 2\log_2(N_L)} - 1$. The outage probability lower bound at relay node after solving Eq. (4.17) is written as:

$$P^{R\_LB}_{out}(\gamma_{th}) \geq F_{\psi_R}(\gamma_{th}) = 1 - \prod_{k=1}^{2}(1 - F_{\gamma^1_{S_k,R}}(\gamma_{th})F_{\gamma^2_{S_k,R}}(\gamma_{th})...F_{\gamma^{N_L}_{S_k,R}}(\gamma_{th})) \quad . \tag{4.18}$$

The above equation is derived in a similar manner as explained in Chapter 2. Using Eq. (2.48), (2.49) and (2.52), Eq. (4.18) can be obtained. For variable number of lasers at each source node, the same analysis can be done in the manner as shown in Chapter 2. To evaluate the above expression, the individual CDF terms need to be evaluated. The channel coefficient $h_{j_{ktx},j_{Rrx}}$ follows G-G distribution. Let $y = (h_{j_{ktx},j_{Rrx}})^2$. The final CDF of SINR, following CDF given in Eq. (4.7), can be written using

Eq. (4.15):

$$F_{\gamma^{j_{Rrx}}_{S_k,R}}(\gamma_{th}) = \frac{(\alpha_G\beta_G)^{(\frac{\alpha_G+\beta_G}{2})}\left(\frac{\gamma_{th}\gamma_{abs}}{\eta_k R_e G_{S_k,R}}\right)^{(\frac{\alpha_G+\beta_G}{4})}}{\Gamma(\alpha_G)\Gamma(\beta_G)} G^{2,1}_{1,3}\left(\begin{matrix}1-(\frac{\alpha_G+\beta_G}{2}) \\ \frac{\alpha_G-\beta_G}{2}, \frac{\beta_G-\alpha_G}{2}, \frac{-\alpha_G-\beta_G}{2}\end{matrix}\middle| \alpha_G\beta_G\left(\frac{\gamma_{th}\gamma_{abs}}{\eta_k R_e G_{S_k,R}}\right)^{\frac{1}{2}}\right) \quad , \tag{4.19}$$

where $\gamma_{abs} = 10^{\gamma_{loss}/10}$. Depending upon the value of k, $G_{S_1,R}$ or $G_{S_2,R}$, and η_1 or η_2 are chosen. j_{ktx} denotes the selected laser source of S_k node and j_{Rrx} denotes the selected photodetector at the relay node. The terms $F_{\gamma^0_{S_k,R}}(\gamma_{th})$, $F_{\gamma^1_{S_k,R}}(\gamma_{th})$ etc. are obtained using Eq. (4.19). These values are put into Eq. (4.18) to obtain the final CDF of ψ_R. Eq. (4.18) basically denotes the outage probability in the first stage when the source nodes send message to te relay. Now our next task is to calculate the outage probability for the second stage. Second stage outage probability can be calculated when we consider that message is received successfully in the first stage. Then the outage probability at the source node S_k, k=1, 2 can be computed as [60]:

$$P^{S_k}_{out}(R_d) \geq P[2\log_2(N_L) + \log_2(1 + \min(\gamma^1_{R,S_k}, \gamma^2_{R,S_k}, ..., \gamma^{N_L}_{R,S_k})) < R_d], k = 1, 2 \ . \tag{4.20}$$

The $2\log_2(N_L)$ term is used due to the same reason as explained earlier in (4.17). For second stage, during relay to a particular source node transmission, outage probability can occur when any of the available links between the lasers at relay node and a photodetector at source node fails. Hence the minimum criteria can satisfy this condition. In this case, out of all the available links, the weakest link is chosen.

Assume $\psi_{S_k} = \min(\gamma^1_{R,S_k}, \gamma^2_{R,S_k}, ..., \gamma^{N_L}_{R,S_k})$. The CDF of ψ_{S_k} is written as:

$$F_{\psi_{S_k}}(\gamma_{th}) = P\left\{\min(\gamma^1_{R,S_k}, \gamma^2_{R,S_k}, ..., \gamma^{N_L}_{R,S_k}) \leq \gamma_{th}\right\} = 1 - \prod_{j_{krx}=1}^{N_L}(1 - F_{\gamma^{j_{krx}}_{R,S_k}}(\gamma_{th})), \quad k = 1, 2 \tag{4.21}$$

The above equation is written using the probability equation of minimum of random variables as explained earlier in Eq. (2.48). $h_{j_{krx},j_{Rtx}}$ follows G-G distribution. Let $y = (h_{j_{krx},j_{Rtx}})^2$. We can write $F_{\gamma^{j_k}_{R,S_k}}(\gamma_{th})$ (following CDF given in Eq. (4.7)) by using Eq. (4.16) as:

$$F_{\gamma^{j_{krx}}_{R,S_k}}(\gamma_{th}) = \frac{(\alpha_G\beta_G)^{(\frac{\alpha_G+\beta_G}{2})}\left(\frac{\gamma_{th}\gamma_{abs}}{\eta_R R_e G_{S_k,R}}\right)^{(\frac{\alpha_G+\beta_G}{4})}}{\Gamma(\alpha_G)\Gamma(\beta_G)} G^{2,1}_{1,3}\left(\begin{matrix}1-(\frac{\alpha_G+\beta_G}{2}) \\ \frac{\alpha_G-\beta_G}{2}, \frac{\beta_G-\alpha_G}{2}, \frac{-\alpha_G-\beta_G}{2}\end{matrix}\middle| \alpha_G\beta_G\left(\frac{\gamma_{th}\gamma_{abs}}{\eta_R R_e G_{S_k,R}}\right)^{\frac{1}{2}}\right) \ . \tag{4.22}$$

where depending upon the value of k, $G_{S_1,R}$ or $G_{S_2,R}$ is chosen. Here j_{krx} denotes the photodetector of the source node S_k. The term $F_{\psi_{S_k}}(\gamma_{th})$ is computed in Eq. (4.21) using Eq. (4.22). The overall outage

probability of the system can be computed by combining the outage probabilities at the source and relay nodes. It is defined as:

$$\begin{aligned} P_{out}^{LB}(\gamma_{th}) &= P_{out}^{R\_LB}(\gamma_{th}) + (1 - P_{out}^{R\_LB}(\gamma_{th}))P_{out}^{S_k}(\gamma_{th}) \\ &\geq 1 - \left[\prod_{k=1}^{2}(1 - F_{\gamma_{S_k,R}^1}(\gamma_{th})F_{\gamma_{S_k,R}^2}(\gamma_{th}), ..., F_{\gamma_{S_k,R}^{N_L}}(\gamma_{th}))\right] \times \left[\prod_{j_{krx}=1}^{N_L}(1 - F_{\gamma_{R,S_k}^{j_{krx}}}(\gamma_{th}))\right] . \end{aligned} \tag{4.23}$$

The total transmission consists of two phases. In the first phase, when the source nodes transmit message to the relay, the outage probability can be defined by the term $P_{out}^{R\_LB}$, obtained from Eq. (4.18). The second phase is the broadcasting stage from the relay. The second term in Eq. (4.23) i.e. $(1 - P_{out}^{R\_LB}(\gamma_{th}))P_{out}^{S_k}(\gamma_{th})$ gives the outage probability for this phase. $P_{out}^{S_k}(\gamma_{th})$ is obtained by solving Eq. (4.22). In Eq. (4.23), we can observe that the term $F_{\gamma_{R,S_k}^{j_{krx}}}(\gamma_{th})$ decreases with increase in SNR η_R (since Meijer G term decreases with increase in SNR value). The subtraction of this term from 1 results in an incremental value. The term $F_{\gamma_{S_k,R}^{j_{Rrx}}}(\gamma_{th})$ contains the Meijer G function, as can be seen from Eq. (4.19), which depends on the SNR η_k. As SNR increases, the Meijer G function decreases resulting in a decrease in value of the overall term $F_{\gamma_{S_k,R}^{j_{Rrx}}}(\gamma_{th})$. Hence the product of such terms also decreases. The subtraction of the resulting product term from 1 gives an increase in the result and the product of two incremented terms is again subtracted from 1, thereby causing an overall decrease in the outage probability value with increase in SNR.

4.3.2.2 Upper Bound of Outage Probability

Our next objective is to find the upper bound of outage probability. The total upper bound has to be evaluated in two stages. For the first stage, outage probability can occur when any of the links fails (either source 1-to-relay or source 2-to-relay link). Maximum outage can occur for each source-to-relay link when any of the available lasers at a particular source node fail to transmit the signal to be received at the relay node. This is in contrast to the lower bound criteria when all the lasers for a particular source-to-relay link had to fail. Thus to fulfil the criteria of failure of any link, minimum of random variables concept has to be used as explained in minimum criteria of Eq. (2.50). Therefore the minimum SINR of all the source nodes and relay links will be computed for upper bound evaluation. Such an upper bound for the first stage can be derived for a data rate of R_d bps as:

$$P_{out}^{R\_UB}(R_d) \leq P[2\log_2(N_L) + \log_2(1 + \min(\gamma_{S_1,R}^1, \gamma_{S_1,R}^2, ..., \gamma_{S_1,R}^{N_L}, \gamma_{S_2,R}^1, \gamma_{S_2,R}^2, ..., \gamma_{S_2,R}^{N_L})) < R_d] . \tag{4.24}$$

The other steps would remain the same as that of lower bound computation.

Assume $\psi_{S_k} = \min(\gamma_{S_1,R}^1, \gamma_{S_1,R}^2, ..., \gamma_{S_1,R}^{N_L}, \gamma_{S_2,R}^1, \gamma_{S_2,R}^2, ..., \gamma_{S_2,R}^{N_L})$ and $\gamma_{th} = 2^{R_d - 2\log_2(N_L)} - 1$. Using Eq. (2.48) and (2.65), the following equation can be derived. The upper bound on outage probability at the

relay is given by:

$$\begin{aligned} P_{out}^{R\_UB}(\gamma_{th}) &\leq F_{\psi_{S_k}}(\gamma_{th}) \\ &= P\left\{\min(\gamma_{S_1,R}^1, \gamma_{S_1,R}^2, ..., \gamma_{S_1,R}^{N_L}, \gamma_{S_2,R}^1, \gamma_{S_2,R}^2, ..., \gamma_{S_2,R}^{N_L}) \leq \gamma_{th}\right\} \\ &= 1 - \prod_{k=1}^{2}(\prod_{j_{Rrx}=1}^{N_L}(1 - F_{\gamma_{S_k,R}^{j_{Rrx}}}(\gamma_{th}))), \quad k = 1, 2 \ , \end{aligned} \tag{4.25}$$

where $F_{\gamma_{S_k,R}^{j_{Rrx}}}(\gamma_{th})$ is defined in Eq. (4.19). Thus the overall upper bound of outage probability of the system (after inserting the values of the corresponding terms) can be defined as:

$$\begin{aligned} P_{out}^{UB}(\gamma_{th}) &= P_{out}^{R\_UB}(\gamma_{th}) + (1 - P_{out}^{R\_UB}(\gamma_{th}))P_{out}^{S_k}(\gamma_{th}) \\ &\leq 1 - \left[\prod_{k=1}^{2}(\prod_{j_{Rrx}=1}^{N_L}(1 - F_{\gamma_{S_k,R}^{j_{Rrx}}}(\gamma_{th})))\right] \times \left[\prod_{j_{krx}=1}^{N_L}(1 - F_{\gamma_{R,S_k}^{j_{krx}}}(\gamma_{th}))\right] \ . \end{aligned} \tag{4.26}$$

In the first phase, when the source nodes transmit message to the relay, the outage probability can be defined by the term $P_{out}^{R\_UB}$. The second phase is the broadcasting stage from the relay. The second term in Eq. (4.26) i.e. $(1 - P_{out}^{R\_UB}(\gamma_{th}))P_{out}^{S_k}(\gamma_{th})$ gives the outage probability for this phase. $P_{out}^{S_k}(\gamma_{th})$ is obtained by solving Eq. (4.22). In Eq. (4.26), we can observe that the term $F_{\gamma_{R,S_k}^{j_{krx}}}(\gamma_{th})$ decreases with an increase in η_R value. This term when subtracted from 1 will give an incremented value. Meanwhile, the term $F_{\gamma_{S_k,R}^{j_{Rrx}}}(\gamma_{th})$ contains the Meijer G function, as can be seen from Eq. (4.19), which depends on the SNR η_k. As SNR increases, the Meijer G function decreases resulting in a decrease in value of the overall term $F_{\gamma_{S_k,R}^{j_{Rrx}}}(\gamma_{th})$. Hence the product of such terms also decreases. The subtraction of the resulting product term from 1 gives an increase in the result. The product of two incremented terms when subtracted from 1 results in an overall decrease in outage probability value with increment in SNR.

4.3.2.3 Outage Probability Analysis for Direct System

A bidirectional system without relay (DFSO) is considered and its outage probability is derived for G-G channel. A laser and a photodetector are present in each of the two devices S_1 and S_2, such that they can exchange data with each other. The SINR at any of the nodes is given by:

$$\gamma_{S_1,S_2} = \frac{\eta_k R_e \left(h_{S_1,S_2}\right)^2}{\frac{I_R}{N_0} + 1}, \quad k = 1, 2 \ , \tag{4.27}$$

where h_{S_1,S_2} denotes the channel coefficient between the two devices S1 and S2, following G-G distribution. Therefore outage probability for DFSO system is given by:

$$\begin{aligned} P_{out} &= P\left\{\gamma_{S_1,S_2} \leq \gamma_{th}\right\} \quad = F_{\gamma_{S_1,S_2}}(\gamma_{th}) \\ &= \frac{(\alpha_G\beta_G)^{(\frac{\alpha_G+\beta_G}{2})}\left(\frac{\gamma_{th}\gamma_{abs}}{\eta_k R_e}\right)^{(\frac{\alpha_G+\beta_G}{4})}}{\Gamma(\alpha_G)\Gamma(\beta_G)} G_{1,3}^{2,1}\left(\begin{matrix} 1-(\frac{\alpha_G+\beta_G}{2}) \\ \frac{\alpha_G-\beta_G}{2}, \frac{\beta_G-\alpha_G}{2}, \frac{-\alpha_G-\beta_G}{2} \end{matrix} \middle| \alpha_G\beta_G\left(\frac{\gamma_{th}\gamma_{abs}}{\eta_k R_e}\right)^{\frac{1}{2}}\right) \ , \end{aligned} \tag{4.28}$$

where $\gamma_{th} = 2^{R_d} - 1$ and CDF can be written using Eq. (4.7) and Eq. (4.27). The distance of separation was 2 Km between the nodes in OSM-DFTWR. For this analysis, distance of separation between the nodes will be 4 Km as no relay is used. Accordingly values of α_G and β_G are calculated for DFSO system. From the expression, it is clear that with an increase in SNR value, the Meijer G term decreases, resulting in an overall decrease of outage probability.

4.3.2.4 Asymptotic Analysis

The asymptotic analysis can be carried out for lower and upper bounds of outage probability. First let us focus on the final lower bound outage probability expression as given in Eq. (4.23). The expression is a product of CDF terms and each CDF term has a Meijer G component. As shown earlier in Chapter 2, the Meijer G function needs to be expressed in terms of basic mathematical functions. For this, the argument in Meijer G function is first inverted using Eq. (6.2.2) in [62]. Hence at very high SNR values, CDF of SINR in Eq. (4.21) can be written as:

$$F_{\gamma_{S_k,R}^{jktx}}(\gamma_{th}) \approx \frac{(\alpha_G\beta_G)^{(\frac{\alpha_G+\beta_G}{2})}(\frac{1}{z})^{(\frac{\alpha_G+\beta_G}{2})}}{\Gamma(\alpha_G)\Gamma(\beta_G)} \sum_{k=1}^{2} z^{a_k-1} \times \frac{\prod_{l=1;l\neq k}^{2}\Gamma(a_k-a_l)\prod_{l=1}^{1}\Gamma(1+b_l-a_k)}{\prod_{l=3}^{3}\Gamma(1+a_l-a_k)}, \tag{4.29}$$

where $z = \left(\frac{\eta_k R_e G_{S_k,R}}{\gamma_{th}\gamma_{abs}}\right)^{1/2}$, $a = [1-(\frac{\alpha_G-\beta_G}{2}), 1-(\frac{\beta_G-\alpha_G}{2}), 1+(\frac{\alpha_G+\beta_G}{2})]$, $b = [\frac{\alpha_G+\beta_G}{2}]$. Similarly CDF of SINR for source node in Eq. (4.18) is also expressed in terms of elementary function for performing asymptotic analysis. For diversity gain, the highest exponent of SNR is selected. In our case, η_k or η_R is the SNR and its highest exponent will be $-\frac{\alpha_G+\beta_G}{4} - \frac{\alpha_G-\beta_G}{4} = -\alpha_G/2$ if $\alpha_G > \beta_G$ or $-\beta_G/2$ if $\alpha_G < \beta_G$. Hence the diversity gain D_g is dependent on the channel condition and is given by negative exponent of SNR i.e. $\alpha_G/2$ if $\alpha_G > \beta_G$ or $\beta_G/2$ if $\alpha_G < \beta_G$. Referring to Eq. (2.73), the final diversity gain is thus given by $D_g = \min(\alpha_G/2, \beta_G/2)$. The overall coding gain for lower bound on outage probability (considering multiplication of CDF terms) is given by:

$$C_g = \left(\frac{(\alpha_G\beta_G)^{(\frac{\alpha_G+\beta_G}{2})}\left(\frac{\gamma_{th}\gamma_{abs}}{R_e G_{S_k,R}}\right)^{(\frac{\alpha_G+\beta_G}{2})}}{\Gamma(\alpha_G)\Gamma(\beta_G)} \sum_{k=1}^{2}\left(\frac{R_e G_{S_k,R}}{\gamma_{th}\gamma_{abs}}\right)^{1/2(a_k-1)} \times \frac{\prod_{l=1;l\neq k}^{2}\Gamma(a_k-a_l)\prod_{l=1}^{1}\Gamma(1+b_l-a_k)}{\prod_{l=3}^{3}\Gamma(1+a_l-a_k)} \right)^{\frac{3N_L}{-D_g}}. \tag{4.30}$$

Thus we can observe that the slope of the outage probability curve is dependent on the atmospheric turbulence parameter. Weaker turbulence results in higher values of β_G (with $\beta_G < \alpha_G$), thereby providing more diversity gain.

4.3.3 Results and Discussion

In this section, analytical results of bounds on outage probability are plotted for various system parameters and validated by means of Monte Carlo simulations. Strong AT, N_L=2 and L (distance between source nodes and relay)=2 Km are considered unless explicitly stated. The influence of different system parameters on the system performance is also studied and valuable insights regarding the system are noted.

The outage performance of OSM based DFTWR system is compared with PLNC evaluating all the lower and upper bounds. It is evident from Fig. 4.2 that outage probability value is least for OSM based DFTWR (OSM-DFTWR). It can be clearly seen that the simulation results follow a tight lower bound for the proposed method, thereby validating our analysis. The simple direct FSO (DFSO) model without relay performs the worst which justifies the use of relay. The PLNC results have been modelled using Eq. (7) in [123]. The parameters used are same as the parameters used for generating outage probability of OSM based DFTWR. Our proposed results are compared with the results in [124] also where the authors have used lognormal channels. The outage probability for PLNC with lognormal channel are calculated using Eq. (14) of [124], and subsequently the results are plotted in Fig. 4.2 of our chapter with the labelling as PLNC-LOG. The outage probability for direct FSO are calculated for our parameters using Eq. (15) of [124] and the results are labelled as DFSO-LOG in Fig. 4.2 of our chapter. Thus we have compared our proposed results with two methods available in literature and we can observe that our proposed methods perform better with the same parameters.

Our proposed system performs better than PLNC because in PLNC multiple lasers operate leading to more inter-optical interference. While in case of OSM-DFTWR, OSM is applied along with PLNC causing a single laser to be activated at a time. This reduces the inter-optical interference leading to better performance. The performance improvement can be studied analytically also from the lower bound and upper bound expressions. The threshold SNR contains a term $(R_d - 2\log_2(N_L))$ for our proposed method while it is only R_d for PLNC. The effective data rate is reduced for OSM-DFTWR method. Our proposed system also performs better than DFSO system. This can be explained from a physical point of view also. In DFSO, the relay is absent, hence the effective distance of separation is 4 Km, while it is only 2 Km for OSM-DFTWR. Due to larger distance of separation in DFSO, the light rays have to travel a larger distance and encounter more turbulence effect. This hampers the light propagation, leading to more chances of error, thereby giving poor performance of DFSO in comparison to OSM-DFTWR. Another interesting fact to note from the graph of Fig. 4.2 is that the DFSO and PLNC methods using lognormal channels behave in a different way. The lognormal channel based systems give poor results at lower SNR values but can match the results of our proposed system (using G-G channel) for higher

SNR values. This is due to the fact that lognormal channels are suitable for weak turbulence conditions. We have done our analysis for strong turbulence conditions for which G-G channel is appropriate and hence our proposed system is giving good results at low SNR values (even when signal power is weak). Now when SNR is very high meaning that signal power is very high (keeping noise power constant), then lognormal channels can give better performance as indicated by the nature of the curve. But optical signal power cannot be raised beyond a threshold limit as it may be hazardous to our eyes. Therefore, the signal power needs to be limited and hence we have to design methods which are capable of yielding better results at low SNR values (even with limited signal power). This justifies the fact that our proposed method is appropriate for FSO communication as it can yield superior performance even at low SNR values under strong turbulence conditions.

The different SNR values required to achieve certain target outage probability values for different methods are tabulated in Table 4.5. Three different target outage probability values are chosen as 0.1, 0.08, and 0.05. The SNR gain of OSM based DFTWR over PLNC is 6 dB or more which justifies the fact that the proposed system is beneficial. The SNR gain of OSM based DFTWR over conventional DFSO is more than 10 dB for all cases. As the outage value decreases, the gain in SNR for our proposed method is much more which is beneficial. This is due to the fact that extra bits are used for activating the transmitting optical source, causing one laser to be active at a time, thereby reducing the inter-optical interference.

Table 4.5: Comparison of lower bounds on outage probability

P_{out}	SNR for various techniques (in dB)				
	OSM-DFTWR	PLNC	DFSO	PLNC-LOG	DFSO-LOG
0.1	19	26	30	33	35
0.08	21	28	32	35	37
0.05	25	31	36	36	38

The upper bounds on outage performance of the proposed method is compared with that of PLNC in Fig. 4.3 analytically and by means of Monte Carlo simulations. The bounds show improvement in performance for OSM based DFTWR for both γ_{loss}=0 dB and γ_{loss}=3 dB. It is observed that the proposed system has 2 bps data rate more than that of PLNC. This is due to the bits which are required for laser selection which in our case is 1. Since the communication is full-duplex, hence the increment factor in data rate will be 2. This can be explained with an example. For γ_{loss}=3 dB and outage probability value of 0.15, PLNC has a data rate of 3 bps while OSM based DFTWR has a data rate of 5 bps. It is also observed that with an increment in data rate, there is an increment in outage probability also, leading to inferior system performance. Higher data rates are difficult to achieve, hence chances of error are more. Therefore, we can conclude that lower target data rates are suitable for better system

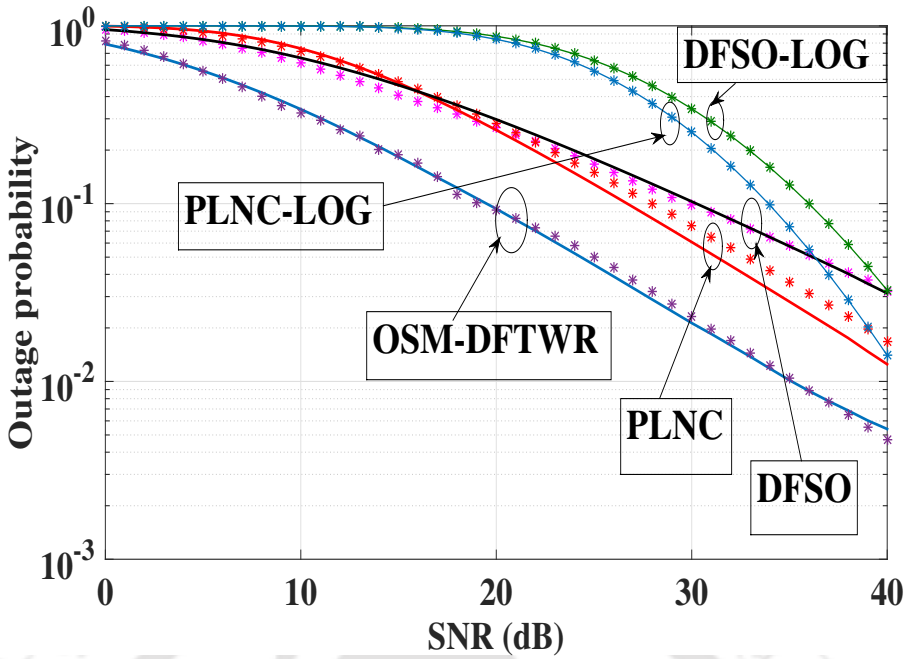

Figure 4.2: Comparison of outage probability between different systems
(Solid line represents lower bound of analytical results while $*$ sign indicates simulation results).

performance.

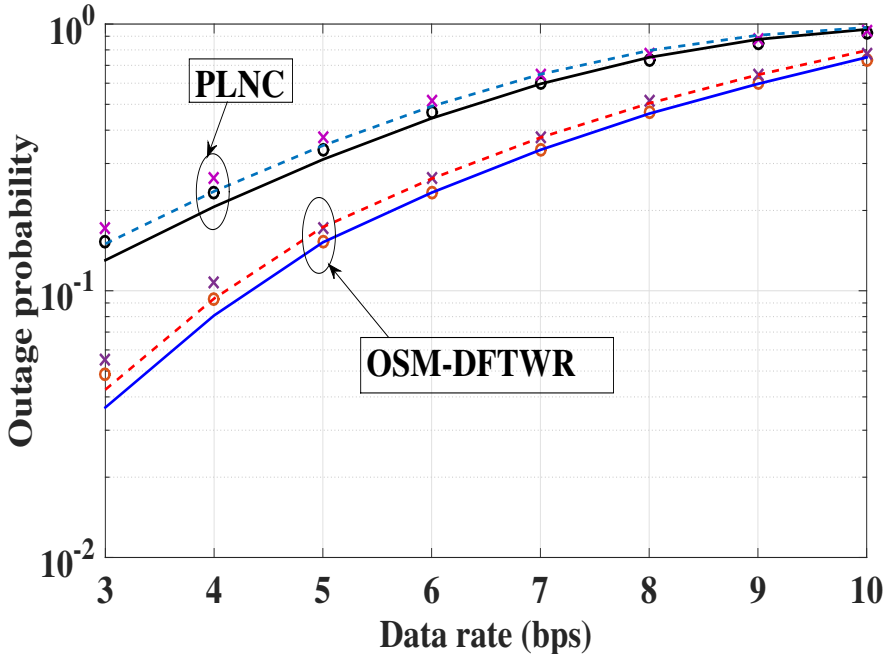

Figure 4.3: Comparison of upper bound on outage performance with respect to data rate
(Solid line represents γ_{loss} = 0 dB analytical results, o sign indicates γ_{loss} = 0 dB simulation results, dashed line indicates γ_{loss} = 3 dB analytical results and x sign indicates γ_{loss} = 3 dB simulation results).

For different SNR loss factors, γ_{loss}=0 dB, γ_{loss}=3 dB and γ_{loss}=6 dB, the lower bounds on outage probabilities are shown in Fig. 4.4. The target data rate is 3 bps and the SNR at relay node is equal to the SNR at the source nodes. It can be observed from the graphs that increase in SNR loss factor

degrades the system performance due to increase in inter-laser optical interference. The analytical and simulation results are validated by asymptotic results also and it is observed that the asymptotic results merge with the analytical and simulation results for high SNR values, thereby justifying our analysis. The increase in self-interference causes an increase in outage probability. For example, for SNR=20 dB, the outage probability value for γ_{loss}=0 dB is 0.08, outage probability value for γ_{loss}=3 dB is 0.09, while for γ_{loss}=6 dB, the value is 0.13. Thus we can observe that the outage probability value increases with increase in SNR loss factor. The analysis can be interpreted in a different manner. As the SNR loss factor increases, it means there is more interference at the relay node due to simultaneous transmission from the source nodes. Hence reception of message by the relay node in the first time slot is not correctly done. The relay is incapable of transmitting the message correctly in the second time slot in presence of interference, leading to more chances of error. Thus the outage probability performance becomes worse with increase in SNR loss factor.

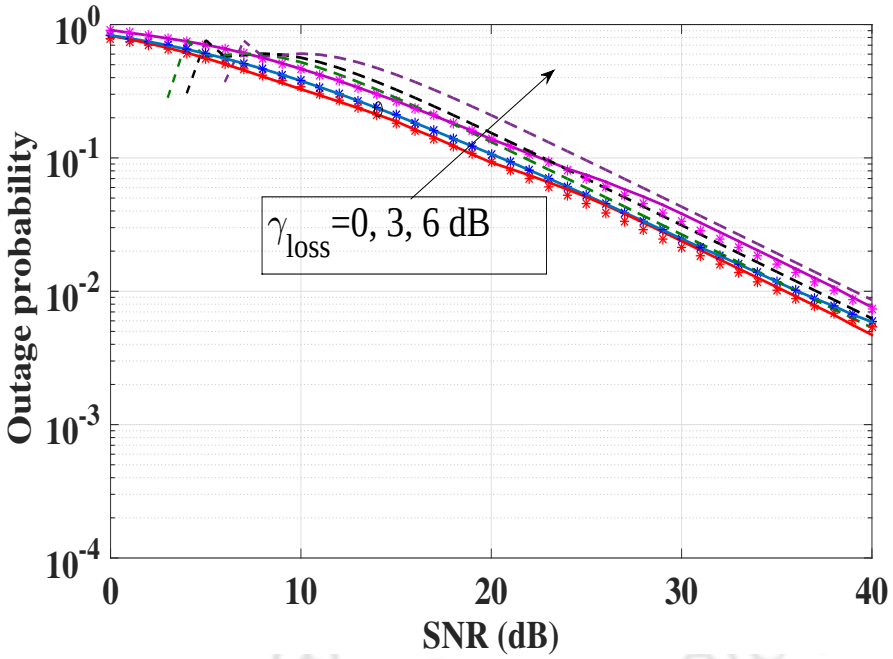

Figure 4.4: Comparison of outage performance of the system with different SNR loss factors (Solid line represents analytical results, $*$ sign indicates simulation results and dashed line represents asymptotic results).

In Fig. 4.5, the performance of OSM based DFTWR is analyzed in terms of link distance. It is evident from the graph that there is an increment in outage probability value with an increment in link distance (as distance between source nodes and relay is increased), thereby leading to inferior system performance. Atmospheric turbulence causes fading which increases with an increase in distance. As the distance increases, the LOS path is blocked due to presence of more obstacles. The optical signal also has to travel through more turbulences. The light rays undergo more scattering and refraction as

the turbulence increases, thereby resulting in reception of poor signal at the receiver located far away. This is the reason for poor performance of the system at large link distances. The analytical results are justified by means of simulation results. The asymptotic results converge with the analytical and simulation results for high SNR values, thereby justifying our analysis.

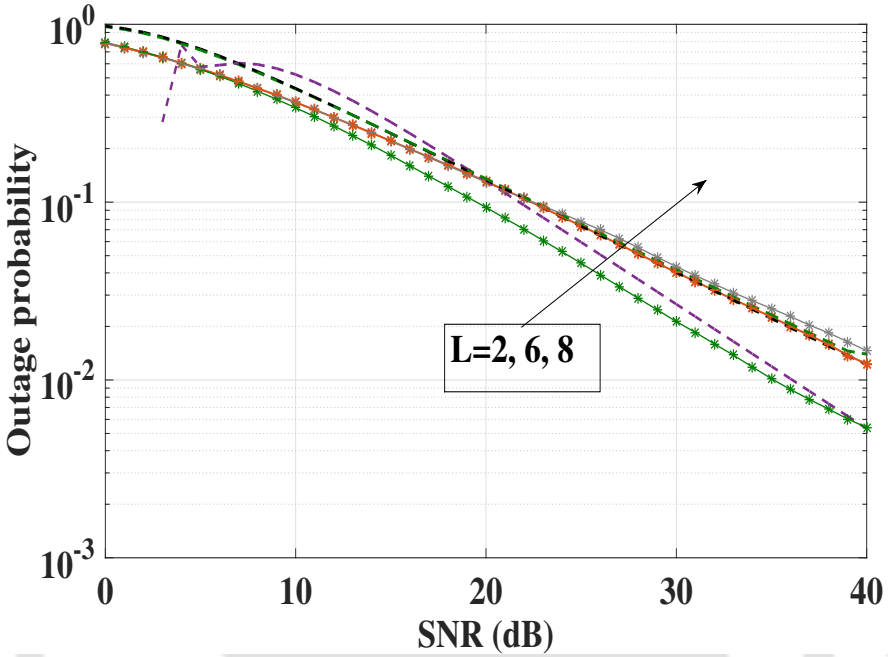

Figure 4.5: Effect of link distance on the lower bound of outage performance of the system (Solid line represents analytical results, $*$ sign indicates simulation results and dashed line represents asymptotic results).

The performance of OSM-DFTWR is verified by Monte Carlo simulations for different atmospheric conditions in Fig. 4.6. The simulation results are in close accordance with the analytical results. The asymptotic results also show close match with the analytical and simulation results at high SNR values, thereby justifying our analysis. This system gives reasonably good performance even under strong and moderate atmospheric turbulences where fluctuations in atmosphere are much more. The outage probability is maximum for strong atmospheric turbulence while it is least for weak condition. Hence it is concluded that G-G channel yields optimum performance even in harsh atmospheric conditions. It is pertinent to note that as the atmospheric turbulence increases, the Rytov variance value increases due to increase in value of the constant C_n^2. Accordingly, the value of α_G and β_G changes to denote the presence of more scattering effects. This hampers the optical signal propagation, leading to more error for higher degrees of turbulence. During daytime when the air gets heated up and the hot air being lighter rises up, more turbulence effect is created leading to increase in C_n^2 value. This also degrades the performance of our proposed system. Again during night, the value of C_n^2 is the least leading to weak turbulence effect, thereby improving our system performance. Fog and snow also influence the

turbulence conditions, thereby changing the system performance accordingly. Thus it can be inferred that the amount of turbulence plays a key role in determining the system performance. We have broadly categorized the varying turbulence conditions into three categories, however for other conditions, values of α_G and β_G can be calculated and accordingly the system performance can be compared.

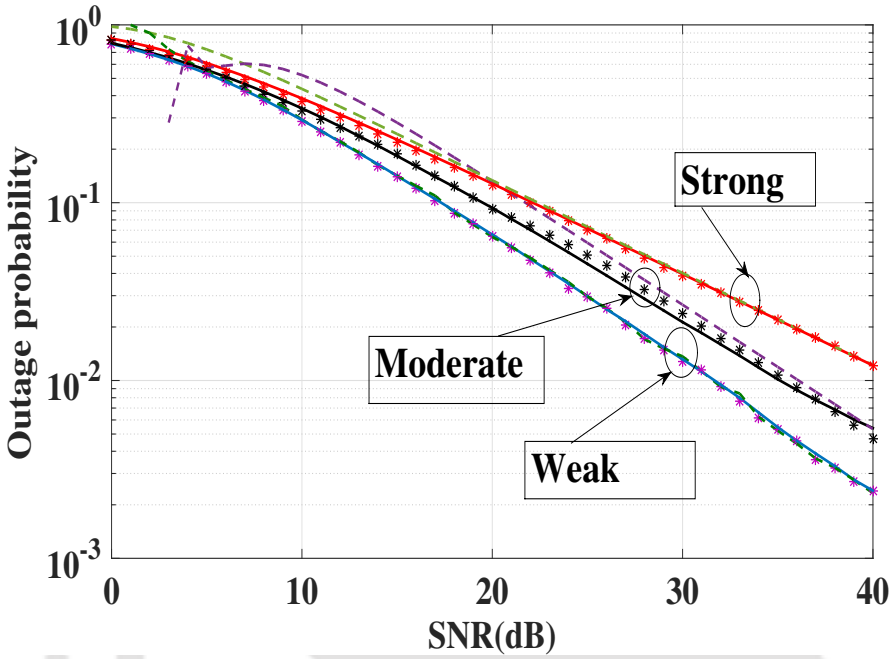

Figure 4.6: Lower bound of outage performance of the system under different atmospheric conditions (Solid line represents analytical results, $*$ sign indicates simulation results and dashed line represents asymptotic results).

The number of transmitting laser is varied and its effect on outage probability for OSM based DFTWR is studied analytically in Fig. 4.7 and verified by means of Monte Carlo simulations also. The results are validated by asymptotic results also. SNR of both the nodes and the relay is varied while N_L is varied as 2, 4, and 8. We know that increase in number of transmit lasers leads to increase in spectral efficiency and outage probability. There will be an increase in bit rate by a factor of 2 if we use N_L=4 system rather than a N_L=2 system, but it also requires an additional 4 dB of SNR to maintain the same outage value as that of N_L=2 system. Similarly to increase the bit rate by a factor of 3 for N_L=8 system, it requires additional 4 + 4 = 8 dB of SNR as compared to N_L=2 system. Thus a compromise between spectral efficiency and error rate is required. The increase in transmit lasers will lead to more inter-laser optical interference, thereby leading to a decrease in performance.

4.4 Transmit Laser Selection for FSO Communication

In the last section, we have seen that OSM can improve system performance for FSO cooperative communication. However, it has some drawbacks which we are going to resolve by some new methods in the subsequent sections. We will also incorporate the effect of pointing error to our channel model

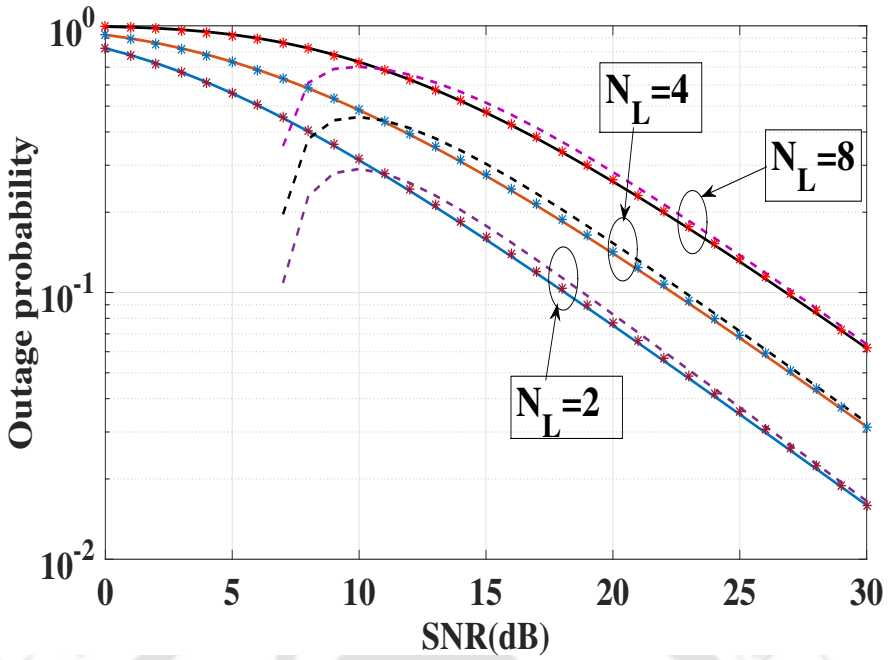

Figure 4.7: Effect of variation in number of transmit lasers on the lower bound of outage performance of the system
(Solid line represents analytical results, $*$ sign indicates simulation results and dashed line represents asymptotic results).

to demonstrate its effect on the performance of FSO systems. Pointing errors generally occur due to misalignment of laser sources due to wind speed, building sways, etc. In practical FSO communication, these type of errors can occur due to wind, building vibrations, etc. Path loss can also occur as the signal on propagating through the atmosphere undergoes an attenuation effect. These effects are incorporated in the G-G channel model for further analysis.

In case of OSM if the chosen link is down or blocked, then the message would not be transmitted and the system performance suffers. This leads to the necessity for transmit laser selection (TLS) depending upon the channel condition. We can either use only TLS or TLS combined with OSM to improve the throughput [129]. TLS is used to select the best set of transmit laser sources out of the available multiple laser sources depending on the channel condition. As light passes through the atmosphere, it undergoes changes in direction and energy due to changes in refractive index. Laser alignment technique cannot yield the optimum performance in such scenarios and TLS can be used to improve the performance. OSM is combined along with TLS to further improve the spectral efficiency. At the receiver, light rays may not be received properly due to attenuation and scattering of the signal. But if we have a set of laser sources to choose from, then we can select the best transmit laser depending on the received SNR. This compensates for the increase in cost due to the use of multiple laser sources, else performance may degrade if a certain optical link is down or blocked. Thus in this work, we have explored the possibility

of laser source selection by selecting one or multiple sources out of the available set of laser sources for cooperative FSO communication. The received SNR at the destination node in both the hops can be maximized by applying TLS. The destination node performs maximal-ratio combining (MRC) to maximize the received SNR.

In Section 4.3, literature related to MIMO FSO communication and OSM have already been presented in detail. Hence literature related to OSM with pointing errors and TLS techniques are presented in this section. Performance analysis for FSO links has been done in terms of outage probability in [130] and the study includes pointing errors, but they have not considered OSM or transmit source selection. Outage probability for cooperative FSO communication including pointing errors has been evaluated in [131]. Symbol error rate for spatial modulation in visible light communication has been computed in [132] using adaptive scheme where modulation order has been varied. The authors in [133] have calculated lower bound of mutual information using channel adaptive scheme for optical spatial modulation. In the literature, authors have performed error analysis over κ-μ [134] and η-μ fading channels [135] for cooperative RF communication. OSSK over G-G channel with pointing error has been analyzed by evaluating BER, coding gain and diversity gain in [136]. OSSK has also been investigated in terms of BER in [137]. Both the works in [136] and [137] consider pointing error for FSO communication. The performance of a coherent FSO system has been analyzed in [138] considering pointing error and geometric spread in addition to atmospheric turbulence effect and path loss.

Outage probability for SM systems with antenna selection for RF communication has also been evaluated in [32]. Previous works have considered transmit antenna selection in conventional RF communication over Rayleigh [139] and Nakagami [140] channels. There are few works related to TLS in FSO communication also. A TLS method for multiple-input-single-output (MISO) FSO communication system has been explored over strong turbulence channel using K distribution in [141]. In this work, the authors have assumed CSI at the transmitter and receiver and depending on the largest scintillation value of the optical path, transmit laser is chosen. TLS scheme has also been studied for FSO communication using K distribution in [142]. Transmit laser selection and receive diversity has been reported in [143] for mobile FSO nodes and the analysis has been conducted over weak lognormal channels. For underwater visible light communication, TLS has been proposed for diver-to-diver MISO system in [144]. Asymptotic error analysis has been performed for TLS based FSO communication over G-G channels with pointing errors in [145]. However this work has not achieved any closed form expressions for error or outage probability. TLS has been combined with space-time trellis code for MISO FSO systems to select two out of available laser sources in [146]. The authors have considered strong turbulence conditions and modelled the channel using negative exponential and K distribution in this work. Another work has

been reported in [147] related to TLS combined with space-time trellis code for MISO FSO systems.

After studying the literature, it is found that a significant research gap exists in the combined application of TLS and OSM for FSO cooperative communication over G-G channels with pointing error and path loss effect. Another gap exists in deriving closed form error expressions for both TLS and TLS-OSM systems over G-G channels with pointing and path loss error. In the literature, TLS has mostly been analyzed for strong turbulence conditions and has not been analyzed for cooperative FSO communication to the best of the author's knowledge. The complexity analysis of TLS and TLS-OSM schemes in terms of power consumption, cost, decoding complexity and overhead bits are not available in the literature also. All these factors motivate us to propose TLS and TLS-OSM schemes for FSO cooperative communication over G-G channel incorporating pointing error and path loss effect.

The contribution of our work is in deriving closed form expressions of outage probability and ASEP for TLS and TLS-OSM schemes in a FSO cooperative system. The performance of such systems are also compared with a system devoid of TLS. Asymptotic analysis is also performed for the proposed schemes and coding and diversity gains are calculated. The power consumption, cost, decoding complexity and overhead feedback bits required are analyzed for TLS and TLS-OSM. G-G channel incorporating pointing error and path loss effect is considered, thereby representing a practical scenario. The importance of our work is highlighted by the fact that closed form expressions are necessary for system analysis. Without closed form expressions, it is difficult to gain proper insight into the system performance. Closed form expressions can be used to understand the nature of system performance by varying certain system parameters. Asymptotic analysis is also possible from the closed form expressions. FSO is basically a LOS communication. Hence to transmit data over large distances (generally of the order of several kilometers), relays are required as it is easier to maintain LOS links between two short distant nodes. Presence of obstacles in urban environment also blocks the LOS path, making cooperative communication all the more necessary. Therefore, we consider performance analysis of TLS and TLS-OSM in cooperative FSO system in the subsequent sections.

4.4.1 Channel Model with Pointing Error

G-G channel model with pointing error is used for this analysis. The turbulence parameters for various atmospheric conditions have been defined in the previous sections. The detailed explanation of pointing error along with the CDF and PDF of channel model after including pointing and path loss error are derived in this section. Misalignment of laser sources causes pointing errors for which certain factors like aperture size of the detector, beam width and jitter variance have to be considered [130]. A circular aperture of radius a and a Gaussian beam profile at the receiver is assumed for this work. Let

detector accumulate h_p fraction of the power. The PDF of h_p is defined as:

$$f_{h_p}(h_p) = \frac{\zeta^2}{A_0^{\zeta^2}} h_p^{\zeta^2-1} \ , \tag{4.31}$$

where h_p can take any value in the interval $[0, A_0]$ and $\zeta = w_{z_{eq}}/2\sigma_s$. ζ can be expressed as the ratio between equivalent beam radius at the receiver ($w_{z_{eq}}$) and twice the pointing error displacement standard deviation at the receiver denoted by σ_s. ζ^2 is the coefficient which mainly denotes the effect of pointing error on the system performance. The above mentioned terms are defined as:

$$A_0 = [erf(\nu)]^2, \ w_{z_{eq}}^2 = w_z^2 \ \frac{\sqrt{\pi} erf(\nu)}{2\nu \exp(-\nu^2)}, \ \nu = \frac{\sqrt{\pi} a}{\sqrt{2} w_z} \ , \tag{4.32}$$

where w_z is the beam waist of a Gaussian beam propagating in atmospheric turbulence and its value is given in [130]. erf is the error function encountered while integrating the normal distribution. The laser beam while propagating through the atmosphere also causes attenuation of laser power which can be calculated by using Beer Lambert Law:

$$h_l(z) = \frac{P(z)}{P(0)} = \exp(-\sigma_{att} z) \ , \tag{4.33}$$

where attenuation coefficient is denoted by σ_{att}, $h_l(z)$ is the power loss which occurs due to laser beam propagation over a distance z, and $P(z)$ is the laser power measured at a distance z. For a long observation period, the term h_l is considered to be a fixed scaling factor. Thus this term accounts for the path loss error. h is the turbulence induced fading coefficient. The total error in FSO communication is the combined effect of pointing, attenuation and turbulence fading induced error. Therefore, the overall PDF of $h_{eq} = h_l h_p h$ after considering attenuation and pointing error can be written as [130]:

$$f_{h_{eq}}(h_{eq}) = \frac{\zeta^2}{A_0 h_l^{\zeta^2}} h_{eq}^{\zeta^2-1} \int_{h_{eq}/A_0 h_l}^{\infty} h^{-\zeta^2} f_h(h) dh \ . \tag{4.34}$$

For strong turbulence when G-G channels are used, then the overall PDF can be modified as [130]:

$$f_{h_{eq}}(h_{eq}) = \frac{2\zeta^2 (\alpha_G \beta_G)^{(\alpha_G+\beta_G)/2)}}{(A_0 h_l)^{\zeta^2} \Gamma(\alpha_G)\Gamma(\beta_G)} h_{eq}^{\zeta^2-1} \int_{h_{eq}/A_0 h_l}^{\infty} h^{(\alpha_G+\beta_G)/2-1-\zeta^2} K_{\alpha_G-\beta_G}(2\sqrt{\alpha_G \beta_G h}) dh \ . \tag{4.35}$$

The modified Bessel function of second kind and order $\alpha_G - \beta_G$ ($K_{\alpha_G-\beta_G}$) can be expressed in terms of Meijer G function and the final equation can be rewritten as [130, 148]:

$$f_{h_{eq}}(h_{eq}) = \frac{\zeta^2 (\alpha_G \beta_G)^{(\alpha_G+\beta_G)/2)}}{(A_0 h_l)^{\zeta^2} \Gamma(\alpha_G)\Gamma(\beta_G)} h_{eq}^{\zeta^2-1} \int_{h_{eq}/A_0 h_l}^{\infty} h^{(\alpha_G+\beta_G)/2-1-\zeta^2} G_{0,2}^{2,0}\left(\alpha_G \beta_G h \mid \begin{matrix} - \\ \frac{\alpha_G-\beta_G}{2}, \frac{\beta_G-\alpha_G}{2} \end{matrix}\right) dh$$

$$= \frac{\zeta^2(\alpha_G\beta_G)}{\Gamma(\alpha_G)\Gamma(\beta_G)A_0h_l} \times G_{1,3}^{3,0}\left(\begin{matrix}\zeta^2\\ \zeta^2-1,\alpha_G-1,\beta-1\end{matrix}\middle|\frac{\alpha_G\beta_Gh_{eq}}{A_0h_l}\right). \tag{4.36}$$

Let received SNR $y = h_{eq}^2$. Considering change in random variables, the PDF of received SNR is given by:

$$f_Y(y) = \frac{\zeta^2(\alpha_G\beta_G)}{(A_0h_l)\Gamma(\alpha_G)\Gamma(\beta_G)2y^{1/2}}G_{1,3}^{3,0}\left(\begin{matrix}\zeta^2\\ \zeta^2-1,\alpha_G-1,\beta_G-1\end{matrix}\middle|\frac{\alpha_G\beta_Gy^{1/2}}{A_0h_l}\right). \tag{4.37}$$

The overall CDF, after considering pointing and path loss error can be evaluated by integrating Eq. (4.36) and can be computed as:

$$F_{h_{eq}}(h_{eq}) = \frac{\zeta^2}{\Gamma(\alpha_G)\Gamma(\beta_G)} \times G_{2,4}^{3,1}\left(\begin{matrix}1,\zeta^2+1\\ \zeta^2,\alpha_G,\beta_G,0\end{matrix}\middle|\frac{\alpha_G\beta_Gh_{eq}}{A_0h_l}\right). \tag{4.38}$$

The CDF of received SNR after integrating Eq. (4.37) can be written as:

$$F_Y(y) = \frac{\zeta^2}{\Gamma(\alpha_G)\Gamma(\beta_G)}G_{2,4}^{3,1}\left(\begin{matrix}1,\zeta^2+1\\ \zeta^2,\alpha_G,\beta_G,0\end{matrix}\middle|\frac{\alpha_G\beta_Gy^{1/2}}{A_0h_l}\right). \tag{4.39}$$

4.4.2 Proposed System Model for TLS and TLS-OSM

The conventional 3 node one-way relay model, composed of source node (SN), relay node (RN) and destination node (DN) is considered, as displayed in Figure 4.8. SN and DN are directly interconnected also. The nodes are half-duplex in nature with N_L lasers at SN and RN and N_D photodetectors at RN and DN nodes. In this model, the nodes exchange data bits by means of DF technique at the relay. For transmission, N_L LED/lasers are utilized while N_D photodetectors of responsivity R_e are used for reception. The relative gains of the links as illustrated in Section II of [51] and Eq. 3 of [52] are written as: $G_{S,R} = (\frac{d_{SD}}{d_{SR}})^\tau$, $G_{R,D} = (\frac{d_{SD}}{d_{RD}})^\tau$ where $G_{S,R}$ and $G_{R,D}$ are the relative gain of the SN to RN link and RN to DN links respectively, d_{SR}, d_{SD} and d_{RD} are the distances between SN and RN, SN and DN, and RN and DN links respectively. The path loss coefficient is denoted by τ. Relative geometrical gain factor $\kappa_{rg} = \frac{G_{S,R}}{G_{R,D}}$ indicates the relative position of RN node. When RN is located closer to DN, κ_{rg} is less than 1, whereas κ_{rg} is greater than 1 if RN is located closer to SN and if RN is equidistant from SN and DN then κ_{rg} is 1.

In the source and relay nodes, source data modulates a RF subcarrier signal and the resulting modulated signal modulates the intensity of optical source like laser. In TLS, among all transmit laser sources, a single laser source is activated which give the maximum receive SNR. This laser source is used for transmission of messages using M-ary modulation scheme such as BPSK in the TLS encoder. For example, in Fig. 4.8 (a), TLI is chosen as 2 at the SN, hence laser 2 will be used for sending optical signals, all other laser sources remain idle. Similarly, TLI is chosen as N_L for RN, therefore only laser

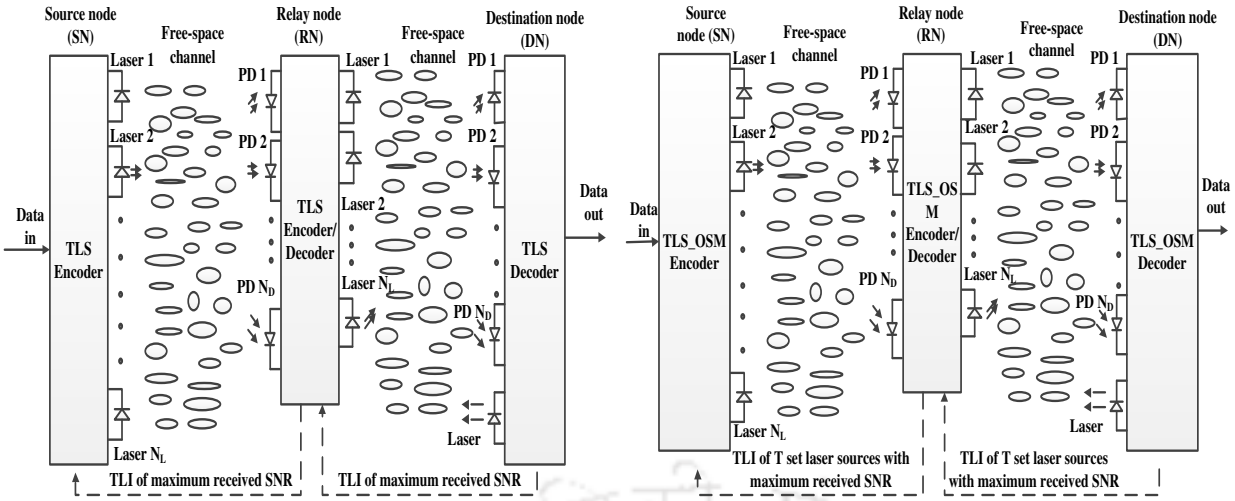

Figure 4.8: Proposed system model for (a) TLS and (b) TLS-OSM (TLI: Transmitter Laser Index/Indices, PD: Photodetector).

N_L will be sending optical signals. For illustration purpose, we have taken TLI=2 and TLI=N_L for SN and RN respectively. In actual scenario, TLI can be estimated before sending a chunk of data and TLI can be sent from the receiver to the transmitter through a low rate partial feedback link [149, 150] using $\log_2(N_L)$ bits. Since RN has N_L laser sources, any of these lasers could be used for sending TLI. In DN, we have intentionally added a laser source for executing this low-rate feedback channel.

In TLS-OSM, among all the transmit laser sources, a set of T laser sources are selected which give the maximum receive SNR at the receiver. On these T laser sources, OSM is applied. In other words, transmit laser source activation and mapping of M-ary modulation scheme such BPSK are performed depending on the incoming message bits. For example, in Fig. 4.8 (b), at SN, second laser is activated for incoming message bit 0001 for T=8. In this case, BPSK symbol will be sent from Laser 2 of SN. OSM decoder will decode the transmit laser index as well as the message bit sent from the transmitter. Thus in TLS-OSM, TLI is sent using $T\log_2(N_L)$ bits through a low rate partial feedback link. TLS-OSM detection process carries information for both TLI and symbol, unlike TLS where the detection is done only for the symbol transmitted.

4.4.3 Complexity Analysis of TLS and TLS-OSM

For power consumption analysis, it is assumed that power consumption of each optical chain and optical switch are P_o and P_{sw} respectively [151]. α_{tr} is the load dependent slope factor while P_{tr} is the optical transmit power. Each optical switch can connect two lasers. The number of optical switches required is denoted by N_{sw}. For spatial multiplexing optical MIMO techniques, N_L optical chains are required, which is the same as the number of lasers required. For TLS and TLS-OSM, only 1 optical chain is required. To achieve a spectral efficiency of η_{SE} bits per channel use (bpcu) for M-ary modulation scheme, switch requirement for TLS is $N_{sw}^{TLS} = N_L/2$ while for TLS-OSM, switch requirement

is $N_{sw}^{TLS-OSM} = 2^{(\eta_{SE}-\log_2(M)-1)}$. Total power consumption of TLS and TLS-OSM scheme is computed by Eq. (4.40) and (4.41) respectively.

$$P_{tot}^{TLS} = P_o + \alpha_{tr} P_{tr} + P_{sw} N_{sw}^{TLS} \ . \tag{4.40}$$

$$P_{tot}^{TLS-OSM} = P_o + \alpha_{tr} P_{tr} + P_{sw} N_{sw}^{TLS-OSM} \ . \tag{4.41}$$

Power consumption of optical MIMO techniques is given by:

$$P_{tot}^{MIMO} = P_o N_L + \alpha_{tr} P_{tr} \ . \tag{4.42}$$

Though there is switch requirement for TLS and TLS-OSM scheme, but the number of switches required to achieve a high spectral efficiency is less. Hence the total power consumption of N_L optical chains in optical MIMO is more than the power consumed by the switches and single optical chain in TLS and TLS-OSM. Similarly from cost perspective, it is assumed that cost of each optical chain and optical switch are C_o and C_{sw} respectively. A S/P converter is also required for TLS and TLS-OSM whose cost is denoted by $C_{S/P}$. Total cost of TLS and TLS-OSM scheme is evaluated as Eq. (4.43) and (4.44) respectively.

$$C_{tot}^{TLS} = C_o + C_{S/P} + C_{sw} N_{sw}^{TLS} \ . \tag{4.43}$$

$$C_{tot}^{TLS-OSM} = C_o + C_{S/P} + C_{sw} N_{sw}^{TLS-OSM} \ . \tag{4.44}$$

Cost of optical MIMO techniques is evaluated as $C_{tot}^{MIMO} = C_o N_L$. The cost of an optical switch is much lower than that of an optical chain and number of switches required in TLS and TLS-OSM is much lesser than the optical chain requirement in optical MIMO. An example is considered where $\eta_{SE} = 8$ bpcu, $N_L = 64$ and $M = 4$. The number of switches required for OSM is $N_{sw}^{OSM} = 32$, while TLS requires $N_{sw}^{TLS} = 32$ switches and TLS-OSM also requires $N_{sw}^{TLS-OSM} = 32$ switches. The parameters considered are $P_o = 53W, \alpha_{tr} = 3.1, P_{tr} = 6.3W, P_{sw} = 0.2W, C_o = 1000\$, C_{S/P} = 2\$, C_{sw} = 220\$$. Please note that these are typical values obtained through quotations and websites [152, 153, 154, 155, 156]. The cost may vary according to location, however the proportion of the values with respect to each other will be similar. An optical chain comprises of intensity modulator, RF modulator, DC bias adder, pulse shaping and I/Q modulator blocks. Hence the cost is calculated accordingly. The power consumption of OSM, TLS and TLS-OSM are thus calculated as $P_{tot}^{OSM} = P_{tot}^{TLS} = P_{tot}^{TLS-OSM} = 78.9$ W while optical MIMO has power consumption of $P_{tot}^{MIMO} = 3411$ W. Similarly, the cost is calculated for OSM, TLS and TLS-OSM as $C_{tot}^{OSM} = C_{tot}^{TLS} = C_{tot}^{TLS-OSM} = 804.2\$$ while the cost of optical MIMO is $C_{tot}^{MIMO} = 64002\$$.

Hence it is conclusive that TLS and TLS-OSM perform better than optical MIMO in terms of power consumption and cost. Decoding complexity of optical MIMO is given by M^{N_L} (as ML decoding is applied), whereas decoding complexity of TLS and TLS-OSM is given by M since single optical chain is used. The complexity comparison table is shown in Table 6.1.

Table 4.6: Complexity comparison of the proposed methods.

Schemes	Power consumption	Cost	Decoding complexity	TLI overhead
Optical MIMO	$P_o N_L + \alpha_{tr} P_{tr}$	$C_o N_L$	M^{N_L}	Nil
TLS	$P_o + \alpha_{tr} P_{tr} + P_{sw} N_{sw}^{TLS}$	$C_o + C_{S/P} + C_{sw} N_{sw}^{TLS}$	M	$\log_2(N_L)$
TLS-OSM	$P_o + \alpha_{tr} P_{tr} + P_{sw} N_{sw}^{TLS-OSM}$	$C_o + C_{S/P} + C_{sw} N_{sw}^{TLS-OSM}$	M	$T log_2(N_L)$

4.4.4 Performance Analysis of TLS and TLS-OSM

Outage probabilities and end-to-end ASEP of the the system are evaluated in this section. First we have analyzed system performance in selecting one optical source and then we have incorporated OSM along with TLS to select a set of optical sources. Assume $\eta_S = \frac{P_S}{N_0}$, $\eta_R = \frac{P_R}{N_0}$, be the SNR at source node and relay node respectively. P_S indicates the source node transmission power and P_R indicates the relay node transmission power.

4.4.4.1 Outage Probability of TLS system

In the first time slot, the message is broadcasted by the source node to the relay node and destination node. The message is decoded at the relay and on successful decoding, the message is encoded by the relay and retransmitted to the destination node in the second time slot. The process is unidirectional in nature.

The j_R photodetector of RN receives the signal in n^{th} time slot which is given by:

$$y_R^{j_R}[n] = \sqrt{R_e P_S G_{S,R}}\; h_{j,i}^{S,R} x[n] + w_S[n] \;, \tag{4.45}$$

where $j_R \in \{1, 2, ..., N_D\}$. At the relay node, the noise is represented by the term $w_S[n]$. R_e is the responsivity of the photodetector. $x[n]$ is the message bit modulated by BPSK scheme in the n^{th} time slot. $h_{j,i}^{S,R}$ is the channel coefficient between the i^{th} transmitting laser of node SN and j^{th} receiving photodetector of node RN. The signal received at RN is decoded by using ML algorithm and the decoded message bit is denoted by $x_R[n]$.

The received signal emitted from the relay and obtained at the j_D photodetector of destination node

in n^{th} time slot is expressed as:

$$y_{RD}^{j_D}[n] = \sqrt{R_e P_R G_{R,D}}\ h_{j,i}^{R,D} x_R[n] + w_R[n]\ . \tag{4.46}$$

$h_{j,i}^{R,D}$ is the channel coefficient between the i^{th} transmitting laser of node RN and j^{th} receiving photodetector of node DN. At the destination node, the overall noise is denoted by $w_R[n]$.

The received signal emitted from the source node, obtained at the j_D photodetector of destination node in n^{th} time slot is expressed as:

$$y_{SD}^{j_D}[n] = \sqrt{R_e P_S}\ h_{j,i}^{S,D} x[n] + w_D[n]\ . \tag{4.47}$$

$h_{j,i}^{S,D}$ is the channel coefficient between the i^{th} transmitting laser of node SN and j^{th} receiving photodetector of node DN. For broadcasting phase, the overall noise is represented by $w_D[n]$. MRC is applied at the destination node to maximize the received SNR at DN in both the time slots.

In case of photodetectors, the major sources of noise are thermal noise, shot noise and dark current noise. We have considered thermal noise ($\sigma_t = \frac{4k_B T_e B_w F_n}{R_L}$) generated due to a load resistance (R_L) of 50 Ω at a temperature (T_e) of 300 K. k_B is the Boltzmann's constant, F_n is the noise figure and B_w is the bandwidth. Shot noise arises due to the random arrival of photons and is given by $\sigma_s = 2q_e R_e P_S B_w$ where q_e is the electron charge. Dark current noise is given by $\sigma_d = 2q_e I_{DC} B_w$ where I_{DC} is the dark current generated in photodetector in absence of light [157]. Hence overall noise variance at the nodes is given by $\sigma_n^2 = \sigma_t^2 + \sigma_s^2 + \sigma_d^2$.

A single transmit optical source is selected according to the following criteria:

$$I^k = \underset{1 \le i \le N_L^k}{arg\ \ max} \left\{ C_i = \sum_{j=1}^{N_D^D} |h_{j,i}^{k,D}|^2 \right\}\ , \tag{4.48}$$

where $k\ \epsilon \{S, R\}$, I^k denotes the transmit laser index of node k which maximizes the received SNR at the destination node, $h_{j,i}^{k,D}$ is the channel coefficient between the i^{th} transmitting laser of node k and j^{th} receiving photodetector of node DN, N_D^D is the count of photodetectors at DN and N_L^k denotes the number of lasers at k^{th} node. Each C_i for $i\ \epsilon\ (1, 2, ...N_L^k)$ for node SN and RN are arranged in ascending order such that $C_1 \le C_2 \le ... \le C_{N_L^k}$. At SN and RN, the transmit laser index is chosen which gives the highest value of $C_{N_L^k}$. Assumption is taken that all channel coefficients $h_{j,i}^{k,D}$ are independent and identically distributed. The CDF of the received SNR after applying TLS, ($F_\gamma(\gamma)$) follows square of G-G distribution with pointing errors. Our next objective is to find the outage probability of the TLS system. The total transmission occurs in two stages. Hence the outage probability has to be

computed in two steps. For the first step, outage probability occurs independently in both the source-to-relay link and source-to-destination link. Thus the first stage outage probability will be the product of outage probability of source-to-relay transmission and the outage probability of source-to-destination transmission. If the relay is able to decode the message successfully in the first stage, then the second stage transmission occurs and the outage probability is computed for relay-to-destination link. Hence the second stage outage probability can be computed as the product of outage probability of relay-to-destination transmission and the complement of outage probability of source-to-relay transmission. Now for TLS, outage probability occurs when all the paths from lasers at one node to photodetector at the other node fails. Due to the presence of diversity, even if one laser is able to transmit successfully, then outage does not occur. This means all links for source-to-destination have to fail for outage condition, meaning maximum of random variables criteria holds true. Therefore, outage probability for a particular link in TLS is given by the product of individual outage probabilities of a particular laser to photodetector link. The outage probability for source-to-relay link is given by $F_{\gamma_{SR}}(\frac{\gamma_{th}}{\bar{\gamma}_{SR}})$, while the outage probability of the overall source-to-destination link (when all link failure occurs for source-to-destination) is given by $\left[F_{\gamma_{SD}}(\frac{\gamma_{th}}{\bar{\gamma}_{SD}})\right]^{N_L^S}$. The outage probability for the overall relay-to-destination link (provided relay can successfully decode the message in the first phase) is given by $\left[F_{\gamma_{SRD}}\left(\frac{\gamma_{th}}{\bar{\gamma}_{SD}+\bar{\gamma}_{RD}}\right)\right]^{\frac{N_L^S+N_L^R}{2}}$. Therefore, the end-to-end outage probability of TLS system can be evaluated as [134], [158]:

$$P_{out}(\gamma_{th}) = F_{\gamma_{SR}}(\frac{\gamma_{th}}{\bar{\gamma}_{SR}})\left[F_{\gamma_{SD}}(\frac{\gamma_{th}}{\bar{\gamma}_{SD}})\right]^{N_L^S} + \left[1 - F_{\gamma_{SR}}(\frac{\gamma_{th}}{\bar{\gamma}_{SR}})\right]\left(F_{\gamma_{SRD}}\left(\frac{\gamma_{th}}{\bar{\gamma}_{SD}+\bar{\gamma}_{RD}}\right)\right)^{\frac{N_L^S+N_L^R}{2}}, \quad (4.49)$$

where $\gamma_{th} = 2^{R_d-1}$ and R_d is the threshold data rate in bps. For analyzing outage probability considering pointing errors, the CDFs follow distribution as given in Eq. (4.39). The CDFs can be expressed as:

$$F_{\gamma_{SR}}\left(\frac{\gamma_{th}}{\bar{\gamma}_{SR}}\right) = \frac{\zeta^2}{\Gamma(\alpha_G)\Gamma(\beta_G)} G_{2,4}^{3,1}\left(\begin{matrix}1,\zeta^2+1\\ \zeta^2,\alpha_G,\beta_G,0\end{matrix}\middle|\frac{\alpha_G\beta_G\left(\frac{\gamma_{th}}{\bar{\gamma}_{SR}}\right)^{1/2}}{A_0 h_l}\right), \quad (4.50)$$

$$F_{\gamma_{SD}}\left(\frac{\gamma_{th}}{\bar{\gamma}_{SD}}\right) = \frac{\zeta^2}{\Gamma(\alpha_G)\Gamma(\beta_G)} G_{2,4}^{3,1}\left(\begin{matrix}1,\zeta^2+1\\ \zeta^2,\alpha_G,\beta_G,0\end{matrix}\middle|\frac{\alpha_G\beta_G\left(\frac{\gamma_{th}}{\bar{\gamma}_{SD}}\right)^{1/2}}{A_0 h_l}\right), \quad (4.51)$$

$$F_{\gamma_{RD}}\left(\frac{\gamma_{th}}{\bar{\gamma}_{RD}}\right) = \frac{\zeta^2}{\Gamma(\alpha_G)\Gamma(\beta_G)} G_{2,4}^{3,1}\left(\begin{matrix}1,\zeta^2+1\\ \zeta^2,\alpha_G,\beta_G,0\end{matrix}\middle|\frac{\alpha_G\beta_G\left(\frac{\gamma_{th}}{\bar{\gamma}_{RD}}\right)^{1/2}}{A_0 h_l}\right), \quad (4.52)$$

where average SNR of SN-to-RN link $(\bar{\gamma}_{SR}) = \eta_S R_e G_{S,R}$, average SNR of SN-to-DN link $(\bar{\gamma}_{SD}) = \eta_S R_e$ and average SNR of RN-to-DN link $(\bar{\gamma}_{RD}) = \eta_R R_e G_{R,D}$. η_S and the η_R are the source and relay node SNR. The CDF terms contain the Meijer G function which depends on the SNR value. The

Meijer G function decreases with an increment in SNR value resulting in decrement of the overall CDF term. Hence there is a reduction in product of such terms. The CDF term $F_{\gamma_{SR}}(\frac{\gamma_{th}}{\bar{\gamma}_{SR}})$ is subtracted from 1 thereby increasing the result which is again compensated by a greater decrease of the term $F_{\gamma_{SRD}}(\frac{\gamma_{th}}{\bar{\gamma}_{SR}+\bar{\gamma}_{RD}})^{\frac{N_L^S+N_L^R}{2}}$, hence resulting in an overall decrement in outage probability with increment in SNR value. The outage probability of the system without considering TLS is evaluated as:

$$[P_{out}(\gamma_{th})]_{No\ selection} = F_{\gamma_{SR}}(\frac{\gamma_{th}}{\bar{\gamma}_{SR}})\left[F_{\gamma_{SD}}(\frac{\gamma_{th}}{\bar{\gamma}_{SD}})\right] + \left[1 - F_{\gamma_{SR}}(\frac{\gamma_{th}}{\bar{\gamma}_{SR}})\right]\left(F_{\gamma_{SRD}}\left(\frac{\gamma_{th}}{\bar{\gamma}_{SD}+\bar{\gamma}_{RD}}\right)\right) \ . \quad (4.53)$$

4.4.4.2 Analysis of TLS-OSM System

To select a set of T laser sources which produce the maximum received power, all the C_is obtained from Eq. (4.48) are arranged in ascending order. The set of T laser sources corresponding to the maximum values of C_is are chosen. Following the order statistics, the PDF of C_i such that $C_1 \leq C_2 \leq ... \leq C_i \leq ...C_{N_L^k}$ is given by [32]:

$$f_{C_i}(\gamma) = \frac{1}{B_t(i, N_L^k - i + 1)}\left\{F_\gamma(\gamma)\right\}^{i-1}\left(1 - F_\gamma(\gamma)\right)^{N_L^k - i} f_\gamma(\gamma) \ , \quad (4.54)$$

where $i = N_L^k - T + 1$, $k \ \epsilon \ \{S, R\}$, beta function is represented by $B_t(.,.)$. Now our next objective is to find the PDF of received SNR where T sources are selected. The set of T sources will correspond to the best set of SNR values arranged in ascending order. After choosing a particular SNR value C_i, the next T set of SNR values need to be chosen. The PDF of the SNR for selection of these T sources needs to be evaluated. For this purpose, the PDF of C_i needs to be calculated for the range $N_L^k - T + 1$ to N_L^k and divided by the range i.e. T. Therfore the SNR received at RN or DN node, follows a PDF which is given by:

$$f_\gamma^i(\gamma) = \frac{1}{N_L^k - i + 1}\sum_{j=i}^{N_L^k}\frac{1}{B_t(j, N_L^k - j + 1)}\left\{F_\gamma(\gamma)\right\}^{j-1}\left(1 - F_\gamma(\gamma)\right)^{N_L^k - j} f_\gamma(\gamma) \ , \quad (4.55)$$

where $f_\gamma(\gamma)$ and $F_\gamma(\gamma)$ are PDF and CDF of square of G-G distribution with pointing error calculated using Eq. (4.37) and (4.39) respectively. PDF of the received SNR for all the three links SN-RN, SN-DN and RN-DN are calculated individually for error analysis.

For $T = 2$, (where T is the number of selected laser sources) the transmit laser source which is activated is chosen as:

$$j_k = \begin{cases} 2, & \text{if } x_k^{LSB}[n] = 1 \\ 1, & \text{if } x_k^{LSB}[n] = 0 \ , \end{cases} \quad (4.56)$$

where the n^{th} time slot is represented by n and k denotes the node which may be SN or RN for this model.

If $T > 2$, then the transmit laser source is activated by using $\log_2 T$ number of bits (from LSB side) and $\log_2 M$ message bit will be applied for symbol constellation mapping. BPSK modulation scheme is utilized for our analysis. Depending on the message bits, laser source is activated and the corresponding mapping has been tabulated in Table 3 and Table 4 of [128] for T=4 and T=8 respectively. OSM is combined with TLS to obtain greater spectral efficiency. The proposed TLS-OSM system can transmit $\log_2(M) + \log_2(T)$ bits per channel use (bpcu) while a normal TLS system can transmit $\log_2(T)$ bpcu.

4.4.4.3 Error Analysis of TLS and TLS-OSM

Our objective is to calculate the end-to-end error probability of TLS and TLS-OSM systems. For error analysis, PDF is required. We start with the end-to-end CDF of TLS system which is obtained from outage probability equation (Eq. 4.49) and is given by:

$$F_{\gamma_{E2E}}(\gamma) = F_{\gamma_{SR}}\left(\frac{\gamma}{\bar{\gamma}_{SR}}\right)\left[F_{\gamma_{SD}}\left(\frac{\gamma}{\bar{\gamma}_{SD}}\right)\right]^{N_L^S} + \left[1 - F_{\gamma_{SR}}\left(\frac{\gamma}{\bar{\gamma}_{SR}}\right)\right] \times \left(F_{\gamma_{SRD}}\left(\frac{\gamma}{\bar{\gamma}_{SD}+\bar{\gamma}_{RD}}\right)\right)^{\frac{N_L^S+N_L^R}{2}}, \tag{4.57}$$

where γ_{E2E} is the end-to-end SNR. It is observed from the end-to-end CDF equation that the CDF is calculated in two phases. The CDF of the first stage transmission is given by the product of the CDF of source-to-relay transmission and CDF of source-to-destination transmission. Both these transmission processes are independent, hence the product of two CDF terms gives the CDF of the first stage. In the next stage, the CDF is calculated by the product of CDF of relay-to-destination transmission and the complement of CDF of source-to-relay transmission. The complement of CDF of source-to-relay transmission signifies that if the message bits are decoded successfully by the relay in the first stage, then only the second stage transmission can occur. The end-to-end PDF of the system obtained by differentiating Eq. (4.57) is given by:

$$\begin{aligned} f_{\gamma_{E2E}}(\gamma) &= \frac{d}{d\gamma}F_{\gamma_{E2E}}(\gamma) \\ &= \frac{1}{\bar{\gamma}_{SR}}f_{\gamma_{SR}}\left(\frac{\gamma}{\bar{\gamma}_{SR}}\right)\left[F_{\gamma_{SD}}\left(\frac{\gamma}{\bar{\gamma}_{SD}}\right)\right]^{N_L^S} + F_{\gamma_{SR}}\left(\frac{\gamma}{\bar{\gamma}_{SR}}\right)\frac{N_L^S}{\bar{\gamma}_{SD}}\left[F_{\gamma_{SD}}\left(\frac{\gamma}{\bar{\gamma}_{SD}}\right)\right]^{N_L^S-1} f_{\gamma_{SD}}\left(\frac{\gamma}{\bar{\gamma}_{SD}}\right) \\ &- \frac{1}{\bar{\gamma}_{SR}}f_{\gamma_{SR}}\left(\frac{\gamma}{\bar{\gamma}_{SR}}\right)\left(F_{\gamma_{SRD}}\left(\frac{\gamma}{\bar{\gamma}_{SD}+\bar{\gamma}_{RD}}\right)\right)^{\frac{N_L^S+N_L^R}{2}} + \left[1 - F_{\gamma_{SR}}\left(\frac{\gamma}{\bar{\gamma}_{SR}}\right)\right]\left(\frac{N_L^S+N_L^R}{2}\right)\frac{1}{\bar{\gamma}_{SD}+\bar{\gamma}_{RD}} \\ &\times \left(F_{\gamma_{SRD}}\left(\frac{\gamma}{\bar{\gamma}_{SD}+\bar{\gamma}_{RD}}\right)\right)^{\frac{N_L^S+N_L^R}{2}-1} f_{\gamma_{SRD}}\left(\frac{\gamma}{\bar{\gamma}_{SD}+\bar{\gamma}_{RD}}\right). \end{aligned} \tag{4.58}$$

For M-ary modulation, overall ASEP is written as [61]:

$$P_e = \int_0^\infty aQ(\sqrt{e\gamma}) f_{\gamma_{E2E}}(\gamma) d\gamma, \tag{4.59}$$

where $f_{\gamma_{E2E}}(\gamma)$ is given by Eq. (4.58). The constellation scheme determines the values of a and e which have been obtained from Eq. 7 of [81]. For BPSK, $a = 1, e = 2$. The integral can be solved in Mathematica.

The error analysis for TLS-OSM scheme is also performed. The PDFs obtained using Eq. (4.55) are used to perform error analysis. The total transmission is a two stage process. Hence the error has to be computed in two steps. For the first step, error can occur both during source-to-relay transmission and source-to-destination transmission. Thus the first stage error probability will be the product of error probability of source-to-relay transmission and the error probability of source-to-destination transmission. If the relay is able to decode the message successfully in the first stage, then the second stage transmission occurs and the error is computed for relay-to-destination transmission. Hence the second stage error probability can be computed as the product of error probability of relay-to-destination transmission and the complement of error probability of source-to-relay transmission. Therefore the end-to-end probability of error is given by [135]:

$$P_e = P_{e(SR)}(\bar{\gamma}_{SR})P_{e(SD)}(\bar{\gamma}_{SD}) + P_{e(SRD)}(\bar{\gamma}_{SRD})\left[1 - P_{e(SR)}(\bar{\gamma}_{SR})\right] , \tag{4.60}$$

where $P_{e(SRD)}(\bar{\gamma}_{SRD})$ is the probability of error at DN when RN is able to decode the data correctly in the first phase, $P_{e(SR)}(\bar{\gamma}_{SR})$ is the probability of error at RN in the first phase and $P_{e(SD)}(\bar{\gamma}_{SD})$ is the error probability at DN in the first phase. $(1 - P_{e(SR)}(\bar{\gamma}_{SR}))$ is the probability that RN has decoded the message successfully in the first stage. All these probability of errors at the individual nodes (P_{node}) can be calculated as:

$$P_{node} = \int_0^\infty Q(\sqrt{2\gamma}) f_n(\gamma) d\gamma , \tag{4.61}$$

where $f_n(\gamma)$ is the PDF of received SNR at the particular node calculated from Eq. (4.55). The integral can be solved in Mathematica.

4.4.4.4 Asymptotic Analysis

Let us carry out the asymptotic analysis of outage probability for TLS. The outage probability of TLS system is given in Eq. (4.49) which is a product of several CDF term. Let us consider a single CDF term which contains Meijer G component. Eq. (4.57) has Meijer G term which can be inverted and written in terms of elementary function at very high SNR values [63] using the formula already explained in Chapter 2. Hence the CDF of any link (SR or RD) can be written as:

$$F_\gamma\left(\frac{\gamma_{th}}{\bar{\gamma}}\right) \approx \frac{\zeta^2}{\Gamma(\alpha_G)\Gamma(\beta_G)} \sum_{k=1}^{3} z^{a_k - 1} \frac{\prod_{l=1, l\neq k}^{3} \Gamma(a_k - a_l) \prod_{l=1}^{1} \Gamma(1 + b_l - a_k)}{\prod_{l=4}^{4} \Gamma(1 + a_l - a_k) \prod_{l=2}^{2} \Gamma(a_k - b_l)} , \tag{4.62}$$

where $z = \frac{A_0 h_l \bar{\gamma}^{1/2}}{\gamma_{th}^{1/2} \alpha_G \beta_G}$, $a = [1-\zeta^2, 1-\alpha_G, 1-\beta_G, 1]$ and $b = [0, \zeta^2]$. The diversity and coding gain can be obtained when the SNR ($\bar{\gamma}$) exponent is maximum. Using Eq. (2.73), we can obtain the diversity gain of our TLS system as $\min(\frac{\zeta^2}{2}, \frac{\alpha_G}{2}, \frac{\beta_G}{2})$. Now the CDF terms are multiplied in Eq. (4.57), which means each Meijer G term is multiplied. We need to consider only the highest exponent of SNR in this case. The negative component of highest exponent of SNR is obtained when the exponent term is multiplied by $\max(N_L^S, (N_L^S + N_L^R)/2)$. Hence the total diversity gain of TLS is given by $D_g = \left(\min(\frac{\zeta^2}{2}, \frac{\alpha_G}{2}, \frac{\beta_G}{2})\right) \times \left(\max(N_L^S, (N_L^S + N_L^R)/2)\right)$. The diversity gain of system without TLS will be $\min(\frac{\zeta^2}{2}, \frac{\alpha_G}{2}, \frac{\beta_G}{2})$ as the CDF term is not raised to the power of number of lasers. Let us illustrate this with an example. If $N_L^S = N_L^R = 2$ and if the channel follows strong turbulence conditions i.e. $\alpha_G = 4.2, \beta_G = 1.4, \zeta^2 = 17.4$, then the diversity gain is $D_g = 0.7 \times 2 = 1.4$. For $N_L^S = N_L^R = 3$, diversity gain is $D_g = 0.7 \times 3 = 2.1$. For system without TLS, diversity gain will be 0.7. We will verify the results from the simulation results later. From this analysis, we can conclude that having more number of lasers at source and relay node gives better diversity and hence the slope of the curve will be more indicating better system performance.

To calculate the coding gain, we separate the SNR terms and the remaining terms in Eq. (4.62). The modified equation is given by:

$$F_\gamma\left(\frac{\gamma_{th}}{\bar{\gamma}}\right) \cong \frac{\zeta^2}{\Gamma(\alpha_G)\Gamma(\beta_G)} \sum_{k=1}^{3} \left(\frac{A_0 h_l}{\gamma_{th}^{1/2} \alpha_G \beta_G}\right)^{a_k - 1} \frac{\prod_{l=1, l\neq k}^{3} \Gamma(a_k - a_l) \prod_{l=1}^{1} \Gamma(1 + b_l - a_k)}{\prod_{l=4}^{4} \Gamma(1 + a_l - a_k) \prod_{l=2}^{2} \Gamma(a_k - b_l)} \times \bar{\gamma}^{(1/2(a_k - 1))}. \tag{4.63}$$

Now with the help of Eq. (2.73), the final coding gain (C_g) for TLS system can be calculated as:

$$C_g = \left(\frac{\zeta^2}{\Gamma(\alpha_G)\Gamma(\beta_G)} \sum_{k=1}^{3} \left(\frac{A_0 h_l}{\gamma_{th}^{1/2} \alpha_G \beta_G}\right)^{a_k - 1} \frac{\prod_{l=1, l\neq k}^{3} \Gamma(a_k - a_l) \prod_{l=1}^{1} \Gamma(1 + b_l - a_k)}{\prod_{l=4}^{4} \Gamma(1 + a_l - a_k) \prod_{l=2}^{2} \Gamma(a_k - b_l)}\right)^{-\frac{\max(N_L^S, (N_L^S + N_L^R)/2)}{D_g}}. \tag{4.64}$$

Thus we can see that with the benefits of tractable closed form expressions we could find out the diversity and coding gain from the expressions itself without doing any numerical simulations which require computational resources and it is time consuming.

Asymptotic analysis for ASEP can also be done in a similar manner. Since the entire derivation will be similar to that of the outage probability asymptotic analysis, hence we are skipping the same expressions to avoid redundancy. The individual CDF and PDF terms contain Meijer G components and can be written in terms of elementary functions for high SNR values as shown earlier. For error analysis the overall PDF is multiplied by a Q function whose SNR component has an exponent of 1/2. Using the relation, $\int_0^\infty erfc(x) x^{a-1} dx = \Gamma((1+a)/2)/(\sqrt{\pi} a)$ (Eq. 6.281 in [48]), we can compare the exponent of SNR terms only. The highest exponent of SNR is observed when the SNR is multiplied $\max(N_L^S, N_L^R)$

times. Hence the final diversity gain obtained from ASEP analysis is also $D_g = \left(\min(\frac{\zeta^2}{2}, \frac{\alpha_G}{2}, \frac{\beta_G}{2})\right) \times \left(\max(N_L^S, (N_L^S + N_L^R)/2)\right)$. Similarly for TLS-OSM system, diversity gain can be obtained. From order statistics (refer to Eq. (4.55)), we can notice that after writing the PDF and CDF terms using Eq. (4.62), the highest exponent of SNR in the expression is again N_L^k. Referring to Eq. (2.73), the final diversity gain of TLS-OSM system can be written as $D_g = \left(\min(\frac{\zeta^2}{2}, \frac{\alpha_G}{2}, \frac{\beta_G}{2})\right) \times \left(\max(N_L^S, (N_L^S + N_L^R)/2)\right)$. However, it is interesting to note that the diversity gain values of TLS and TLS-OSM will be different. In TLS, let there be 2 sources at relay and source node. Hence $N_L^S = N_L^R = 2$. But in TLS-OSM, we have to select T out of total sources. Hence let $N_L^S = 4, N_L^R = 4$ and $T = 2$. Therefore, diversity gain for TLS-OSM will be more as number of lasers at source and relay is more than that of OSM. Considering strong turbulence conditions i.e. $\alpha_G = 4.2, \beta_G = 1.4, \zeta^2 = 17.4$, diversity gain of TLS is then $0.7 \times 2 = 1.4$ while that of TLS-OSM is $0.7 \times 4 = 2.8$. Similarly for the case when $N_L^S = N_L^R = 6, T = 2$, TLS-OSM will have a diversity gain of 4.2. These values will be verified from the simulation results later on.

4.4.5 Results

System performance of TLS is done in terms of ASEP and outage probability. Strong turbulence conditions are considered for all simulations unless explicitly specified. It is assumed that source and relay nodes have identical SNR and transmit power. Responsivity of the photodetector (R_e) is taken as 0.5. The relay node is situated midway between SN and DN, meaning κ_{rg}=0 dB. The distance of separation between SN and RN and the distance between RN and DN are taken as 2 Km. The parameters considered for our work (as in [130]) are listed in Table 4.7. The G-G channel model incorporating pointing errors is considered.

Table 4.7: Parameter values.

Parameter	Symbol	Rate
Transmitter/receiver optical efficiency	$\eta_{Tx} = \eta_{Rx}$	0.8
Responsivity	R_e	0.5
Standard deviation of noise	σ_n	10^{-7}
Receiver diameter	2a	20cm
Distance between two nodes	L	2 Km
Corresponding beam radius at 1Km	w_z	2.5m
Corresponding jitter standard deviation	σ_s	30cm
Transmitter aperture	T_{ap}	7.5cm
Transmitter aperture separation	T_{sep}	40mm
Divergence angle	θ	2 mrad

The laser selection diversity (TLS) can be illustrated by means of Table 4.8. The G-G channel

incorporating pointing error case is considered for analysis. As the number of available lasers for selection increases, the proposed system has an increment in transmit power gain. The transmit optical power required to achieve certain outage probabilities have been tabulated in the table. It can be observed that to achieve a particular outage probability value of 0.01, the TLS system having 2 laser sources at each node requires 16 dBm of power while the TLS system having 3 laser sources at each node requires 11 dBm of power. Hence in this case, the system having 3 laser sources can achieve a coding gain of 5 dBm. The coding gain increases as the target outage probability value decreases. The reason for better performance of the system having more laser sources is the fact that more channel diversity is available to select the channel with best SNR, and accordingly the transmit laser can be selected.

Table 4.8: Comparison of outage probability results for TLS.

Outage probability	Transmit optical power for various combinations (in dBm)	
	$N_L^S = N_L^R = 2$	$N_L^S = N_L^R = 3$
0.1	8	5
0.01	16	11
0.005	19	13

To visualize the effect of different SNR at source and relay node, the transmit power at relay node is varied (keeping noise fixed) for various configurations of TLS scheme in Fig. 4.9. The G-G channel with pointing errors is used for this analysis. It is observed that an increment in optical transmit power at relay node (P_R) and an increment in number of transmit sources results in performance improvement, as was the trend earlier in case of equal SNR values at source and relay nodes. At a particular source transmit power value, increase in the relay transmit power can improve the performance. This is because if relay transmit power is increased, then the chances of successful message transmission in the second time slot is more. It means that even if DN is unable to receive message from SN in the first time slot, still the DN can receive the message successfully in second time slot as the message from SN is routed through the RN with a higher relay transmit power.

The outage probabilities for various configurations of TLS are compared with that of a model where there is no laser source selection. G-G channel with pointing error is used for analysis. Outage probabilities for different number of transmit laser sources at the source and relay node are plotted in Fig. 4.10. The analytical results are verified by means of Monte Carlo simulations. The target data rate (R_d) is taken as 2 bps. It is deduced from the graph that the system performance gets enhanced with increase in source and relay transmit sources. The proposed system gives better performance over the scenario when there is no transmit laser selection, obtained using Eq. (4.53). The analytical results for G-G channel

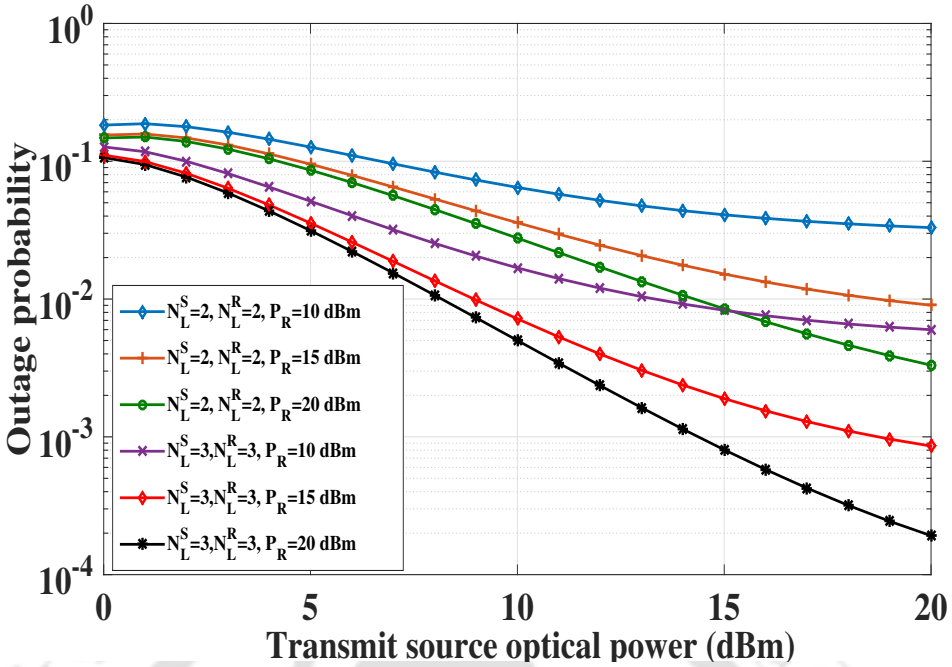

Figure 4.9: Outage probability results for various number of transmit sources for TLS scheme at various relay node transmit power values.

with pointing error are obtained using Eq. (4.49). The results can be interpreted in a different manner also. As the number of laser sources increases, more diversity is obtained and the optimum channel with the best SNR can be selected even if a few links are of poor quality. By having the chance of selecting a channel from a larger pool of channels increases the chances of obtaining the best channel. Thus the best laser can be selected for transmission if more diversity is available. In case of system without TLS, there is no chance of selection of channel depending upon channel quality. Hence if the selected link is down, system performance is affected. Therefore, system without TLS gives poorer performance as compared to TLS system. Let us calculate the diversity gains from Fig. 4.10. For the system without TLS and considering the SNR range of 10-20 dB, the diversity gain is given by the slope of outage probability curve and its value is $\log_{10}(0.26/0.058) = 0.65$. It is close to the theoretical value of 0.7. For TLS system with $N_L^S = N_L^R = 2$ and considering the SNR range of 10-20 dB, the diversity gain is given as $\log_{10}(0.064/0.003) = 1.33$. It is close to the theoretical value of 1.4. For TLS with $N_L^S = N_L^R = 3$ and SNR range of 10-20 dB, the diversity gain is given by $\log_{10}(0.017/0.00019) = 1.95$. This is close to the theoretical value of 2.1 also.

The ASEP results of the proposed TLS system are analyzed for different transmit laser source arrangements ($N_L^S = 2, N_L^R = 2$ and $N_L^S = 3, N_L^R = 3$) in Fig. 4.11. The results are compared with that of FSO links over Gamma channels in presence of pointing errors, as available in [159]. The results from [159] are recreated using our system parameters and denoted in the graph as Ref. Paper. Our proposed

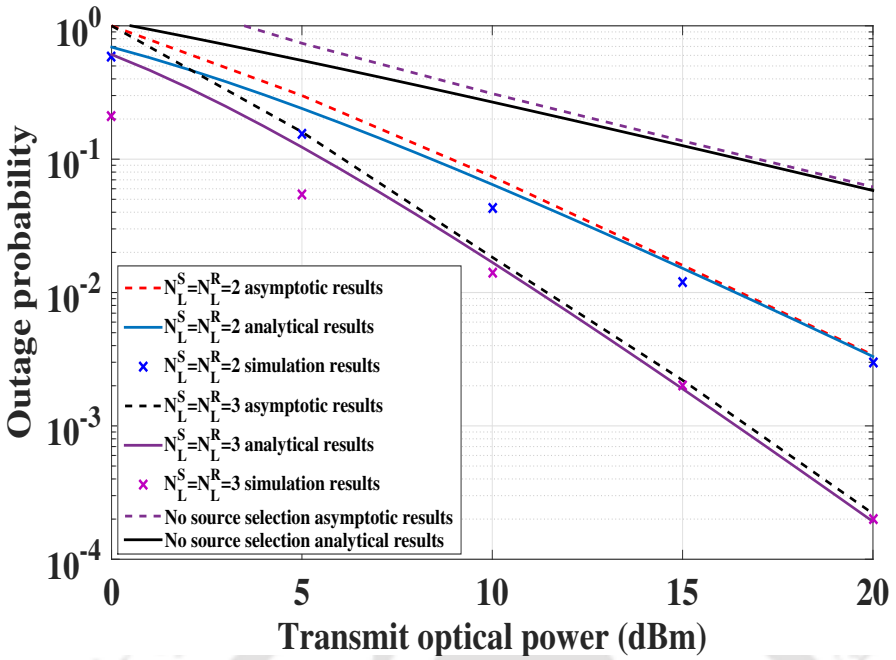

Figure 4.10: Outage probability results for various number of transmit sources for different models.

TLS system outperforms the existing method in [159]. The ASEP performance improves with diversity i.e. one source is selected from a set of available multiple sources. As explained in the outage probability results, the same logic of multiple diversity being available holds true for ASEP results also. Hence the system with multiple laser sources yields better performance. For example, to achieve an ASEP of 0.001, the transmit power required for $N_L^S = N_L^R = 2$ case is 14 dBm, while for $N_L^S = N_L^R = 3$ case, the transmit power required is 9 dBm. To achieve an ASEP of 0.0005, the transmit power required for $N_L^S = N_L^R = 2$ case is 17 dBm, while for $N_L^S = N_L^R = 3$ case, transmit power is 11 dBm. Therefore, the coding gain of system having 3 laser sources is at least 5 dBm over the system having 2 laser sources. It is noticed from the results that as number of transmit sources at source and relay nodes increases, there is more possibility of obtaining the best channel for transmission, thereby resulting in selection of the best laser. From the closed form expressions of outage probability derived earlier, it can be seen that as number of transmit sources increases, the term $\left(F_{\gamma_{SD}}\left(\frac{\gamma_{th}}{\bar{\gamma}_{SD}}\right)\right)^{N_L^S}$ decreases more with an increment in SNR (since Meijer G term decreases with an increase in SNR), thereby leading to a further decrement in total outage probability value. It means that if more lasers are available at source node to transmit the message, then there is more possibility of reception of the signal at the destination node, leading to lesser chances of outage probability. It can also be inferred that relay is beneficial as performance improves with an increment in number of relay node lasers. If relay node laser count increases, the term $\left(F_{\gamma_{SRD}}\left(\frac{\gamma_{th}}{\bar{\gamma}_{SD}+\bar{\gamma}_{RD}}\right)\right)^{\frac{N_L^S+N_L^R}{2}}$ decreases further because a single CDF term contains a Meijer G term which decreases with increase in SNR. Since the overall CDF term decrements further with an increase in N_L^R

value, hence the total outage probability value also decreases further. It also indicates that if more number of lasers at relay node are present, then there is more chance that there will be at least one link possible between laser at relay node and photodetector at destination node for message transmission.

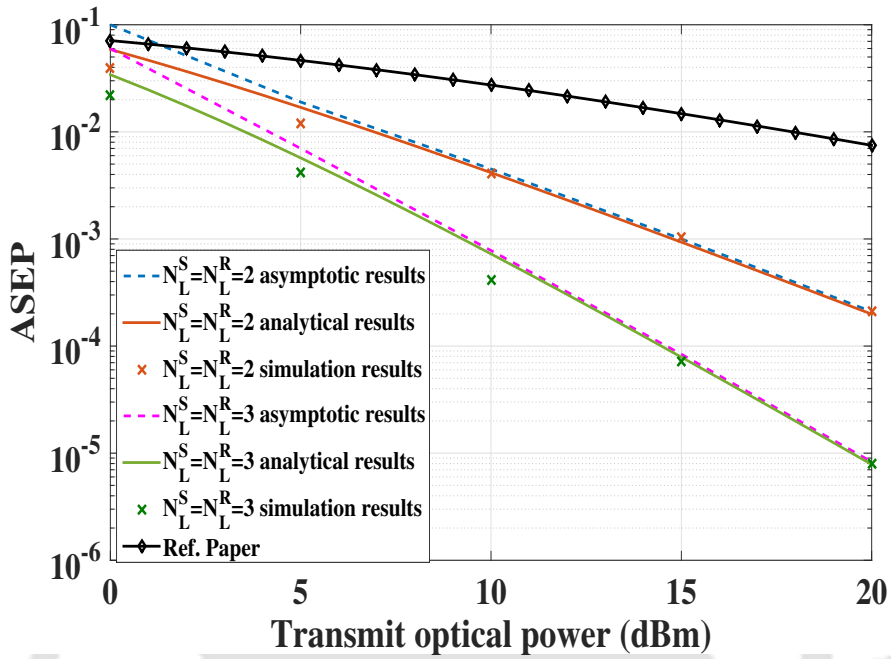

Figure 4.11: ASEP analytical results for various number of transmit sources and system models.

In Fig. 4.12, the ASEP results are displayed for TLS-OSM scheme where 2 lasers are selected for applying OSM technique. The results are compared with only TLS scenario having $N_L^S = N_L^R = 2$. It is evident from the graph that as number of available laser sources for selection increases, the performance improves. TLS-OSM scheme outperforms the conventional TLS scheme because we are selecting the best optical channel out of the available channels and then applying OSM where the sources are activated depending on the message bit. In case of TLS, the laser is selected depending on the channel condition only. Meanwhile in TLS-OSM, the laser selection is much more optimized in the sense that a set of T laser sources are selected depending on the channel condition, thereby making more diversity available. Out of those T best sources, a single one is chosen depending on the value of the message bits. This is the reason for better performance of TLS-OSM as compared to TLS. Let us calculate the diversity gain of TLS and TLS-OSM from Fig. 4.12. For TLS scheme, considering SNR range of 10-20 dB, the slope of ASEP curve is calculated. Hence diversity gain is $\log_{10}(0.0041/0.00019) = 1.32$ which is close to the theoretical value of 1.4 calculated earlier. For TLS-OSM scheme when $N_L^S = N_L^R = 4, T = 2$ and SNR range is 10-20 dB, slope of the ASEP curve is calculated. Diversity gain is $\log_{10}(0.0013/0.000016) = 2.9$ which is close to the theoretical value of 2.8 calculated earlier. Again for TLS-OSM scheme, when $N_L^S = N_L^R = 4, T = 2$ and SNR range is 10-20 dB, diversity gain is given as $\log_{10}(0.00014/(4 \times 10^{-8})) = 3.5$. There is slight

difference between this value and theoretical value of 4.2.

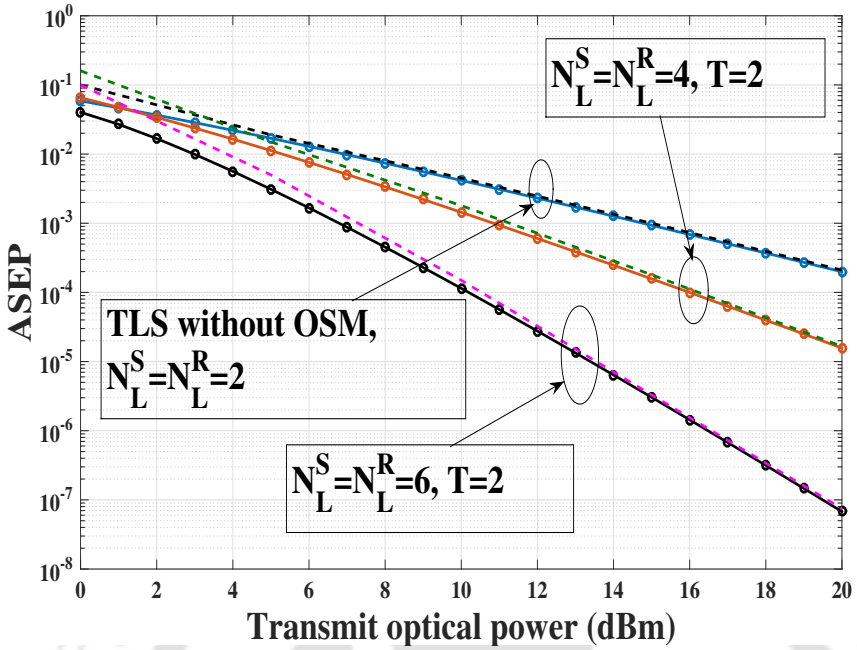

Figure 4.12: ASEP results for TLS with OSM and without OSM
(Solid line represents analytical results, • represents simulation results and dashed line represents asymptotic results).

4.5 Advanced Optical Spatial Modulation Schemes for FSO systems

The single optical chain requirement in OSM can be relaxed for more advanced schemes to obtain higher spectral efficiencies. Literature survey in this field reveals the proposal of some advanced spatial modulation based schemes in RF domain. Enhanced spatial modulation (ESM) in RF domain has been extensively explored in [85] where single or double antennas are activated depending on the message bits. Improved quadrature spatial modulation (IQSM) in RF domain has been investigated in [160], where transmission of double modulated symbols takes place over double layer of antennas in a single symbol interval. Generalized spatial modulation (GSM) in RF domain has been explored in [161], where the authors proposed transmission of multiple modulated symbols by activating multiple antennas. An improved spatial modulation scheme in RF domain has been studied in [162], where multiple antennas are activated depending on the message bits to transmit the same symbol. Differential quadrature spatial modulation (DQSM) [163] has been implemented for RF communication, where the real and imaginary parts of modulated symbols are transmitted in separate time blocks to mitigate the issue of pilot symbols. A few of the advanced SM schemes have been studied for optical indoor channels also. GSM for indoor visible light communication (VLC) has been analyzed in [164] in terms of average PEP. Another work in [165] also analyzes GSM for VLC communication. BER analysis of spatial quadrature modulation for VLC has been performed in [166] where the spatial domain is used to convey the orthogonality and

polarity of the complex signals. An angular diversity receiver approach for VLC can effectively reduce the channel correlation for SM MIMO VLC system as shown in [167]. Differential OSM (DOSM) for FSO communication has been proposed in [127] where the authors have proposed to resolve the problems of pilot signalling required for updating the CSI at the receiver.

To sum up the literature survey, several works are available in the literature regarding advanced SM schemes in RF communication. Some advanced OSM schemes are available for indoor visible light communication also. However, a significant research gap exists in the implementation of such advanced OSM schemes for outdoor FSO communication. The presence of atmospheric turbulence in FSO communication leads to a turbulence induced fading based channel model. The channel model is deterministic in case of indoor VLC channels. The research field of advanced OSM schemes for FSO systems, which has the potential to enhance the spectral efficiency of OSM systems, remains vastly unexplored. Another major research gap exists in the method of calculation of BER for all these advanced OSM schemes in various domain. The BER calculation methods mostly neglect the error involved in detection of the laser index at the receiver, and only consider the error encountered due to symbol detection. This is primarily due to the fact that the PDF of the difference of G-G random variables (generally used for FSO communication) is relatively unknown. Another important factor called pointing error for outdoor FSO communication has been ignored in literature while analyzing advanced OSM schemes. There is no available work regarding the analysis of advanced OSM schemes in terms of power consumption and cost. Some of the schemes may also be common in RF domain, but they cannot be implemented directly in optical domain due to the presence of pointing errors, atmospheric turbulences, different nature of optical transmitter and receiver used with respect to their RF counterparts. All these factors motivate us to propose advanced OSM schemes for FSO communication.

The novelty of our work lies in the fact that performance analysis of new schemes like optical enhanced spatial modulation (OESM), optical generalized spatial modulation (OGSM) and optical improved quadrature spatial modulation (OIQSM) are investigated for FSO communication for the first time. BER expressions for the same are derived and the results are compared with OSM, thereby justifying the performance improvement. The novelty of our work also involves defining all system parameters required for transmitter and receiver, incorporating pointing error and path loss effect into the G-G channel model and providing cost and performance analysis of the systems in FSO domain. We have considered both spatial and symbol modulation error while deriving upper bounds of BER for all the schemes, which highlights the contribution of our work. Laser index detection error was not taken into account in majority of the works in literature, which we have tried to address, thereby adding value to our work.

In the subsequent sections, we have analyzed performance of advanced OSM schemes in terms of BER, cost and power consumption. In OESM, single or double laser activation takes place depending upon the message bits. Therefore, a maximum of 2 optical chains are present in OESM. In OGSM, a certain number of lasers are activated depending upon the message bits. The number of optical chains is less than the number of lasers. While in OIQSM, single or double lasers are activated depending on the message bits. Two symbols are transmitted in one symbol duration as two layers of lasers are utilized to transmit the real and imaginary parts of two symbols. Keeping in mind that we are sending two modulated symbols in OIQSM, the requirement of 4 optical chains is constant.

4.5.1 System Model for Advanced Schemes of OSM

G-G channel model is used for analysis as described earlier and in [128]. For all the proposed schemes, the source node (SN) and destination node (DN) are separated by a distance of L. There are N_L lasers with its corresponding apertures at SN and N_D photodetectors with its corresponding apertures at DN. The photodetector has a responsivity of R_e. In an optical transmit chain, source data initially modulates a RF subcarrier signal. The modulated signal contains negative data, which needs to be eliminated in order to drive the laser. Therefore, DC bias adder is used to make the modulated signal positive. Laser intensity is modulated by the positively modulated signal. At the receiver, direct detection by photodetector is performed in absence of local oscillator. The information varies according to the optical signal intensity. This property helps us to retrieve the electrical signal subsequently followed by RF coherent demodulation. In OESM, two optical chains are used, while OGSM requires N_{opt} optical chains where $N_{opt} < N_L$. Note that N_L denotes the number of source lasers. OIQSM has 4 optical chains. There is a switch or controller in all the systems which activates the necessary optical chain according to the message bits.

4.5.2 Optical Enhanced Spatial Modulation

In OESM, two optical transmit chains are used and single or double laser activation takes place depending upon the message bits. A primary constellation and two secondary constellation schemes are required for this technique. The size of the secondary constellation is half of the size of the primary constellation scheme. When single laser is activated, the symbol is mapped according to the primary constellation, while for double laser activation, two symbols are mapped to either of the two secondary constellation schemes. For example, if primary constellation size is m where $m = \log_2(M)$, then size of secondary constellation is $m/2$ or $\sqrt{M}$. The total number of possible combinations of symbol transmission is N_L^2 where N_L denotes the number of lasers. Hence spectral efficiency of OESM is given by $\eta_{ESM} = \log_2(N_L^2) + \log_2(M)$.

For example if $N_L = 4$ and M=4, then primary constellation will be quadrature phase shift keying

(QPSK) and secondary constellation will be binary phase shift keying (BPSK). 4-QAM and QPSK are same and the constellation schemes can take symbols from the set $\{\pm 1 \pm j\}$. $BPSK_0$ and $BPSK_1$ are the secondary constellation schemes given by $BPSK_0 = \{\pm 1\}$ and $BPSK_1 = \{\pm j\}$. In this case, OESM can transmit 6 bpcu while normal OSM can transmit only 4 bpcu with $N_L = 4$ and M=4. Thus this OESM scheme has been named as 4t6b. The scheme *atyb* represents a as number of lasers and y as spectral efficiency. For the particular 4t6b OESM scheme, 16 total combinations are possible out of which the first 4 combinations are same as that of OSM with single optical source being active. Double source activation is done for the next 6 cases where symbol mapping is done according to one of the secondary constellation scheme $BPSK_0$, while the secondary constellation scheme $BPSK_1$ is used for the next 6 cases. The active laser combination for this scheme is explained in Chapter 3.

An example of OESM is illustrated in Fig. 4.13 where the information stream is given by [1 0 0 1 1 1] and $N_L = 4, M = 4$. Thus the first four bits are used as control bits which corresponds to decimal number 9 i.e. the combination labelled P_{10} where the third and fourth lasers will be active (according to Table 3.8). Decimal number 0 corresponds to combination P_1 and so on. According to the secondary constellation scheme $BPSK_0$, the modulated bits would be [1 1]. Hence the transmitted symbol vector will be $\mathbf{x} = [0\ 0\ 1\ 1]^T$. $[\,]^T$ denotes the transpose of a matrix. The other OESM schemes can be similarly implemented for higher modulation schemes and transmit sources.

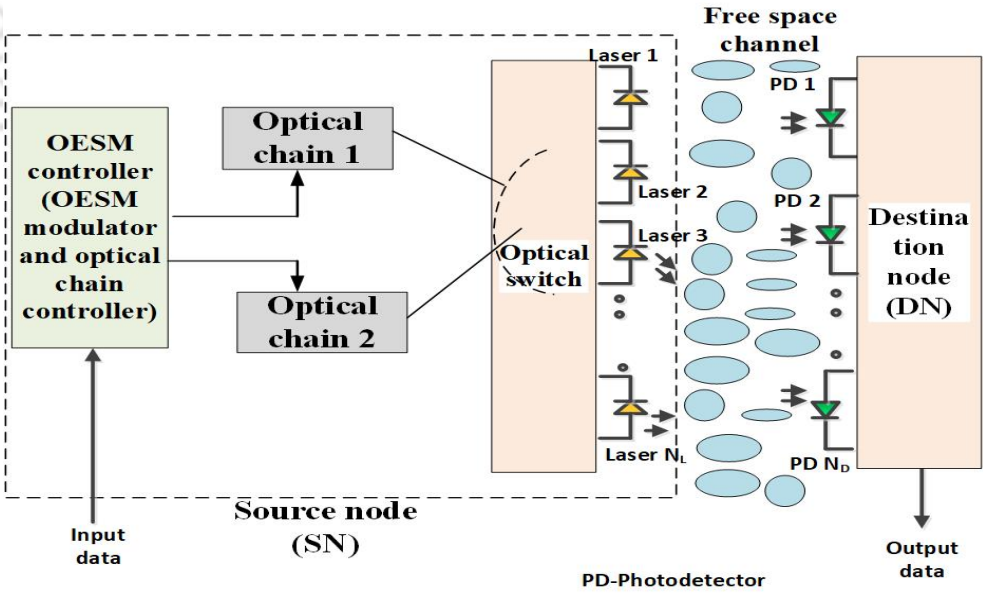

Figure 4.13: Proposed system model for OESM.

4.5.3 Optical Improved Quadrature Spatial Modulation

A new scheme called OIQSM is proposed for FSO system to enhance the spectral efficiency. Transmission of two symbols occurs in a single symbol interval. The real and imaginary parts of two constellation

symbols are transmitted using two different sets of laser sources. By deploying a much reduced constellation state, OIQSM can generate the same spectral efficiency as that of OSM, thereby resulting in improved error performance. The input data stream is partitioned into laser index data and constellation data. The laser index data is partitioned into in-phase laser index and quadrature phase laser index. Constellation data is divided into two data streams. The real parts of both the streams are transmitted through the active in-phase laser sources and imaginary parts are transmitted through active quadrature phase laser sources. The activated laser sources which are selected according to the incoming bits for $N_L = 4$ are listed in Table 4.9. Thus 2 layers of lasers are activated in one symbol duration. The spectral efficiency of OIQSM is given by [160] $2\left\lfloor \log_2 \binom{N_L}{2} \right\rfloor + 2\log_2 M$ bpcu. Its benefit is that the count of the transmit sources need not be a power of 2. Hence to obtain the identical spectral efficiency as that of OIQSM, OSM requires a higher constellation scheme which gives much more error.

Table 4.9: Activated lasers for OIQSM with $N_L = 4$

Index	Activated lasers
00	1,2
01	1,3
10	1,4
11	2,3

For our proposed OIQSM based FSO system, let us consider an example where input data stream is [11010110]. The part of the data stream which will be used for activating the corresponding laser source, is [1101] while the remaining part [0110] will be used for constellation mapping. Therefore according to Table 4.9, the lasers which are activated for transmitting real and imaginary parts are $\{2, 3\}$ and $\{1, 3\}$ respectively. 4-QAM modulation scheme is used in this case and accordingly the symbols will be $[1 - j, -1 + j]$. The real and imaginary parts will be separated as follows. Note that real parts of the above two symbols are 1 and -1. They will be sent from laser 2 and laser 3 respectively. Similarly, imaginary parts of the above two symbols are -1 and +1. They will be sent from laser 1 and laser 3 respectively. Hence we can write $\mathbf{x_r} = [0, 1, -1, 0]^T$ and $\mathbf{x_i} = [-1, 0, 1, 0]^T$. The overall signal which is transmitted is $\mathbf{x} = \mathbf{x_r} + j\mathbf{x_i} = [-j, 1, -1 + j, 0]^T$. The in-phase and quadrature phase laser activation is shown in Fig. 4.14 and 4.15 respectively.

4.5.4 Optical Generalized Spatial Modulation

This technique can exploit the selection of both transmit optical chains and laser sources to yield better spectral efficiencies than OSM. However, decoding complexity and cost also increase with use of multiple laser sources. Hence an optimum combination of optical chains and laser sources need to be selected. The OGSM system comprises of N_{opt} optical chains and N_L laser sources. A multiple pole multiple throw (N_{opt}, N_L) switch is used for connecting the optical chains to the lasers. Out of N_L laser

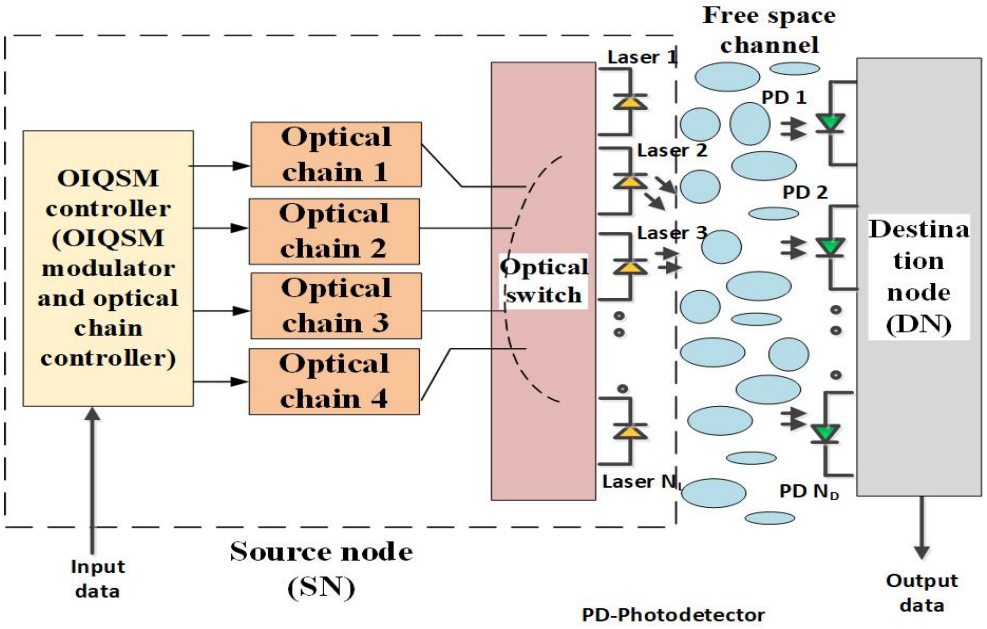

Figure 4.14: Proposed system model for OIQSM during in-phase activation for input bit stream [1100 0110].

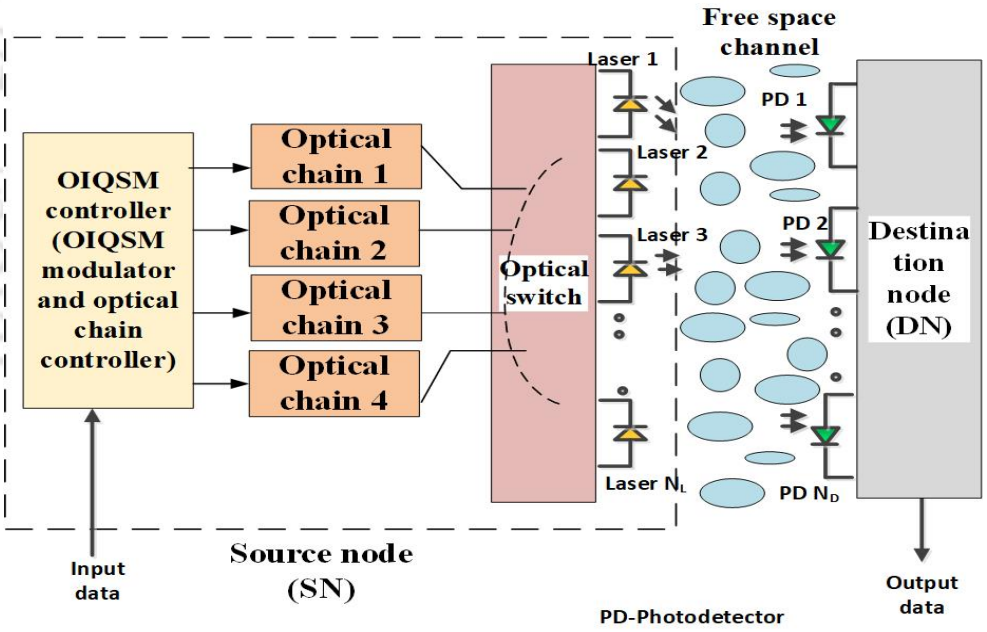

Figure 4.15: Proposed system model for OIQSM during quadrature phase activation for input bit stream [1100 0110].

sources, N_{opt} lasers are chosen to be activated. The modulated symbol is split into N_{opt} groups and each group is composed of m bits (where $M = 2^m$), which are transmitted from each laser. The constellation mapping is done according to the M-ary modulation scheme. Hence the spectral efficiency can be defined as $\eta_{OGSM} = \left\lfloor \log_2 \binom{N_L}{N_{opt}} \right\rfloor + mN_{opt}$. C is defined as the control bits used to choose the set of active laser sources and is defined by $C = \left\lfloor \log_2 \binom{N_L}{N_{opt}} \right\rfloor$. The set of valid laser patterns to be activated is given by K having dimension of 2^C.

The optimum selection of number of optical chains N_{opt} is a matter of concern in OGSM systems. The selection has to be done in such a way that it maximizes the spectral efficiency. The first part of the spectral efficiency expression increases from $N_{opt} = 0$ to $N_{opt} = \lfloor N_L/2 \rfloor$ and then decreases. However, the second part of the expression increases linearly with N_{opt} keeping the modulation term constant. Thus the optimum value of N_{opt} for which the spectral efficiency is maximum should be between $\lfloor N_L/2 \rfloor$ and N_L.

OGSM is illustrated with an example. $N_L = 4, N_{opt} = 2, M = 4$ are the parameters considered which gives $C = 2$ and $\eta_{OGSM} = 6$ bpcu (bits per channel use). The laser pattern set is given by $K = [1,1,0,0],[1,0,1,0],[0,1,0,1],[0,0,1,1]$. The pattern can be different, but should be fixed before transmission and should have a cardinality of 2^C. Let the incoming message bits be given by the sequence [1 0 0 1 1 1]. Therefore, the first 2 bits will define the control bits indicating that the 3rd pattern from set K will be used for activating the lasers. The remaining bits [0 1 1 1] will be used for constellation mapping. Since second and fourth lasers will be activated, therefore 2 symbols each of size 2 bits (4-QAM is used) will be modulated. The modulated bits are given by $1 - j$ and $-1 - j$ respectively. Thus the transmitted signal vector is given by $\mathbf{x} = [0, 1-j, 0, -1-j]^T$. The example is pictorially illustrated in Fig. 4.16.

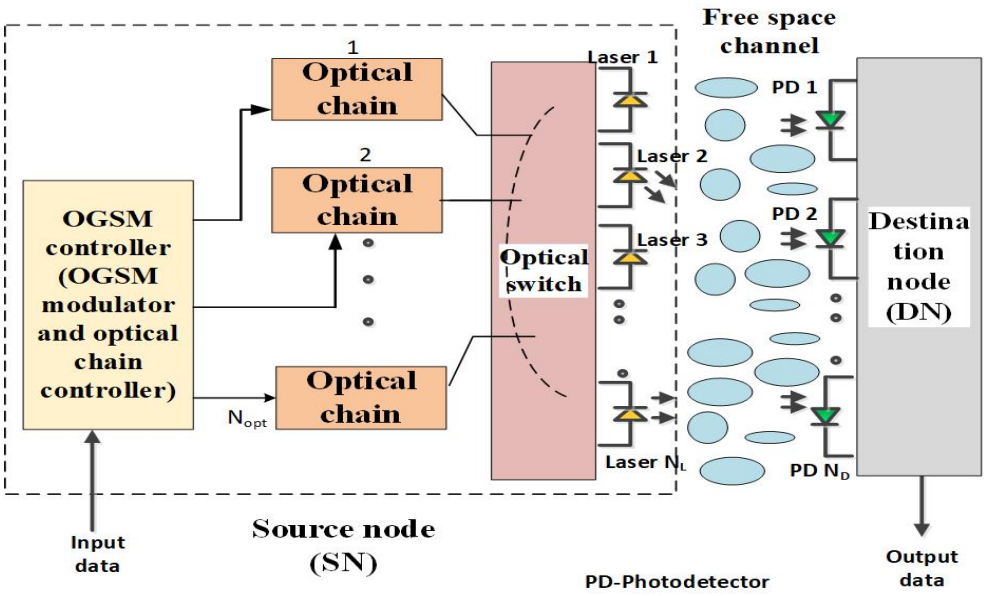

Figure 4.16: Proposed system model for OGSM.

4.5.5 Performance Analysis of Advanced OSM Schemes

Source node transmits message bits to destination node in a single time slot and the output at the receiver is given by $\mathbf{y} = [y_1\ y_2 ...\ y_{N_D}]^T$ where $[\ ]^T$ denotes transpose of a matrix. $\mathbf{s}$ is the transmitted signal vector where $\mathbf{s} = \sqrt{R_e O_{eff} E}\ \mathbf{x}$. $\mathbf{E}$ denotes the average symbol energy, O_{eff} is the optical efficiency

of the system.

$$\mathbf{y} = \mathbf{H}\mathbf{s} + \mathbf{n} \ . \tag{4.65}$$

At the photodetector, thermal, shot and background noise are the major sources of noise. The total noise variance ($\mathbf{n}$) is computed by adding up the variances of the three types of noises. Ambient light generates thermal noise which is represented by additive white Gaussian noise of zero mean and variance N_0. The random arrival of photons results in shot noise. Dark current noise arises in the absence of light. $\mathbf{x}$ is the transmitted source vector. Decoding at the receiver takes place by maximum likelihood (ML) decoding which is evaluated as:

$$\hat{\mathbf{s}} = \arg\min_{\mathbf{s}\in\mathbb{S}} \|\mathbf{y} - \mathbf{H}\mathbf{s}\|^2 \ , \tag{4.66}$$

where $\mathbb{S}$ is the set of normalized transmit symbol vectors. Each scheme - OSM, OESM, OIQSM and OGSM - has its own predefined set $\mathbb{S}$, containing all the symbol vectors for that particular scheme. Pairwise Error Probability (PEP) is the probability of symbol vector $\mathbf{s}$ being decoded as $\mathbf{s}'$. For detection of symbol mapping bits, the average PEP can be computed as:

$$\begin{aligned} APEP(s \to s')^{Symbol} &= \frac{1}{|\mathbb{S}|}\mathbb{E}_{\mathbf{H}}\left[\mathcal{Q}\left(\frac{1}{N_D}\sqrt{\frac{\gamma_{eff}||\mathbf{H}s - \mathbf{H}s'||^2}{2}}\right)\right] \\ &= \frac{1}{|\mathbb{S}|}\int_0^\infty \mathcal{Q}\left(\frac{1}{N_D}\sqrt{\frac{\gamma_{eff}\sum_{j=1}^{N_D}\sum_{i=1}^{N_L}||h_{ij}s - h_{ij}s'||^2}{2}}\right) f_{\gamma_{SM}}(h)dh \ , \end{aligned} \tag{4.67}$$

where average received SNR is $\bar{\gamma} = \frac{E}{N_0}$, $\gamma_{eff} = \frac{R_e O_{eff} E}{N_0}$ and $\gamma_{SM} = \sum_{j=1}^{N_D}(\sum_{i=1}^{N_L} h_{ij})^2$. $\mathbf{H}$ is the channel matrix having dimension of $N_D \times N_L$ and h_{ij} is an element of the channel matrix which follows G-G distribution with pointing errors as in Eq. (4.36). The integration involves multi-dimensional integration over the channel gains from each laser to photodetector. Hence exact closed form expressions cannot be derived and analytical results are obtained using numerical methods. The average BER (ABER) (denoted by P_s) occurring during detection of the symbol mapping bits is bounded by [85]:

$$P_s \leq \frac{1}{|\mathbb{S}|log_2(|\mathbb{S}|)}\sum_{\mathbf{s}\in\mathbb{S}}\sum_{\mathbf{s}'\in\mathbb{S}} n(\mathbf{s}\to\mathbf{s}')APEP(\mathbf{s}\to\mathbf{s}')^{Symbol} \ , \tag{4.68}$$

where $n(\mathbf{s}\to\mathbf{s}')$ is the number of bit errors that occur when $\mathbf{s}$ is decoded as $\mathbf{s}'$. Next we come to the calculation of error involved in laser index detection. During detection of the laser index, the APEP (where the laser index $\mathbf{j}$ can be incorrectly detected as $\mathbf{i}$) for G-G channel with pointing errors can be

computed as:

$$APEP(j \to i) = \frac{1}{|\mathbb{S}|} \sum_{\mathbf{j}\in\mathbb{S}} \sum_{\mathbf{i}\in\mathbb{S}} \sum_{k=0}^{\infty} \frac{(2N_D)^{k+N_D}\Gamma(\frac{k+N_D+1}{2})}{\gamma_{eff}^{(k+N_D)/2}\sqrt{\pi}(k+N_D)\Gamma((k+N_D)/2)} \times \left(C\frac{(-\alpha_G\beta_G/(A_0h_l))^k}{\gamma_{eff}^{(k+1)/2}k!} G_{5,5}^{3,4}\left(\begin{matrix} 0,k+1-\zeta^2,k+1-\alpha_G,k+1-\beta_G,\zeta^2 \\ \zeta^2-1,\alpha_G-1,\beta_G-1,k-\zeta^2,k \end{matrix} \middle| 1 \right) \right)^{N_D}, \quad (4.69)$$

where $C = \frac{\alpha_G\beta_G\zeta^4}{A_0h_l(\Gamma(\alpha_G)\Gamma(\beta_G))^2}$. The details of this derivation is shown in Appendix.

This expression contains summation of terms where $k = 0$ to ∞. To solve this infinite summation series, we are going to explore the upper limit value of k for which the series is convergent. The Cauchy ratio test can be used to check the convergence of the infinite series. The series is convergent if:

$$\lim_{k\to\infty} |\frac{a_{k+1}}{a_k}| \leq 1 \ . \quad (4.70)$$

The series coefficient of $(k+1)^{th}$ and k^{th} terms are obtained only from Eq. (4.69). The ratio of two Meijer G functions will always be a nonzero real number for all values of k. This can be derived in a similar manner as shown in [100]. On solving the ratio, it can be observed that the degree of k in the denominator exceeds that of the numerator by one. Hence on applying the limit condition, the ratio equation will result in zero indicating that the infinite series is convergent. The upper bound of k for which the series is convergent is investigated in Mathematica. It is observed that at higher SNR values (or higher values of transmit power), the PEP expression converges to a fixed value at lower k values. For example at transmit power value of 10 dBm, PEP for $k = 0$ is 0.044, for $k = 2$ value is 0.074, for $k = 4$ value is 0.088 while for $k \geq 6$ value is 0.095. Thus at 10 dBm transmit power, PEP is convergent for $k \geq 6$. Similarly for 15 dBm transmit power, PEP for $k = 0$ is 0.0139, for $k = 2$ value is 0.0149 while for $k \geq 4$ value is 0.015. Hence it is convergent for $k \geq 4$ at 15 dBm transmit power. Now for 20 dBm transmit power, PEP value for $k \geq 0$ is 0.0044, while for 30 dBm transmit power, PEP value for $k \geq 0$ is 0.000442. Thus the PEP converges to a value for $k \geq 0$ at high values of transmit power exceeding 20 dBm. It is to be noted that as the value of k increases, the computation time also increases. The study of upper bound of k for which the series is convergent, is also done for moderate ($\alpha_G = 4.0, \beta_G = 1.9$) and weak turbulence conditions ($\alpha_G = 11.6, \beta_G = 10.1$). For moderate turbulence conditions the PEP is convergent at $k \geq 0$ for more higher transmit power values of 30 dBm or more. At transmit power value of 20 dBm, PEP under moderate turbulence conditions is convergent for $k \geq 4$. Similarly under weak turbulence conditions, PEP is convergent for $k \geq 3$ at transmit power value of 30 dBm while for transmit power value of 20 dBm, it is convergent for $k \geq 5$. Hence it is concluded that as the turbulence conditions

decrease, the upper bound of k is a large number at a particular value of transmit power. Another fact to note is that for more numbers of photodetectors, the bound of k is greater for a particular value of transmit power. For $N_D = 2$, PEP is convergent for $k \geq 4$ at transmit power value of 30 dBm. The detailed analysis of the upper limit of summation variable k is shown in Table 4.10 and the PEP values are considered to be accurate till 5 places of decimal. In this work we have considered strong turbulence conditions ($\alpha_G = 4.2, \beta_G = 1.4$) and a single photodetector scenario. Hence considering all values of transmit power, we have considered the upper bound of k as 10. Thus the upper bound results will be tight for the considered range of transmit power values for strong turbulence conditions.

Table 4.10: Upper bound of k analysis

Parameters	$10dBm$ power		$15dBm$ power		$20dBm$ power		$30dBm$ power	
	k	PEP	k	PEP	k	PEP	k	PEP
$\alpha_G = 4.2$, $\beta_G = 1.4$, $N_D = 1$	6	0.09554	4	0.01522	0	0.00444	0	0.00044
$\alpha_G = 4.0$, $\beta_G = 1.9$, $N_D = 1$	8	0.05544	6	0.00724	4	0.00312	0	0.00024
$\alpha_G = 11.6$, $\beta_G = 10.1$, $N_D = 1$	10	0.00554	8	0.00084	5	0.0003	3	0.00002
$\alpha_G = 4.2$, $\beta_G = 1.4$, $N_D = 2$	10	0.00844	8	0.00112	6	0.00018	4	0.0000012

The average bit error rate for laser index detection (denoted by P_{lide}) is given by:

$$P_{lide} \leq \frac{1}{|\mathbb{S}|log_2(|\mathbb{S}|)} \sum_{j \in \mathbb{S}} \sum_{i \in \mathbb{S}} n(j \to i) APEP(j \to i) \ . \tag{4.71}$$

It is interesting to note that closed form expressions are possible for laser index detection while it is not possible for symbol error detection. This is because laser index detection involves difference of one-dimensional channel gain where laser index is kept fixed and the photodetector index at the receiver may vary. PDF of such summation of the difference of channel gains can be obtained as shown in Appendix for laser index detection error. While in case of symbol detection, there is multi-dimensional channel gain difference where both laser and photodetector index can vary. Thus the PDF of double summation of the difference of channel gains need to be evaluated, which is unknown to us. This is the reason for not obtaining closed form expressions of this symbol error detection part. Future work can try to derive the PDF of difference of two G-G random variables over double summation terms.

The total BER of the system can occur either when there is an error in laser index estimation or when there is an error in symbol estimation. Hence the total error bound follows the minimum criteria as explained in Eq. (2.50). Therefore, the total bit error rate of the system (P_e) can be upper bounded as:

$$P_e \leq P_s + P_{lide} - P_s P_{lide} \ . \tag{4.72}$$

The BER bounds depend on the different OSM schemes. Depending upon the number of transmit lasers

being active, the corresponding channel gains will vary and accordingly the integration over the channel gains will be done. The predefined set of possible symbol vectors also vary according to the schemes, thereby changing the BER values.

Since closed form expressions have not been obtained for symbol detection error, hence coding and diversity gain cannot be calculated from the asymptotic analysis. In the absence of closed form expressions, it is difficult to predict the behaviour of the system at high SNR values by observing the multi-dimensional integration. It is pertinent to note that the diversity gain can be calculated from BER expression of the laser index detection error equation. It is observed that the highest exponent of SNR in Eq. (4.69) is $-N_D$. Therefore, the diversity gain is N_D i.e. it is dependent on the number of receiving photodetector only and is independent of the channel parameters or pointing error effect. More number of photodetectors at the receiver means more diversity is available and chances of correct laser index estimation is more. In future, closed form expressions for asymptotic analysis of such advanced OSM schemes will be pursued.

4.5.6 Comparison of Performance Metrics

Power consumption, cost and complexity analysis of the proposed methods are done in this section. Power consumption of optical chain and optical switch are considered as P_o and P_{sw} [151]. α_{tr} is the slope dependent load factor and P_{tr} is the total transmitted optical power. Power consumption of OSM, OESM, OGSM and OIQSM are given by Eq. (4.73), (4.74), (4.75) and (4.76) respectively.

$$P_{tot}^{OSM} = P_o + \alpha_{tr} P_{tr} + P_{sw} N_{sw}^{OSM} \ . \tag{4.73}$$

$$P_{tot}^{OESM} = 2P_o + \alpha_{tr} P_{tr} + P_{sw} N_{sw}^{OESM} \ . \tag{4.74}$$

$$P_{tot}^{OGSM} = P_o N_{opt} + \alpha_{tr} P_{tr} + P_{sw} N_{sw}^{OGSM} \ . \tag{4.75}$$

$$P_{tot}^{OIQSM} = 4P_o + \alpha_{tr} P_{tr} + P_{sw} N_{sw}^{OIQSM} \ . \tag{4.76}$$

Power consumption of optical MIMO is given by $P_{tot}^{MIMO} = P_o N_L + \alpha_{tr} P_{tr}$. Number of switches are different for each scheme and number of switch requirement for OSM, OESM, OGSM (assuming $N_{opt} = 2$) and OIQSM to achieve a spectral efficiency of η_{SE}, are given by Eq. (4.77), (4.78), (4.79) and (4.80) respectively.

$$N_{sw}^{OSM} = 2^{(\eta_{SE} - log_2(M) - 1)} \ . \tag{4.77}$$

$$N_{sw}^{OESM} = 2^{(\eta_{SE} - log_2(M))/2 - 1} \ . \tag{4.78}$$

$$N_{sw}^{OGSM} = \lfloor 1/4 \left(1 + \sqrt{1 + 4 \times 2^{((\eta_{SE} - 2log_2(M))+1)}}\right) \rfloor \ . \tag{4.79}$$

$$N_{sw}^{OIQSM} = 1/4 \left(1 + \sqrt{1 + 4 \times 2^{((\eta_{SE} - 2log_2(M))/2+1)}}\right) \ . \tag{4.80}$$

The hardware cost is calculated for all the schemes. C_o, $C_{S/P}$, C_{sw} are assumed to be the costs of optical chain, serial to parallel converter and optical switch respectively. Total hardware costs of OSM, OESM, OGSM and OIQSM are given by Eq. (4.81), (4.82), (4.83) and (4.84) respectively.

$$C_{OSM} = C_o + C_{S/P} + C_{sw} N_{sw}^{OSM} \ . \tag{4.81}$$

$$C_{OESM} = 2C_o + C_{S/P} + C_{sw} N_{sw}^{OESM} \ . \tag{4.82}$$

$$C_{OGSM} = C_o N_{opt} + C_{S/P} + C_{sw} N_{sw}^{OGSM} \ . \tag{4.83}$$

$$C_{OIQSM} = 4C_o + C_{S/P} + C_{sw} N_{sw}^{OIQSM} \ . \tag{4.84}$$

Total cost of optical spatial multiplexing based MIMO system is given by $C_{tot}^{MIMO} = C_o N_L$. The number of switches required for OGSM, OESM and OIQSM are much lesser than the requirement in OSM for a particular spectral efficiency and M-ary modulation scheme. Hence, the switch cost and power consumption of switches are much lesser for higher spectral efficiencies in OESM, OGSM and OIQSM as compared to that of OSM. However, these advanced OSM schemes require more optical chains in comparison to OSM. The power consumption of an optical chain is more than that of a switch while the cost of an optical chain is more than that of an optical switch. An example is considered where $\eta_{SE} = 8$ bpcu, $N_L = 64$ and $M = 4$. For OESM 4 switches are required, for OGSM 3 switches are required (assuming $N_{opt} = 2$), for OIQSM switch requirement is 2, while the switch requirement is 32 for OSM. The parameters considered are $P_o = 53W, \alpha_{tr} = 3.1, P_{tr} = 6.3W, P_{sw} = 0.2W, C_o = 1000\$, C_{S/P} = 2\$, C_{sw} = 220\$$. Thus for a larger value of N_L, which is required to obtain a greater η_{SE} value, the total cost of OSM is more than that of the proposed methods due to excessive requirement of switches. The power consumption of OSM is relatively lesser than the other schemes, however this trend is not fixed for all values of spectral efficiency and modulation scheme. As the spectral efficiency increases, the number of switches in OSM increase by a power of 2 whereas for other schemes, the growth in switches is linear. For example if $\eta_{SE} = 20$ bpcu and M=4, number of switches in OSM is 131072 while number of switches in OESM is 256, number of switches in OGSM is 362 and number of switches in OIQSM is 11. In this case, we can clearly notice that the total power consumption of OSM will exceed that of the other advanced OSM schemes due to excessive requirement of switches. The slight increase in the power consumption of multiple optical chains in advanced OSM schemes is negated by the excessive

power consumption of switches in OSM for very high spectral efficiency values. The total cost of OSM also exceeds the cost of other advanced OSM schemes for such high spectral efficiency values. Another fact to note is that the excessive requirement of switches in OSM also consumes lot of space in OSM. Thus we can conclude from this detailed analysis that as spectral efficiency value increases, advanced OSM schemes perform better than OSM both in terms of power consumption and cost. The example of $\eta_{SE} = 8$ bpcu, M=4 and $N_L = 64$ is pictorially illustrated in Fig. 4.17 where the overall power consumption and cost of the proposed methods are compared with that of OSM and optical spatial multiplexing (Optical SMX) MIMO techniques. It is evident that the proposed methods perform better than OSM in terms of overall cost at this particular spectral efficiency. However as explained earlier, for more higher spectral efficiencies, the proposed methods can perform better than OSM even in terms of power consumption also.

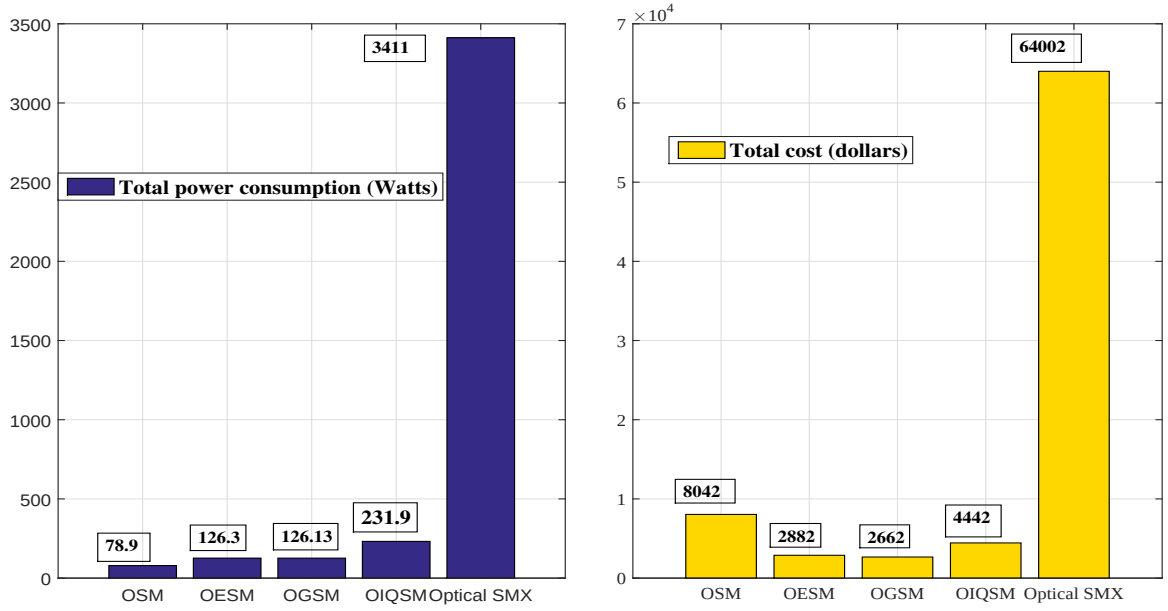

Figure 4.17: (a) Power consumption and (b) cost comparsion of the proposed methods.

4.5.7 Results related to Advanced OSM Schemes

Strong turbulence conditions with $N_L = 4$, $N_D = 1$ and $L = 2$ Km are considered for all simulations unless mentioned explicitly. The other parameters are defined in Table 4.7. For Monte Carlo simulations, 10^6 G-G channel realizations are generated. The source bits are randomly generated and the symbol mapping is done according to the particular scheme. Thus for 10^6 bits, number of erroneous bits are computed by activating the corresponding lasers and transmitting the bits across the particular channel. At the receiver, symbol detection is done in two steps- first the laser activation bits are estimated to know the particular laser index and in the next step the symbol mapping bits are decoded.

The performance of the proposed methods- OESM and OGSM are compared with that of OSM and other techniques used in literature, in terms of BER in Fig. 4.18. The results from [168, 169, 100] are used for performance comparison. In [168], single-input-single-output (SISO) optical system has been implemented over G-G channel deploying on-off keying (OOK) and assuming plane wave strong turbulence conditions. BER has been computed over G-G channel assuming light fog and strong turbulence conditions, and 4-QAM modulation in [169]. The results of BER for space shift keying (SSK) based FSO system under strong turbulence (with $N_L = 4$, $N_D = 1$) are recreated from [100]. The results of all these methods are obtained for our values of transmit optical power and plotted in the figure. $N_L = 4$ and spectral efficiency of 6 bpcu are considered for our analysis of the proposed methods. $N_{opt} = 2$ and 4-QAM modulation is used for OGSM, 4-QAM is also used for OESM, while OSM uses 16-QAM to achieve the same spectral efficiency. OESM and OGSM easily outperform OSM as OSM uses a higher modulation scheme which has closer spacing between constellation points, thus causing more error in symbol detection. OESM outperforms OGSM as sometimes single laser activation also occurs in OESM, while OGSM always activates 2 lasers for the above scenario, hence OESM suffers from less optical interference as compared to OGSM. It is also interesting to note that successful decoding of more number of laser indices is more difficult, thereby leading to an increase in P_{lide} value (BER for laser index detection). It is evident from the figure that our proposed methods perform better than the existing methods. Our methods use techniques to select the best laser for transmission, thereby offering more diversity. Hence it can perform better than the existing SISO technique where only a single laser is available for transmission. In SSK based FSO system (optical SSK), the information is only conveyed over space by the laser index and no symbol mapping is done by any modulation scheme. Meanwhile in our proposed methods, information is conveyed both by laser indices and modulated symbols, thereby giving superior performance. Optical SSK is a spatial case of OSM where information is transmitted in spatial domain only, thereby giving better performance than 4-QAM and SISO cases in literature. 4-QAM scenario in the graph corresponds to the case where no OSM is applied. Hence, no diversity is available and the laser is selected irrespective of message bit value and channel condition. This is the reason for its worst performance.

The comparison of OGSM, OIQSM and OSM is carried out in terms of BER in Fig. 4.19 for $N_L = 4$ and a spectral efficiency of 8 bpcu. OGSM uses $N_{opt} = 3$ and 4-QAM modulation while OESM utilize 16-QAM modulation. OIQSM uses 4-QAM modulation while OSM uses 64-QAM modulation. OSM uses the highest modulation scheme, thereby yielding the most inferior performance. As modulation scheme increases, the symbols are more closely packed and chances of making error in detection of such closely spaced symbols is more. Thus the BER involved in symbol detection (P_s) increases, leading to

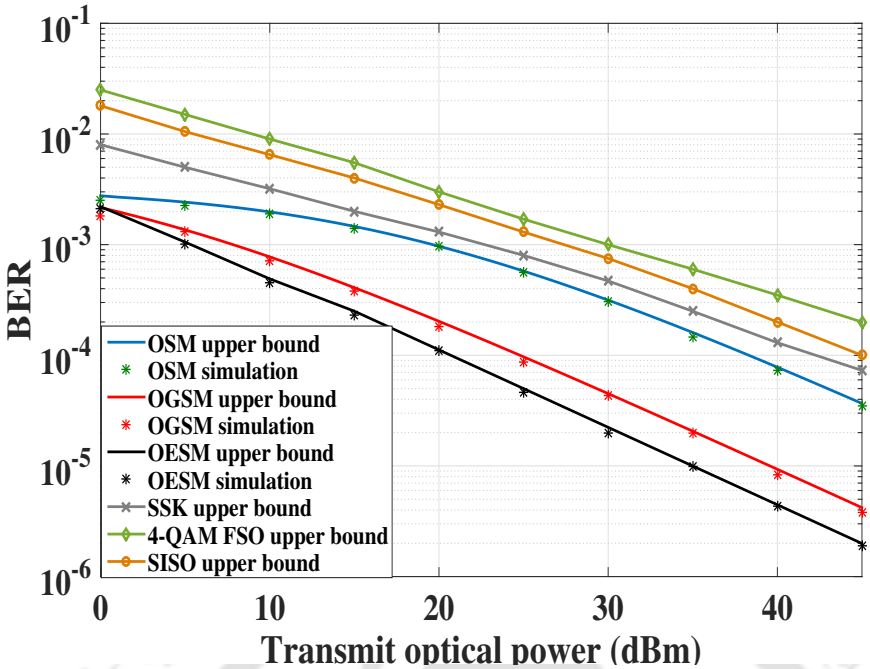

Figure 4.18: Performance comparison of the proposed methods for spectral efficiency of 6bpcu.

overall increase in system bit error rate. OESM uses lower modulation scheme than OSM, but a higher modulation scheme than OGSM and OIQSM. Thus performance of OESM is better than OSM, but inferior as compared to OGSM and OIQSM. OIQSM and OGSM uses the same modulation scheme, but OIQSM uses only 2 optical chains while OGSM uses 3 optical chains, leading to lesser optical interference in OIQSM and contributing to improved performance of OIQSM over OGSM. It is pertinent to note that OIQSM uses 2 activated lasers and OGSM uses 3 activated lasers for transmission in this particular case for comparison. It means that receiver will face greater difficulty in correctly decoding the three laser indices of OGSM, while it is relatively easier to decode 2 laser indices correctly in OIQSM. More decoding of laser indices means more chances of error. Thus if error involved in detection of laser index (P_{lide}) is more, the total BER of the system will also be more.

From Fig. 4.19, diversity gain of the various methods can be calculated by calculating the slope of BER curves. For OESM, considering power range of 35-45 dBm, the diversity gain is given by $\log_{10}(\frac{0.000082}{0.000016}) = 0.71$. Diversity gain of OGSM for the same power range is $\log_{10}(0.00003/0.0000052) = 0.76$. OIQSM within the same power range has a diversity gain of $\log_{10}(0.000013/0.000003) = 0.64$. From the results we can observe that the diversity gains of the schemes more or less are similar to one another. This is because it depends mainly on the receiver diversity i.e. number of photodetectors. For equal number of photodetectors diversity gains are nearly equal. Irrespective of the number of lasers activated for any scheme, a larger number of photodetectors available for reception is capable of increasing the diversity gain. Let us estimate the coding gain from the horizontal shift of the curves. If we consider

a BER of 0.00006, OIQSM achieves a coding gain of around 5 dBm over OGSM, 12 dBm over OESM and 20 dBm over OSM. This coding gain is achieved due to the combined effect of lower modulation scheme and lower number of lasers activated. The coding gain of OESM over OSM at 0.0004 BER value is 6 dBm, while the coding gain of OGSM over OSM at 0.0004 BER is around 13 dBm. These results highlight the fact that advanced OSM schemes are beneficial than OSM in terms of coding gain, although they may consume a little extra power than OSM for this spectral efficiency value. The slight extra power consumption is balanced by the benefit in coding gain of the proposed methods.

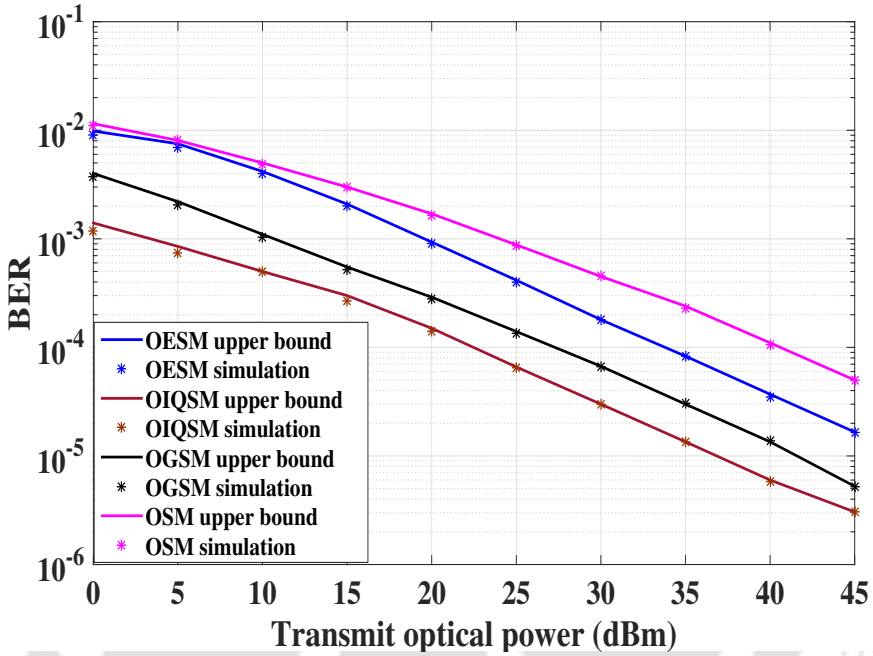

Figure 4.19: Performance comparison of the proposed methods for spectral efficiency of 8bpcu.

The performance of OESM and OGSM for different parameter variations are compared in Fig. 4.20. It is observed that performance of OGSM and OESM degrades with increase in spectral efficiency as higher target data rates are difficult to achieve. With increase in modulation scheme, the performance also degrades. For example OESM uses 16-QAM for $N_L = 4, \eta_{SE} = 8bpcu$ while OESM uses 4-QAM for $N_L = 4, \eta_{SE} = 6bpcu$. Similarly, OGSM with $\eta_{SE} = 6bpcu$ and OGSM with $\eta_{SE} = 8bpcu$ uses 4-QAM but have different number of optical chains. As N_{opt} value increases in OGSM, more lasers are active and the performance degrades due to increase in optical interference. It is pertinent to note that OGSM having 3 optical chains performs better than OESM with 2 optical chains at the same spectral efficiency of 8 bpcu. This is because OGSM uses 4-QAM and OESM uses 16-QAM to attain the same spectral efficiency. As constellation size increases, the symbol vector spacing decreases leading to more chances of error. Again for same spectral efficiency of 6 bpcu, OESM having 2 optical chains performs better than OGSM having 2 optical chains. This is because of the fact that OESM sometimes activates

single laser and optical chain also depending on the message bits, which reduces the optical interference as compared to OGSM with 2 optical chains, where 2 lasers and 2 optical chains are always activated. Another interpretation of this result is that when more lasers are activated, it becomes difficult for the receiver to decode multiple laser indices correctly. Hence the bit error rate for laser index detection increases, contributing to the overall increase in BER of the system. In all the figures, the analytical upper bounds are tight and validated by Monte Carlo simulations, thereby justifying our analysis.

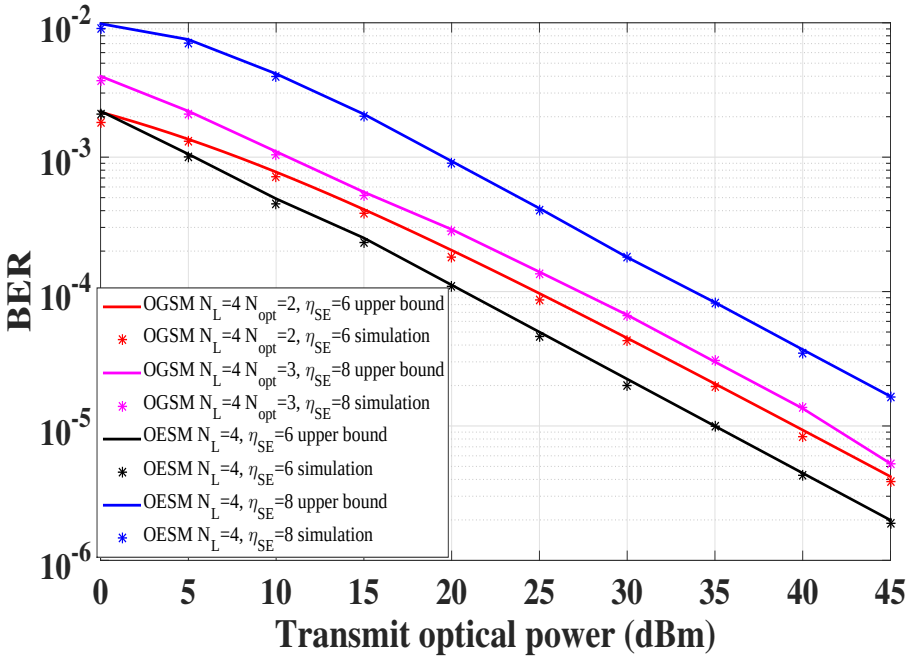

Figure 4.20: Effect of parameter variations on system performance.

4.6 Conclusion

In this chapter, OSM and advanced OSM schemes for FSO communication have been analyzed. Initially OSM combined with PLNC for full-duplex decode-and-forward FSO cooperative systems was studied. To eliminate the drawbacks of OSM, TLS and TLS-OSM schemes were studied for half-duplex FSO cooperative communication. Next, to further increase the spectral efficiency of OSM, advanced OSM methods were studied for FSO systems which can offer benefits of improved error performance. Cost and power consumption analysis of all the methods have been provided. In future, these advanced OSM schemes can be combined with TLS to achieve higher spectral efficiencies for FSO cooperative communication. Future work can be extended to the derivation of exact outage probability and BER expressions for OSM and PLNC based bidirectional FSO cooperative system, and derivation of closed form expressions for exact error analysis of advanced OSM schemes.

5. Spatial Modulation for Underwater Optical Wireless Communication

Optical wireless communication has been studied for free-space communication in the earlier chapter. In a similar manner, optical wireless communication can be implemented in underwater environment also with some modifications. In this chapter, underwater optical wireless communication (UOWC) with SISO case and MIMO cases are explored. The chapter after a broad overview regarding UOWC technology (Section 5.1) and the concerned channel model (Section 5.2), is divided into three major parts. The first part (Section 5.3) deals with AF based UOWC SISO scenario. Outage probability and ASEP expressions for one-way and two-way relay based SISO UOWC systems are derived. The second part (Section 5.4) extends UOWC to MIMO scenario and proposes OIQSM for UOWC cooperative communication. BER, cost and power consumption analysis are carried out for such systems. The subsequent part of the chapter (Section 5.5) proposes TLS and TLS-OSM schemes to resolve the drawbacks of OSM for UOWC cooperative systems. Outage probability and ASEP closed form expressions are derived for such systems. The chapter is finally summarized in Section 5.6.

5.1 Introduction to UOWC

In underwater communication, message is propagated underwater by using some carriers. The system performance in aquatic environment is affected by the water salinity and presence of diverse marine organisms. RF and acoustic underwater communication suffer from the problem of limited bandwidths and lower data rates. While on the other hand, higher data rates can be achieved by using UOWC. UOWC has many similarities with atmospheric FSO communication [13], however the environmental conditions are different. In underwater conditions, absorption takes place due to collision between the propagating photons and water molecules, and other suspended molecules, and suffer energy loss. The optical signals undergo directional change due to scattering [170]. The absorption coefficient $a(\lambda)$ and scattering coefficient $b(\lambda)$ are considered to take these effects into account [171].

Acoustic form of underwater communication has some disadvantages. The frequency of operation is very low leading to poor data rates. The delay time in acoustic links is also large (typically in seconds).

Acoustic transceivers are also expensive and not energy efficient. The RF method suffers from the problem of short link range. It also requires expensive energy inefficient transceivers and large antennas. Hence one can opt for underwater optical wireless communications as a possible alternative. Speed of light (which is the carrier in UOWC) is much greater than acoustic wave. Thus UOWC links are immune to link latency and provide more security also [172, 173].

The underwater environment is dynamic resulting in the need of a complex channel model. UOWC equipment are affected by water flow, temperature, salinity and turbidity of water. Power crisis in the aquatic environment requires the devices to be energy efficient. In underwater environment, light absorption occurs due to the presence of coloured dissolved organic material (CDOM) and chlorophyll. This hinders light propagation and the turbidity of water increases. The concentration of CDOM also fluctuates with ocean depth variations, thereby changing the corresponding light attenuation coefficients. The temperature and pressure of ocean currents vary rapidly causing fluctuations of refractive index of water. This phenomenon is known as turbulence [174].

Monte Carlo based numerical simulations of the channel in UOWC has been performed in literature which has shown that the fading free impulse response (FFIR) of the channel, with absorption and scattering effects taken into account, cannot be adopted like FSO channel links. The tremendous amount of multiple scattering of the propagating light causes temporal dispersion on the channel FFIR and consequently on the received optical signal. Turbulence induced fading must be considered while designing the channel. The channel FFIR is multiplied by a positive fading coefficient to characterize the fading induced channel turbulence. Beer-Lambert's Law can suitably describe the attenuation effect in sea water. But in this work, blue/green region of the visible spectrum has been chosen, as 450-550 nm spectral range (corresponding to blue/green region) has the least attenuation and scattering coefficient. Hence we have considered turbulence induced fading in our channel model and ignored the attenuation error. The distance of communication between UOWC devices is typically within the range of 100 m [175]. Hence the effect of pointing and misalignment errors caused due to floating oceanic currents has been neglected in the analysis, but it may be included in the analysis and this has been kept for future research works. Background noise is weak in underwater environment; hence the receiving apertures have large diameters. This results in a weak turbulence effect which can be effectively described by a lognormal channel model. Lognormal models are used in scenarios where single scattering phenomenon occur. The assumption that the magnitude of the scattered optical field is less than the unperturbed phase gradient is valid for underwater environments due to the presence of weak turbulence induced fading. Hence use of lognormal channel model is justified for UOWC under weak oceanic turbulences, as has been reported in literature [175, 176, 177, 178].

In UOWC systems, optical sources like LED/Laser are intensity modulated at the transmitting side while for reception, direct detection by photo-detector is done [96]. Binary phase shift keying (BPSK) or some higher constellation schemes like M-quadrature amplitude modulation (QAM) [179, 180] can be used as modulation schemes for UOWC systems. Usually, deep underwater ocean explorations will need longer distance communication since the ocean depths are generally in kilometers. For this, cooperative communication with amplify-and-forward (AF) technique at the relay can be beneficial. In a bidirectional cooperative UOWC system, transmission of two packets in either direction takes place in two time slots only thereby saving bandwidth. Both the source nodes transmit their messages to the relay and the relay then amplifies and forwards them to the corresponding destination nodes. Thus all the nodes can operate in full-duplex mode in a bidirectional system.

5.2 Channel Model

Note that UOWC experiences a single scattering phenomenon which induces weak turbulence effects as stated by Rytov theory earlier. The channel fading coefficient has an amplitude envelope which is considered to be represented by a random variable $h \geq 0$ following lognormal distribution. From the Rytov theory as seen earlier $h = e^{2Y}$ where Y is a normal random variable with μ^{lg} and σ^2 as the mean and variance of $Y = 1/2\ln(h)$. Therefore, the PDF of lognormal fading coefficient for UOWC link is given by:

$$f_h(h) = \frac{1}{h\sqrt{8\pi\sigma^2}} \exp\left(-\frac{\left(\ln(h) - 2\mu^{lg}\right)^2}{8\sigma^2}\right) . \tag{5.1}$$

Usually, we take the mean of h as 1. Hence, taking $E[h] = \mu_h^{lg} = \exp(2\mu^{lg} + 2\sigma^2) = 1$, we get $\mu^{lg} = -\sigma^2$ [181]. Note that variance of h, $\sigma_h^2 = E[h^2] - (E[h])^2 = (e^{4\sigma^2} - 1)e^{(4\mu_x^{lg} + 4\sigma^2)}$ can be simplified as $\sigma_h^2 = e^{4\sigma^2} - 1$. For $\sigma^2 << 1$, then $\sigma_h^2 \approx 4\sigma^2$. Let $\gamma = |h|^2$. Therefore, the PDF of received SNR γ can be written as [182]:

$$f_\gamma(\gamma) = \frac{1}{\sqrt{32\pi}\gamma\sigma} \exp\left(\frac{-\left(\ln(\frac{\gamma}{\bar{\gamma}}) + 4\sigma^2\right)^2}{32\sigma^2}\right) , \tag{5.2}$$

where $\bar{\gamma}$ represents the average electrical SNR of the UOWC links. The CDF can be expressed as [182]:

$$F_\gamma(\gamma) = 1 - \frac{1}{2} erfc\left(\frac{\ln\left(\frac{\gamma}{\bar{\gamma}}\right) + 4\sigma^2}{\sqrt{32}\sigma}\right) . \tag{5.3}$$

where $erfc(\cdot)$ denotes the complementary error function given as $erfc(x) = \frac{2}{\sqrt{\pi}} \int_x^\infty e^{-t^2} dt$.

Scintillation index denoted by σ_I^2 is used to describe the fluctuations of refractive index for turbulent seawater. Its value indicates the nature of turbulence. For example, σ_I >1 indicates strong turbulence,

while $0 < \sigma_I < 1$ denotes weak turbulence. In weak turbulence environments, we assume that σ^2=-μ^{lg} and $\sigma_I^2 = e^{4\sigma^2} - 1$ [177]. It may be noted as σ^2 increases, σ_I^2 also increases. The parameter σ_I^2 is calculated using other parameters like wavelength, link distance and refractive index constant depending on the type of sea water and turbulence. Coastal sea water is considered for our analysis which is symbolized by the parameter ω_{wat}. σ_I^2 value is calculated using other parameters as shown below:

$$\sigma_I^2 = -\frac{24.832\pi^5}{\lambda^3 \times 10^8} \int_0^\infty \kappa_f^{-14/3} \epsilon^{-1/3} [1 + 2.35(\kappa_f \ \eta_{km})^{2/3}] \times \frac{\chi_T}{\omega_{wat}^2} (\omega_{wat}^2 e^{-A_T \delta} + e^{-A_s \delta} - 2\omega e^{-A_{Ts} \delta}) \times \sin\left(\frac{L\kappa_f^2 \lambda}{2\pi}\right) d\kappa_f \ , \quad (5.4)$$

where κ_f denotes the scalar spatial frequency, ϵ is the rate of dissipation of turbulent kinetic energy per unit mass of fluid, λ is the wavelength, η_{km} represents Kolmogorov microscale, the rate of dissipation of mean-square temperature is represented by χ_T, ω_{wat} is the relative strength of temperature and salinity fluctuations and L is the distance between two nodes. A_T, A_S and A_{Ts} are all constants. $\delta = 8.284(\kappa_f \ \eta_{km})^{4/3} + 12.978(\kappa_f \ \eta_{km})^2$. The values are later given in Results section. Thus the lognormal channel model has a variance σ^2 which is dependent on σ_I^2 and takes into account all the conditions available underwater.

5.3 Amplify-and-Forward Based UOWC Systems

Now we come to the first contribution of this chapter, which deals with the performance analysis of unidirectional and bidirectional AF based UOWC SISO systems in terms of outage probability and ASEP. AF relaying is a technique where the relay just amplifies and forwards the signal without actually decoding it. In the literature, optical pre-amplification for UOWC systems has been explored in [176]. In [183], a suitable channel model for UOWC systems, which considers effects like turbulence, absorption and scattering, has been proposed. The performance of UOWC system for random sea surface has been analyzed in [184]. Experimental investigation of temporal properties of optical communication signals in turbid underwater environments has been performed under various coherent modulation schemes like phase shift keying and quadrature amplitude modulation [180]. Decode-and-forward and amplify-and-forward based multi-hop UOWC communication has been analyzed in terms of a Lambertian based channel model in [185]. In [175], a point-to-point multi-hop UOWC has been investigated in terms of BER. The influence of different number of relays and the effect of transmit power have been studied for optical wireless communication in turbid water in [186]. Capacity analysis of UOWC under weak turbulence conditions has been performed in [177]. Optimization of power allocation and relay location has been proposed for AF multi-hop systems over lognormal channels. Half-duplex and full-duplex AF

and DF relaying with energy harvesting has been studied over lognormal channels in [187]. Exact outage probability and symbol error rate analysis for two-way AF relay networks has been done over Nakagami-m fading channels [188]. Performance analysis of AF FSO system has been proposed over lognormal channels in [189]. BER analysis over G-G and lognormal based FSO systems has been done in [190].

Based on the above literature survey, quite a few research gaps have been observed. There are few works dealing with AF based systems over lognormal channels in FSO communication, but limited works based on lognormal channels in UOWC. In UOWC, the lognormal channel has to take into account scattering, weak turbulence induced fading and attenuation factors due to the behaviour of optical signals underwater. Such a study is not required for FSO communication, even though the channel model may be same. Another research gap observed is that closed form expressions of BER for AF relay based systems over lognormal channel could not be derived in literature. Either some approximations were done by using asymptotic analysis or by some numerical methods. Tractable closed form BER expressions for such systems are lacking. All these factors motivate us to propose closed form outage probability analysis and error analysis for AF based UOWC systems over lognormal channel using MG distribution.

The novelty of this work is as follows. The closed form expressions for outage probability lower bounds of one-way relay (OWR) and two-way relay (TWR) based UOWC are derived by approximating lognormal underwater fading channel with mixture of Gamma (MG) distributions. The exact analysis of outage probability is also provided and the difficulties involved in obtaining exact analysis are also listed, thereby justifying the reason to opt for calculation of bounds. The challenging part of the error evaluation is to derive closed form expressions as lognormal distribution contains intractable integrals which prevents us from getting closed form expressions. Without closed form expressions, it is difficult to analyze the system performance by varying a particular parameter. Numerical methods take up a lot of time and has high computational complexity, and hence closed form analytical expressions are required for gaining valuable insight into the system performance and also for further system optimization. With approximation of lognormal distribution by MG distribution, MIMO UOWC analysis can become tractable. In the subsequent sections, system models are provided. The closed form expressions for outage probability and ASEP for OWR and TWR based UWOC are derived by approximating lognormal distribution with 5-MG distribution. Asymptotic analysis is also carried out to evaluate coding and diversity gains.

5.3.1 System Model and Performance Analysis for AF based UOWC Systems

The model which is used for UOWC can be explained through Fig. 5.1. The ROVs and sensors need to interact through optical wireless links, leading to the necessity of point-to-point communication between the devices. Since the UOWC is a short range communication, hence there is need for a

cooperative model. The simplest form of 3 node cooperation model, comprising of SN, RN and DN nodes, is considered, as shown in Fig. 5.2. SN denotes the source node, RN denotes the relay node and DN denotes the destination node as depicted in Fig. 5.2. SR signifies the channel path from SN to RN whereas RD is the channel path from RN to DN. h_{SR} denotes the channel coefficient from SN to RN and h_{RD} is the channel coefficient from RN to DN. For our proposed dual-hop relay system, there is no direct link between SN and DN. One can extend this analysis to multi-hop relay system [191] for further extending the link range. For transmitting purpose, lasers are used and for receiving side, a photodetector of responsivity R_e is used.

5.3.1.1 Outage Probability for One-Way Relay System (OWR based UOWC)

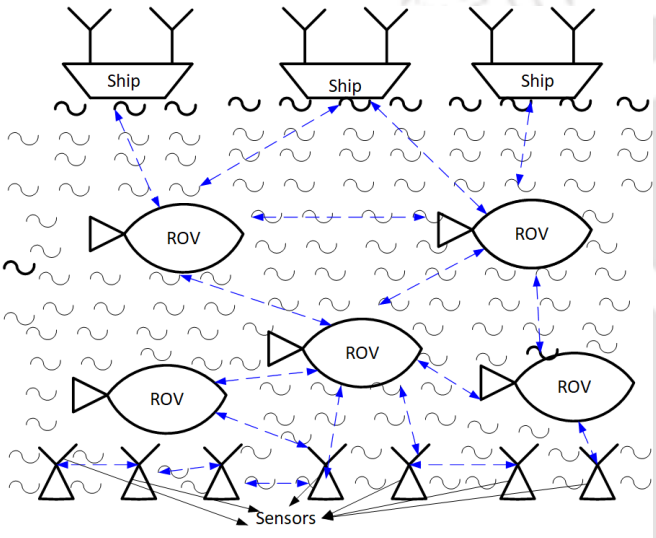

Figure 5.1: Practical system model for UOWC (Dashed arrows represents optical links).

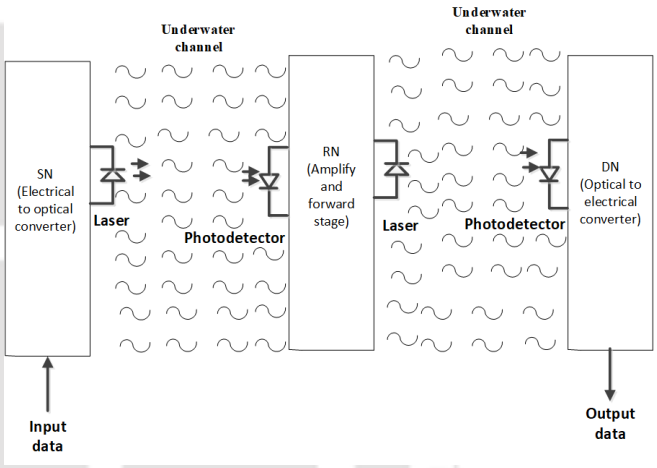

Figure 5.2: System model for OWR based UOWC

The total AF process is a dual time slot process. In the first time slot, source node sends its message to the relay node while in the second time slot, relay node amplifies it with a gain and forwards the signal to the destination node. The received signal r_{SR} at RN at the end of first time slot can be written as:

$$r_{SR} = \sqrt{ER_e}h_{SR}x + n_{SR} \ . \tag{5.5}$$

where x denotes the transmitted signal, n_{SR} is the zero mean complex Gaussian random variable with variance $N_0/2$. Time slots are the smallest division of a communication channel that is assigned to particular users in a communication system. Hence the nodes can transmit information in a particular time slot only. The total energy required for transmission in the two time slots by SN and RN is 2E. The received signal r_{RD} at DN at the end of second time slot can be written as:

$$r_{RD} = \sqrt{cER_e}h_{SR}h_{RD}x + n_{RD} \ , \tag{5.6}$$

where n_{RD} is the zero mean complex Gaussian random variable with variance $N_0/2$. For AF relaying the variable-gain c can be defined as [192, 193]:

$$c = \frac{R_e E/N_0}{1 + R_e|h_{SR}|^2 E/N_0 + R_e|h_{RD}|^2 E/N_0} \ . \tag{5.7}$$

CSI at the receiver is obtained by sending training sequence or pilot signals. For slow fading, channel stability enables the receiver to acquire the CSI. In fast fading case, the channel coefficients vary at a fast rate and reliable channel estimation may not be possible. It is to be kept in mind that for variable-gain relaying, the channel gains are varying and exact knowledge of the channel statistics must be known to the nodes. Thus for variable-gain relaying scheme, CSI needs to be known at the destination node. The destination requires CSI for both source-to-relay links and relay-to-destination links to decode the message. Therefore, channel estimation and channel exchange are required for both relay and destination nodes. The channel estimations of the source-to-relay link and relay-to-destination links can be assumed as a multi-user channel estimation problem [194]. The results of channel estimation can be used in interference cancellation in this case. This technique follows the principle of periodic insertion of a unique training sequence into each data sequence and also allows the time variation of the channels within and between the training sequences. Interference mitigation techniques is an interesting field of research and can be considered as a future scope of work for such UOWC systems.

For calculation of end-to-end outage probability, end-to-end SNR calculation is required. Thus from Eq. (5.6) and (5.7), the equivalent end-to-end SNR at the DN node is written as:

$$\gamma_{SRD}^{owr} = \frac{\gamma_{SR}\gamma_{RD}}{1 + \gamma_{SR} + \gamma_{RD}} \ , \tag{5.8}$$

where,

$$\gamma_{SR} = \frac{R_e|h_{SR}|^2 E}{N_0} \ , \quad \gamma_{RD} = \frac{R_e|h_{RD}|^2 E}{N_0} \ . \tag{5.9}$$

Now we will try to evaluate the exact outage probability for such a system. Let the threshold SNR γ_{th} be denoted by x. The total end-to-end outage probability ($F_{\gamma_{SRD}^{owr}}(x)$) is given by:

$$\begin{aligned} F_{\gamma_{SRD}^{owr}}(x) &= P\left(\frac{\gamma_{SR}\gamma_{RD}}{\gamma_{SR} + \gamma_{RD} + 1} < x\right) \\ &= \int_{y=0}^{\infty} P\left(\frac{\gamma_{SR} y}{\gamma_{SR} + y + 1} < x\right) f_{\gamma_{RD}}(y)dy \\ &= \int_{y=0}^{\infty} P\left(\gamma_{SR} < \frac{(y+1)x}{y - x}\right) f_{\gamma_{RD}}(y)dy \\ &= F_{\gamma_{RD}}(x) + \int_{x}^{\infty} F_{\gamma_{SR}}(z)\, f_{\gamma_{RD}}(y)dy \ . \end{aligned} \tag{5.10}$$

For the last step of the above equation, we have split the limit of integration into two parts $y = 0$ to x and the other $y = x$ to ∞. Let $z = \frac{(y+1)x}{y-x}$. The value of $P\left(\gamma_{SR} > \frac{(y+1)x}{y-x}\right)$ in the range of $y = 0$ to x is 1, since the random variable γ_{SR} is always positive and will always be greater than the negative value of $\frac{(y+1)x}{y-x}$ when $0 < y < x$. The PDF and CDF of the terms are inserted from Eq. (5.2) and Eq. (5.3) respectively to obtain the following simplified equation:

$$F_{\gamma_{SRD}^{owr}}(x) = 1 - \frac{1}{2}erfc\left(\frac{\ln\left(\frac{x}{\bar{\gamma}_{RD}}\right) + 4\sigma^2}{\sqrt{32}\sigma}\right) + \int_x^{\infty} \frac{1}{\sqrt{32\pi\sigma_{RD}^2 y}}\left(1 - \frac{1}{2}erfc\left(\frac{\ln\left(\frac{z}{\bar{\gamma}_{SR}}\right) + 4\sigma^2}{\sqrt{32}\sigma}\right)\right)\exp\left(-\frac{\left(\ln\left(\frac{y}{\bar{\gamma}_{RD}}\right) + 8\sigma_{RD}^2\right)^2}{32\sigma_{RD}^2}\right) dy \ . \tag{5.11}$$

From the above integral equation, we can observe that the second term's integral is intractable. No closed form expressions are available to the best of the author's knowledge. Such integrals need to be solved numerically in Mathematica. But our goal is to obtain closed form expressions to gain valuable insights regarding system performance. Hence we opt for bounds of outage probability scenario now. High SNR case is considered and end-to-end SNR is approximated as:

$$\gamma_{SRD}^{owr} = \frac{\gamma_{SR}\gamma_{RD}}{1 + \gamma_{SR} + \gamma_{RD}} \cong \frac{1}{2}\frac{2}{\frac{1}{\gamma_{SR}} + \frac{1}{\gamma_{RD}}} = \gamma_{approx} \ . \tag{5.12}$$

An upper bound can be obtained by the inequality:

$$\gamma_{approx} < \gamma_{up} \approx \min(\gamma_{SR}, \gamma_{RD}) \ . \tag{5.13}$$

This is explained by the condition that when either of the links fails (source-to-relay or relay-to-destination), then outage can occur. Since the SNR is upper bounded, hence the CDF will be lower bounded as CDF is inversely proportional to SNR. A tight lower bound on CDF of γ_{SRD}^{owr} can be evaluated by considering the minimum of two random variables condition (which corresponds to either of the link failure condition). $P(\gamma_{SR} < \gamma)$ is the CDF of source-to-relay link and $P(\gamma_{RD} < \gamma)$ is the CDF of relay-to-destination link. Thus, the overall lower bound of CDF is given by a closed form expression [195]:

$$F_{\gamma_{SRD}^{owr}}(\gamma) \geq P(\gamma_{SR} < \gamma) + P(\gamma_{RD} < \gamma) - P(\gamma_{SR} < \gamma)P(\gamma_{RD} < \gamma) \ . \tag{5.14}$$

Using Eq. (5.14) and Eq. (5.3), the outage probability for a threshold SNR of γ_{th} is lower bounded as:

$$P_{out}(\gamma_{th}) \geq P(\min(\gamma_{SR}, \gamma_{RD}) < \gamma_{th})$$
$$= 1 - \frac{1}{4} erfc\left(\frac{\ln\left(\frac{2^{R_d}-1}{R_e\bar{\gamma}_{SR}}\right) + 4\sigma_{SR}^2}{\sqrt{32}\sigma_{SR}}\right) erfc\left(\frac{\ln\left(\frac{2^{R_d}-1}{R_e\bar{\gamma}_{RD}}\right) + 4\sigma_{RD}^2}{\sqrt{32}\sigma_{RD}}\right) , \quad (5.15)$$

where $\gamma_{th} = 2^{R_d} - 1$, $\bar{\gamma}_{SR} = E/N_0$, $\bar{\gamma}_{RD} = E/N_0$ (assuming that SNR at both SN and RN nodes are equal) and R_d is the target data rate in bps. Let us analyze the outage probability from the closed form expression. The analysis can be easily understood by the analysis of a single erfc function term. If the SNR increases, the log term becomes more and more negative. As the argument in erfc function becomes more and more negative, the erfc function value increases in a positive manner. Thus the product of two erfc function values will also increase. The total increment when subtracted from 1 will give decreasing values with increment in SNR value. Therefore, the total outage probability value decreases with increment in SNR value.

The next step is to evaluate the lower bound of PDF which will be required for error analysis. For the PDF evaluation, CDF needs to be calculated first. The CDF of lower bound using Eq. (5.14), can be written as:

$$F_{\gamma_{SRD}^{owr}}(\gamma) \geq 1 - \frac{1}{4} erfc\left(\frac{\ln\left(\frac{\gamma}{R_e\bar{\gamma}_{SR}}\right) + 4\sigma_{SR}^2}{\sqrt{32}\sigma_{SR}}\right) erfc\left(\frac{\ln\left(\frac{\gamma}{R_e\bar{\gamma}_{RD}}\right) + 4\sigma_{RD}^2}{\sqrt{32}\sigma_{RD}}\right) . \quad (5.16)$$

The corresponding PDF can be obtained by differentiating (5.16) and the final expression of PDF lower bound can be written as:

$$f_{\gamma_{SRD}^{owr}}(\gamma) \geq \frac{1}{8\sqrt{2\pi}\gamma}\left[\frac{1}{\sigma_{SR}} \exp\left(\frac{-\left(\ln(\frac{\gamma}{R_e\bar{\gamma}_{SR}}) + 4\sigma_{SR}^2\right)^2}{32\sigma_{SR}^2}\right) erfc\left(\frac{\left(\ln(\frac{\gamma}{R_e\bar{\gamma}_{RD}}) + 4\sigma_{RD}^2\right)}{\sqrt{32}\sigma_{RD}}\right)\right.$$
$$\left. + \frac{1}{\sigma_{RD}} \exp\left(\frac{-\left(\ln(\frac{\gamma}{R_e\bar{\gamma}_{RD}}) + 4\sigma_{RD}^2\right)^2}{32\sigma_{RD}^2}\right) erfc\left(\frac{\left(\ln(\frac{\gamma}{R_e\bar{\gamma}_{SR}}) + 4\sigma_{SR}^2\right)}{\sqrt{32}\sigma_{SR}}\right)\right] . \quad (5.17)$$

While differentiating some steps are required. For example, assume $z = \frac{\ln\left(\frac{\gamma}{R_e\bar{\gamma}_{RD}}\right)+4\sigma_{RD}^2}{\sqrt{32}\sigma_{RD}}$ and the relation $erfc(x) = \frac{2}{\sqrt{\pi}}\int_x^\infty e^{-t^2}dt$ is used.

5.3.1.2 Outage Probability for Two-Way Relay System (UOWC_TWR)

For two-way relay system in Fig. 5.3, both the nodes (SN and DN) send information to the relay. All the nodes work in full-duplex mode. The SNR at DN can be expressed as [188]:

$$\gamma_{SRD}^{twr} = \frac{\gamma_{SR}\gamma_{RD}}{1 + \gamma_{SR} + 2\gamma_{RD}} , \quad (5.18)$$

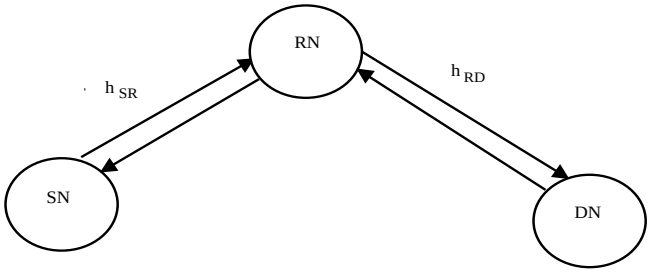

Figure 5.3: System model for UOWC_TWR

where the terms have been explained earlier. Again if we do exact analysis as shown for OWR case, then closed form outage probability expressions cannot be achieved. Hence we opt for high SNR analysis. For high SNR case, the end-to-end SNR can be approximated as:

$$\gamma_{SRD}^{twr} = \frac{\gamma_{SR}\gamma_{RD}}{1+\gamma_{SR}+2\gamma_{RD}} \cong \frac{1}{2}\frac{2}{\frac{2}{\gamma_{SR}}+\frac{1}{\gamma_{RD}}} = \gamma_{approx} \ . \tag{5.19}$$

A tight upper bound of the SNR needs to be calculated. As the SNR is upper bounded, hence the CDF, outage probability and PDF will be lower bounded. A tight lower bound on CDF of γ_{SRD}^{twr} is given by a closed form expression as in earlier case:

$$F_{\gamma_{SRD}^{twr}}(\gamma) \geq P\{\frac{1}{2}\min(\gamma_{SR}, 2\gamma_{RD}) < \gamma\} \ . \tag{5.20}$$

The CSI has to be made available to all the nodes and interference has to be mitigated. Channel estimation techniques are applied for updating the CSI and mitigating the interference as discussed earlier in OWR based systems. Outage occurs when either of the links fails. This condition can be satisfied by the minimum criteria of the SNR of the two links. In this case the 1/2 term is due to the full-duplex nature of the system. The outage probability of TWR system is thus lower bounded as:

$$\begin{aligned} P_{out}(\gamma_{th}) &\geq P\{\tfrac{1}{2}\min(\gamma_{SR}, 2\gamma_{RD}) < \gamma_{th}\} \\ &= P(\gamma_{SR} < 2\gamma_{th}) + P(\gamma_{RD} < \gamma_{th}) - P(\gamma_{SR} < 2\gamma_{th})P(\gamma_{RD} < \gamma_{th}) \\ &= 1 - \tfrac{1}{4} erfc\left(\frac{\ln\left(\frac{2(2^{R_d}-1)}{Re\tilde{\gamma}_{SR}}\right)+4\sigma_{SR}^2}{\sqrt{32}\sigma_{SR}}\right) erfc\left(\frac{\ln\left(\frac{2^{R_d}-1}{Re\tilde{\gamma}_{RD}}\right)+4\sigma_{RD}^2}{\sqrt{32}\sigma_{RD}}\right) \ . \end{aligned} \tag{5.21}$$

Let us analyze the outage probability from the closed form expression. The analysis can be easily understood by the analysis of a single erfc function term. If the SNR increases, the log term becomes more and more negative. As the erfc component becomes more and more negative, the erfc function value increases in a positive manner. Thus the product of two erfc function value will also increase. The total increment when subtracted from 1 will give decreasing values with increment in SNR value.

Therefore, the total outage probability value decreases with increment in SNR value.

For error analysis, the PDF of lower bound is required. The PDF can only be evaluated from the CDF equation. Hence first we calculate the CDF for UOWC_TWR system which can be written as:

$$F_{\gamma_{SRD}^{twr}}(\gamma) \geq 1 - \tfrac{1}{4} erfc\left(\frac{\ln\left(\frac{2*\gamma}{R_e\bar{\gamma}_{SR}}\right)+4\sigma_{SR}^2}{\sqrt{32}\sigma_{SR}}\right) erfc\left(\frac{\ln\left(\frac{\gamma}{R_e\bar{\gamma}_{RD}}\right)+4\sigma_{RD}^2}{\sqrt{32}\sigma_{RD}}\right) . \tag{5.22}$$

Similarly the PDF of lower bound for this system can be expressed by differentiating the CDF. Hence the lower bound PDF is expressed as:

$$\begin{aligned} f_{\gamma_{SRD}^{twr}}(\gamma) \geq \frac{1}{8\sqrt{2\pi}\gamma}\Bigg[\frac{1}{\sigma_{SR}} \exp\left(\frac{-\left(\ln(\frac{2\gamma}{R_e\bar{\gamma}_{SR}})+4\sigma_{SR}^2\right)^2}{32\sigma_{SR}^2}\right) erfc\left(\frac{\left(\ln(\frac{\gamma}{R_e\bar{\gamma}_{RD}})+4\sigma_{RD}^2\right)}{\sqrt{32}\sigma_{RD}}\right) \\ + \frac{1}{\sigma_{RD}} \exp\left(\frac{-\left(\ln(\frac{\gamma}{R_e\bar{\gamma}_{RD}})+4\sigma_{RD}^2\right)^2}{32\sigma_{RD}^2}\right) erfc\left(\frac{\left(\ln(\frac{2\gamma}{R_e\bar{\gamma}_{SR}})+4\sigma_{SR}^2\right)}{\sqrt{32}\sigma_{SR}}\right)\Bigg] . \end{aligned} \tag{5.23}$$

5.3.2 ASEP Calculation for UOWC AF Systems

Let $P_q(\mathrm{x})$ denote the symbol error probability (SEP) of the M-ary modulation scheme deployed. The average ASEP over the entire fading channel for OWR based UOWC can be written as [80]:

$$P_e \cong \int_0^\infty aQ(\sqrt{e\gamma}) f_{\gamma_{SRD}^{owr}}(\gamma) d\gamma . \tag{5.24}$$

For a TWR based UOWC system, the PDF is replaced by $f_{\gamma_{SRD}^{twr}}$. The PDF of OWR and TWR systems have been evaluated earlier. However the closed form expression of ASEP cannot be evaluated. Hence the integral is obtained using software like Mathematica. In this work, binary phase shift keying (BPSK) modulation scheme is used. The values of a and e depend on the constellation scheme and has been taken from Eq. (7) of [81].

It is observed from the expressions that lognormal distribution poses a lot of problems for analyzing UOWC system performance, as the distribution contains intractable integrals. Closed form expressions for ASEP cannot be obtained due to higher computational complexities of lognormal distribution. Thus lognormal distribution can be approximated by a MG distribution [82], which offers ease of calculation.

5.3.3 PDF, CDF and Error Analysis using MG Distributions

After approximating lognormal distribution with MG distribution, the outage probability and error expressions need to be derived. For outage probability, CDF equation of MG distribution is required and for error analysis, PDF equation of MG distribution is required. The PDF of MG distribution can be written as defined earlier in Eq. (3.8). Number of mixing coefficients is denoted by n, Γ denotes the

Gamma function, P_i is the mixing coefficient of the i^{th} Gamma distribution having properties like $P_i > 0$ and $\sum_{i=1}^{n} P_i = 1$. The shape and scale parameters of the i^{th} Gamma distribution for $x > 0$ are α_i^{MG} and β_i^{MG} respectively. CDF of MG distribution can be obtained by integrating the PDF and can be written as defined in Eq. (3.9). Outage probability for UOWC_OWR system can be calculated as:

$$P_{out} = \sum_{i=1}^{n} P_i \left(1 - \frac{1}{\Gamma(\alpha_i^{MG})} G_{1,2}^{2,0}\left(\begin{matrix}1\\0,\alpha_i^{MG}\end{matrix}\middle|\frac{\beta_i^{MG}\gamma_{th}}{R_e\bar{\gamma}}\right)\right) , \tag{5.25}$$

where $\gamma_{th} = 2^{R_d} - 1$ for UOWC_OWR systems, R_d is the data rate, $\bar{\gamma}$ is the average SNR. For asymptotic analysis of outage probability, the argument in Meijer G function is first inverted using Eq. (6.2.2) in [62] and the expression is written as:

$$P_{out} = \sum_{i=1}^{n} P_i \left(1 - \frac{1}{\Gamma(\alpha_i^{MG})} G_{2,1}^{0,2}\left(\begin{matrix}1,1-\alpha_i^{MG}\\0\end{matrix}\middle|\frac{R_e\bar{\gamma}}{\beta_i^{MG}\gamma_{th}}\right)\right) . \tag{5.26}$$

Let $z = \frac{R_e\bar{\gamma}}{\beta_i^{MG}\gamma_{th}}$. Then the Meijer G function at very high values of its argument can be written as described in Eq. (41) in [63]. Thus the overall asymptotic expression is written as:

$$P_{out}^{asym} \approx \sum_{i=1}^{n} P_i \left(1 - \frac{1}{\Gamma(\alpha_i^{MG})} \sum_{k=1}^{2} z^{a_k-1} \frac{\prod_{l=1,l\neq k}^{2} \Gamma(a_k - a_l)}{\prod_{l=1}^{1} \Gamma(a_k - b_l)}\right) , \tag{5.27}$$

where $a = \left[1, 1 - \alpha_i^{MG}\right]$, $b = [0]$. To obtain the diversity gain from this expression, the highest exponent of SNR is required which is given by $-\min(\alpha_i^{MG})$. Therefore the negative value of this exponent, according to Eq. (2.73) give us the value of diversity gain which is $\min(\alpha_i^{MG})$ in our case. The coding gain is given by:

$$C_g = \left(\sum_{i=1}^{n} P_i \left(1 - \frac{1}{\Gamma(\alpha_i^{MG})} \sum_{k=1}^{2} \left(\frac{R_e}{\beta_i^{MG}\gamma_{th}}\right)^{a_k-1} \frac{\prod_{l=1,l\neq k}^{2} \Gamma(a_k - a_l)}{\prod_{l=1}^{1} \Gamma(a_k - b_l)}\right)\right)^{-\frac{1}{\min(\alpha_i^{MG})}} . \tag{5.28}$$

Our next goal is to evaluate closed form expressions of ASEP using 5-MG distributions. For AF based UOWC systems, end-to-end CDF of the entire system is computed and then end-to-end PDF is computed by differentiating the CDF. For ASEP calculation of UOWC_OWR, Eq. (5.24) is used, Q function is expressed in terms of Meijer G function. The end-to-end PDF of the UOWC_OWR system can be defined as:

$$\begin{aligned} f_{E2E}(\gamma) &= f_{\gamma_{SR}}(\gamma_{SR}) + f_{\gamma_{RD}}(\gamma_{RD}) - f_{\gamma_{SR}}(\gamma_{SR})F_{\gamma_{RD}}(\gamma_{RD}) - f_{\gamma_{RD}}(\gamma_{RD})F_{\gamma_{SR}}(\gamma_{SR}) \\ &= f_{\gamma_{SR}}(\gamma_{SR})(1 - F_{\gamma_{RD}}(\gamma_{RD})) + f_{\gamma_{RD}}(\gamma_{RD})(1 - F_{\gamma_{SR}}(\gamma_{SR})) . \end{aligned} \tag{5.29}$$

For γ_{SR}=γ_{RD}=γ,

$$\begin{aligned} f_{E2E}(\gamma) &= 2f_{\gamma}(\gamma)(1 - F_{\gamma}(\gamma)) \\ &= 2f_{\gamma}(\gamma) \sum_{i=1}^{n} \left[(1 - P_i) + \frac{P_i}{\Gamma(\alpha_i^{MG})} G_{1,2}^{2,0}\left(\begin{matrix}1\\0,\alpha_i^{MG}\end{matrix}\middle|\frac{\gamma\beta_i^{MG}}{\bar{\gamma}R_e}\right)\right] , \end{aligned} \tag{5.30}$$

where the values of $f_\gamma(\gamma)$ and $F_\gamma(\gamma)$ are computed using MG distribution. Now the overall ASEP for BPSK modulation can be written as:

$$P_e \cong \int_0^\infty f_{E2E}(\gamma) Q(\sqrt{2\gamma}) d\gamma \ . \tag{5.31}$$

Now, $P_e = f_1 + f_2$, where

$f_1 = \int_0^\infty 2 f_\gamma(\gamma) \sum_{i=1}^n (1-P_i) Q(\sqrt{2\gamma}) d\gamma$ and $f_2 = \int_0^\infty 2 f_\gamma(\gamma) \sum_{i=1}^n \frac{P_i}{\Gamma(\alpha_i^{MG})} G_{1,2}^{2,0}\left({}^{1}_{0,\alpha_i^{MG}} \middle| \frac{\gamma \beta_i^{MG}}{\bar{\gamma} R_e} \right) Q(\sqrt{2\gamma}) d\gamma$.

We will be treating the terms f_1 and f_2 separately. One contains multiplication of a variable with exponential term and a Meijer G component, and the other term contains multiplication of a variable with exponential terms and two Meijer G components. We can write Q function in terms of Meijer G function [46]:

$$Q(\sqrt{2x}) = \frac{1}{2\sqrt{\pi}} G_{1,2}^{2,0}\left({}^{1}_{0,1/2} \middle| x \right) \ . \tag{5.32}$$

Therefore we can write f_1 and f_2 as:

$$\begin{aligned} f_1 &= \int_0^\infty \sum_{i=1}^n \frac{P_i(1-P_i)\gamma^{\alpha_i^{MG}-1}(\beta_i^{MG})^{\alpha_i^{MG}}}{\Gamma(\alpha_i^{MG})} e^{-\beta_i^{MG}\gamma} \frac{1}{\sqrt{\pi}} G_{1,2}^{2,0}\left({}^{1}_{0,1/2} \middle| \gamma \right) d\gamma \\ &= \sum_{i=1}^n P_i(1-P_i) \int_0^\infty \frac{(\beta_i^{MG})^{\alpha_i^{MG}}}{\Gamma(\alpha_i^{MG})\sqrt{\pi}} \gamma^{\alpha_i^{MG}-1} G_{0,1}^{1,0}\left({}^{-}_{0} \middle| \frac{\beta_i^{MG}\gamma}{\bar{\gamma} R_e} \right) G_{1,2}^{2,0}\left({}^{1}_{0,1/2} \middle| \gamma \right) d\gamma \\ &= \sum_{i=1}^n \frac{P_i(1-P_i)}{\Gamma(\alpha_i^{MG})\sqrt{\pi}} G_{2,2}^{2,1}\left({}^{1-\alpha_i^{MG},1}_{0,1/2} \middle| \frac{\bar{\gamma} R_e}{\beta_i^{MG}} \right) \ , \end{aligned} \tag{5.33}$$

$$\begin{aligned} f_2 &= \int_0^\infty \sum_{i=1}^n \frac{P_i \gamma^{\alpha_i^{MG}-1}(\beta_i^{MG})^{\alpha_i^{MG}}}{\Gamma(\alpha_i)\Gamma(\alpha_i)} e^{-\beta_i^{MG}\gamma} \frac{1}{\sqrt{\pi}} P_i G_{1,2}^{2,0}\left({}^{1}_{0,\alpha_i} \middle| \frac{\beta_i^{MG}\gamma}{\bar{\gamma} R_e} \right) G_{1,2}^{2,0}\left({}^{1}_{0,1/2} \middle| \gamma \right) d\gamma \\ &= \int_0^\infty \sum_{i=1}^n \frac{P_i \gamma^{\alpha_i-1}(\beta_i^{MG})^{\alpha_i}}{\Gamma(\alpha_i)\Gamma(\alpha_i)} G_{0,1}^{1,0}\left({}^{-}_{0} \middle| \frac{\beta_i^{MG}\gamma}{\bar{\gamma} R_e} \right) \frac{1}{\sqrt{\pi}} P_i G_{1,2}^{2,0}\left({}^{1}_{0,\alpha_i} \middle| \frac{\beta_i^{MG}\gamma}{\bar{\gamma} R_e} \right) G_{1,2}^{2,0}\left({}^{1}_{0,1/2} \middle| \gamma \right) d\gamma \\ &= \sum_{i=1}^n \frac{P_i^2}{(\Gamma(\alpha_i^{MG}))^2\sqrt{\pi}} G_{1,0:1,2:1,2}^{0,1:2,0:2,0}\left(\begin{matrix} 1-\alpha_i^{MG} \\ - \end{matrix} \middle| \begin{matrix} 1 \\ 0, \alpha_i^{MG} \end{matrix} \middle| \begin{matrix} 1 \\ 0, 1/2 \end{matrix} \middle| 1, \frac{\bar{\gamma} R_e}{\beta_i^{MG}} \right) \ . \end{aligned} \tag{5.34}$$

By combining the terms f_1 and f_2 we can write the overall ASEP as:

$$\begin{aligned} P_e \cong & \sum_{i=1}^n P_i(1-P_i) \frac{1}{\Gamma(\alpha_i^{MG})\sqrt{\pi}} G_{2,2}^{2,1}\left({}^{1-\alpha_i^{MG},1}_{0,1/2} \middle| \frac{\bar{\gamma} R_e}{\beta_i^{MG}} \right) \\ & + \sum_{i=1}^n \frac{P_i^2}{(\Gamma(\alpha_i^{MG}))^2\sqrt{\pi}} G_{1,0:1,2:1,2}^{0,1:2,0:2,0}\left(\begin{matrix} 1-\alpha_i^{MG} \\ - \end{matrix} \middle| \begin{matrix} 1 \\ 0, \alpha_i^{MG} \end{matrix} \middle| \begin{matrix} 1 \\ 0, 1/2 \end{matrix} \middle| 1, \frac{\bar{\gamma} R_e}{\beta_i^{MG}} \right) \ . \end{aligned} \tag{5.35}$$

The following formulae have been used [46, 196]:

$$\int_0^\infty \tau^{\alpha-1} G_{u,v}^{s,t}\left({}^{c_1,c_2,\ldots,c_t,c_{t+1},c_u}_{d_1,d_2,\ldots,d_s,d_{s+1},\ldots,d_v} \middle| \tau w \right) G_{p,q}^{m,n}\left({}^{a_1,a_2,\ldots,a_n,a_{n+1},\ldots a_p}_{b_1,b_2,\ldots,b_m,b_{m+1},\ldots,b_q} \middle| \tau z \right) d\tau$$

$$= w^{\alpha} G_{v+p,u+q}^{m+t,n+s}\left(\begin{matrix} a_1,....,a_n,1-\alpha-d_1,...,1-\alpha-d_s,...,a_{n+1},...,a_p \\ b_1,....,b_m,1-\alpha-c_1,....,1-\alpha-c_t,...b_{m+1},...,b_q \end{matrix}\middle| \frac{z}{w}\right), \quad (5.36)$$

$$\int_0^{\infty} t^{\alpha-1} G_{p_1,q_1}^{m_1,n_1}\left(\begin{matrix} a_1,a_2,...,a_{n_1},a_{n_1+1},,...a_{p_1} \\ b_1,b_2,...,b_{m_1},b_{m_1+1},....,b_{q_1} \end{matrix}\middle| zt\right) G_{p_2,q_2}^{m_2,n_2}\left(\begin{matrix} a_1,a_2,...,a_{n_2},a_{n_2+1},,...a_{p_2} \\ b_1,b_2,...,b_{m_2},b_{m_2+1},....,b_{q_2} \end{matrix}\middle| xt\right)$$
$$\times G_{p_3,q_3}^{m_3,n_3}\left(\begin{matrix} a_1,a_2,...,a_{n_3},a_{n_3+1},,...a_{p_3} \\ b_1,b_2,...,b_{m_3},b_{m_3+1},....,b_{q_3} \end{matrix}\middle| yt\right) dt$$
$$= z^{-\alpha} G_{q_1,p_1:p_2,q_2:p_3,q_3}^{n_1,m_1:m_2,n_2:m_3,n_3}\left(\begin{matrix} 1-\alpha-b_1,...,1-\alpha-b_{q1} \\ 1-\alpha-a_1,...,1-\alpha-a_{p1} \end{matrix}\middle| \begin{matrix} a_1,a_2,...,a_{p2} \\ b_1,b_2,...,b_{q2} \end{matrix}\middle| \begin{matrix} a_1,a_2,...,a_{p3} \\ b_1,b_2,...,b_{q3} \end{matrix}\middle| x/z, y/z\right). \quad (5.37)$$

Thus it is seen that the ASEP and outage probability expressions are now available in closed form. Asymptotic analysis can also be performed for Meijer G function in ASEP expression. The Meijer G function has to be expressed in terms of basic mathematical functions. For this, the argument in Meijer G function is first inverted using Eq. (6.2.2) in [62]. Then the Meijer G function at very high values of its argument can be written as described in Eq. (41) in [63]. Some key facts can be observed from the closed form ASEP expressions. Meijer G function decreases with increasing value of SNR. Hence both the Meijer G components decreases leading to lesser error values with an increment in SNR values. A bivariate Meijer G term is also present in the expression which is a function of two variables basically.

The benefit of these closed form expressions of outage probability and ASEP using MG distribution is that the expressions are tractable in nature. Asymptotic expressions are also tractable and diversity and coding gain could be easily obtained. The expressions could be used in understanding the system performane with parameter variations. It will be easier for wireless engineers to optimize the system performance with these closed form expressions, rather than going for the cumbersome numerical methods.

5.3.4 Results for AF Based UOWC Systems

We have considered the average SNRs and the fading coefficients of both the SN-RN and RN-DN links to be equal. For outage probability calculation, the threshold data rate (R_d) is assumed as 3 bps. Link range (L) is the distance between SN and RN, and RN and DN. The RN has been assumed to be equidistant from SN and DN. Transmit optical power is 1 W. 7.5 cm is the transmitter aperture diameter, 6 mm denotes the transmitter aperture separation, receiver aperture diameter is 25 cm and photodetector responsivity is 0.85. $A_T = 1.863 \times 10^{-2}$, $A_s = 1.9 \times 10^{-4}$, $A_{Ts} = 9.41 \times 10^{-3}$, $\eta_{km} = 10^{-3}$ m, $\epsilon = 10^{-5} m^2/s^3$, $\chi_T = 10^{-6} K^2/s$, $\omega_{wat} = -2.5$ are the parameters considered [197]. These parameters are considered throughout the chapter unless mentioned explicitly.

It is observed from Fig. 5.4 that outage probability performance of the system improves with a

decrease in σ^2 value for which the link distance and turbulence is less. Note that the outage probability lower bounds of OWR and TWR based UOWC are calculated using Eq. (5.15) and (5.21) respectively. It has been reported in [198] that the σ^2 and σ_I^2 increases with the link distance. Thus smaller value of σ^2 may be interpreted for shorter link distance. σ^2 has been varied as 0.04, 0.09 and 0.16 for both one-way and two-way relay. TWR based UOWC suffers from self-interference effect as the nodes are transmitting and receiving simultaneously. Therefore it shows more outage than its counterpart. TWR can give more data rate as it is transmitting and receiving simultaneously, but it can suffer from more outage due to interference. Thus a compromise is required between spectral efficiency and outage probability performance. In future, interference cancellation schemes can be worked out to improve the outage probability performance of TWR system. The analytical results are validated by means of Monte Carlo simulations too. For example, to achieve an outage probability value of 0.1, OWR based UOWC system requires 25 dB of SNR while TWR based UOWC requires 27 dB of SNR. Thus there is a SNR gain of 2 dB for one-way relaying method. This is clearly illustrated by means of Table 5.1 for $\sigma^2 = 0.09$ where the SNR required to achieve different outage probability values are depicted.

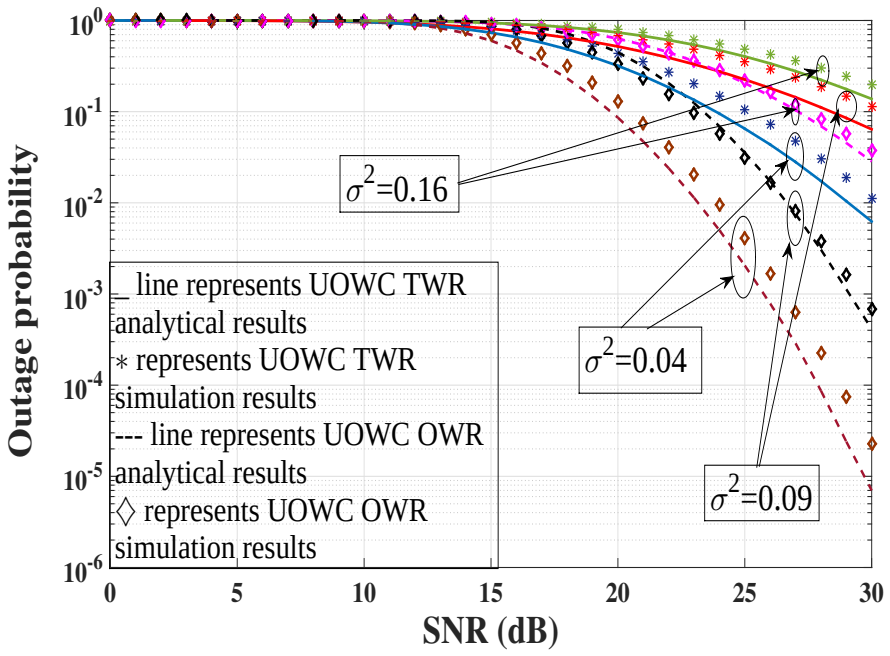

Figure 5.4: Outage probability for amplify and forward relay based UOWC.

Table 5.1: Comparison of lower bounds on outage probability for $\sigma^2 = 0.09$

P_{out}	SNR for various techniques (in dB)	
	UOWC_OWR	UOWC_TWR
0.5	19	21
0.1	25	27
0.05	27	29

MG distribution is the best fit for lognormal distribution as shown by simulation results in Fig. 5.5. It is observed from the PDF curves, that higher components of MG distributions closely matches with that of lognormal curve but as components goes on increasing, computational complexity also grows. Therefore there is a trade-off between complexity and error. 5-MG distribution shows almost perfect match with lognormal distribution and hence is considered for further system analysis. The parameters chosen obtained using Expectation maximization algorithm [82] are $\alpha_i^{MG} = 4.9987, 6.99, 8.996, 0.9938, 6.9977$, $\beta_i^{MG} = 3.884, 7.351, 9.716, 1.166, 13.075$, $P_i = 0.3021, 0.107, 0.1720, 0.1061, 0.3119$.

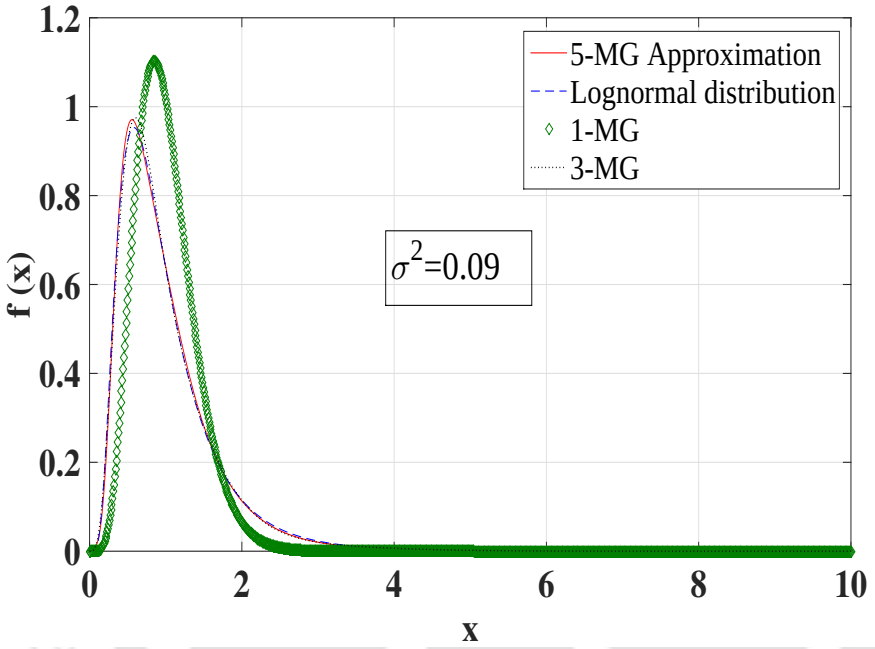

Figure 5.5: The comparison between lognormal and different MG distributions.

In Fig. 5.6, the outage probability for OWR based UOWC system is verified using 5-MG distributions. The analytical results of outage probability for OWR based UWOC are calculated using Eq. (5.21). σ^2=0.09 and σ^2=0.16 are considered for this case. The 5-MG analytical results are verified by means of Monte Carlo simulations also. The results obtained are in close agreements. The results are justified using asymptotic analysis also. In case of higher SNR values, the aysmptotic results gradually merge with the analytical results, thereby justifying our analysis. Let us calculate diversity gain from the graph. Considering the SNR range of 25-30 dB for $\sigma^2 = 0.09$, the diversity gain is $10\log_{10}(0.008/0.0023)/5 = 1.15$. The theoretical value of diversity gain is $\min(\alpha_i^{MG}) = 0.9938$. Thus the theoretical and practical values are almost close to each other. Similarly for $\sigma^2 = 0.16$ and considering SNR range of 25-30 dB, diversity gain is $10\log_{10}(0.14/0.048)/5 = 0.93$ which is again close to the theoretical value of 0.9938. For coding gain, let us calculate the horizontal shift of curves between $\sigma^2 = 0.09$ and $\sigma^2 = 0.16$ for an outage probability value of 0.1. The coding gain is $26 - 18.5 = 7.5$ dB. Hence it can be inferred that lower

turbidity gives better coding gain and better performance. As sea water turbidity increases, the light propagation in water is hampered. The refractive index of water changes more rapidly due to varying temperature, pressure and humidity of ocean currents. This results in the failure of light rays to reach the receiver properly resulting in more error.

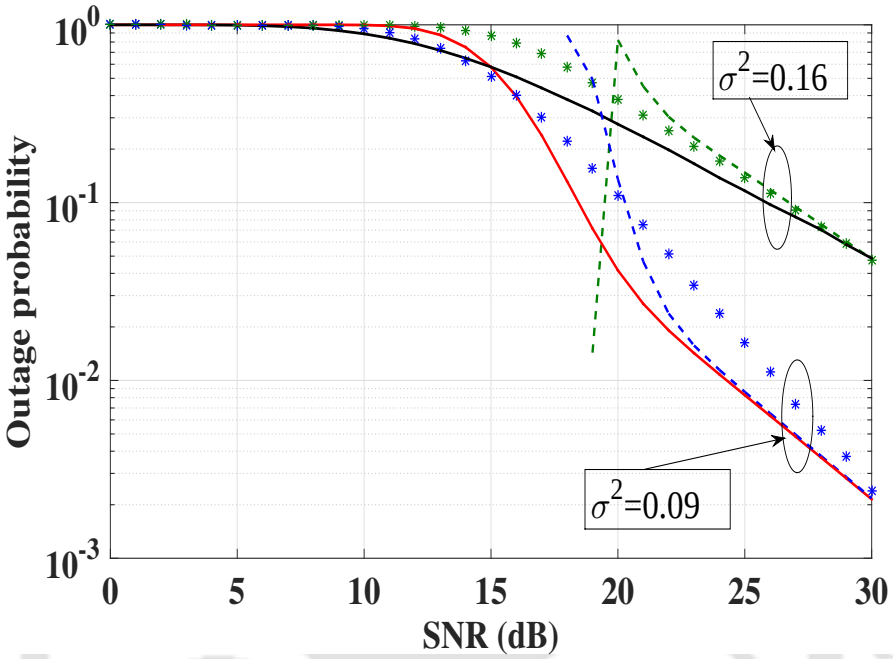

Figure 5.6: Outage probability for OWR based UOWC using 5-MG distributions for different values of σ^2 (Solid line represents analytical results, dashed line represents asymptotic results, and * represents simulation results).

The error performance of the system for BPSK modulation scheme is observed from Fig. 5.7. The analytical results for lognormal distribution are obtained using Eq. (5.24). As mentioned before, no closed form expression is available, hence integral is numerically evaluated using Mathematica. The closed form expression is obtained for ASEP by approximating lognormal distribution by MG distributions using Eq. (5.35). It is evident that lesser values of σ^2 gives better performance. In this case, σ^2 is varied as 0.09 and 0.16. ASEP results obtained from 5-MG distributions closely matches with the results obtained from lognormal distribution. It can be observed that lesser values of sea water turbidity give better results. As the turbid nature of sea water decreases, light propagation is better and proper reception of the signals by photodetector can occur. Another interpretation of the results can be that sea water turbidity and hence variance values of lognormal distribution increase with an increase in link distance. Thus as the distance of propagation increases, it becomes increasingly difficult for the light rays to reach the receiver, thereby giving poor performance for such high σ^2 values.

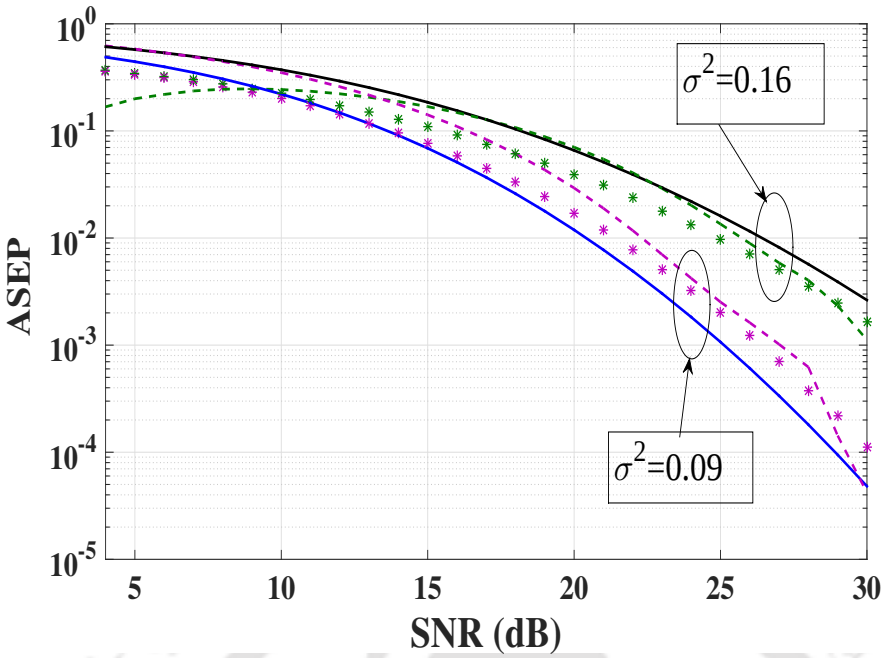

Figure 5.7: ASEP of OWR based UOWC (Solid line represents analytical results using lognormal distribution, dashed line represents analytical results using 5-MG distribution, and * represents simulation results using lognormal distribution).

5.4 Optical Improved Quadrature Spatial Modulation for UOWC

In the earlier section, we have studied how cooperative AF based UOWC system behaves for SISO scenario. However, SISO systems have the drawback that in any case if the particular link between laser and photodetector is down, then the communication cannot take place due to lack of diversity. This leads to the necessity of MIMO UOWC systems. To reduce the optical interference in MIMO UOWC systems, OSM technology can be used. In the earlier chapter, the basic concepts of OSM have been described already. In the forthcoming sections, advanced OSM scheme like optical improved quadrature spatial modulation (OIQSM) will be studied for BER performance improvement over SISO AF based UOWC systems. The channel model and other concepts of UOWC remain the same as defined earlier. Literature survey regarding basic UOWC cooperative systems [175, 185, 186, 187] have been presented in earlier sections already. UOWC employing spatial diversity and multi-pulse position modulation techniques has been analyzed in [199] by deriving approximate analytical BER expressions using lognormal channels. Spatial diversity has been exploited to calculate the BER of SIMO and MIMO based UOWC links in [200]. Space division multiplexing for underwater transmission has been proposed in [201]. MIMO UOWC systems employing spatial modulation has been proposed in [202], where upper bound expressions of BER have been evaluated under weak turbulence conditions using lognormal channels. UOWC systems with optical spatial modulation has been proposed in [178]. SM and other advanced versions of SM for RF

domain have been analyzed in [203]. Improved quadrature spatial modulation (IQSM) in RF domain has been investigated in [160], where transmission of double modulated symbols takes place over double layer of antennas in a single symbol time interval. To enhance the spectral efficiency of OSM, quadrature spatial modulation [204] can be implemented in optical domain also known as optical quadrature spatial modulation (OQSM), where different lasers are used to transmit the real and imaginary parts of a modulated symbol. OQSM has a spectral efficiency of $\log_2(M) + \log_2(N_L)^2$ bpcu (bits per channel use), since the total combination of active lasers is N_L^2. N_L denotes the number of lasers and M is the M-ary modulation scheme. In order to achieve higher spectral efficiencies, without increasing the number of laser sources or constellation size, new schemes have to be proposed for UOWC systems. A few of the advanced SM schemes have been studied for optical indoor channels [164, 165, 166], but not for underwater channels. Certain works are available for OSM in FSO communication, as shown in the earlier chapter. However, the application of OSM and other advanced versions of OSM have not yet been explored for UOWC links.

Based on the above literature survey, following research gaps have been observed. No work exists regarding advanced OSM schemes to increase the spectral efficiency of UOWC based systems over lognormal channels. UOWC cooperative systems exploiting the use of OSM techniques are also not available in the literature. In UOWC systems, the distance of propagation of the signals is very limited. Hence to increase the effective link range of communication, relays are needed. Therefore, advanced OSM methods need to be studied for cooperative UOWC systems. Cost and power consumption analysis of such advanced schemes in UOWC is also not reported. Closed form expressions for such advanced OSM schemes in UOWC cooperative systems over lognormal channels need to be investigated for tractable analysis. Motivated by the existing research gaps, we have proposed an advanced OSM scheme called OIQSM for UOWC cooperative systems.

The novelty of our work is explained by the fact that OIQSM analysis for underwater cooperative systems for weak oceanic turbulence conditions is done in terms of BER along with cost and power consumption analysis for the first time. The BER expressions are achieved in closed form which makes it tractable for gaining valuable insights about the system performance. Solving intractable integrals in lognormal distributions are a challenge in obtaining such closed form expressions, but the issue is resolved by using frustration function. The cost and power consumption of OIQSM is compared with that of OSM and optical MIMO. Sea water turbidity in UOWC is a big challenge. Hence we have also analyzed the effect of sea water turbidity on the system performance. The performance of OIQSM is also studied for various positions of the relay. The effect on diversity gain after applying multiple lasers in OIQSM is also highlighted. All these studies will be illustrated in detail in the forthcoming sections

of this chapter.

5.4.1 Optical Improved Quadrature Spatial Modulation

In OIQSM, real and imaginary portions of the two symbols are transmitted through two layers of optical sources at a time. Thus 4 optical chains are required as compared to the single optical chain requirement in OSM, but the reduction of overall cost and power minimization in OIQSM overshadows the use of extra optical chains in comparison to OSM. Keeping in mind that we are sending two modulated symbols in OIQSM at a time, the requirement of 4 optical chains is constant. To increase the spectral efficiency, multiple modulated symbols can be transmitted by a precoding based scheme, as proposed for RF domain [205], but the downfall for oceanic channels is that more lasers will be activated and more optical chains will be required. More optical chains and lasers will consume more power and generating more power is a matter of concern in the aquatic environment. Therefore there should be a trade-off between spectral efficiency and energy efficiency. Hence we are restricting it to transmission of two modulated symbols at a time only in OIQSM, but it can be extended for any number of modulated symbols easily.

The OIQSM process is the same as explained for FSO communication in Section 4.5.3. The table of laser activation is also provided in Table 4.9. For our proposed UOWC cooperative system, let us consider an example where input data stream is [11010110]. The part of the data stream which will be used for activating the corresponding laser source, is [1101] while the remaining part [0110] will be used for constellation mapping. Thus according to Table 4.9, the lasers at source and relay node are activated correspondingly for bits 11 and 01. Hence the index of lasers transmitting real and imaginary parts of the two symbols are $\{2, 3\}$ and $\{1, 3\}$ respectively. 4-QAM modulation scheme is used in this case and accordingly the symbols for bits 01 and 10 will be $[-1 + j, 1 - j]$. The real parts of the above two symbols are +1 and -1. They will be sent from laser 2 and laser 3 respectively. Similarly, imaginary parts of the above two symbols (-1 and +1) will be sent from laser 1 and laser 3 respectively. The same lasers are activated in both the nodes because the same message bits are transmitted and lasers are activated according to the bits. For different bit patterns, different set of lasers are activated at the nodes. Hence we can write $\mathbf{x_r} = [0, 1, -1, 0]^T$ and $\mathbf{x_i} = [-1, 0, 1, 0]^T$. The overall signal which is transmitted is $\mathbf{x} = \mathbf{x_r} + j\mathbf{x_i} = [-j, 1, -1 + j, 0]^T$.

Fig. 5.8 and Fig. 5.9 shows the system model for OIQSM for the above example. The spectral efficiency of OIQSM has been explained earlier in the previous chapter. For OIQSM performance analysis, a 3 node cooperative system model is considered, as shown in Fig. 5.8 and 5.9 where source node (SN) and destination node (DN) are directly and indirectly connected. The real parts of the modulated symbol are transmitted during in-phase laser activation as shown in Fig. 5.8 for the above example. Fig. 5.9

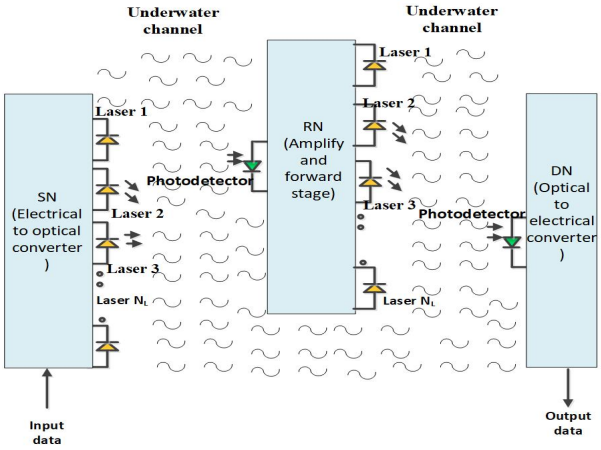

Figure 5.8: Proposed system model for OIQSM in-phase activation for input bit stream [1100 0110].

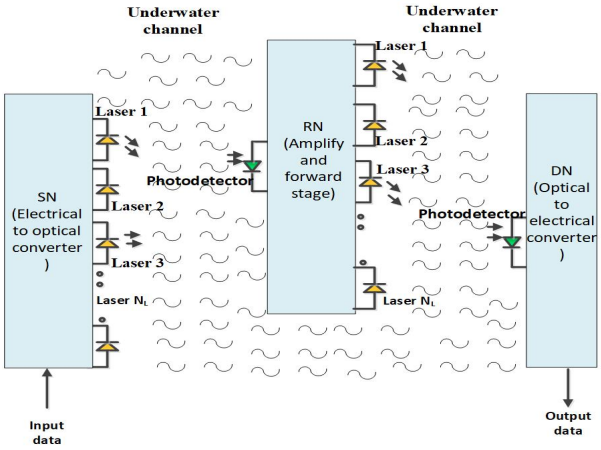

Figure 5.9: Proposed system model for OIQSM quadrature phase activation for input bit stream [1100 0110].

shows the quadrature phase laser activation where the imaginary parts of the modulated symbol are transmitted for the same example. Lasers are used as transmitter and a photodetector of responsivity R_e is used as receiver. Thus in SN and relay node (RN), N_L lasers are used while a photodetector is present in RN and DN.

5.4.2 Performance Analysis of OIQSM UOWC Systems

The performance analysis of AF based OIQSM system is done in terms of BER. To compute BER, pairwise error probability (PEP) expressions are derived as explained below. Lognormal channel model is used for performance analysis. Let κ_{rg} denote the relative geometrical gain given by $\kappa_{rg} = \frac{G_{S,R}}{G_{R,D}} = \left(\frac{d_{RD}}{d_{SR}}\right)^{\tau}$. τ is the path loss coefficient [51]. $G_{S,R} = (\frac{d_{SD}}{d_{SR}})^{\tau}$, $G_{R,D} = (\frac{d_{SD}}{d_{RD}})^{\tau}$ where d_{SR}, d_{RD} and d_{SD} denote the distances between SN and RN, RN and DN, and SN and DN respectively. In this AF based OIQSM model, the source node transmits message to the relay and destination in the first time slot, while the relay retransmits the message received from source to the destination in second time slot. The source terminal transmits message $\mathbf{x}$ in the first phase with fraction KE power. The received signal at relay in the first time slot is denoted by r_R, while the signal received by destination in the first time slot is denoted by r_{D1}. The relay normalizes the signal r_R and retransmits it to destination in the second time slot with fraction $(1-K)E$ power. The destination node receives this signal in second time slot and is denoted by r_{D2}. Thus the total energy used by OIQSM is $KE + (1-K)E = E$. The expressions for r_R, r_{D1} and r_{D2} can be written as [206]:

$$r_R = \sqrt{G_{S,R}KE}\mathbf{h_{SR}x} + n_R,\ r_{D1} = \sqrt{KE}\mathbf{h_{SD}x} + n_{D1}\ , \tag{5.38}$$

$$r_{D2} = \sqrt{cE}\mathbf{h_{RD}}.*\mathbf{h_{SR}x} + n_{D2}\ . \tag{5.39}$$

where .∗ denotes element wise multiplication between two vectors, $\mathbf{x}$ has a size of $N_L \times 1$, channel coefficients $\mathbf{h_{SR}}$, $\mathbf{h_{SD}}$ and $\mathbf{h_{RD}}$ have a size of $1 \times N_L$. $\mathbf{h_{SR}}$ and $\mathbf{h_{RD}}$ have elements of the form $[h_{SR,1}, ..., h_{SR,N_L}]$ and $[h_{RD,1}, ..., h_{RD,N_L}]$ respectively. Element wise multiplication is done between the vectors i.e. $h_{SR,1} \times h_{RD,1}$, $h_{SR,2} \times h_{RD,2}$ and so on. The variable-gain c for proposed system is defined as:

$$c = \frac{K(1-K)G_{S,R}G_{R,D}E/N_0}{1 + KG_{S,R}|h_{SR}|^2E/N_0 + (1-K)G_{R,D}|h_{RD}|^2E/N_0} \ . \tag{5.40}$$

n_R, n_{D1} and n_{D2} are noise parameters which are independent complex Gaussian random variables with zero mean and variance N_0. The noise variance is computed by considering the variances of thermal noise, shot noise and dark current noise. $\mathbf{h_{SR}}$ is the channel between transmitting laser of SN and receiving photodetector of RN, $\mathbf{h_{SD}}$ is the channel between transmitting laser of SN and receiving photodetector of DN, $\mathbf{h_{RD}}$ is the channel between transmitting laser of RN and receiving photodetector of DN. All the channel coefficients follow lognormal distribution as discussed earlier. PEP is defined as the probability that the maximum likelihood (ML) decoder decodes a symbol vector $\mathbf{s}'$ instead of transmitted symbol vector $\mathbf{s}$. PEP of lognormal cooperative communication can be expressed as [206]:

$$PEP(\mathbf{s} \to \mathbf{s}') = Q\left(\sqrt{\frac{\|\mathbf{Hs} - \mathbf{Hs}'\|^2}{2N_0}}\right) \leq \frac{1}{2}\exp\left(-\frac{\|\mathbf{Hs} - \mathbf{Hs}'\|^2}{4N_0}\right) \ , \tag{5.41}$$

where $\mathbf{H}$ is the channel matrix whose elements follow lognormal distribution. Let us denote X as the Euclidean distance between two symbol vectors given by $X = \|\mathbf{s} - \mathbf{s}'\|^2$. Q denotes the Q function. After calculating the Euclidean distance in terms of variance and signal power and doing some algebraic manipulations, the final PEP expression for our proposed system is written as:

$$PEP(\mathbf{s} \to \mathbf{s}') \leq \frac{1}{2\sqrt{\pi}} \int_{-\infty}^{\infty} \exp(-v^2) Fr(TD_1; 0; \sigma_{SR}) \ Fr(2TK; 0; \sigma_{SD}) dv \ , \tag{5.42}$$

where $v = (a_{RD} + \sigma_{RD}^2)/\sqrt{2\sigma_{RD}^2}$, $a_{RD} = 20\log_{10} h_{RD}$, $D_1 = \frac{2G_{S,R}K}{1+\frac{C_1}{\exp[v\sqrt{8\sigma_{RD}^2} - 2\sigma_{RD}^2]}}$, $C_1 = \frac{2G_{S,R}KE/N_0+1}{2G_{R,D}(1-K)E/N_0}$, E/N_0 is the SNR, $T = \frac{EX}{4N_0}$, $Fr(A; B; \sigma)$ is the frustration function defined as [207]:

$$Fr(A; B; \sigma) = \int_{-\infty}^{\infty} \frac{1}{\sqrt{2\pi\sigma^2}} I_0(2Bu\sqrt{A}) \exp(-Au^2) \times \exp(-(\ln u + \sigma^2)^2/2\sigma^2) du, \tag{5.43}$$

where $I_0(\cdot)$ is the modified Bessel function of order zero. The worst case PEP occurs when squared Euclidean distance between the symbol vectors is minimum and is given by $L_{min}^2 = \underset{s \neq s'}{min} \|\mathbf{s} - \mathbf{s}'\|^2$. For $\kappa_{rg} << 1$, (i.e. $d_{SR} >> d_{RD}$) PEP can be evaluated as [206]:

$$PEP(\mathbf{s} \rightarrow \mathbf{s}') \leq \frac{1}{2} Fr\left(\frac{KEX}{2N_0}; 0; \sigma_{SD}\right) \times Fr\left(\frac{KEX}{2N_0}; 0; \sigma_{SR}\right) . \tag{5.44}$$

Similarly for $\kappa_{rg} >> 1$, (i.e. $\mathrm{d}_{SR} << d_{RD}$) PEP can be evaluated as [206]:

$$PEP(\mathbf{s} \rightarrow \mathbf{s}') \leq \frac{1}{2} Fr\left(\frac{KEX}{2N_0}; 0; \sigma_{SD}\right) \times F_r\left(\frac{(1-K)EX}{2N_0}; 0; \sqrt{\sigma_{SR}^2 + \sigma_{RD}^2}\right) . \tag{5.45}$$

We have considered the scenarios $\kappa_{rg} << 1$ and $\kappa_{rg} >> 1$ for simpler tractable expressions. For other scenarios, Eq. (5.42) holds valid, but closed form expression cannot be achieved. $\kappa_{rg} << 1$ means that the relay is located closed to the destination node and $\kappa_{rg} >> 1$ means that the relay is located closer to the source node. Our goal is to achieve closed form expressions of BER for easier tractable analysis. That is the reason for this assumption of relative location of relay node. For other positions, numerical methods can be applied to calculate the exact value. For analyzing system performance, BER of all the systems are compared. The BER performance is union bounded by [206]:

$$P_b \leq \frac{1}{|\mathbb{S}| log_2(|\mathbb{S}|)} \sum_{\mathbf{s}} \sum_{\mathbf{s} \neq \mathbf{s}'} n(\mathbf{s} \rightarrow \mathbf{s}') PEP(\mathbf{s} \rightarrow \mathbf{s}') . \tag{5.46}$$

$PEP(\mathbf{s} \rightarrow \mathbf{s}')$ is the PEP, $n(\mathbf{s} \rightarrow \mathbf{s}')$ is the count of information bit errors occurred in selecting wrong codeword $\mathbf{s}'$ at the receiver instead of the original codeword $\mathbf{s}$ transmitted and $\mathbb{S}$ is the predefined set containing all the symbol vectors for a particular scheme. For our proposed system, the (L_{min}^2) value varies, thereby changing the PEP and union bound. From this expression, some key facts can be noted. According to the particular spectral efficiency and number of laser sources in OIQSM, the modulation scheme is applied. This determines the distance between symbol vectors which affects the PEP and consequently the BER value. The BER is predominantly dependent on the variance values of the UOWC links.

5.4.3 Complexity Analysis of OIQSM

The complexity comparison of OIQSM with other methods like optical multiple-input-multiple-output (MIMO) based spatial multiplexing schemes are tabulated in Table 5.3. For power consumption analysis [151], P_o is assumed as the power consumption of each optical chain, α_{tr} is the slope of the load dependent power consumption, while P_{tr} is the total optical transmit power. P_{sw} is the power consumption of each optical switch and N_{sw} is the number of optical switches required for a particular scheme. In OSM, a single optical chain is used, while 4 optical chains are used in OIQSM. Spatial multiplexing techniques of optical MIMO require N_L optical chains (same as the number of lasers). An optical switch can connect two lasers. Considering a target spectral efficiency of η_{SE}, the number of switches required for OIQSM

can be computed as in Eq. (4.80). Number of switches for OSM will be same as in SM [151] and is given by Eq. (4.77). Total power consumption of OSM is given in Eq. (4.73). Similarly, power consumption of OIQSM is given by Eq. (4.76). Power consumption of spatial multiplexing (SMX) techniques in optical MIMO is given by $P_t^{SMX} = P_o N_L + \alpha_{tr} P_{tr}$. Thus it can be observed that power consumption of optical SMX is greater than that of OSM and OIQSM because N_L optical chains are used in optical SMX. Though optical switches are used in OSM and OIQSM, but the power consumption in OSM and OIQSM is greatly reduced because of lower optical chain requirement. The number of switches required for OIQSM is much lesser than the requirement in OSM. An example has been considered where $\eta_{SE} = 8$ bpcu, $N_L = 64$ and $M = 4$. For OIQSM, number of switches required is 2 while the switch requirement is 32 for OSM. For more higher spectral efficiency values like $\eta_{SE} = 20$ bpcu, the switch requirement in OSM is excessive in comparison to OIQSM. Thus for a larger value of N_L, which is required to obtain a greater η_{SE} value, the total power consumption of OSM exceeds that of OIQSM due to excessive requirement of switches.

Table 5.2: Complexity comparison of the proposed methods.

Schemes	Power consumption	Cost	Decoding complexity
Optical SMX	$P_o N_L + \alpha_{tr} P_{tr}$	$C_o N_L$	M^{N_L}
OSM	$P_o + \alpha_{tr} P_{tr} + P_{sw} \times N_{sw}^{OSM}$	$C_o + C_{S/P} + C_{sw} N_{sw}^{OSM}$	M
OIQSM	$4P_o + \alpha_{tr} P_{tr} + P_{sw} \times N_{sw}^{OIQSM}$	$4C_o + C_{S/P} + C_{sw} N_{sw}^{OIQSM}$	M^4

For cost analysis, C_o is considered as the cost of a single optical chain, $C_{S/P}$ is the cost of a serial/parallel converter while C_{sw} is the cost of an optical switch. Total cost of spatial multiplexing techniques in optical MIMO is given by $C_{SMX} = C_o N_L$, whereas total cost in OSM is computed in Eq. (4.81). The total cost for our proposed method OIQSM is calculated as $C_{OIQSM} = 4C_o + C_{S/P} + C_{sw} N_{sw}^{OIQSM}$. The number of switches required for OIQSM is much lesser than the requirement in OSM. Hence the switch cost is much lesser for higher spectral efficiencies in OIQSM. This compensates the extra cost incurred in optical chain. In optical SMX, total cost is greater than that of OSM and OIQSM because N_L optical chains are used in optical SMX and optical chain cost is much greater than the cost of an optical switch or S/P converter. Decoding complexity is given by M^{N_L} for optical MIMO, whereas it is given by M^4 for OIQSM. Therefore, OIQSM is beneficial from cost and power consumption perspective to achieve very high spectral efficiencies. A graphical analysis of the power consumption and cost of OIQSM has been provided already in the previous chapter for FSO communication. The same power consumption and cost analysis holds true for UOWC systems.

5.4.4 Results of OIQSM Based UOWC Systems

The minimum distance between symbol vectors depend on the constellation scheme. OIQSM uses a smaller constellation size than OSM to achieve a particular spectral efficiency, thus minimum distance between symbol vectors (L^2_{min}) is always greater in OIQSM. The L^2_{min} values for OIQSM can be obtained similar to what has been given in Table IV of [85]. Power allocation factor $K = 0.5$ is considered. For $\kappa_{rg} << 1$, $d_{SR} = 60\ m$ and $d_{RD} = 10\ m$, while for $\kappa_{rg} >> 1$, $d_{SR} = 10\ m$ and $d_{RD} = 60\ m$ are chosen. Clear ocean water is considered for which the absorption and scattering coefficient values are given in [177]. These parameters are used to calculate the turbulence value. For $\kappa_{rg} << 1$, $\sigma_{SR} = 0.3$ and $\sigma_{RD} = 0.01$ with $\sigma^2 \cong \sigma^2_{SR}$ are taken, while for $\kappa_{rg} >> 1$, $\sigma_{SR} = 0.01$ and $\sigma_{RD} = 0.3$ with $\sigma^2 \cong \sigma^2_{RD}$ are considered for oceanic channel generation unless mentioned explicitly. Eq. (5.42) is used for calculating PEP values for $\kappa_{rg} = 1$, while Eq. (5.44) is used for calculating PEP values for $\kappa_{rg} << 1$ in Fig. 5.10.

The results of OIQSM are compared with 4-quadrature amplitude modulation (QAM) orbital angular momentum shift keying modulation based UOWC systems (OAMSK) using Laguerre-Gauss beam based channel [208], AF one-way relaying method (AFOWR) [79]. The corresponding bit error rate (BER) of the AFOWR system (which has been illustrated in the initial part of this chapter) have been plotted using Fig. 8 of [79]. To achieve the spectral efficiency of 8 bpcu, OIQSM requires 4-QAM while OSM requires 64-QAM for $N_L = 4$. For performance analysis in Fig. 5.10, OIQSM and OSM results are obtained for σ^2=0.09 (for $\kappa_{rg} << 1$ and $\kappa_{rg} = 1$) and spectral efficiency of 8 bpcu. For AFOWR same value of σ^2=0.09 with BPSK scheme is considered. For BPSK, average symbol error probability (ASEP) and BER are the same. The results for $\kappa_{rg} << 1$ and $\kappa_{rg} >> 1$ are almost similar, hence only $\kappa_{rg} << 1$ and $\kappa_{rg} = 1$ cases are shown in the figure. $\kappa_{rg} = 1$ signifies relay is equidistant from the two nodes. Since a direct source-to-destination path exists in our system model, hence the relay being closer to the source or destination node does not have much impact on the system performance, hence giving similar results for $\kappa_{rg} << 1$ and $\kappa_{rg} >> 1$. Thus under the same turbulence conditions and system model, performance of our proposed method OIQSM outperforms the existing AFOWR system. For instance, at SNR of 10 dB the BER for our proposed scheme (for $\kappa_{rg} << 1$) is 0.009, whereas BER for AFOWR and OSM (for $\kappa_{rg} << 1$) are 0.22 and 0.11 respectively. This huge improvement in the BER for our proposed scheme is possible for any κ_{rg} value, due to deployment of a lower modulation scheme in OIQSM for the same spectral efficiency. We can interpret from the results that OSM and OIQSM (using multiple laser sources) are better than the SISO based AFOWR model. This is due to the fact that more laser-to-photodetector links are available for selection in OSM and OIQSM, which nullifies the poor channel condition.

Let us compare the diversity gain of the methods from the graph of Fig. 5.10 by calculating the slope of BER curve for SNR range of 10-20 dB. For AFOWR, diversity gain is $\log_{10}(0.12/0.011) = 1.04$.

The diversity gain of our proposed OIQSM method for $\kappa_{rg} << 1$ is $\log_{10}(0.0094/0.0000016) = 3.77$. The diversity gain of OIQSM for $\kappa_{rg} = 1$ is $\log_{10}(0.004/(1.2 \times 10^{-7})) = 4.52$. The diversity gain of OSM for $\kappa_{rg} << 1$ is $\log_{10}(0.12/0.0008) = 2.17$ while for $\kappa_{rg} = 1$, the diversity gain is $\log_{10}(0.078/0.00013) = 2.78$. Hence we can infer that by applying multiple laser sources, diversity gains of OSM and OIQSM have increased in comparison to the earlier SISO case. OIQSM yields much more diversity gain than OSM signifying that by using more optical chains and activating more lasers than OSM, performance improvement can be obtained for any position of the relay node. Also if the relay is exactly midway between the two nodes for either OSM or OIQSM, then performance is optimum and more diversity gain can be obtained. This is because both the links on either side of the relay node can perform optimally in this case, whereas if the relay is located closer to a particular node, then the other link performance suffers due to larger propagation distance of light.

The performance improvement of OIQSM is elaborated by means of Table 5.3. The SNR values required to achieve the target BER values for different methods are tabulated. It is clearly evident that OIQSM outperforms OSM by a minimum SNR gain of about 5.5 dB for any BER value. It also outperforms AFOWR and 4-OAMSK by more than 10 dB and 12 dB respectively for any BER value, thereby justifying our claim that OIQSM is the superior method. All the obtained results could not be plotted for higher SNR values in the graph due to lack of space, but are included in the table for comparison.

Table 5.3: Comparison of BER values

BER	SNR for various techniques (in dB)			
	4-OAMSK	AFOWR	OSM $\kappa_{rg} << 1$	OIQSM $\kappa_{rg} << 1$
0.1	13	13	10	0
0.01	22	20	16.5	9.8
0.001	27	25	19.5	14
0.0001	31	29	22	16.5

The effects of sea water turbulence on OIQSM performance is investigated in Fig. 5.11. σ^2 value depends on scintillation index σ_I^2 which describes the turbidity of sea water. $\kappa_{rg} << 1$ case is considered with σ^2 varying as 0.09, 0.16 and 0.25. As value of σ^2 increases, sea water turbidity increases and system performance decreases. For this analysis, OIQSM with 4-QAM modulation is employed to achieve spectral efficiency of 8 bpcu. For this modulation scheme and symbol vector arrangement, L_{min}^2 is calculated by computing the minimum of the distances between the symbol points in the constellation diagram, which is evaluated as 1. All analytical results obtained using Eq. (5.46) are validated by means of Monte Carlo simulations. Another physical interpretation of the result can be done. As sea water turbidity increases, it means light propagation is hampered due to the rapid changes in refractive index,

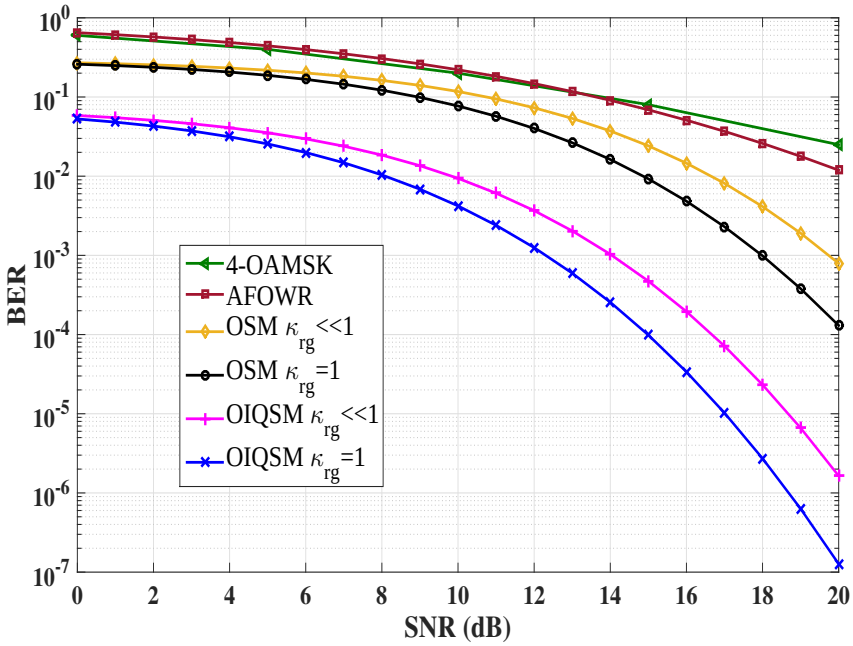

Figure 5.10: Performance comparison of proposed system.

pressure and temperature of oceanic currents. As light fails to propagate effectively, poor reception of signal occurs at the photodetector, thereby causing more error.

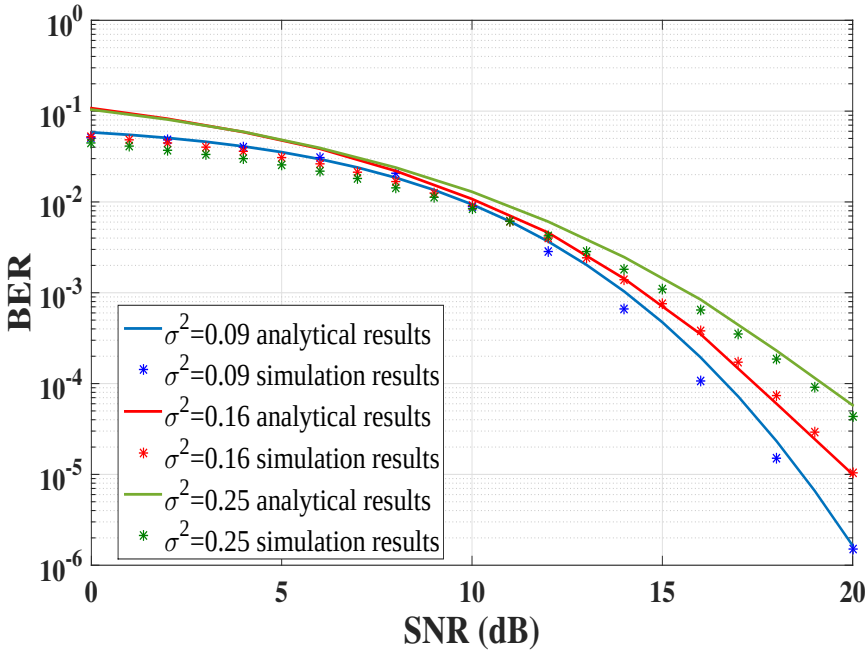

Figure 5.11: Analysis of OIQSM system with different σ^2 values.

5.5 Transmit Laser Selection Based UOWC Systems

OSM is used in UOWC systems to enhance the spectral efficiency and improve the error performance. However, the drawback of OSM is that the transmit laser is chosen according to the message bits, hence

irrespective of the condition of the channel path, the message is transmitted through the selected channel. Therefore in case of inferior channel conditions, system performance may suffer. In such scenarios, channel feedback should be considered while selecting the transmit laser. To resolve the drawbacks of OSM, we have proposed the scheme of TLS in UOWC systems, which selects a single transmit laser source for transmission based on the best channel path. TLS may be combined with OSM to further enhance the spectral efficiency of UOWC systems. In TLS-OSM scheme, a group of optical sources are selected from a larger set of optical sources and OSM is applied on the selected sources to combine the benefits of both TLS and OSM.

In the earlier sections of this chapter, we have done literature survey of various MIMO UOWC systems [199, 200, 202], cooperative UOWC systems [175, 185, 186, 187] and OSM based UOWC system [178]. Let us have a look at some of the works related to TLS schemes. There are quite a few works based on application of TLS in FSO systems. MISO FSO communication system with TLS has been explored over strong turbulence channel using K distribution in [141]. The transmit laser is chosen depending on the largest value of scintillation of a particular path. TLS scheme has also been studied for FSO communication using K distribution in [142]. For mobile FSO nodes with weak lognormal channels, TLS and receive diversity has also been implemented in [143]. TLS based FSO systems have been analyzed over G-G channels with pointing error, in terms of asymptotic error expressions in [145]. However, this work has not achieved any closed form expressions for error or outage probability. A transmit alternate laser selection scheme for FSO communication has been proposed in [209] where a time diversity order is selected for the available lasers depending on greater values of scintillation of the optical path. The analysis has been done over G-G channel with pointing errors. TLS combined with space-time trellis code has been reported in [147] for MISO FSO systems over G-G channel and asymptotic BER expressions have been derived. For underwater visible light communication, TLS has been proposed for diver-to-diver MISO system in [144], where only asymptotic BER analysis has been reported. The source with the highest received instantaneous SNR is chosen, but the system model is a point-to-point link and not a cooperative model.

After studying the literature, it is inferred that study of TLS schemes for UOWC systems in terms of closed form expressions of BER or outage probability are yet to be reported. A combined study of TLS and TLS-OSM for such UOWC systems are also not available. Most of the works have focussed on analyzing TLS schemes over G-G channel. The technique of TLS depending on received SNR and its analysis in UOWC cooperative systems over lognormal channel is not available in literature. All these research gaps motivate us to propose TLS and TLS-OSM schemes for UOWC cooperative communication. Such systems can be beneficial in extending the link range of spectral efficiency of short range UOWC

system communication.

The novelty of our work lies in the fact that TLS and TLS-OSM schemes are proposed for UOWC cooperative systems for the first time. TLS and TLS-OSM schemes are proposed to activate the transmit lasers depending on the maximum received SNRs. OSM scheme, when combined with TLS, can offer much better performance as illustrated by us in the forthcoming sections. The performance analysis of such systems is carried out in terms of outage probability and ASEP, and the corresponding expressions for UOWC system analysis are derived by us. The cost and power consumption analysis of TLS and TLS-OSM schemes are also proposed by us, adding to the contribution of our work. The challenge involved in this task is to implement the feedback path to send the transmit laser index and not the exact channel gains, thereby consuming less bits. The evaluation of PDF of received SNRs for the group of selected lasers in TLS-OSM is another intricate problem involved in this work. Thus the performance analysis of such schemes along with the system model will be illustrated in the next few subsections.

5.5.1 Proposed System Model for TLS-Based UOWC Systems

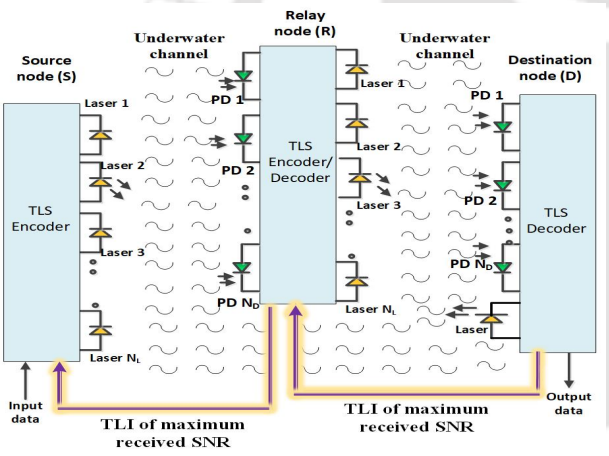

Figure 5.12: Proposed system model for TLS

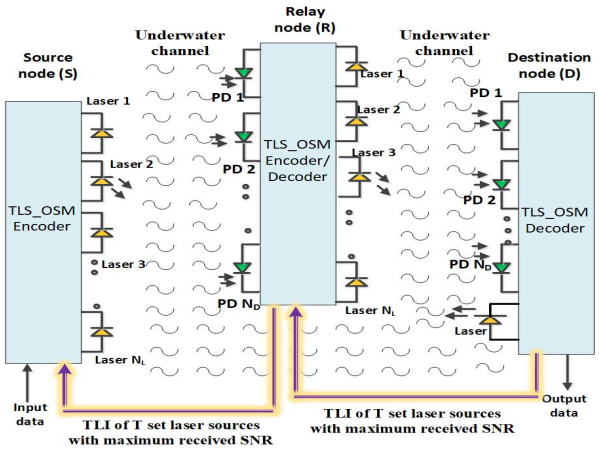

Figure 5.13: Proposed system model for TLS-OSM

For both TLS and TLS-OSM in UOWC systems, a 3 node cooperative model is used. Source node (S) can directly interact with relay node (R) and destination node (D). The relay node can decode and forward the message of the source node to the destination node. Thus source and relay nodes possess N_L lasers each, while relay and destination nodes possess N_D photodetectors each having responsivity of R_e. d_{SR}, d_{SD} and d_{RD} are assumed to be the distances between S and R, S and D, and R and D links respectively. $G_{S,R}$ and $G_{R,D}$ are the relative gains of S-R and R-D links respectively.

For TLS and TLS-OSM, a single transmit optical chain is used. The transmit laser index (TLI) needs to be estimated according to the maximum received SNR and this TLI data is provided as a feedback from the receiver to the transmitter before the actual data payload is sent from the transmitter. This

feedback is sent through a low rate partial feedback link [149, 150] using $\log_2(N_L)$ bits for TLS scheme. Relay node has lasers, hence any of these lasers can be utilized in conveying the TLI for TLS and TLS-OSM. However, for destination node, an extra laser has been incorporated for sending the TLI estimate to the relay. In TLS scheme as shown in Fig. 5.12, according to the TLI received, a single laser yielding the maximum received SNR, is activated. Similarly for TLS-OSM process as portrayed in Fig. 5.13, TLI estimate is sent as feedback by using $T\log_2(N_L)$ bits. In this process, a subset of T laser sources from the set of all the laser sources are chosen based on the maximum received SNR yielded at the receiver. OSM is applied on these T sources. Thus information regarding symbol detection is conveyed in TLS, whereas both symbol and TLI detection information are conveyed in TLS-OSM. In both Fig. 5.12 and 5.13, PD denotes photodetector and TLI denotes transmit laser index. The complexity analysis of TLS and TLS-OSM has already been provided earlier in Table 4.6. Thus it can be observed from the table that TLS and TLS-OSM are beneficial than optical MIMO techniques in terms of cost, power consumption, and decoding complexity.

5.5.2 Performance Analysis of TLS and TLS-OSM UOWC System

The source node SNR is given by $\eta_S = \frac{P_S}{N_0}$ and relay node SNR is given by $\eta_R = \frac{P_R}{N_0}$, where P_S and P_R are the transmit power of source and relay node respectively.

5.5.2.1 TLS System Analysis

In the first time slot, the j_R photodetector of relay node and j_D photodetector of destination node receive the message transmitted from the source node. The signals received at R and D in the first time slot are given by $y_{SR}^{j_R}$ and $y_{SD}^{j_D}$ respectively. Let $D_1 = \sqrt{R_e P_S G_{S,R}}$, $D_2 = \sqrt{R_e P_S}$. Thus the received signals are written as:

$$y_{SR}^{j_R}[n] = D_1\, h_{j,i}^{S,R} x[n] + w_{SR}[n]\ , \tag{5.47}$$

$$y_{SD}^{j_D}[n] = D_2\, h_{j,i}^{S,D} x[n] + w_{SD}[n]\ . \tag{5.48}$$

During the second time slot, the signal emitted from the relay after successful decoding, is received at the destination node by the j_D photodetector and is given by $y_{RD}^{j_D}$. The relay node deploys DF technique. Let $D_3 = \sqrt{R_e P_R G_{R,D}}$.

$$y_{RD}^{j_D}[n] = D_3\, h_{j,i}^{R,D} x_R[n] + w_{RD}[n]\ . \tag{5.49}$$

w_{SR} and w_{SD} denote the noise term received at the relay and destination node respectively in the first time slot, while w_{RD} denotes the noise term received at the destination node in the second time slot. $h_{j,i}^{S,R}$ represents the channel between i^{th} transmitting laser at source and j^{th} receiving photodetector of relay node. $h_{j,i}^{S,D}$ represents the channel between i^{th} transmitting laser at source and j^{th} receiving photodetector of destination node. $h_{j,i}^{R,D}$ represents the channel between i^{th} transmitting laser at relay and j^{th} receiving photodetector of destination node.

During both the time slots, thermal noise is generated at R and D nodes due to the presence of ambient light, which can be represented as zero mean white Gaussian random noise having variance N_0. The dominant noise sources in case of photodetectors are thermal noise, dark current noise and shot noise. Thermal noise ($\sigma_t = \frac{4k_B T_e B_w F_n}{R_L}$) is considered equivalent to the noise produced due to a load resistance (R_L) of 50 Ω at a temperature (T_e) of 300 K. F_n is the noise figure, k_B is the Boltzmann's constant and B_w is the bandwidth. The random arrival of photons creates shot noise and is given by $\sigma_s = 2q_e R_e P_S B_w$ where q_e is the electron charge. $\sigma_d = 2q_e I_{DC} B_w$ represents the dark current noise, where the dark current produced in absence of light at the photodetector is denoted by I_{DC} [157]. Therefore, total noise variance is computed by $\sigma_n^2 = \sigma_t^2 + \sigma_s^2 + \sigma_d^2$.

The SNR received at the destination node in both time slots is maximized by applying MRC. The selection of a single transmit optical source is done in accordance with the following condition:

$$O^t = \underset{1 \le i \le N_L^t}{arg\ max} \left\{ C_i = \sum_{j=1}^{N_D^D} |h_{j,i}^{t,D}\ ,|^2 \right\} \tag{5.50}$$

where $t \epsilon (S, R)$. Number of lasers at the particular node t is denoted by N_L^t, whereas number of photodetectors at destination node is given by N_D^D. The laser index at source or relay node ensuring maximum received SNR at the output is denoted by O^t. Each C_i for $i\ \epsilon\ (1, 2, ...N_L^t)$ for S and R nodes are arranged in ascending order such that $C_1 \le C_2 \le ... \le C_{N_L^t}$. At S and R, the transmit laser index is selected yielding the maximum value of $C_{N_L^t}$. The channel coefficients $h_{j,i}^{t,D}$ are assumed to be independent and identically distributed. Our next objective is to find the outage probability of the TLS system. The total transmission is a dual stage process. For the first step, outage probability occurs independently in both the source-to-relay link and source-to-destination link. Second stage outage probability is calculated considering there is no outage in the first stage. Hence the second stage outage probability can be computed as the product of outage probability of relay-to-destination transmission and the complement of outage probability of source-to-relay transmission. Outage occurs in TLS for a particular link, when there is not a single path available from any of the lasers to a photodetector. Hence outage probability is given by the condition that all links must fail for a particular node-to-node link. The TLS system has

an end-to-end (E2E) outage probability, calculated as Eq. (5) in [134]:

$$P_{out}^{E2E} = P_{out}(SR)\left[P_{out}(SD)\right]^{N_L^S} + (1 - P_{out}(SR))\left[P_{out}(SRD)\right]^{\frac{N_L^S + N_L^R}{2}} , \tag{5.51}$$

where $P_{out}(SR) = F_{\gamma_{SR}}(\frac{\gamma_{th}}{\bar{\gamma}_{SR}})$, $P_{out}(SD) = F_{\gamma_{SD}}(\frac{\gamma_{th}}{\bar{\gamma}_{SD}})$, $P_{out}(SRD) = \left(F_{\gamma_{SRD}}\left(\frac{\gamma_{th}}{\bar{\gamma}_{SD}+\bar{\gamma}_{RD}}\right)\right)$, $\gamma_{th} = 2^{R_d} - 1$ and the threshold data rate is given by R_d in bps. The system performing without TLS has an outage probability which is computed as Eq. (5) in [129] and has already been explained in the previous chapter. The respective CDFs follow lognormal distribution explained earlier, where $\bar{\gamma}_{SR} = \eta_S R_e G_{S,R}$, $\bar{\gamma}_{RD} = \eta_R R_e G_{R,D}$. From the closed form expression of outage probability, it is clear that we can analyze the system performance from the nature of each outage term. Each outage term is inversely proportional to SNR. Thus an increment in SNR value decreases each outage probability value. There will be a decrement in the product of two such outage probability values also. In the second stage, the complement of one outage probability value will get incremented, but its product with decreased outage probability value of second stage will result in an overall decrement of E2E outage probability value.

5.5.2.2 TLS-OSM System Analysis

The objective is to calculate error of TLS-OSM scheme. Hence, the PDF of received SNR needs to be evaluated. For the selection of a subset of T laser sources yielding the maximum received SNR, all the C_is calculated using Eq. (5.50) are arranged in ascending order. According to the maximum C_i values, the subset of T laser sources is selected. Obeying the order statistics, the PDF of C_i such that $C_1 \leq C_2 \leq ... \leq C_i \leq ...C_{N_L^t}$ is given by [32]:

$$f_{C_i}(\gamma) = \frac{1}{B_t(i,T)}\left\{F_\gamma(\gamma)\right\}^{N_L^t - T} \times \left(1 - F_\gamma(\gamma)\right)^{T-1} f_\gamma(\gamma) , \tag{5.52}$$

where $i = N_L^t - T + 1$, $B_t(.,.)$ symbolizes the beta function. The next objective is to calculate the PDF of received SNR when T sources are selected. The set of T largest SNRs have to be selected. For this purpose, the PDF of C_i needs to be calculated for the range $N_L^t - T + 1$ to N_L^t and divided by the range i.e. T. The PDF of the SNR received at R or D is evaluated as:

$$f_\gamma^i(\gamma) = \frac{1}{T}\sum_{j=i}^{N_L^t} A \times \left\{F_\gamma(\gamma)\right\}^{j-1}\left(1 - F_\gamma(\gamma)\right)^{N_L^t - j} f_\gamma(\gamma) , \tag{5.53}$$

where $A = \frac{1}{B_t(j, N_L^t - j + 1)}$, $f_\gamma(\gamma)$ and $F_\gamma(\gamma)$ are PDF and CDF of lognormal distribution given in Eq. (5.2) and Eq. (5.3) respectively. For all the three paths S-R, S-D and R-D, the received SNR has a PDF which is evaluated for performance analysis. For $T = 2$, (where T is the number of selected laser sources) the

activation of transmit laser source (j_t) is done by the criteria:

$$j_t = \begin{cases} 2, & \text{if } x_t^{LSB}[n] = 1 \\ 1, & \text{if } x_t^{LSB}[n] = 0 \ , \end{cases} \tag{5.54}$$

where the n^{th} time slot is represented by n and t denotes the node which may be S or R for this model. x represents the message bit to be transmitted. If $T > 2$, then $\log_2 T$ number of bits (from LSB side) is used for activating the transmit laser, while constellation mapping is done by the remaining $\log_2 M$ message bits. $\log_2(M)+\log_2(T)$ bpcu is transmitted by the proposed TLS-OSM system, while only $\log_2(M)$ bpcu is transmitted by a conventional TLS system. Thus it is observed that TLS-OSM is capable of increasing the spectral efficiency as compared to TLS scheme at the expense of more lasers.

5.5.3 TLS and TLS-OSM Error Analysis

The E2E CDF of the TLS system is computed from outage probability equation (Eq. (5.51)) by replacing γ_{th} with γ. The E2E CDF is differentiated to produce E2E PDF of TLS system ($f_{\gamma_{E2E}}(\gamma)$). For BPSK modulation, the fading channel has an ASEP which is computed as [129]:

$$P_e = \int_0^\infty Q(\sqrt{2\gamma}) f_{\gamma_{E2E}}(\gamma) d\gamma \tag{5.55}$$

There is no direct solution for the ASEP equation, hence Mathematica software is used to solve this integral. The error performance analysis for TLS-OSM system is also achieved. The process of TLS-OSM occurs in two steps, hence the error is calculated separately for the two steps. In the first stage, error can occur during transmission from source-to-relay, as well as for source-to-destination path. The second stage error occurs during transmission from relay-to-destination assuming that relay is able to decode the message successfully in the first stage. The error analysis is done using the PDFs obtained from Eq. (5.53). E2E error probability is evaluated as [134]:

$$P_e^{E2E} = P_e(SR)P_e(SD) + P_e(SRD)\left[1 - P_e(SR)\right] \ , \tag{5.56}$$

where $P_e(SRD)$ is the probability of error at D on successful decoding by relay node, $P_e(SR)$ is the error probability at R in the first stage and the error probability at D in the first stage is denoted by $P_e(SD)$. P_e^{node} denotes the error probabilities at the individual nodes which can be computed as $P_e^{node} = \int_0^\infty Q(\sqrt{2\gamma}) f_n(\gamma) d\gamma$ where the particular node has received SNR following PDF of $f_n(\gamma)$. The system performance analysis can be obtained from the closed form error expressions. If each error term is treated separately, then it can be observed that the resultant error term decreases with increment in

SNR value. The product of such error terms also decreases with increment in SNR value. The increment in error value is compensated by the decrement in error value for second stage error calculation. Thus an overall decrement in error value is obtained with increase in SNR values.

5.5.4 Results for TLS and TLS-OSM UOWC Systems

Certain parameters are taken for the performance analysis. Clear ocean water is considered. $\sigma^2 = \sigma_{SR}^2 = \sigma_{RD}^2$ are considered for oceanic channel generation unless mentioned explicitly. For $\sigma^2 = 0.09$ value, $d_{SR} = d_{RD} = 60\ m$ while for $\sigma^2 = 0.16$ value, $d_{SR} = d_{RD} = 80\ m$. It is assumed that the SNR and transmit power at source and relay nodes are equal. This assumption is taken for easier analysis, else all observations are valid without such assumptions also. The quantity of lasers at source node S is given by N_L^S, while N_L^R indicates the quantity of lasers at relay node R.

In Fig. 5.14, the bit error rate (BER) value of our proposed TLS scheme is compared with other existing methods in literature. For BPSK, BER and ASEP values are same. The results of TLS are compared with other methods available in literature like 4-quadrature amplitude modulation (QAM) orbital angular momentum shift keying (OAMSK) modulation based UOWC systems using Laguerre-Gauss beam based channel [208], and AF one-way relaying method (AFOWR) [79]. The corresponding BER of the systems are plotted using Fig. 5 (c) of [208] and Fig. 8 of [79]. SISO case is considered in [208] and [79]. A single optical chain is thus used for the models in [79] and [208] resulting in power consumption of $P_o + \alpha_{tr} P_{tr}$ and cost of $C_o + C_{S/P}$. The OSM results are plotted for $\sigma^2 = 0.09$ and $N_L^S = 4, N_L^R = 4$ and 16-QAM scheme. For TLS scheme with $\sigma^2 = 0.09$, 2 cases are considered- $N_L^S = N_L^R = 2$ and $N_L^S = N_L^R = 3$. It is clearly visible that TLS scheme for both cases outperforms the other methods.

The outage probability analysis for various source combinations of TLS scheme is achieved in Fig. 5.15. The turbidity of water is varied as $\sigma^2 = 0.09$ and 0.16. For any value of σ^2, performance improves with an increase in number of transmit laser sources. The results of TLS system are also better than the system without TLS. All the analytical results are corroborated by Monte Carlo simulations. The results can be interpreted from a physical perspective also. As the number of available laser sources in TLS increases, the best laser can be selected due to more diversity being available. Out of the multiple channel links available, the best one can be selected and the corresponding laser can be activated. This is far better than the scenario where there is no TLS and the single laser has to be switched on irrespective of the channel link condition. As σ^2 value increases, the light propagation and detection at photodetector is affected severely due to more disturbances in sea water, causing more chances of the system failing to reach the target data rate.

For various arrangement of laser sources and turbidity values, the ASEP results of the TLS scheme

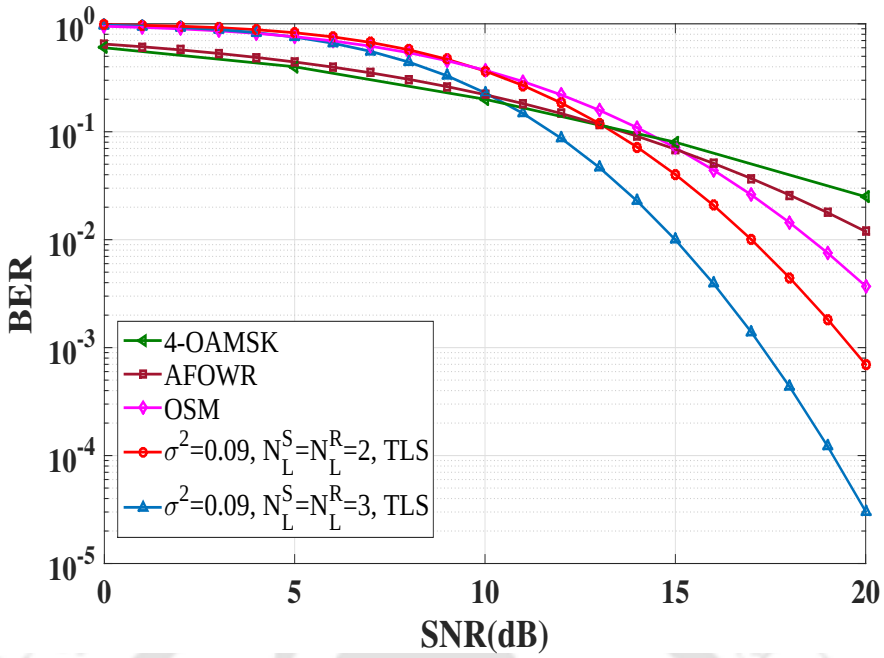

Figure 5.14: Comparison of TLS with other systems in literature.

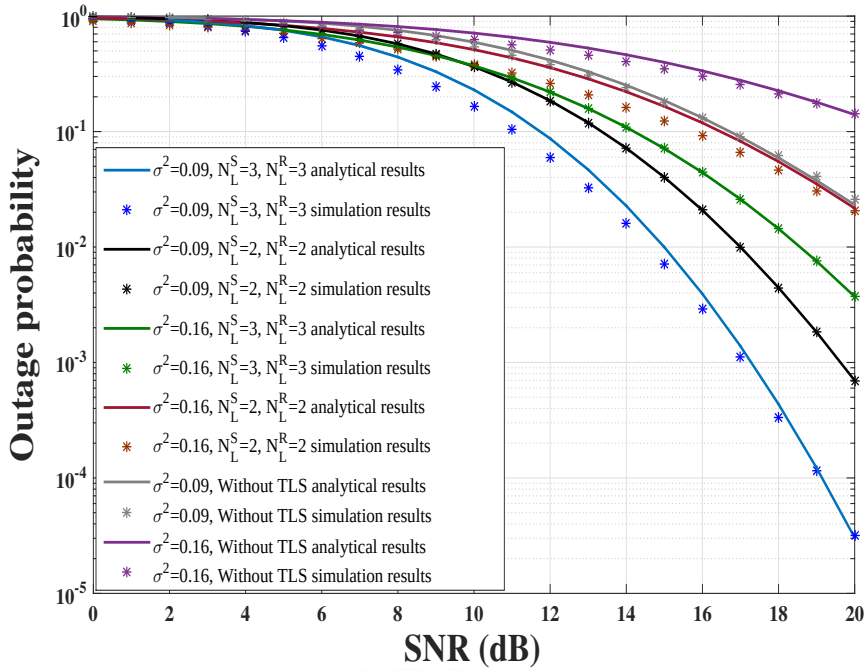

Figure 5.15: Outage probability analysis of TLS.

are depicted in Fig. 5.16. For any value of σ^2, performance improves with an increase in number of transmit laser sources. The ASEP value decreases with in an increase in transmit laser source value. The TLS system shows better performance than the system without TLS. All the analytical results are corroborated by Monte Carlo simulations. The interpretation of the results can be done from another aspect. If σ^2 value increases, it means sea water turbidity increase either due to more variations in refractive index, temperature and pressure of sea water, or due to increase in link distance between

the two nodes. Such increase in link distance or more disturbances in the sea water can hamper the signal reception at the photodetector, thereby leading to more error. If more number of laser sources are available for TLS, then the best one can be chosen due to presence of more diversity. Out of multiple channels, the best one depending on received SNR can be chosen which increases the chance of good quality transmission, rather than having to forcibly transmit out of the single or fewer lasers available.

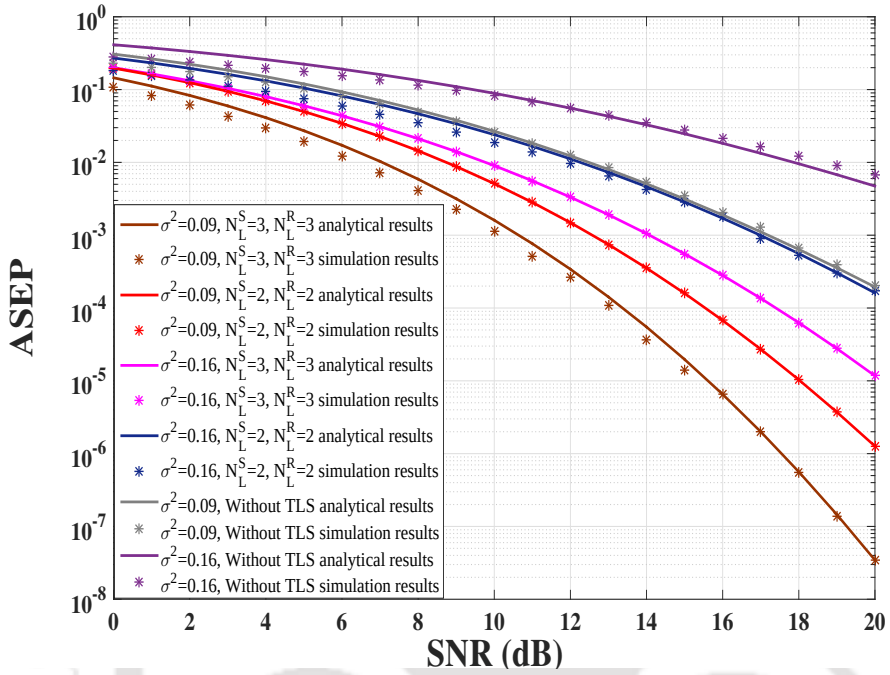

Figure 5.16: ASEP performance analysis of TLS scheme.

The outage probability results for different values of target data rates (R_d) are shown in Fig. 5.17. R_d has been varied as 1, 3 and 5 bps. It is evident from Fig. 5.17 that performance of TLS system degrades with an increment in value of R_d. This is because it is difficult to achieve higher data rates, which results in performance degradation at higher values of R_d. The analytical results are validated by Monte Carlo simulations.

The performances of TLS and TLS-OSM are analyzed in terms of ASEP in Fig. 5.18. For different values of σ^2 and different number of transmit laser sources, performances of TLS and TLS-OSM are compared. For TLS with $N_L^S = N_L^R = 2$, 2 scenarios having $\sigma^2 = 0.09$ and 0.16 are considered, while for TLS-OSM, 3 scenarios ($\sigma^2 = 0.09, N_L^S = 4, N_L^R = 4, T = 2; \sigma^2 = 0.16, N_L^S = 4, N_L^R = 4, T = 2$ and $\sigma^2 = 0.16, N_L^S = 6, N_L^R = 6, T = 2$) are considered. It is noticed that as diversity increases (with a larger set of laser sources available to be chosen from), the performance improves. TLS-OSM scheme also yields better performance than TLS scheme, justifying that it is beneficial to select the best laser sources before applying OSM. The analytical results are corroborated by Monte Carlo simulations. From all the above figures it is also evident that performance degrades with an increase in σ^2 value, indicating that the

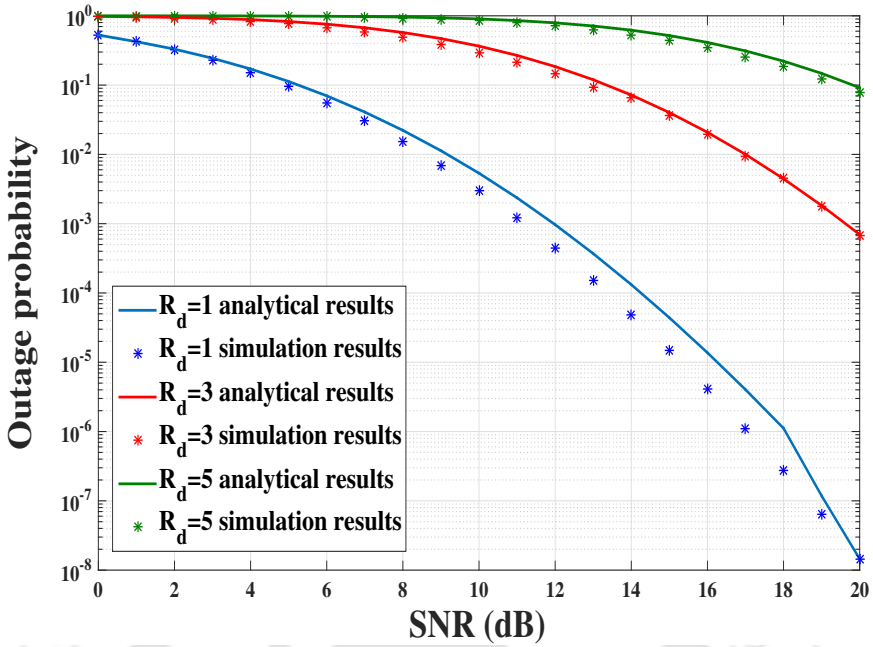

Figure 5.17: Performance analysis of TLS for different values of target data rate.

turbidity of water hampers the light propagation in water. Let us calculate the diversity gains from Fig. 5.18. For $\sigma^2 = 0.16$ and TLS scheme having 2 laser sources at each node, diversity gain for 10-20 dB SNR range is $\log_{10}(0.019/0.00017) = 2.05$. Diversity gain of TLS-OSM scheme ($N_L^S = 4, N_L^R = 4, T = 2$), considering same SNR range and σ^2 value, is calculated as $\log_{10}(0.007/0.00001) = 2.84$. Similarly for $N_L^S = 6, N_L^R = 6, T = 2$ TLS-OSM scheme at the same σ^2 value, diversity gain is $\log_{10}(0.001/(8\times10^{-8})) = 4.1$. Now for σ^2 value of 0.09, TLS scheme has a diversity gain of $\log_{10}(0.004/(1 \times 10^{-6})) = 3.6$. Hence from the results, it is conclusive that as number of laser sources in TLS-OSM scheme increases, the diversity gain increases due to the presence of diversity i.e. more lasers are available for the best selection. Diversity also increases with decrement in sea water turbidity signifying that less turbid sea water is beneficial for light propagation thereby yielding better system performance. Another fact to note is that TLS-OSM scheme offers more diversity gain than TLS scheme because TLS-OSM offers more number of lasers from which the best laser can be selected for applying OSM. Thus the diversity gain depends on the number of lasers available and the channel parameters. It is pertinent to note that for lognormal channels, theoretical asymptotic expressions are not possible because the decreasing rate of error probability does not converge to a finite value for high SNR values [206].

5.6 Conclusion

In this chapter UOWC cooperative systems have been analyzed for both SISO and MIMO cases. For SISO, closed form expressions of outage probability and ASEP have been obtained by approximating lognormal distribution with MG distribution. For MIMO case, OSM has been exploited to create a new

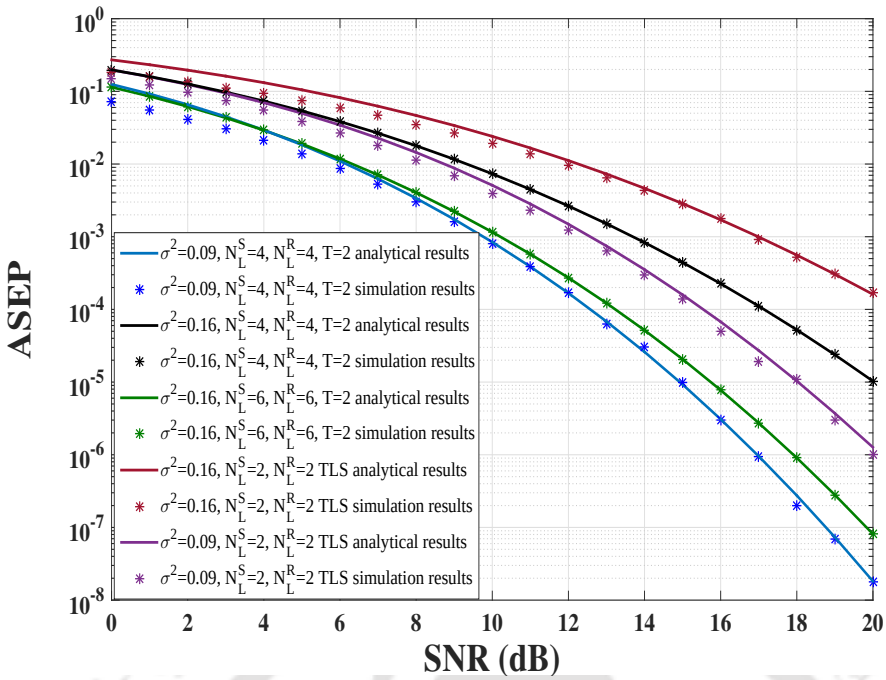

Figure 5.18: Performance comparison of TLS and TLS-OSM.

scheme called OIQSM which gives better performance for UOWC systems at the same spectral efficiency and same number of lasers. The drawbacks of OSM have been resolved by the introduction of TLS which can further be combined with OSM to form TLS-OSM scheme. It has been justified that TLS, TLS-OSM and OIQSM schemes can outperform SISO case at the expense of extra laser sources. Future work can be extended to applying more advanced versions of OSM like OGSM, OESM for UOWC systems along with TLS scheme to achieve better spectral efficiencies. Interference cancellation schemes at the relay can be explored to resolve the issue of interference and acquiring CSI for variable-gain relaying. Study of OIQSM can also be extended for multiple photodetectors to study the receive diversity. The effect of misalignment of laser sources due to floating oceanic currents can be incorporated into the channel model in future.

6. Spatial Modulation for Hybrid FSO/RF Communication

6.1 Introduction

In the last few chapters, we have seen various types of spatial modulation schemes in RF and optical domain. In this chapter, both RF and optical versions of spatial modulation will be combined to form new advanced schemes. The benefits and drawbacks of both FSO and RF communication motivate us to propose a hybrid FSO/RF system, which can exploit the benefits of both FSO and RF communication in cellular systems and achieve high data rates. Since a hybrid FSO/RF system works in both RF and optical domain, hence it comprises of sources and detectors both in RF and optical domain. Optical to electrical and electrical to optical converters are required along with the components of an optical and RF chain. Cooperative hybrid FSO/RF systems are used to improve the link distance where base station (BS) interacts with access points (AP) through FSO links and AP interacts with mobile users (MU) through RF links. Interference occurs between the multiple optical/RF sources and there is unnecessary power use because of the fact that multiple RF/optical chains operate simultaneously in MIMO based hybrid FSO/RF systems. Hybrid spatial modulation (HSM) technique can be used at the BS and AP to reduce the inter-laser and inter-antenna interference, as only one antenna/laser will be activated. The optical/RF source is selected according to the message bit. HSM employs optical/RF spatial modulation depending on whether the channel being considered is for optical or RF communication. But the main drawback of this technique is that the channel corresponding to the selected laser/antenna may give poor performance because we are just selecting the transmit optical/RF source depending upon the message bit, without taking into consideration the channel condition. Therefore, optical/RF source selection is necessary based on the channel feedback from the destination to the source and the resulting system is named as transmit source selection (TSS) system. Atmospheric turbulences and fading effect causes directional and energy changes in the RF or optical waves. Hence the signal may not be detected properly at the receiver. But if there is a large collection of optical/RF sources to choose from, then we can select

the best source depending upon the received SNR. This compensates for the increase in cost due to the use of multiple laser sources/antenna. The transmit source selection is done to maximize the received SNR in both hops. The hybrid system which employs HSM technique along with TSS is named as TSS-HSM, and it will combine both the benefits of HSM and TSS in one system.

In case of HSM and TSS, a single transmit optical/RF chain (comprising of encoders, DC bias adders, modulators, upconverters, etc.) is present, although multiple laser/antenna are present. However in case of spatial multiplexing or MIMO techniques, multiple optical/ RF chains are present both at the transmitting and receiving side which enhances the system cost significantly. Thus HSM and TSS have reduced space and cost complexities. Also in MIMO, the channels are highly correlated as multiple sources are operating simultaneously but in case of HSM and TSS, the channel is uncorrelated due to transmission from a single source. The decoding complexity is also reduced in case of HSM and TSS, and still we are getting better error and spectral efficiency performance. Spatial multiplexing achieves better spectral efficiency, but at the expense of increased decoding complexity. Decoding complexity is directly proportional to the size of constellation scheme which in turn depends on the number of active transmit sources. Considering all these factors, HSM and TSS are beneficial in terms of cost, space, power and performance.

AF and DF techniques can be used at the relay [210] for hybrid FSO/RF systems. Many types of modulation schemes are deployed in FSO communication. On-off keying (OOK) is one of the modulation schemes used, but it requires adaptive threshold making it unsuitable for dynamic environmental conditions. Pulse position modulation (PPM) has lower spectral efficiency than OOK, thus it is not a good choice. Subcarrier intensity modulation (SIM) [96] can overcome these drawbacks, but require carrier phase and frequency synchronization. BPSK modulation scheme can be used by using optical modulators. BPSK is preferred as it is not affected by scintillation. The AP used in our proposed model helps in increasing the effective link distance of hybrid FSO/RF system. It is the node which is equipped with both optical and RF chain. The node consumes resources and escalates system cost, but it is overshadowed by the fact that performance improves after the addition of AP, thereby justifying the use of AP. AP can be used to serve multiple mobile users also, although it is out of scope of this work.

There are several works in the literature on SM techniques in FSO and RF communication. Transmit source techniques in RF and FSO communication are also available. Different configurations of hybrid FSO/RF models exist in the literature too. Outage probability for cooperative FSO communication over turbulent channels with pointing errors has been evaluated in [131]. Outage probability for spatial modulation (SM) systems with antenna selection for RF communication has also been investigated in [32]. Using an adaptive mapping scheme, BER for SM in RF communication has been calculated by the authors

in [33]. The notion of OSM has been proposed for FSO links [84, 114]. SM for visible light communication has been analyzed by calculating the symbol error rate, with an adaptive modulation scheme, in [132]. The authors in [133] have calculated lower bound of mutual information using channel adaptive scheme for optical spatial modulation. In [120], OSM has been implemented for outdoor FSO networks, with a mixture of pulse position and pulse amplitude modulation techniques. Previous works have considered transmit antenna selection in conventional RF communication over Rayleigh [139] and Nakagami [140] channels. Transmit laser selection (TLS) has also been implemented for FSO communication. A TLS method for multiple-input-single-output (MISO) FSO communication system has been explored over strong turbulence channel using K distribution in [141]. In this work, the authors have assumed that perfect CSI is known at the transmitter and receiver and depending on the largest scintillation value of the optical path, transmit laser is chosen. TLS scheme has also been studied for FSO communication using K distribution in [142]. Transmit laser selection and receive diversity has been reported in [143] for mobile FSO nodes and the analysis has been conducted over weak lognormal channels.

Diversity based hybrid FSO/RF system has been proposed in [211] where the same information is transmitted over both FSO and RF links, and selection combining and maximal ratio combining have been used at the receiver. BER analysis for such system has been reported. Such diversity based systems limit the data rate to the lower rate of RF link. Hence capacity benefits can be obtained by splitting the jointly coded data stream between the two FSO and RF links. Such a system has been analyzed in [212] where CSI is not available at the transmitter. Effective coding scheme and power allotment criteria have been studied in this work. A cost efficient hybrid FSO/RF backhaul system has been reported in [213]. Outage analysis of practical FSO/RF hybrid system with adaptive combining has been investigated in [214], where depending on a certain threshold, optical/RF link is chosen. Multiuser hybrid FSO/RF relaying with buffers has been proposed in [215]. In this model, multiple mobile users can interact through RF links with the relay node. The relay is connected to the destination by means of parallel RF and FSO links. FSO transmission takes place as long as the channel condition is above a threshold SNR and when the channel quality degrades below the threshold, then RF backup link is utilized. The buffers at the relay is capable of storing the data from multiple mobile users. Another work in [216] also mentions the use of buffers at the relay for a hybrid FSO/RF model where the source and relay is connected by a RF link, and the relay is connected to the destination by parallel RF and FSO links. Performance analysis of such systems have been carried out in terms of outage probability and ASEP. Performance analysis of cooperative hybrid FSO/RF communication over generalized M-channels has been analyzed in [217]. In this work, the authors have proposed FSO links between relay and destination, and a RF link between source and relay node. But they have considered only fixed-gain AF model and reported

ASEP expressions. The authors in [218] have proposed a parallel hybrid FSO/RF system where the FSO link is active as long as the SNR is above a threshold. When the channel condition degrades and the SNR drops below the threshold, then the parallel RF link is activated. The authors have assumed a point-to-point model with parallel RF and FSO links, where FSO link is modelled by G-G channel with pointing errors and RF channel is modelled by Rician distribution, and performance analysis has been done in terms of outage probability and BER. Multiuser diversity using parallel hybrid FSO/RF links has been investigated in [219]. In this work, the authors have proposed a hybrid access point, a set of FSO users and a set of RF users. Depending on the link quality, any one RF or FSO user can be connected to the access point. Outage probability and BER performance using asymptotic analysis has been reported by the authors.

To sum up, transmit antenna selection and spatial modulation for RF communication have been performed in literature to improve the spectral efficiency and error performance by using only one RF chain. Different configurations of hybrid FSO/RF model have been used in literature. One approach is to achieve diversity by simultaneously transmitting the same information through FSO and RF link; another approach is to achieve capacity enhancement by splitting the information and transmitting it through FSO and RF links. RF link deployment as a backup link when FSO link is down, also serves as a different alternative.

The following research gaps can be observed based on the literature survey. No study has been made regarding any source selection or spatial modulation techniques for hybrid FSO/RF systems. Analysis of cost and power consumption of such hybrid schemes is missing in the literature. The concept of source selection in hybrid FSO/RF systems depending on the maximum received SNR and transmitting only the source index instead of the exact channel gains, has not been investigated in literature. Asymptotic analysis to calculate diversity and coding gains of such systems have not been performed in literature. Based on these research gaps, performance analysis of advanced schemes is proposed for hybrid FSO/RF cooperative systems. Such a hybrid FSO/RF system can exploit the benefits of both FSO and RF systems and will find its application in cellular communication.

The novelty of our work is determined by the fact that HSM, TSS and TSS-HSM schemes (based on DF relaying) are proposed for the first time in hybrid FSO/RF systems, which can be implemented in future cellular communication networks. Performance analysis of such schemes along with that of amplify-and-foward one-way relay (AFOWR) and amplify-and-forward two-way relay (AFTWR) are compared in terms of closed form expressions of outage probability. The challenges involved in deriving exact outage probability expressions are also highlighted. Closed form expressions are essential for wireless engineers to optimize the system performance by studying the influence of different system parameters. Such

tractable closed form expressions saves the time and complexity of numerical simulations. Asymptotic analysis is also carried out to evaluate the diversity and coding gain expressions. Such expressions help us in gaining valuable insight regarding the system performance. The effect of pointing and path loss errors are also considered in the channel model, thereby making our work valid for a practical scenario. The cost and power consumption complexity analysis is also performed for all the proposed schemes, which is another major contribution of our work. The challenges involved in this work include achieving closed form expressions for outage probability of the schemes. The laser or antenna selection depending on the maximum received SNR is completely new. For DF relaying the optical signal has to be converted to electrical signal at AP and then transmitted through antenna. This process involves hardware complexity and cost which is another challenge and a detailed analysis is provided regarding this issue. Overall the chapter includes a detailed analysis of advanced schemes of hybrid FSO/RF system utilizing the concept of spatial modulation and transmit laser selection which has been discussed in the earlier chapters.

6.2 Channel Model

In hybrid FSO/RF communication for cellular use, FSO links are modelled by G-G channels and RF links are modelled by Rayleigh channel model. LOS transmission takes place between BS and AP, while non-line-of-sight (NLOS) transmission takes place between AP and MU in a crowded environment. In NLOS transmission, signal transmitted from the transmitter reaches the receiver after several reflections from the obstacles in its path. Hence deep fading effects occur, which is prevalent in cellular communication, and such signal transmission can be accurately modelled by a Rayleigh channel. On the other hand, the LOS path between AP and BS for FSO communication can be accurately modelled by G-G channel. It is pertinent to note that the hybrid FSO/RF model is being designed for cellular communication. If it would have been modelled for D2D communication without involving BS, then fading models such as cascaded $\alpha - \mu$ model could have been used for hybrid FSO/RF communication. In our model, transmission occurs between an antenna at a very low height located at the mobile equipment and a higher altitude antenna (almost at the building level) at the AP. The AP being at a greater height and being stationary in nature, is relatively free from scattering effects while the MU side being mobile and at a lower height, suffers from scattering effects. Such fading effects can be effectively modelled by fading model such as Rayleigh fading.

For LOS FSO link, G-G channel with pointing error is used which has been described earlier. This channel model is appropriate as it can account for weak to strong turbulences and also incorporate the pointing error effect caused by wind speeds, building sways, etc. The PDF and CDF of received SNR of G-G channel with pointing error is given by Eq. (4.37) and (4.39) respectively. For RF link, Rayleigh

channel is used whose PDF of the SNR is given by $f_\gamma(\gamma) = \frac{1}{\bar{\gamma}} e^{-\frac{\gamma}{\bar{\gamma}}}$ [217], where $\bar{\gamma}$ represents average SNR. CDF of the received SNR for Rayleigh channel is obtained by integrating the PDF and is given by:

$$F_\gamma(\gamma) = 1 - e^{-\frac{\gamma}{\bar{\gamma}}} \ . \tag{6.1}$$

6.3 Proposed System Model

The hybrid FSO/RF system model as shown in Fig. 6.1 comprises of a BS connected to the access point AP with FSO links, while the AP is connected to the mobile user (MU) with the help of RF links. In any cooperative system, source and destination are connected by means of a relay. In our hybrid FSO/RF cooperative model, BS and MU act as source and destination node respectively, while AP act as relay node. Thus our model can be related to any conventional cooperative model. Although not shown in Fig. 6.1, all the nodes are working in half-duplex mode with N_L lasers at the BS and N_D photodetectors at the AP. The AP further comprises of N_A antennas for RF communication, while the MU comprises of N_A antennas for reception purpose. The relative gains of the links as described in Section II of [51] and Eq. 3 of [52] are given as: $G_{S,R} = (\frac{d_{SD}}{d_{SR}})^\tau$, $G_{R,D} = (\frac{d_{SD}}{d_{RD}})^\tau$ where $G_{S,R}$ and $G_{R,D}$ are the relative gain of the BS to AP link and AP to MU links respectively, τ is the path loss coefficient, d_{SD}, d_{SR} and d_{RD} are the distances between BS and MU, BS and AP, and AP and MU links respectively. In the optical node i.e at BS, a RF subcarrier signal is modulated by source data and the modulated signal is then used to modulate the intensity of optical source like laser. The sinusoidal nature of the modulated signal in RF domain causes a necessity of addition of DC bias to make the signal positive in order to drive the optical source. The negative part of the BPSK modulated signal is removed by adding a DC bias signal. This positive signal can then modulate the laser output. The intensity modulated signal transmitted by the laser is sent into free-space by means of an aperture. At the AP node, the received signal is detected by a photodetector and the corresponding electrical signal is generated. The signal undergoes demodulation to get back the original data. For the RF channel, a RF signal is modulated by the data and transmitted into free-space by the antenna at AP. The signal is received by the antenna at MU node and undergoes corresponding demodulation. However for AF technique, the electrical signal output from photodetector at AP is further amplified and transmitted by the antenna without decoding the data.

In HSM, as shown in Fig. 6.2, one out of the laser sources at BS is activated depending on the message bit. Similarly at the AP, photodetectors receive the optical signal and after conversion to electrical signals, one out of the N_A antennas is selected depending on the bit.

In TSS, a single transmit source (optical or RF source) is activated among all the available transmit

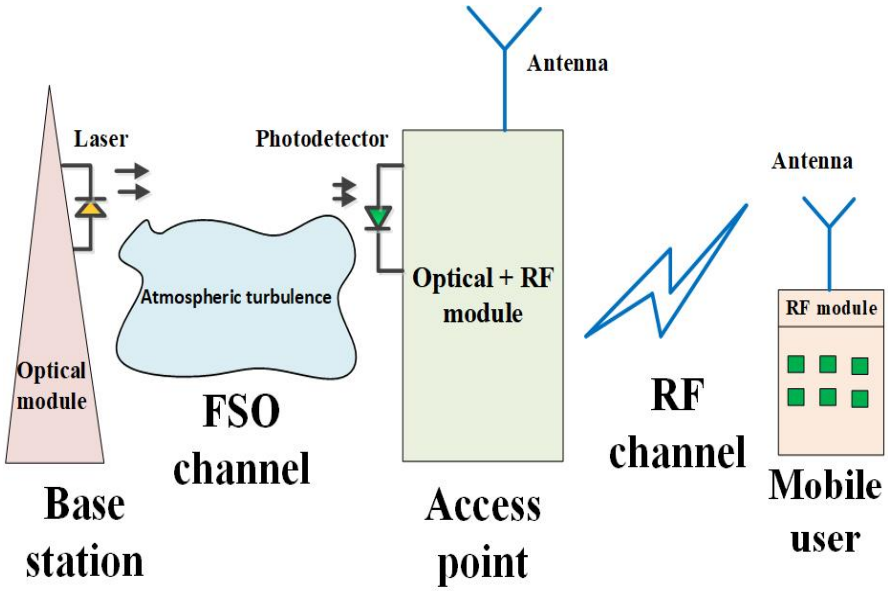

Figure 6.1: Proposed system model

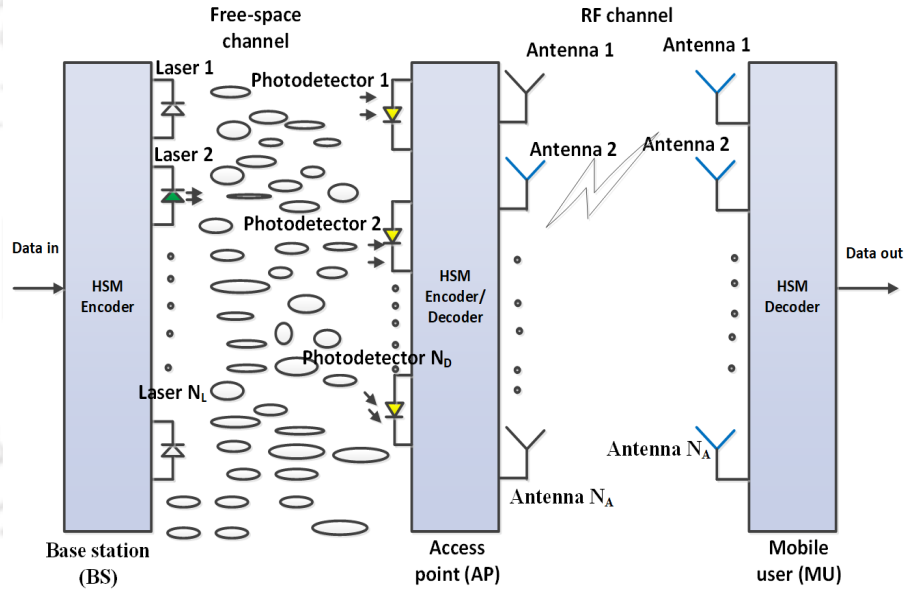

Figure 6.2: Proposed system model for HSM

sources, which yields the maximum received SNR. This particular source is used for transmission using a M-ary modulation scheme which is depicted by the TSS encoder. For example, in Fig. 6.3(a), transmit source index (TSI) is chosen as 2 at the BS, hence laser 2 will be used for sending optical signals, all other lasers remain idle. Similarly, TSI is chosen as 2 for AP, therefore only antenna 2 will be sending RF signals. In actual scenario, TSI can be estimated before sending a chunk of data and TSI can be sent from the receiver to the transmitter through a partial feedback link [149, 150] using $\log_2(N_L)$ or $\log_2(N_A)$ bits. In AP, the low-rate feedback channel is implemented by the addition of an extra laser. MU already has antenna to execute this low-rate feedback channel.

In TSS-HSM as shown in Fig. 6.3(b), among all the transmit sources, a set of T transmit sources

(either optical or RF) are selected which give the maximum received SNR at the receiver. On these T sources, HSM is applied which means transmit source activation and M-ary modulation scheme are done based on the incoming message bits. For TSS-HSM, $T\log_2(N_L)$ or $T\log_2(N_A)$ number of feedback bits are required depending on whether the source is optical or RF based. TSS-HSM detection process carries information for both TSI and symbol unlike TSS, where the detection is done only for the symbol sent from the transmitter.

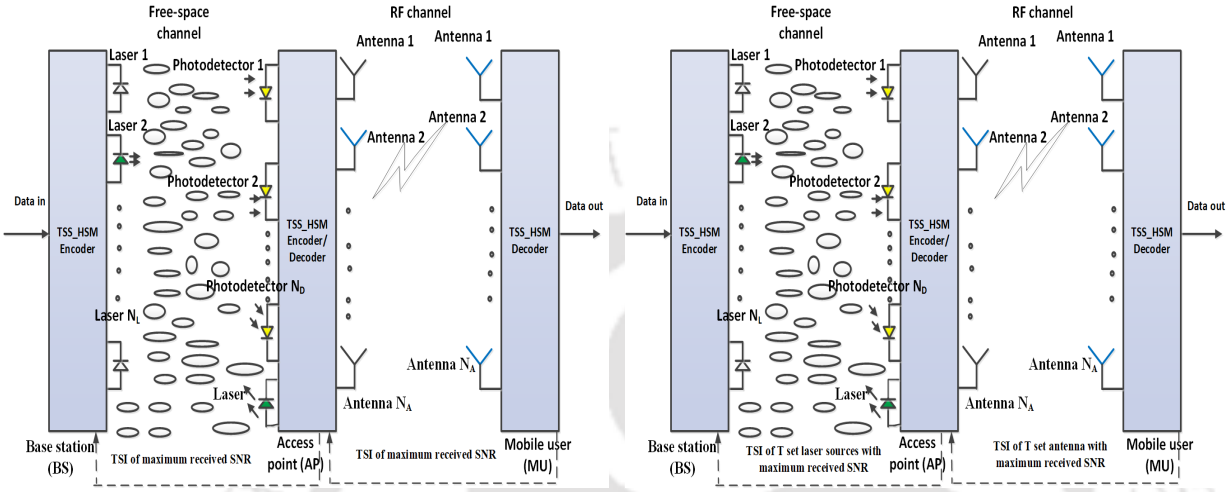

Figure 6.3: Proposed system model for (a) TSS and (b) TSS-HSM (TSI: Transmitter Source Index/Indices).

6.4 Performance Analysis

This section evaluates the outage probability expressions for various systems. P_S indicates the transmit power at BS and P_R denotes the transmission power for AP node. The BS transmits message to AP in the first time slot. The AP decodes the message and on successful decoding, it encodes it and retransmits it to MU in the second time slot. The process is called DF relaying and is unidirectional in nature. The j_{Rrx} photodetector of AP receives signal in n^{th} time slot which is given by:

$$y_R^{j_{Rrx}}[n] = \sqrt{\eta_{tx} R_e P_S G_{S,R}}\, h_{j_S,j_{Rrx}} x_S[n] + w_S[n] \ , \tag{6.2}$$

where $j_{Rrx} \in \{1, 2, ..., N_D\}$. η_{tx} symbolizes the transmitter efficiency. Ambient light at AP node generates thermal noise which is denoted by $w_S[n]$. It can be expressed as white Gaussian zero mean random noise with variance N_0. R_e is the responsivity of the photodetector. In case of photodetectors, the major sources of noise are thermal noise, shot noise and dark current noise. In high speed optical wireless systems, for lower SNR values, thermal noise is the dominant source of noise as evident from Chapter 1 of [220]. Hence, we have considered only thermal noise generated due to a load resistance of 50 Ω at a temperature of 300 K. $x_S[n]$ is the message bit modulated by BPSK scheme in the n^{th} time slot. $h_{j_S,j_{Rrx}}$

is the channel coefficient between the j_S transmitting laser of node BS and j_{Rrx} receiving photodetector of node AP. The signal received at AP is decoded by using maximum likelihood (ML) algorithm and the decoded message bit is denoted by $x_R[n]$. The received signal emitted from the AP and obtained at the j_D antenna of MU is expressed as:

$$y_D^{j_D}[n] = \sqrt{P_R \eta_{rx} G_{R,D}}\; h_{j_{Rtx},j_D} x_R[n] + w_R[n] \;, \tag{6.3}$$

where $j_D \epsilon \{1, 2, ..., N_A\}$. h_{j_{Rtx},j_D} is the channel coefficient between the j_{Rtx} transmitting antenna of AP and j_D receiving antenna of MU. At MU node, Gaussian noise is represented by $w_R[n]$. η_{rx} represents the receiver efficiency. j_{Rrx} denotes photodetector index of AP and j_{Rtx} indicates antenna index of AP. Antenna index of MU is denoted by j_D, whereas j_S indicates laser index of BS.

6.4.1 Hybrid System with AF Protocol

AFOWR is the amplify-and-forward based cooperative hybrid FSO/RF system where no spatial modulation is involved. In this model, single laser is present at BS while single photodetector is present at AP. A single antenna is present at AP and MU. AFTWR is the bidirectional amplify-and-forward based cooperative hybrid FSO/RF model where no spatial modulation in involved. The BS and MU can receive and transmit message simultaneously. Thus it is a full-duplex system and self-interference effect is more. In case of AFOWR variable-gain c is considered which can be defined as [192, 193]:

$$c = \frac{R_e P_S \eta_{tx} G_{S,R} E/N_0}{1 + R_e P_S \eta_{tx} G_{S,R} |h_{j_S,j_{Rrx}}|^2 E/N_0 + P_R \eta_{rx} G_{R,D} |h_{j_{Rtx},j_D}|^2 E/N_0} \;. \tag{6.4}$$

The instantaneous SNR of various links are given as $\gamma_{FSO} = \frac{R_e P_S \eta_{tx} G_{S,R} |h_{j_S,j_{Rrx}}|^2 E}{N_0}$, $\gamma_{RF} = \frac{P_R \eta_{rx} G_{R,D} |h_{j_{Rtx},j_D}|^2 E}{N_0}$ and $\bar{\gamma} = E/N_0$. Thus the second slot transmission will be governed by the following equation for AF relaying:

$$y_D^{j_D}[n] = \sqrt{c P_R \eta_{rx} G_{R,D}}\; h_{j_{Rtx},j_D} x_R[n] + w_R[n] \;. \tag{6.5}$$

For AFOWR system having adaptive gain, the equivalent system SNR is given by [221]:

$$\gamma_{FSO/RF} = \frac{\gamma_{FSO}\gamma_{RF}}{\gamma_{FSO} + \gamma_{RF} + 1} \;, \tag{6.6}$$

where γ_{FSO} and γ_{RF} are the instantaneous SNR for FSO and RF links respectively. Now we will try to evaluate the exact outage probability for such a system and observe the challenges involved. Let the

threshold SNR γ_{th} be denoted by x. The total end-to-end outage probability ($F_{\gamma_{FSO/RF}}(x)$) is given by:

$$\begin{aligned} F_{\gamma_{FSO/RF}}(x) &= P\left(\frac{\gamma_{FSO}\gamma_{RF}}{\gamma_{FSO}+\gamma_{RF}+1} < x\right) \\ &= \int_{y=0}^{\infty} P\left(\frac{\gamma_{FSO}y}{\gamma_{FSO}+y+1} < x\right) f_{\gamma_{RF}}(y)dy \\ &= \int_{y=0}^{\infty} P\left(\gamma_{FSO} < \frac{(y+1)x}{y-x}\right) f_{\gamma_{RF}}(y)dy \\ &= F_{\gamma_{RF}}(x) + \int_{x}^{\infty} F_{\gamma_{FSO}}(z)\, f_{\gamma_{RF}}(y)dy \ . \end{aligned} \tag{6.7}$$

For the last step of the above equation, we have split the limit of integration into two parts $y = 0$ to x and the other $y = x$ to ∞. Let $z = \frac{(y+1)x}{y-x}$. The value of $P\left(\gamma_{FSO} > \frac{(y+1)x}{y-x}\right)$ in the range of $y = 0$ to x is 1, since the random variable γ_{FSO} is always positive and will always be greater than the negative value of $\frac{(y+1)x}{y-x}$ when $0 < y < x$. The PDF and PDF of the terms are inserted according to the PDF and CDF of G-G and Rayleigh channel to obtain the following simplified equation:

$$\begin{aligned} F_{\gamma_{FSO/RF}}(x) = 1 - \exp\left(-\frac{x}{P_R\eta_{rx}G_{R,D}\bar{\gamma}}\right) + \int_{x}^{\infty} \frac{\zeta^2}{\Gamma(\alpha_G)\Gamma(\beta_G)} G_{2,4}^{3,1}\left(\begin{matrix}1,\zeta^2+1\\ \zeta^2,\alpha_G,\beta_G,0\end{matrix}\middle|\, \frac{\alpha_G\beta_G\left(\frac{z}{R_eP_S\eta_{tx}G_{S,R}\bar{\gamma}}\right)^{1/2}}{A_0h_l}\right) \\ \times \frac{1}{P_R\eta_{rx}G_{R,D}\bar{\gamma}} \exp\left(-\frac{y}{P_R\eta_{rx}G_{R,D}\bar{\gamma}}\right) dy \ . \end{aligned} \tag{6.8}$$

From the above integral equation, we can observe that the second term's integral is intractable. No closed from expressions are available to the best of the authors's knowledge. Such integrals need to be solved numerically in Mathematica. But our goal is to obtain closed form expressions to gain valuable insights regarding system performance. Hence, we opt for bounds of outage probability now. For evaluating the lower bounds of outage probability, we need the SNR to be upper bounded. Thus at high SNR, the equivalent SNR is approximated by $\gamma_{FSO/RF} \cong \min(\gamma_{FSO}, \gamma_{RF})$ [61]. The end-to-end outage probability can be lower bounded as:

$$P_{out}^{AF}(\gamma_{th}) \geq F_{\gamma_{FSO/RF}}(\gamma_{th}) = F_{\gamma_{FSO}}(\gamma_{th}) + F_{\gamma_{RF}}(\gamma_{th}) - F_{\gamma_{FSO}}(\gamma_{th})F_{\gamma_{RF}}(\gamma_{th}) \ , \tag{6.9}$$

where $\gamma_{th} = 2^{R_d} - 1$ and R_d is the target data rate. For AFTWR, $\gamma_{th} = 2^{2R_d} - 1$. It is to be kept in mind that for variable-gain relaying, exact knowledge of the channel statistics must be known to the nodes. Therefore, channel estimation and channel exchange are required for both AP and MU nodes. The channel estimations of both the links can be assumed as a multi-user channel estimation problem [194]. The results of channel estimation can be used in interference cancellation in this case. This technique follows the principle of periodic insertion of a unique training sequence into each data sequence and also

allows the time variation of the channels within and between the training sequences. However, there are many such interference cancellation schemes based on the principle of sending pilot signals. Interference mitigation techniques is an interesting field of research and can be considered as a future scope of work for such hybrid FSO/RF systems.

6.4.2 Analysis for HSM System

At the BS side, out of N_L lasers, the transmit laser is activated depending on the value of $\log_2(N_L)$ number of bits from LSB side. An example of transmit laser activation is shown for $N_L = 2$, where the transmit laser source index (j_S) which is activated is selected as

$$j_S = \begin{cases} 2, & \text{if } c^{LSB}[n] = 1 \\ 1, & \text{if } c^{LSB}[n] = 0 \ , \end{cases} \tag{6.10}$$

where n denotes the n^{th} time slot. $c[n]$ represents the bits which may be 0 or 1 in this scenario. The BS transmits data using BPSK to AP which is given by $x_S[n] = 2c[n] - 1$. If $N_L > 2$, then the transmit laser source is activated by using $\log_2 N_L$ number of bits (from LSB side) and the remaining $\log_2 M$ message bits will be applied for symbol constellation mapping. Symbol mapping is done according to the constellation scheme to obtain $x_S[n]$ from $c[n]$. Thus $x_s[n]$ represents the modulated symbol. If channel state information (CSI) is available at the AP, the parameters j_S, $x_S^{MSB}[n]$ are detected using ML detection method [54] and the estimated symbols at the AP are $\hat{j}_S$ and $\hat{x}_S^{MSB}$.

$$(\hat{j_S}, \hat{x}_S^{MSB}[n]) = \underset{(j_S, x_S^{MSB}[n])}{min} \left| y_R^{j_{Rrx}}[n] - \sqrt{\eta_{tx} R_e P_S G_{S,R}} h_{j_S, j_{Rrx}} x_S^{MSB}[n] \right|^2 . \tag{6.11}$$

According to the estimated value of $\hat{j_S}$, the value of LSB bits $c^{LSB}[n]$ can be estimated which is denoted by $\hat{c}^{LSB}[n]$. Similarly for RF channel, the transmit antenna index at AP is made active according to the bits. If $\hat{c}^{LSB}[n] = 0$, $j_R = 1$ is made active while if $\hat{c}^{LSB}[n] = 1$, $j_R = 2$ is activated. Assuming MU node has CSI, ML method detects the parameters j_R, $x_R^{MSB}[n]$ [54] and the estimated symbols are $\hat{j}_R$ and $\hat{x}_R^{MSB}$. Assumption of the CSI being available to the particular nodes is taken. However in practical scenarios, channel estimation techniques can be used to estimate the channel conditions during message transmission. This can be done by using a feedback channel using certain overhead bits. Before transmission, CSI can be sent through this feedback link if channel fading is slowly varying in nature. However, this channel estimation is out of scope of the thesis and can be considered in future research works. Thus assuming known CSI, the subsequent operations are done:

$$\hat{x}_S^{LSB}[n] = \hat{j_R} \oplus j_S, \ \hat{x}_S^{MSB}[n] = \hat{x}_R^{MSB}[n] \oplus x_S^{MSB}[n] \ . \tag{6.12}$$

Readers may note that due to the problem of deriving tractable end-to-end CDF and PDF closed form expressions, bounds of outage probability for HSM are investigated. However in future, analysis can be done in solving end-to-end SNR, PDF and CDF expressions in closed form, which will make analysis of exact outage probability for HSM all the more tractable. For a data rate of R_d bits/s, the AP node has a lower bound of outage probability which is defined as:

$$P_{out}^{R\_LB}(R_d) \geq P[\log_2(N_L) + \log_2(1 + \min(\gamma_{S,R}^1, \gamma_{S,R}^2, ..., \gamma_{S,R}^{N_L})) < R_d] \ . \tag{6.13}$$

Assumption is taken that laser selection involves no error, hence $\log_2 N_L$ bits are used for activating a particular laser. Spatial domain mutual information is upper bounded by $\log_2(N_L)$ as explained in Chapter 2. This assumption is taken because if laser selection error is considered, then it will be difficult to achieve closed form expressions of outage probability. Numerical analysis has to be done which defeats our initial motive of obtaining closed form expressions to gain key facts about the system performance. The PDF of the random variable obtained from the difference of two G-G random variable is not known. Without the difference PDF, the outage probability cannot be evaluated. Research is going on to solve the nature of the difference PDF and this can be a scope for future work. In practical scenarios there is error involved in estimating the laser index properly. However, such errors are very less as compared to the error due to incorrect symbol estimation. Hence the laser selection error is ignored in this work, but can be included in future works. In this calculation, minimum of SNR is calculated. This is because lowest chances of error is when any one of the links from BS to AP fails. Even if one laser is able to transmit from BS to AP, message transmission can take place. Hence, maximum error will occur when all the links fail and minimum error will occur when any one of the links fails. To compute lower bounds of outage probability, minimum condition (either of the link failure) is thus considered. Assume $\psi_R = \min(\gamma_{S,R}^1, \gamma_{S,R}^2, ..., \gamma_{S,R}^{N_L})$. Thus $\gamma_{th} = 2^{(R_d - \log_2(N_L))} - 1$. From Eq. (2.48), the CDF of minimum of random variables can be calculated and using that result, the CDF of ψ_R is computed as [50]:

$$\begin{aligned} P_{out}^{R\_LB}(\gamma_{th}) \geq F_{\psi_R}(\gamma_{th}) &= P\left\{\min(\gamma_{S,R}^1, \gamma_{S,R}^2, ..., \gamma_{S,R}^{N_L}) \leq \gamma_{th}\right\} \\ &= 1 - P\left\{\min(\gamma_{S,R}^1, \gamma_{S,R}^2, ..., \gamma_{S,R}^{N_L}) > \gamma_{th}\right\} \\ &= 1 - P(\gamma_{S,R}^1 > \gamma_{th})P(\gamma_{S,R}^2 > \gamma_{th})....P(\gamma_{S,R}^{N_L} > \gamma_{th}) \\ = 1 - (1 - P(\gamma_{S,R}^1 \leq \gamma_{th}))(1 - P(\gamma_{S,R}^2 \leq \gamma_{th}))....(1 - P(\gamma_{S,R}^{N_L} \leq \gamma_{th})) \\ &= 1 - \textstyle\prod_{j_{Rrx}=1}^{N_L}(1 - F_{\gamma_{S,R}^{j_{Rrx}}}(\gamma_{th})) \ . \end{aligned} \tag{6.14}$$

The SNR received by j_{Rrx} numbered photodetector at AP is given by:

$$\gamma_{S,R}^{j_{Rrx}} = \frac{\eta_{tx} R_e P_S G_{S,R} \left(h_{j_S,j_{Rrx}}\right)^2 E}{N_0}, \qquad where \ \bar{\gamma} = \frac{E}{N_0} \ . \quad (6.15)$$

The SNR received by j_D numbered antenna at MU is given by:

$$\gamma_{R,D}^{j_D} = \frac{\eta_{rx} P_R G_{R,D} \left(h_{j_{Rtx},j_D}\right)^2 E}{N_0} \ . \quad (6.16)$$

$(h_{j_S,j_{Rrx}})^2$ follows square of G-G distribution with pointing errors. We can write outage probability of FSO link by using Eq. (4.39) and Eq. (6.15):

$$F_{\gamma_{S,R}^{j_{Rrx}}}(\gamma_{th}) = \frac{\zeta^2}{\Gamma(\alpha_G)\Gamma(\beta_G)} G_{2,4}^{3,1}\left(\begin{matrix} 1,\zeta^2+1 \\ \zeta^2,\alpha_G,\beta_G,0 \end{matrix} \middle| \frac{\alpha_G \beta_G (\frac{\gamma_{th}}{\eta_{tx} P_S R_e G_{S,R} \bar{\gamma}})^{\frac{1}{2}}}{A_0 h_l} \right) \ . \quad (6.17)$$

The CDF obtained from Eq. (6.17) is put into Eq. (6.14) to obtain the outage probability lower bound for AP node. The next step is to calculate the outage probability for transmission through RF links between AP and MU. Similarly for a data rate of R_d bits/s, the MU node has an outage probability for HSM which can be defined as [50]:

$$P_{out}^{D}(R_d) \geq P[\log_2(N_A) + \log_2(1 + \min(\gamma_{R,D}^1, \gamma_{R,D}^2, ..., \gamma_{R,D}^{N_A})) < R_d] \ . \quad (6.18)$$

Again the minimum SNR condition is considered. This is because lowest chance of outage is when any one of the RF links fails from AP to MU. Any of the link failure condition is given by the minimum SNR of all links. The CDF of minimum of random variables can be calculated from Eq. (2.48). Assume $\psi_D = \min(\gamma_{R,D}^1, \gamma_{R,D}^2, ..., \gamma_{R,D}^{N_A})$ and $\gamma_{th} = 2^{(R_d - \log_2(N_A))} - 1$. $\log_2(N_A)$ number of bits are used for activating the particular antenna. Hence the extra term is required for outage probability calculation. The CDF of ψ_D is thus written as [50]:

$$\begin{aligned} F_{\psi_D}(\gamma_{th}) &= P\left\{\min(\gamma_{R,D}^1, \gamma_{R,D}^2, ..., \gamma_{R,D}^{N_A}) \leq \gamma_{th}\right\} \\ &= 1 - P\left\{\min(\gamma_{R,D}^1, \gamma_{R,D}^2, ..., \gamma_{R,D}^{N_A}) > \gamma_{th}\right\} \\ &= 1 - P(\gamma_{R,D}^1 > \gamma_{th}) P(\gamma_{R,D}^2 > \gamma_{th}) .... P(\gamma_{R,D}^{N_L} > \gamma_{th}) \\ &= 1 - (1 - P(\gamma_{R,D}^1 \leq \gamma_{th}))(1 - P(\gamma_{R,D}^2 \leq \gamma_{th})) .... (1 - P(\gamma_{R,D}^{N_A} \leq \gamma_{th})) \\ &= 1 - \textstyle\prod_{j_D=1}^{N_A} (1 - F_{\gamma_{R,D}^{j_D}}(\gamma_{th})) \ , \end{aligned} \quad (6.19)$$

where the outage probability of RF link is given by (using Eq. (6.16) and (6.1)):

$$F_{\gamma_{R,D}^{j_D}}(\gamma_{th}) = 1 - e^{-\frac{\gamma_{th}}{\eta_R P_R G_{R,D} \bar{\gamma}}} \ . \quad (6.20)$$

Thus, after putting the value of outage probability of particular AP-MU link obtained from Eq. (6.20) in Eq. (6.19), we derive the outage probability at MU node as:

$$P_{out}^{D}(\gamma_{th}) \geq 1 - \prod_{j_D=1}^{N_A} e^{-\frac{\gamma_{th}}{\eta_{rx} P_R G_{R,D} \bar{\gamma}}} \ . \tag{6.21}$$

The summation of the outage probabilities at the AP and MU nodes yields the overall system outage probability. It is thus lower bounded by [50]:

$$\begin{aligned} P_{out}^{LB}(\gamma_{th}) &= P_{out}^{R\_LB}(\gamma_{th}) + (1 - P_{out}^{R\_LB}(\gamma_{th}))P_{out}^{D}(\gamma_{th}) \\ &\geq 1 - (\textstyle\prod_{j_{Rrx}=1}^{N_L}(1 - F_{\gamma_{S,R}^{j_{Rrx}}}(\gamma_{th}))) \prod_{j_D=1}^{N_A} e^{-\frac{\gamma_{th}}{\eta_{rx} P_R G_{R,D} \bar{\gamma}}} \ . \end{aligned} \tag{6.22}$$

The overall transmission is a two stage DF process. The BS transmits message to AP in the first stage, whose outage probability can be defined by the term $P_{out}^{R\_LB}$, obtained from Eq. (6.14). The second stage is the transmission stage from the AP node, which is given by $(1 - P_{out}^{R\_LB}(\gamma_{th}))P_{out}^{D}(\gamma_{th})$. $P_{out}^{D}(\gamma_{th})$ is obtained from Eq. (6.21). Some valuable insights can be gained from this analysis. Each CDF term has Meijer G or exponential component whose value decreases with an increase in SNR. Thus product of such CDF values will also give a decrement. The multiplication of CDF values subtracted from 1 gives an increment, but it is again subtracted from 1 to indicate an overall decrement. Hence, there will be an overall decrement in the total outage probability value of HSM with increment in SNR value. The readers may note that in DF process, where there is no direct link between the BS and MU, the system performance may suffer if there is too much error in the first stage. If the AP is unable to decode the message correctly, then further transmission to MU in second time slot will cause more error. Therefore, the overall outage probability is dominated by the outage probability over G-G channel. Hence it is necessary, that the first stage transmission occurring for FSO links, generates minimum error. The FSO communication serving as a LOS communication between BS and AP can minimize this error. However, to further resolve the drawbacks of DF based HSM system, TSS is proposed which aims to select the best source dependent on the maximum received SNR. This prevents the system from suffering too much error in the first stage of transmission.

6.4.3 Analysis for TSS System

In TSS, the antenna or laser source selection is done based on the maximum received SNR. A particular link for which the received SNR is maximum is chosen, and the TSI of that particular source for which the link generates maximum SNR, is sent as a feedback. Transmission between BS and AP occurs with the help of FSO links. The criteria which is used for selecting a single transmit optical source

is given by:

$$I^S = \underset{1\leq j_S\leq N_L}{arg\ max}\left\{C_i = \sum_{j_{Rrx}=1}^{N_D}|h_{j_S,j_{Rrx}}|^2\right\}, \tag{6.23}$$

where I^S denotes the transmit laser index of node BS which maximizes the received SNR at AP, $j_S \in (1, N_L), j_{Rrx} \in (1, N_D)$. Similarly, a single transmit antenna for the transmission between AP and MU is selected according to the following criteria:

$$I^R = \underset{1\leq j_{Rtx}\leq N_A}{arg\ max}\left\{C_i = \sum_{j_D=1}^{N_A}|h_{j_{Rtx},j_D}|^2\right\}, \tag{6.24}$$

where I^R denotes the transmit antenna index of node AP which maximizes the received SNR at MU.

Each C_i for $i\ \epsilon\ (1, 2, ...N_L)$ for node AP and $i\ \epsilon\ (1, 2, ...N_A)$ for MU are arranged in ascending order such that $C_1 \leq C_2 \leq ... \leq C_{N_L}$ for FSO link and $C_1 \leq C_2 \leq ... \leq C_{N_A}$ for RF link. At AP and MU, the transmit laser and antenna index are chosen respectively which gives the highest value of C_i respectively. The end-to-end outage probability can be written as [134, 158]:

$$P_{out}(\gamma_{th}) = F_{\gamma_{SR}}\left(\frac{\gamma_{th}}{\bar{\gamma}_{SR}}\right)^{N_L} + \left[1 - F_{\gamma_{SR}}\left(\frac{\gamma_{th}}{\bar{\gamma}_{SR}}\right)\right]\left(F_{\gamma_{RD}}\left(\frac{\gamma_{th}}{\bar{\gamma}_{RD}}\right)\right)^{N_A}, \tag{6.25}$$

where $\bar{\gamma}_{SR} = \eta_{tx}P_S R_e G_{S,R}\bar{\gamma}$ and $\bar{\gamma}_{RD} = \eta_{rx}P_R G_{R,D}\bar{\gamma}$. From the outage probability expression of TSS, it is clear that the first term denotes the outage probability of the first phase when the transmit laser is chosen such that the received SNR is maximized at AP. Outage occurs in first phase when none of the FSO links from lasers at BS to photodetectors at AP are available. Even if one link is working, then message can be transmitted. All link failure is satisfied by the condition of maximum SNR of all links. In the second phase, it is considered that message is successfully received by AP from the first phase. Again outage occurs if all the RF links between AP and MU fail. Even if a single link is working between any of the antennas of AP and MU node, transmission can take place. Hence the second term in Eq. (6.25) gives the outage probability of the second phase. One fact is clear from the expression that if FSO link is severely affected such that all links are down, then the outage probability of the first phase will be very high and this will severely degrade the system performance by increasing the overall outage probability value of the TSS system. If $N_L > N_A$, then the severity in performance degradation will be much more as the outage probability of first phase contains a term which is raised to the power of N_L.

6.4.4 Analysis of TSS-HSM System

To calculate the outage probability of TSS-HSM system, the CDF of the received SNR after selection of a set of T sources, is required. Hence we need to calculate the PDF of received SNR first in order to

find CDF. To choose a group of T laser sources/ RF antenna which yields the maximum received power, all the C_is obtained from Eq. (6.23) and (6.24) are arranged in ascending order. The set of T laser sources corresponding to the highest values of C_is are selected. Following the order statistics, the PDF of C_i, such that $C_1 \leq C_2 \leq ... \leq C_i \leq ...C_{N_L}/C_{N_A}$, is given by [32]:

$$f_{C_i}(\gamma) = \frac{1}{B_t(i, N_L - i + 1)} \{F_\gamma(\gamma)\}^{i-1} (1 - F_\gamma(\gamma))^{N_L - i} f_\gamma(\gamma) \ , \tag{6.26}$$

where $i = N_L - T + 1$, $B_t(.,.)$ is the beta function. Now the received SNR of selecting T sources has to be evaluated. The SNRs are arranged in ascending order. Hence the set of SNRs from $N_L - T + 1$ to N_L are chosen. The PDF of the received SNR at AP is evaluated as:

$$f^i_{\gamma_{SR}}(\gamma) = \frac{1}{N_L - i + 1} \sum_{j=i}^{N_L} \frac{1}{B_t(j, N_L - j + 1)} \{F_{\gamma_{SR}}(\gamma)\}^{j-1} (1 - F_{\gamma_{SR}}(\gamma))^{N_L - j} f_{\gamma_{SR}}(\gamma) \ . \tag{6.27}$$

$f_{\gamma_{SR}}(\gamma)$ and $F_{\gamma_{SR}}(\gamma)$ follow PDF and CDF of square of G-G distribution with pointing error. Similarly for RF link, the PDF of received SNR at MU is expressed as:

$$f^i_{\gamma_{RD}}(\gamma) = \frac{1}{N_A - i + 1} \sum_{j=i}^{N_A} \frac{1}{B_t(j, N_A - j + 1)} \{F_{\gamma_{RD}}(\gamma)\}^{j-1} (1 - F_{\gamma_{RD}}(\gamma))^{N_A - j} f_{\gamma_{RD}}(\gamma) \ , \tag{6.28}$$

where $f_{\gamma_{RD}}(\gamma)$ and $F_{\gamma_{RD}}(\gamma)$ follow PDF and CDF of square of Rayleigh distribution and $i = N_A - T + 1$. The corresponding CDF of the received SNRs at AP and MU are calculated by integrating the corresponding PDFs. The end-to-end outage probability of the system is given by:

$$P_{out} = F^i_{\gamma_{SR}}(\gamma_{th}) + (1 - F^i_{\gamma_{SR}}(\gamma_{th}))F^i_{\gamma_{RD}}(\gamma_{th}) \ . \tag{6.29}$$

From this expression, it is clear that the overall outage probability divided into two parts. Thus if we treat the individual terms, we can observe that the CDF terms are Meijer G components (for FSO links) or exponential components (for RF links), which basically decrease with an increment in SNR. The first stage outage probability value subtracted from 1 gives an increment, but it is compensated by the decrease in outage probability value of the second stage. Therefore, the total outage probability will decrease with an increment in SNR.

For $T = 2$, (where T is the number of selected laser/antenna sources), if $x^{LSB}_k[n] = 0$ then 1^{st} source is activated and if $x^{LSB}_k[n] = 1$, then 2^{nd} source is activated, where n represents the n^{th} time slot and k indicates the node which may be MU or AP in this case. We will consider BPSK modulation scheme for our case. The table of laser/antenna source activation depending upon the message bits has been

listed in Table 3 and Table 4 of [128] for T=4 and T=8 respectively, and explained in Chapter 4 also. The proposed TSS-HSM system can transmit $\log_2(M) + \log_2(T)$ bpcu while a normal TSS system can transmit $\log_2(M)$ bpcu.

6.5 Asymptotic Results

In this section, asymptotic analysis of HSM, TSS and TSS-HSM schemes will be performed. In any of the schemes, there are two channels- G-G and Rayleigh. We are interested in only the highest component of SNR which is given by G-G channel component. The Rayleigh channel will have a SNR exponent less than that of G-G channel. The G-G channel CDF has a Meijer G component, which can be written in terms of elementary functions. Referring to Eq. (6.17), the Meijer G function in the equation is first inverted and written as:

$$F_{\gamma_{S,R}^{j_{Rrx}}}(\gamma_{th}) = \frac{\zeta^2}{\Gamma(\alpha_G)\Gamma(\beta_G)} G_{4,2}^{1,3}\left(\begin{matrix} 1-\zeta^2, 1-\alpha_G, 1-\beta_G, 1 \\ 0, -\zeta^2 \end{matrix} \middle| z \right), \tag{6.30}$$

where $z = \frac{A_0 h_l \left(\eta_{tx} P_S R_e G_{S,R} \bar{\gamma}\right)^{\frac{1}{2}}}{\alpha_G \beta_G \gamma_{th}^{1/2}}$. Now the Meijer G function can be written in terms of elementary functions as shown in Eq. (2.69):

$$F_{\gamma_{S,R}^{j_{Rrx}}}(\gamma_{th}) \approx \frac{\zeta^2}{\Gamma(\alpha_G)\Gamma(\beta_G)} \sum_{k=1}^{3} z^{a_k - 1} \frac{\prod_{l=1, l\neq k}^{3} \Gamma(a_k - a_l) \prod_{l=1}^{1} \Gamma(1 + b_l - a_k)}{\prod_{l=4}^{4} \Gamma(1 + a_l - a_k) \prod_{l=2}^{2} \Gamma(a_k - b_l)}, \tag{6.31}$$

where $a = [1-\zeta^2, 1-\alpha_G, 1-\beta_G, 1]$ and $b = [0, \zeta^2]$. The diversity and coding gain can be obtained when the SNR ($\bar{\gamma}$) exponent is maximum. Using Eq. (2.73), we can obtain the diversity gain of Eq. (6.31) as $\min(\frac{\zeta^2}{2}, \frac{\alpha_G}{2}, \frac{\beta_G}{2})$. Now the CDF terms in Eq. (6.22) are multiplied, which means each Meijer G term is multiplied. We have to focus only on the highest exponent of SNR in this case. Hence, the exponential SNR component in Rayleigh distribution is ignored. The highest negative exponent of SNR can be obtained when the SNR term is multiplied by N_L. At very high SNR values, the total diversity gain of HSM (by referring to Eq. (2.73)), is given by $D_g^{HSM} = \left(\min(\frac{\zeta^2}{2}, \frac{\alpha_G}{2}, \frac{\beta_G}{2})\right) \times N_L$. Similarly diversity gain of TSS system can be obtained using Eq. (6.25) and (6.31). The CDF terms are multiplied in the outage probability equation of TSS. Hence the diversity gain of TSS system is $D_g^{TSS} = \left(\min(\frac{\zeta^2}{2}, \frac{\alpha_G}{2}, \frac{\beta_G}{2})\right) \times N_L$. Diversity gain of TSS-HSM is similarly calculated by $D_g^{TSS-HMS} = \left(\min(\frac{\zeta^2}{2}, \frac{\alpha_G}{2}, \frac{\beta_G}{2})\right) \times N_L$. Now with the help of Eq. (2.73) and (6.31), the final coding gain (C_g) for HSM system can be calculated as:

$$C_g = \left(\frac{\zeta^2}{\Gamma(\alpha_G)\Gamma(\beta_G)} \sum_{k=1}^{3} \left(\frac{A_0 h_l \left(\eta_{tx} P_S R_e G_{S,R} \bar{\gamma}\right)^{\frac{1}{2}}}{\gamma_{th}^{1/2} \alpha_G \beta_G} \right)^{a_k - 1} \frac{\prod_{l=1, l\neq k}^{3} \Gamma(a_k - a_l) \prod_{l=1}^{1} \Gamma(1 + b_l - a_k)}{\prod_{l=4}^{4} \Gamma(1 + a_l - a_k) \prod_{l=2}^{2} \Gamma(a_k - b_l)} \right)^{-\frac{N_L}{D_g^{HSM}}}. \tag{6.32}$$

The coding gain of TSS system is similarly obtained by replacing the D_g^{HSM} with D_g^{TSS} term. For TSS-HSM, coding gain is evaluated by replacing D_g^{HSM} with $D_g^{TSS-HSM}$. Let us gain some insights from the asymptotic calculation of diversity gain. Suppose strong turbulence conditions are considered having values of $\alpha_G = 4.2, \beta_G = 1.4, \zeta^2 = 17.1$. Let there be 2 laser sources and 2 antennas. Hence diversity gain of HSM is $\min(\zeta^2/2, \alpha_G/2, \beta_G/2) \times N_L = 1.4$. Diversity gain of TSS is $\min(\zeta^2/2, \alpha_G/2, \beta_G/2) \times N_L = 1.4$. Diversity gain of TSS with 3 antenna and laser sources is $0.7 \times 3 = 2.1$. Diversity gain of TSS-HSM with $N_L = 4, N_A = 4, T = 2$ is given by $0.7 \times 4 = 2.8$. Hence the diversity gain of TSS-HSM is more than that of TSS because of the presence of more optical/RF sources from which the best T sources can be chosen depending on channel condition. TSS having more sources has more diversity gain for the same reason that it has more sources from which it can select the best one.

6.6 Complexity Analysis

The detailed complexity analysis of the proposed schemes- HSM, TSS and TSS-HSM will be done in terms of overall cost and power consumption. The results will be compared to that of spatial multiplexing MIMO scenario where all the lasers and antennas operate simultaneously. An optical chain at the BS comprises of intensity modulators, RF modulators, DC bias adders, S/P converter, filters, etc. On the other hand, RF chain at AP comprises of RF modulators, S/P converters, filters, etc. Let the power consumption of each optical chain and RF chain be P_o and P_{RF} respectively. The cost of each optical chain and RF chain are assumed to be C_o and C_{RF} respectively. α_{tr} is the slope dependent load factor. P_{tr} is the optical transmit power, while P_{trf} is the RF transmit power. The cost of each serial-to-parallel converter is given by $C_{S/P}$. The cost of each optical switch is considered as C_{sw}, while the cost of each RF switch is considered as C_{swrf}. The power consumption of each optical switch is P_{sw} and the power consumption of each RF switch is P_{swrf}. Now in HSM, TSS and TSS-HSM, only one optical or RF chain is required as single laser/antenna is activated. However for MIMO techniques, N_L or N_A number of optical/RF chains are required (same as the number of transmit sources). A single pole dual throw optical/RF switch is used. The overall power consumption of both BS and AP nodes are calculated. It is to be kept in mind that the BS uses optical components while AP uses RF components. For a target spectral efficiency of η_{SE} bpcu and a M-ary modulation scheme, the number of switches required are computed for each scheme. The number of optical switches required for HSM at BS is $N_{sw}^{HSM} = 2^{(\eta_{SE} - \log_2 M - 1)}$, while RF switches required at AP is $N_{swrf}^{HSM} = 2^{(\eta_{SE} - \log_2 M - 1)}$. The number of optical switches required for TSS at BS is $N_{sw}^{TSS} = N_L/2$, while RF switches required at AP is $N_{swrf}^{TSS} = N_A/2$. Similarly for TSS-HM, number of optical switches required at BS $N_{sw}^{TSS-HSM} = 2^{(\eta_{SE} - \log_2 M - 1)}$, while RF switches required at AP is $N_{swrf}^{TSS-HSM} = 2^{(\eta_{SE} - \log_2 M - 1)}$. The total power consumption of HSM,

TSS and TSS-HSM are given by Eq. (6.33), (6.34) and (6.35) respectively.

$$P_{tot}^{HSM} = P_o + \alpha_{tr}P_{tr} + P_{sw}N_{sw}^{HSM} + P_{RF} + \alpha_{tr}P_{trf} + P_{swrf}N_{swrf}^{HSM} \ , \tag{6.33}$$

$$P_{tot}^{TSS} = P_o + \alpha_{tr}P_{tr} + P_{sw}N_{sw}^{TSS} + P_{RF} + \alpha_{tr}P_{trf} + P_{swrf}N_{swrf}^{TSS} \ , \tag{6.34}$$

$$P_{tot}^{TSS-HSM} = P_o + \alpha_{tr}P_{tr} + P_{sw}N_{sw}^{TSS-HSM} + P_{RF} + \alpha_{tr}P_{trf} + P_{swrf}N_{swrf}^{TSS-HSM} \ . \tag{6.35}$$

The total power consumption of MIMO techniques is given by $P_{tot}^{MIMO} = P_oN_L + \alpha_{tr}P_{tr} + P_{RF}N_A + \alpha_{tr}P_{trf}$. Hence it can be noted that the total power consumption of HSM, TSS and TSS-HSM schemes are less than MIMO due to the use of single optical/RF chain in our proposed methods. The overall cost is similarly calculated for HSM, TSS and TSS-HSM in Eq. (6.36), (6.37) and (6.38) respectively.

$$C_{tot}^{HSM} = C_o + C_{S/P} + C_{sw}N_{sw}^{HSM} + C_{RF} + C_{S/P} + C_{swrf}N_{swrf}^{HSM} \ , \tag{6.36}$$

$$C_{tot}^{TSS} = C_o + C_{S/P} + C_{sw}N_{sw}^{TSS} + C_{RF} + C_{S/P} + C_{swrf}N_{swrf}^{TSS} \ , \tag{6.37}$$

$$C_{tot}^{TSS-HSM} = C_o + C_{S/P} + C_{sw}N_{sw}^{TSS-HSM} + C_{RF} + C_{S/P} + C_{swrf}N_{swrf}^{TSS-HSM} \ . \tag{6.38}$$

The cost of MIMO techniques is given by $C_{tot}^{MIMO} = C_oN_L + C_{RF}N_A$. Hence it can be noted that the total cost consumption of HSM, TSS and TSS-HSM schemes are less than MIMO due to the use of single optical/RF chain in our proposed methods. An example is considered to illustrate the power consumption and cost benefits of the proposed methods. The spectral efficiency considered as $\eta_{SE} = 8$ bpcu, while number of lasers and antennas are taken as $N_L = 64, N_A = 64$ and $M = 4$. The number of switches required for HSM is $N_{sw}^{HSM} = N_{swrf}^{HSM} = 32$, while TSS requires $N_{sw}^{TSS} = N_{swrf}^{TSS} = 32$ switches and TSS-HSM also requires $N_{sw}^{TSS-HSM} = N_{swrf}^{TSS-HSM} = 32$ switches. The parameters considered are $P_o = 53W, \alpha_{tr} = 3.1, P_{tr} = 6.3W, P_{sw} = 0.2W, C_o = 1000\$, C_{S/P} = 2\$, C_{sw} = 220\$, P_{RF} = 53W, P_{trf} = 6.3W, P_{swrf} = 5mW, C_{swrf} = 2\$, C_{RF} = 180\$$ [151, 153, 155, 222]. The values of power consumption of HSM, TSS and TSS-HSM schemes are computed as 151.6 W for each, while MIMO consumes 6822 W. The cost consumption of HSM, TSS and TSS-HSM schemes are computed as 1050 $ for each, while MIMO consumes 75522 $. From this, it is clear that our proposed methods like HSM, TSS and TSS-HSM can offer considerable benefits in terms of power consumption and cost. As the spectral efficiencies increase, the number of sources required will be more and the power consumption and cost of MIMO will increase significantly.

6.7 Results

In this section, the performance of our proposed systems- HSM, TSS and TSS-HSM are compared with existing models in terms of outage probability. For performance analysis, G-G channel (with pointing errors) with strong turbulence is considered for FSO link, while Rayleigh channel is considered for RF link. The distance of separation between each node (L)= 2 Km is considered. It is assumed that BS and AP nodes have identical SNR. Transmitter aperture size is 7.5 cm, transmitter aperture separation is 40 mm, receiver aperture diameter is 20 cm, divergence angle is 2 mrad, responsivity is 0.5, transmitter/receiver optical efficiency is 0.8, corresponding jitter standard deviation is 30 cm, corresponding beam radius at 1 Km is 2.5 m [130]. Turbulence parameters for strong turbulence are $\alpha_G = 4.2$, $\beta_G = 1.4$. The analysis is performed considering BPSK modulation scheme. For the sake of simplicity, $N_L = N_A = 2$ is assumed. However for any value of optical/RF sources, results can be obtained as all analytical formulas are obtained for generalized number of sources. The target data rate (R_d) is considered as 3 bps. These parameters are considered throughout the work unless explicitly specified otherwise.

The system performance of HSM, TSS and TSS-HSM are compared with other methods in literature. The methods used are parallel Hybrid FSO/RF [214] with $\gamma_{th} = 10dB$ and $\gamma_{th} = 11dB$ and they are named as FSO_10 and FSO_11 respectively in our work for comparison. FSO_10 and FSO_11 involve a point-to-point hybrid FSO/RF system where FSO links are active as long as the received SNR is above the defined threshold, else RF link will be activated. The thresholds of the two methods FSO_10 and FSO_11 are 10 dB and 11 dB respectively. A multiuser hybrid FSO/RF has been used by the authors in [219] and we have considered the case of single user for our comparison. Eq. (19) from [219] has been used to evaluate the outage probability for our desired conditions and the results are denoted by HFSO in our comparison. The results from Fig. 5 (moderate turbulence with $\phi = 0.6$) in [218] have been used in our work and is denoted by MOD. It involves a point-to-point hard switching hybrid FSO/RF system where FSO link is active when atmospheric conditions are perfect; however beyond a certain threshold SNR when channel quality degrades, RF link is activated. The results of SC2 in [215] for two different thresholds ($\gamma_{th}^1 = 8dB, \gamma_{th}^2 = 10dB$ and $\gamma_{th}^1 = 5dB, \gamma_{th}^2 = 7dB$) in Fig. 3 of [215] have been used for our comparison also and are named as HFSO_8 (for threshold $\gamma_{th}^1 = 8dB, \gamma_{th}^2 = 10dB$) and HFSO_5 (for threshold $\gamma_{th}^1 = 5dB, \gamma_{th}^2 = 7dB$) in our work. HFSO_8 and HFSO_5 both involve mixed RF and hybrid FSO/RF system. Multiple mobile users interact with the destination through a relay in this model. Mobile user-to-relay links are in RF domain, while relay-to-destination links are of both FSO and RF type. Depending upon predefined SNR thresholds γ_{th}^1 and γ_{th}^2 and $\gamma_{th}^1 < \gamma_{th}^2$, RF and FSO link switching is done at destination node. If SNR received at destination is more than or equal to γ_{th}^2

Table 6.1: Comparison of outage probabilities for different methods

SNR(dB)	Outage probability values of different methods										
	FSO_10	FSO_11	HFSO	MOD	HFSO_8	HFSO_5	HSM	TSS	TSS-HSM	AFOWR	AFTWR
0	0.65	1	0.95	$9*10^{-4}$	1	1	$5.3*10^{-4}$	$1.2*10^{-4}$	$2.7*10^{-6}$	0.001	0.0048
5	0.6	1	0.81	$7.5*10^{-4}$	1	0.85	$2.3*10^{-4}$	$5*10^{-5}$	$7*10^{-7}$	$4.6*10^{-4}$	0.0022
10	0.1	0.4	0.41	$6*10^{-4}$	0.7	0.4	$1*10^{-4}$	$2*10^{-5}$	$1.7*10^{-7}$	$2*10^{-4}$	$9.6*10^{-4}$
15	0.009	0.07	0.12	$4*10^{-4}$	0.25	0.12	$4*10^{-5}$	$7*10^{-6}$	$4.4*10^{-8}$	$9.2*10^{-5}$	$4.3*10^{-4}$
20	0.0007	0.002	0.02	$2.5*810^{-4}$	0.07	0.03	$2.1*10^{-5}$	$3*10^{-6}$	$1.1*10^{-8}$	$4.1*10^{-5}$	$1.9*10^{-4}$

then FSO link is used or else RF link is used. γ_{th}^{1} is the threshold for outage probability calculation. Here FSO is the cooperative hybrid based model without any spatial modulation scheme. Basically it refers to the conventional/standard approach, under fading scenario. In this FSO model, link between BS and AP follows G-G distribution while the link between AP and MU follows Rayleigh distribution. Table 6.1 lists the outage probability values of different methods at specific SNR values. It is noticed that our proposed methods- HSM, TSS and TSS-HSM outperform the other methods in terms of outage probability for any SNR values. The outage probability results of different techniques at different SNR values are graphically illustrated in Fig. 6.4. HSM can outperform the other methods because of its ability to select the transmit source depending on message bit value. The SNR gain of HSM over the other methods is over 20 dB at any outage probability value beyond 0.001.

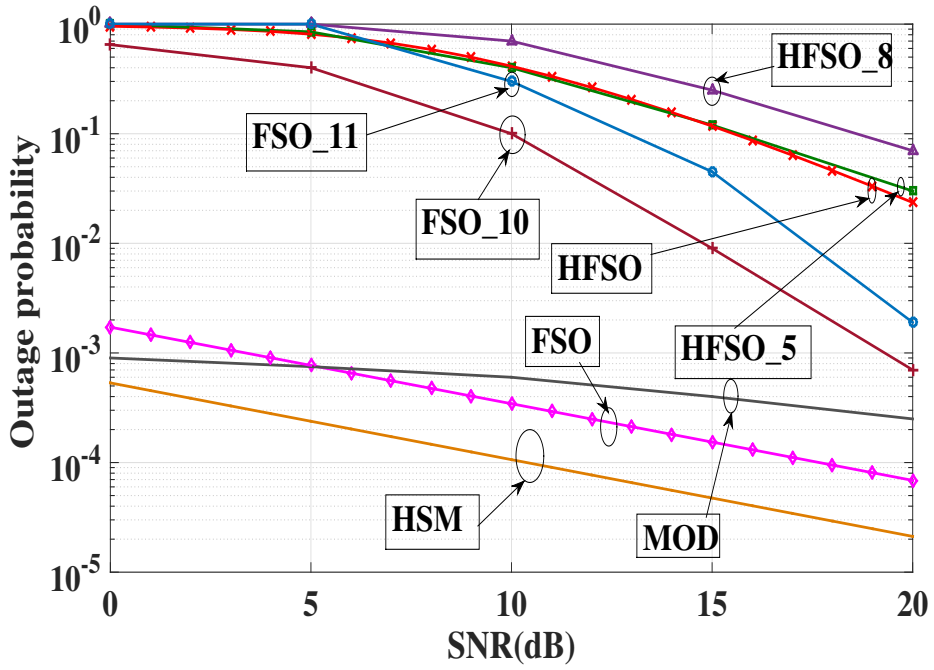

Figure 6.4: Performance comparison of proposed HSM system with other existing systems.

The performance of our proposed HSM system is compared with other systems like AFOWR, AFTWR and FSO in Fig. 6.5. It can be noted that HSM system performs better than the others because of its ability to activate the corresponding optical/RF source depending on the message bit. FSO system

does not implement any spatial modulation technique, hence it cannot choose the source depending on message bits. It has to transmit irrespective of the channel condition and message bit value, thereby leading to poorer performance. AFTWR suffers from more self-interference effect that AFOWR as all the nodes are operating in full-duplex mode. AFOWR also suffers in performance as compared to HSM, because it simply amplifies the signal without decoding it. Hence if error is there, it is also transmitted, whereas in DF protocol, the bits are decoded and regenerated at AP node.

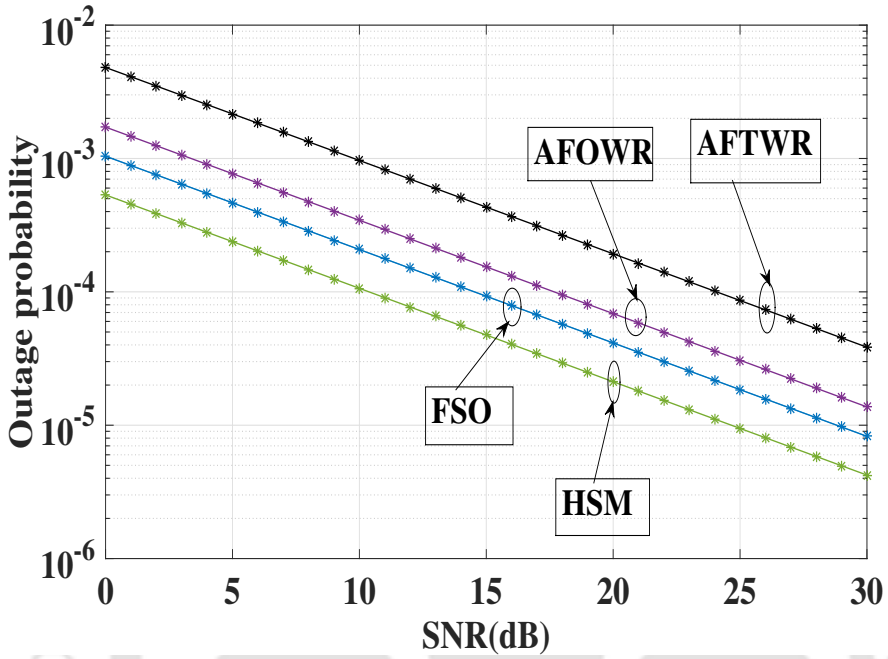

Figure 6.5: Performance comparison of proposed HSM system
(Solid line indicates analytical results while '*' symbol indicates simulation results).

The impact of variation of target data rates on the outage probability results of HSM is studied. R_d is varied as 3, 5, 8 and 10 bps. It is evident from Fig. 6.6 that with an increment in the value of R_d, the system performance degrades indicating that it is more difficult to achieve higher target data rates. To attain higher data rates, quality of channel condition should be good. But due to turbulence effects and fading effects, the system is not able to achieve high data rates and suffers from more error.

The impact of different atmospheric turbulences on the performance of HSM system is explored. Strong, moderate and weak turbulences are considered, according to which the parameters α_G and β_G for FSO links are varied. It is observed from Fig. 6.7 that as turbulence effect weakens, the system performance improves. The available turbulence offers more scattering and absorption effects, which hampers light propagation for the FSO link. This severly impacts the ability of the photodetector at the AP to receive the signal correctly in presence of high degrees of turbulence. It can also be noted that during daytime, turbulence is more as air gets heated up and rises up rapidly because of hot air being light. This creates more turbulence effect than night time. Hence system performance can be severely

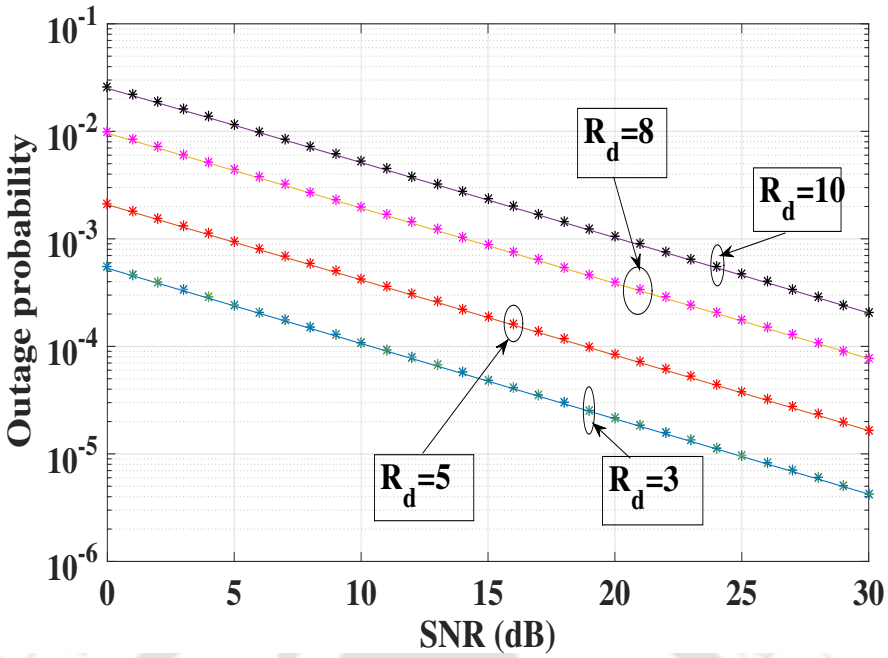

Figure 6.6: Performance of HSM for various data rates
(Solid line indicates analytical results while '*' symbol indicates simulation results).

affected during daytime or in presence of high amounts of turbulence in FSO link.

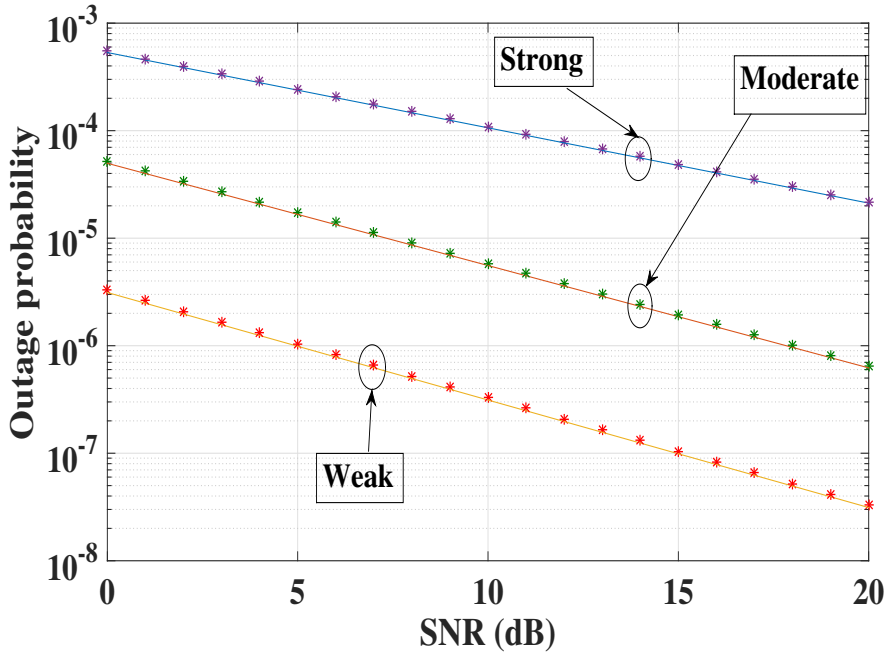

Figure 6.7: HSM performance for varying atmospheric turbulences
(Solid line indicates analytical results while '*' symbol indicates simulation results).

The performance of TSS system is explored for various combinations of source arrangements and the results are compared with that of HSM system. TSS is applied for $N_L = N_A = 2$ and $N_L = N_A = 3$ sources implying that out of the multiple optical/RF sources available at the nodes, only one of the

source will be selected for transmission depending upon the maximum received SNR. HSM scheme has $N_L = N_A = 2$ out of which one optical/RF source is activated depending on the message bit. In case of TSS-HSM, the number of available optical/RF sources at the BS and AP are denoted by N while the number of optical/RF sources selected for applying HSM are denoted by T. The results are depicted in Fig. 6.8 and it is observed that TSS and TSS-HSM schemes outperform HSM because TSS and TSS-HSM selects the source depending upon the channel condition, while HSM performance can degrade if an inferior channel is selected according to the message bit-not based on the channel condition. As the diversity increases in number of sources, the performance improves because we have more available sources and corresponding channels to choose a single one. If HSM is applied after TSS, then it can perform much better than TSS and HSM, because the best set of sources are chosen depending on the best channels available. Hence if HSM is applied on the best channel links available, then system performance will improve than the scenario where HSM is applied irrespective of the channel condition. Therefore, the complexity of sending feedback bits in case of TSS and TSS-HSM is justified by the performance improvement over HSM. TSS can achieve a coding gain of around 10 dB over HSM at an outage probability value of 0.0001, as is observed from the graph. Asymptotic results also merge with the analytical values at high SNR values, indicating that our analysis is valid for high SNR regime.

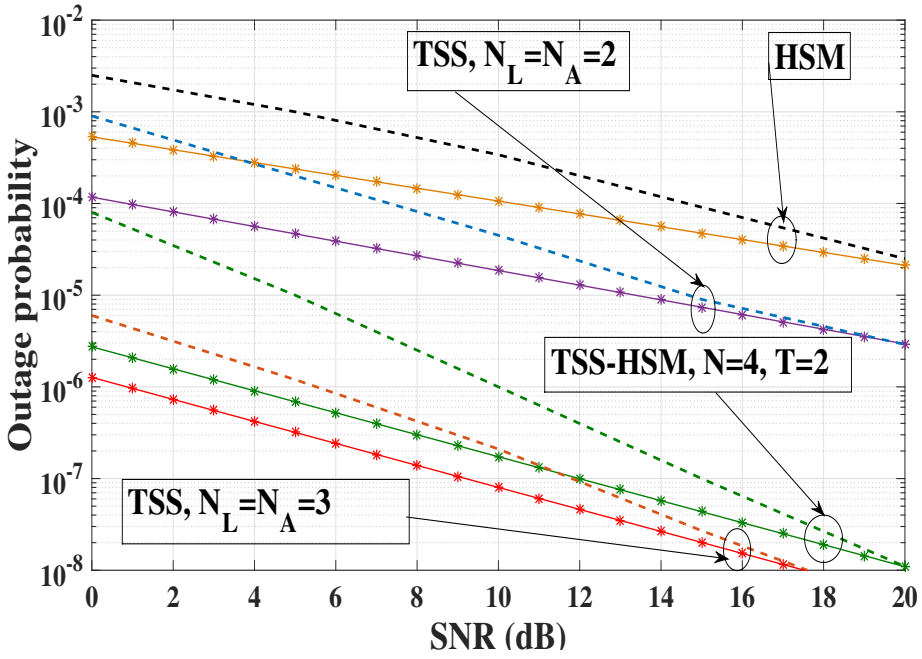

Figure 6.8: Performance of TSS and TSS-HSM system
(Solid line represents analytical results, '*' represents simulation results while dashed line represents asymptotic results).

6.8 Conclusion

New methods for cellular communication have been proposed in this chapter. The escalated system cost and complexity involved in a hybrid FSO/RF system is overshadowed by the performance improvement in hybrid FSO/RF system as it combines the benefits of both FSO and RF communication. To account for the misalignment of laser sources, pointing errors have been incorporated in the G-G channel for FSO links. Some new techniques like HSM, TSS and TSS-HSM have been proposed which yield better results than the existing methods. It has been inferred that TSS-HSM is the best method in terms of performance. In future, TSS, HSM and TSS-HSM can be analyzed for hybrid FSO/RF systems in terms of error performance using other modulation schemes also. Future works can also be extended to applying different forms of spatial modulation like improved spatial modulation, extended spatial modulation, quadrature spatial modulation, etc. for hybrid FSO/RF systems to increase the spectral efficiency of such systems. The concept of multi-user hybrid FSO/RF system can be investigated in future by using access point to serve multiple mobile users. Channel estimation techniques can be introduced for HSM to update the CSI regularly. Hybrid FSO/RF models can also be analyzed for D2D communication using generalized fading models in future.

7. Conclusion and Future Work

This thesis aims to enhance the performance of point-to-point communication for both RF and optical wireless communication. This can be beneficial for future 5G and 6G communication. Performance enhancement is proposed by the incorporation of various advanced spatial modulation schemes for D2D, BAN, FSO, UOWC and hybrid FSO/RF systems. It has been observed that MIMO systems can increase the performance of any system in various domains by using multiple antennas/lasers. However, such MIMO systems require multiple RF/optical chains which escalates the system cost and leads to unnecessary power consumption. There is also excessive inter-antenna or inter-optical interference due to simultaneous operation of multiple sources. These drawbacks motivated us to opt for spatial modulation in this thesis. Various advanced versions of SM have been proposed to enhance the spectral efficiencies of the systems. Thus performance analysis of advanced spatial modulation schemes has been carried out for a diverse range of applications in this thesis. The overall thesis can be summarized as follows:

- A brief survey of the various technologies like BAN, FSO, UOWC and hybrid FSO/RF has been presented along with the motivation and contribution of the thesis in Chapter 1. The basics of SM, PLNC and the various performance metrics have also been provided in this chapter.

- SM for RF cooperative systems have been proposed for improving the error performance in Chapter 2. SM along with PLNC have been analyzed over cascaded $\alpha - \mu$ channels for bidirectional communication and the system model has the potential to be applicable for D2D communication. The PDF and CDF of the cascaded $\alpha - \mu$ channel have been evaluated. Closed form expressions of lower and upper bounds of outage probability have been derived for the proposed system and the results show that our proposed system can perform better than AFOWR and AFTWR systems. Asymptotic expressions have also been derived to evaluate the coding and diversity gains. The effect of self-interference at the relay has also been studied. From the results, it can be inferred that lower self-interference effect, lower number of cascaded components of the channel and midway location of the relay are beneficial for the system performance. It has been observed from the results that our proposed system offers a SNR gain of 8 dB over PLNC scheme.

- BAN communication has been analyzed for sporting activities like running and cycling for both SISO and MIMO cases in Chapter 3. Advanced versions of SM like ESM and SMBM have been proposed for MIMO BAN communication to enhance the spectral efficiencies. Closed form expressions of BER have been achieved for such systems by approximating the LN-4 channel with MG distribution. Asymptotic analysis has been carried out for all schemes to illustrate the diversity and coding gain benefits of our proposed methods. It has been obtained from the results that SMBM can perform better than SM, ESM and SISO scenario. SMBM uses a single RF chain and lower modulation scheme, thereby generating superior performance. The effect of side-by-side and back-to-back running and cycling on the performance of these proposed methods have been studied. The influence of body movements on BAN channel and their effect on system performance have been explored. The impact of various types of body height, weight, etc. on the system performance have been analyzed by incorporating a BMI factor in the analysis of the proposed methods. It has been inferred from the results that cycling is better than running for any scenario and scheme because of the stationarity of the outstretched arms in case of cycling, while in running the arms are in oscillatory motion.

- Chapter 4 deals with various forms of OSM in FSO systems. OSM along with PLNC has been proposed for FSO cooperative bidirectional systems and its performance has been analzyed. Lower and upper bounds of outage probability expressions have been derived in closed form to study the performance of the proposed system. The analysis has been performed over G-G channel which can model various turbulence effects suitably. Asymptotic analysis has been carried out with tractable expressions to compute the diversity and coding gain of our proposed system. The effect of self-interference at the relay due to simultaneous data transfer from the source nodes has been studied. The impact of various parameters on the system has been investigated and it has been concluded from the results that lesser turbulence, lower self-interference, and lesser link distances are beneficial for the system performance. From the results, it is also conclusive that our proposed system can perform better than PLNC and point-to-point FSO systems (without relay). OSM activates the laser without considering the channel condition and this drawback can be mitigated by the use of TLS technique. TLS and TLS-OSM have been studied for FSO cooperative systems and the complexity analysis of the proposed methods have also been analyzed in terms of power consumption and cost. Closed form expressions of outage probability have been derived for TLS and TLS-OSM which makes the analysis easy and tractable. The analysis has been done over G-G channel incorporating pointing and path loss errors. Asymptotic analysis has been carried out to evaluate coding and diversity gain. It has been observed from the results that TLS-OSM scheme

can produce the best results due to the presence of more diversity in the set of laser sources, from which the transmitting laser is to be chosen. Further, the spectral efficiency of OSM is enhanced by the proposal of more advanced schemes like OESM, OGSM and OIQSM. The performance analysis has been done in terms of BER over G-G channel with pointing error, and considers both spatial domain error and modulation domain error. The power consumption and cost complexity analysis of the proposed schemes have been proposed. The effect of different modulation schemes and spectral efficiencies have been studied for these OSM based schemes. It is conclusive from the results that these advanced OSM schemes can perform better than OSM in terms of BER, cost and power consumption for attaining very high spectral efficiencies.

- UOWC cooperative communication has been studied both for SISO and MIMO cases in Chapter 5. Initially performance of both one-way and two-way relay based SISO UOWC cooperative communication have been analyzed in terms of outage probability and ASEP over weak turbulence induced fading, modelled by lognormal channels. Closed form expressions in terms of outage probabiity and ASEP have been derived for such SISO scenario by approximating the intractable lognormal distribution with MG distribution. Asymptotic analysis has also been carried out for SISO scenario. It has been inferred from the results that lower values of sea water turbulence is beneficial for the system performance. The analysis is then extended for MIMO scenario with the implementation of OIQSM scheme for UOWC cooperative system. Closed form expression of BER for such scheme has been achieved and complexity analysis in terms of power consumption and cost has also been performed. Results show that OIQSM can perform better than OSM and SISO case for any amount of turbulence. To resolve the issues of OSM, TLS and TLS-OSM schemes have also been proposed for UOWC cooperative systems and the performance analysis is achieved in terms of closed form expressions of outage probability and ASEP. Cost and power consumption analysis of such schemes have also been done. It has been concluded from the results that TLS and TLS-OSM schemes can perform better than OSM and SISO scenario in terms of BER. TLS-OSM scheme is the most superior method due to the presence of more diversity.

- The concepts of both FSO and RF communication have been combined to propose ASM schemes for hybrid FSO/RF cooperative system in Chapter 6. Various ASM schemes like HSM, TSS and TSS-HSM have been proposed for such hybrid cooperative systems that can be implemented in future cellular communication. The performance analysis of such systems are achieved in terms of tractable closed form outage probability expressions. Asymptotic analysis of such schemes give valuable insights regarding diversity and coding gain. Cost and power consumption analysis of such

systems have also been illustrated in detail. The performance of these proposed methods are found to outperform AF based one-way and two-way relaying methods. It is inferred from the results that TSS-HSM is the most superior method because of the presence of a larger set of available optical/RF sources. HSM, TSS and TSS-HSM also use a single RF/optical chain, thereby saving cost and power consumption as compared to MIMO schemes.

In future, several of the works listed in this thesis can be further expanded or some of the drawbacks exposed in these schemes can be studied. Some of the possible future works are listed below:

- Performance analysis of SM and PLNC based RF cooperative systems for D2D communication can be achieved in terms of other generalized fading models like $\kappa - \mu$ and $\eta - \mu$.

- Channel state information can be updated at regular intervals for RF, FSO, UOWC and hybrid FSO/RF systems and made available to all the nodes by using some channel estimation technique. Channel estimation techniques by using the least amount of feedback bits as overhead, should be explored such that system efficiency is not hampered.

- The end-to-end expressions of SNR, PDF and CDF of SM-PLNC based systems can be derived in terms of tractable closed form expressions. Such expressions are needed both for cascaded $\alpha - \mu$ and G-G channels for exact outage probability evaluation of SM-PLNC based bidirectional systems for both RF and optical wireless domain.

- More advanced SM schemes like quadrature spatial modulation, generalized spatial modulation, etc. can be analyzed for cooperative BAN communication and expressions of BER and outage probability can be evaluated. The potentiality of BAN cooperative communication in sports and healthcare industry can be explored further.

- G-G channel in FSO communication can be replaced by Malaga channel which is a more generalized channel model. Closed form expressions of BER and channel capacity need to be derived for such systems.

- Advanced OSM schemes like OGSM, OIQSM and OESM can be combined with TLS for performance benefits of FSO systems. Performance analysis of such systems can be investigated. Exact expressions for symbol detection and laser index detection for calculation of BER for such schemes can be derived. Asymptotic analysis of such schemes can also be done in terms of closed form tractable expressions.

- OSM techniques can be investigated for visible light communication (VLC) for point-to-point communication in indoor environment. More advanced OSM schemes can be implemented for performance analysis of such VLC systems.

- Pointing error and error arising due to floating nodes in oceanic currents can be incorporated in UOWC channel model. The performance analysis of TLS, TLS-OSM and other schemes like OIQSM, OESM, OGSM, etc. can be studied for UOWC cooperative systems in presence of pointing errors.

- Interference cancellation schemes at the relay can be explored to resolve the interference for variable-gain relay based UOWC cooperative systems. Channel estimation techniques by frequent updation of training signal can be one way of implementing this.

- Receiver diversity effect on OIQSM for UOWC cooperative systems can be studied by considering multiple photodetectors and closed form expressions of BER can be derived for such MIMO systems.

- The concept of multi-user hybrid FSO/RF system can be explored by incorporating multiple AP in the system model. Schemes like HSM, TSS and TSS-HSM can be implemented for such multi-user models and its performance analysis can be studied in terms of outage probability or BER. Different advanced forms of SM can also be combined with TSS to study the performance benefits on hybrid FSO/RF systems.

- The concept of channel coding can also be introduced to spatially modulated systems for both RF and optical domain to design an effective codebook. Spatial modulation schemes can also be investigated across various time slots to study the interference effect and mitigate it.

- SM concept can be introduced in the field of ambient backscattering communication. Following the principle of harvesting the energy from ambient RF communication, a device called tag can transmit data to another device called reader located nearby, by changing the reflection coefficient of the antenna. If the tag has multiple antennas, a single one can be activated depending on the message value according to the concept of SM. Such SM based backscattering communication can enhance the performance of point-to-point communication in a closed environment for IoT devices without requiring power sources.

भारतीय प्रौद्योगिकी संस्थान गुवाहाटी
Indian Institute of Technology Guwahati

Bibliography

[1] L. Xu, H. Zhang, J. Wang, W. Shi, and T. A. Gulliver, "End-to-end performance analysis of AF relaying M2M cooperative system," *International Journal of Multimedia and Ubiquitous Engineering*, vol. 10, no. 9, pp. 211–224, 2015.

[2] S. Mumtaz, "Direct mobile-to-mobile communication: Paradigm for 5G," *IEEE Wireless Communications*, vol. 21, no. 5, pp. 14–23.

[3] M. Cheffena and M. Mohamed, "The application of lognormal mixture shadowing model for B2B channels," *IEEE Sensors Letters*, vol. 2, no. 3, pp. 1–4, Sep. 2018.

[4] M. Cheffena, "Time-varying on-body wireless channel model during walking," *EURASIP Journal on Wireless Communications and Networking*, vol. 2014, no. 29, pp. 1–11, 2014.

[5] R. Khan and M. M. Alam, "Body-to-body communication: Applications, system design aspects and performance evaluation," in *2018 12th International Symposium on Medical Information and Communication Technology (ISMICT)*, March 2018, pp. 1–2.

[6] H. A. Willebrand and B. S. Ghuman, "Fiber optics without fiber," *IEEE Spectrum*, vol. 38, no. 8, pp. 40–45, Aug 2001.

[7] W. P. Z. Ghassemlooy and S. Rajbhandari, *Optical Wireless Communications: System and channel modelling with Matlab*. CRC Press, 2013.

[8] M. R. Bhatnagar and Z. Ghassemlooy, "Performance analysis of *g*amma *g*amma fading FSO MIMO links with pointing errors," *Journal of Lightwave Technology*, vol. 34, no. 9, pp. 2158–2169, May 2016.

[9] I. S. Ansari, M. M. Abdallah, M. S. Alouini, and K. A. Qaraqe, "Outage performance analysis of underlay cognitive RF and FSO wireless channels," in *2014 3rd International Workshop in Optical Wireless Communications (IWOW)*, Sept 2014, pp. 6–10.

[10] E. Friedman and L. John, Miller, *Photonics Rules of Thumb*. McGraw-Hill Professional, 2003.

[11] H. Weichel, *Laser Beam Propagation in the atmosphere.* Bellingham, WA: SPIE, 1990.

[12] D. Chadha, *Terrestrial Optical wireless communication.* McGraw-Hill, 2013.

[13] P. Kaur, V. K. Jain, and S. Kar, "Performance analysis of FSO array receivers in presence of atmospheric turbulence," *IEEE Photonics Technology Letters*, vol. 26, no. 12, pp. 1165–1168, June 2014.

[14] V. V. Mai and A. T. Pham, "Adaptive multi-rate designs for hybrid FSO/RF systems over fading channels," in *2014 IEEE Globecom Workshops (GC Wkshps)*, Dec 2014, pp. 469–474.

[15] S. Liew, "Physical-layer network coding: Tutorial, survey and beyond," *Elsevier Journal in Physical Communication*, vol. 6, no. 3, pp. 4–42.

[16] S. Buyukcorak, M. Vural, and G. K. Kurt, "Lognormal mixture shadowing," *IEEE Transactions on Vehicular Technology*, vol. 64, no. 10, pp. 4386–4398, Oct 2015.

[17] B. Talha and M. Patzold, "Channel models for mobile-to-mobile cooperative communication systems," *IEEE Vehicular Technology Magazine*, vol. 6, no. 2, pp. 33–43.

[18] G. K. Karagiannidis, N. C. Sagias, and T. Mathiopoulos, "The N- Nakagami fading channel model," in *2005 2nd International Symposium on Wireless Communication Systems*, Sep. 2005, pp. 185–189.

[19] F. Gong, "Cooperative mobile-to-mobile communications over double nakagami-M fading channels," *IET Communications*, vol. 6, no. 18, pp. 3165–3175.

[20] B. S. Paul, A. Hasan, H. Madheshiya, and R. Bhattacharjee, "Time and angle of arrival statistics of mobile-to-mobile communication channel employing circular scattering model," *IETE Journal of Research*, vol. 55, no. 6, pp. 275–281.

[21] M. Patzold, B. O. Hogstad, N. Youssef, and D. Kim, "A MIMO mobile-to-mobile channel model: Part i- the reference model," in *IEEE 16th International Symposium on Personal, Indoor and Mobile Radio Communications*, Berlin, Germany, 10.1109/PIMRC.2005.1651501.

[22] K. Baltzis, "A simplified geometric channel model for mobile-to-mobile communications," *Radio-Engineering*, vol. 20, no. 4, pp. 961–967.

[23] P. T. Samarasinghe, T. A. Lamahewa, T. D. Abhayapala, and R. A. Kennedy, "3D mobile-to-mobile wireless channel model," in *2010 Australian Communications Theory Workshop (AusCTW)*, Feb 2010, pp. 30–34.

[24] M. Riaz, S. J. Nawaz, and N. M. Khan, "3D ellipsoidal model for mobile-to-mobile radio propagation envrionments," *Wireless Pers. Commun.*, vol. 72, no. 4, pp. 2465–2479.

[25] A. Zajic, "Three dimensional modelling, simulation and capacity analysis of space-time correlated mobile-to-mobile channels," *IEEE Transactions on Vehicular Technology*, vol. 57, no. 4, pp. 2042–2054.

[26] M. Riaz, N. M. Khan, and S. J. Nawaz, "A generalized 3-D scattering channel model for spatiotemporal statistics in mobile-to-mobile communication environment," *IEEE Transactions on Vehicular Technology*, vol. 64, no. 10, pp. 4399–4410.

[27] J. Salo, "The distribution of the product of independent rayleigh random variables," *IEEE Transactions on Antennas and Propagation*, vol. 54, no. 2, pp. 639–643.

[28] I. Trigui, A. Laourine, S. Affes, and A. Stephenne, "On the performance of cascaded generalized K fading channels," in *Global Telecommunications Conference*, Honolulu, HI, USA, 10.1109/GLOCOM.2009.5426028.

[29] E. J. Leonardo and M. D. Yacoub, "Product of α-μ variates," *IEEE Wireless Communications Letters*, vol. 4, no. 6, pp. 637–640, Dec 2015.

[30] E. J. Leonardo and M. D. Yacoub, "Statistics of the product of arbitrary α-μ variates with applications," in *2014 IEEE 25th Annual International Symposium on Personal, Indoor, and Mobile Radio Communication (PIMRC)*, Sep. 2014, pp. 73–76.

[31] F. Yilmaz and M. S. Alouini, "Product of the powers of generalized nakagami-m variates and performance of cascaded fading channels," in *IEEE Globecom*, Honolulu, HI, USA, 10.1109/GLOCOM.2009.5426254.

[32] B. Kumbhani and R. S. Kshetrimayum, "Outage probability analysis of spatial modulation systems with antenna selection," *Electronics Letters*, vol. 50, no. 2, pp. 125–126, January 2014.

[33] S. Guo, H. Zhang, P. Zhang, and D. Yuan, "Adaptive mapper design for spatial modulation with lightweight feedback overhead," *IEEE Transactions on Vehicular Technology*, vol. 66, no. 10, pp. 8940–8950, Oct 2017.

[34] X. Xie, Z. Zhao, M. Peng, and W. Wang, "Spatial modulation in two-way network coded channels: Performance and mapping optimization," in *2012 IEEE 23rd International Symposium on Personal, Indoor and Mobile Radio Communications - (PIMRC)*, 2012, pp. 72–76.

[35] Y. Zhou, H. Zhang, D. Yuan, P. Zhang, and H. Liu, "Differential spatial modulation with BPSK for two-way relay wireless communications," *IEEE Communications Letters*, vol. 21, no. 6, pp. 1361–1364, 2017.

[36] S. Guo, H. Zhang, P. Zhang, D. Wu, and D. Yuan, "Generalized 3-D constellation design for spatial modulation," *IEEE Transactions on Communications*, vol. 65, no. 8, pp. 3316–3327, 2017.

[37] K. Yang, "Relay antenna selection in MIMO two-way relay networks over nakagami-m fading channels," *IEEE Trans. Vehicular Tech.*, vol. 63, no. 5, pp. 2349–2362.

[38] E. Nasab, "Multi-antenna AF-two way relaying over nakagami-m fading channels," *Wireless Pers. Commun.*, vol. 73, no. 3, pp. 717–729.

[39] G. Amarasuriya, "Two-way amplify-and-forward multiple-input multiple-output relay networks with antenna selection," *IEEE Journal on Selected Areas in Communications*, vol. 30, no. 8, pp. 1513–1529.

[40] S. O. Ata and I. Altunbas, "Fixed-gain AF PLNC over cascaded Nakagami-m fading channels for vehicular communications," *AEU - International Journal of Electronics and Communications*, vol. 70, no. 4, pp. 510 – 516, 2016.

[41] M. Shirkhani, Z. Tirkan, and A. Taherpour, "Performance analysis and optimization of two-way cooperative communications in inter-vehicular networks," in *2012 International Conference on Wireless Communications and Signal Processing (WCSP)*, 2012, pp. 1–6.

[42] R. Shakeri, H. Khakzad, A. Taherpour, and S. Gazor, "Performance of two-way multi-relay inter-vehicular cooperative networks," in *2014 IEEE Wireless Communications and Networking Conference (WCNC)*, 2014, pp. 520–525.

[43] S. Zhang, S. C. Liew, and P. Lam, "Hot topic: Physical layer network coding," in *Annual International Conference on Information, Communications and Signal Processing*, Los Angeles, CA, USA, 10.1145/1161089.1161129.

[44] R. Rajesh, P. Velmurugan, S. Thiruvengadam, and P. Mallick, "Spatial modulation and physical layer network coding based bidirectional relay network with transmit antenna selection over nakagamim fading channels," *Int. Journal of Commun. Syst.*, vol. e3742, 2018.

[45] S. Ustunbas, U. Aygolu, and E. Basar, "Spatially modulated bidirectional cognitive cross network design with physical-layer coding," *IEEE Transactions on Vehicular Technology*, vol. 67, no. 7, pp. 6185–6192, 2018.

[46] Wolfram research. [Online]. Available: http://functions.wolfram.com/HypergeometricFunctions/MeijerG/21/ShowAll.html

[47] I. Gradshteyn, *Table of Integrals, Series and Products*. New York, NY, USA: Academic Press, ISBN 978-0-12-294760-5.

[48] A. Prudnikov, Y. Brychkov, and O. Marichev, *Integrals and Series: Special Functions, Additional Chapters*. Moscow, Russia: Fizmatlit Press, ISBN 978-2881246821.

[49] E. J. Leonardo and M. D. Yacoub, "The product of two α-μ variates and the composite α-μ multipathâĂŞshadowing model," *IEEE Transactions on Vehicular Technology*, vol. 64, no. 6, pp. 2720–2725, 2015.

[50] A. Bhowal and R. S. Kshetrimayum, "Outage probability bound of decode and forward two-way full-duplex relay employing spatial modulation over cascaded $\alpha-\mu$ channels," *International Journal of Communication Systems*, vol. 32, no. 3, 2019.

[51] H. Ilhan, "Cooperative diversity of intervehicular communciation: Performance analysis and optimization," *IEEE Transactions on Vehicular Technology*, vol. 58, no. 7, pp. 3301–3310.

[52] H. Ochiai, "Variable-rate two-phase collaborative communication protocols for wireless networks," *IEEE Transactions on Vehicular Technology*, vol. 52, no. 9, pp. 4299–4313.

[53] B. Jiao, "Spatial modulated full duplex," *IEEE Wireless Communications Letters*, vol. 3, no. 6, pp. 641–644, Dec 2014.

[54] M. Ju, "Error performance analysis of BPSK modulation in physical-layer network-coded bidirectional relay networks," *IEEE Transactions on Communication*, vol. 58, no. 10, pp. 2770–2775.

[55] Y. Shi, M. Ma, Y. Yang, and B. Jiao, "Optimal power allocation in spatial modulation systems," *IEEE Transactions on Wireless Communications*, vol. 16, no. 3, pp. 1646–1655, March 2017.

[56] G. Altin, U. Aygolu, E. Basar, and M. E. Celebi, "Outage probability analysis of cooperative spatial modulation systems," in *2016 23rd International Conference on Telecommunications (ICT)*, May 2016, pp. 1–5.

[57] H. Brahathesa, P. G. S. Velmurugan, and S. J. Thiruvengadam, "Outage analysis of spatial modulation in cognitive radio networks," in *2017 International Conference on Wireless Communications, Signal Processing and Networking (WiSPNET)*, March 2017, pp. 1892–1896.

[58] F. Yarkin and I. Altunbas, "Outage performance of spatial modulation with transmit antenna selection over nakagami-m fading channels with arbitrary m," in *2016 8th International Congress on Ultra Modern Telecommunications and Control Systems and Workshops (ICUMT)*, Oct 2016, pp. 438–442.

[59] M. Eslamifar, C. Yuen, W. H. Chin, and Y. L. Guan, "Max-min antenna selection for bi-directional multi-antenna relaying," in *2010 IEEE 71st Vehicular Technology Conference*, May 2010, pp. 1–5.

[60] Y. Liu, P. Dharmawansa, and M. R. McKay, "Max-flow min-cut outage characterization of dual-hop relay channels," in *2012 50th Annual Allerton Conference on Communication, Control, and Computing (Allerton)*, Oct 2012, pp. 1659–1665.

[61] A. Bhowal and R. S. Kshetrimayum, "End to end performance analysis of M2M cooperative communication over cascaded α-μ channels," in *2017 9th International Conference on Communication Systems and Networks (COMSNETS)*, Jan 2017, pp. 116–122.

[62] M. Springer, *The Algebra of random variables*. Hoboken, NJ, USA: Wiley, 1979.

[63] I. S. Ansari, F. Yilmaz, and M. S. Alouini, "Performance analysis of free-space optical links over malaga ($\mathcal{M}$) turbulence channels with pointing errors," *IEEE Transactions on Wireless Communications*, vol. 15, no. 1, pp. 91–102, Jan 2016.

[64] Z. Zhang, "Full-duplex two way and one way relaying: average rate, outage probability and tradeoffs," *IEEE Transactions on Wireless Communications*, vol. 15, no. 6, pp. 3920–3933.

[65] A. Meharouech, J. Elias, and A. Mehaooua, "Moving towards body-to-body sensor networks for ubiquitous applications:a survey," *Journal of Sensor and Actuator Networks*, vol. 8, no. 2, pp. 1–27, 2019.

[66] Y. Fu and J. Liu, "Monitoring system for sports activities using body area networks," in *Proceedings of the 8th International Conference on Body Area Networks*, ser. BodyNets '13, 2013, pp. 408–413.

[67] S. L. Cotton, R. D'Errico, and C. Oestges, "A review of radio channel models for body centric communications," *Radio Science*, vol. 49, no. 6, pp. 371–388, June 2014.

[68] D. B. Smith, D. Miniutti, T. A. Lamahewa, and L. W. Hanlen, "Propagation models for body-area networks: A survey and new outlook," *IEEE Antennas and Propagation Magazine*, vol. 55, no. 5, pp. 97–117, Oct 2013.

[69] J. Salo, L. Vuokko, H. M. El-Sallabi, and P. Vainikainen, "An additive model as a physical basis for shadow fading," *IEEE Transactions on Vehicular Technology*, vol. 56, no. 1, pp. 13–26, Jan 2007.

[70] F. Mani and R. D. Errico, "A spatially aware channel model for body-to-body communications," *IEEE Transactions on Antennas and Propagation*, vol. 64, no. 8, pp. 3611–3618, Aug 2016.

[71] R. Rosini, R. Verdone, and R. D'Errico, "Body-to-body indoor channel modeling at 2.45 GHz," *IEEE Transactions on Antennas and Propagation*, vol. 62, no. 11, pp. 5807–5819, Nov 2014.

[72] X. Yang, S. A. Shah, A. Ren, N. Zhao, Z. Zhang, D. Fan, J. Zhao, W. Wang, and M. Ur-Rehman, "Freezing of gait detection considering leaky wave cable," *IEEE Transactions on Antennas and Propagation*, vol. 67, no. 1, pp. 554–561, Jan 2019.

[73] S. Sangodoyin and A. F. Molisch, "A measurement-based model of BMI impact on UWB multi-antenna PAN and B2B channels," *IEEE Transactions on Communications*, vol. 66, no. 12, pp. 6494–6510, Dec 2018.

[74] X. Yang, S. A. Shah, A. Ren, N. Zhao, D. Fan, F. Hu, M. Ur Rehman, K. M. vonDeneen, and J. Tian, "Wandering pattern sensing at S-band," *IEEE Journal of Biomedical and Health Informatics*, vol. 22, no. 6, pp. 1863–1870, Nov 2018.

[75] X. Yang, S. A. Shah, A. Ren, D. Fan, N. Zhao, S. Zheng, W. Zhao, W. Wang, P. J. Soh, and Q. H. Abbasi, "S-band sensing-based motion assessment framework for cerebellar dysfunction patients," *IEEE Sensors Journal*, pp. 1–1, 2019.

[76] A. Samanta and Y. Li, "Distributed pricing policy for cloud-assisted body-to-body networks with optimal QoS and energy considerations," *IEEE Transactions on Services Computing*, pp. 1–1, 2018.

[77] C. Bussler, "Is semantic web technology taking the wrong turn?" *IEEE Internet Computing*, vol. 12, no. 1, pp. 75–79, Jan 2008.

[78] M. Mohamed, M. Cheffena, and A. Moldsvor, "Characterization of the body-to-body propagation channel for subjects during sports activities," *Sensors*, vol. 18, no. 2, pp. 1–14, 2018.

[79] A. Bhowal and R. S. Kshetrimayum, "Performance analysis of one- and two-way relays for underwater optical wireless communications," *OSA Continuum*, vol. 1, no. 4, pp. 1400–1413, Dec 2018. [Online]. Available: http://www.osapublishing.org/osac/abstract.cfm?URI=osac-1-4-1400

[80] I. S. Ansari, S. Al-Ahmadi, F. Yilmaz, M. S. Alouini, and H. Yanikomeroglu, "A new formula for the BER of binary modulations with dual-branch selection over generalized-K composite fading channels," *IEEE Transactions on Communications*, vol. 59, no. 10, pp. 2654–2658, October 2011.

[81] G. W. H. Cui and Y. Wang, "Effects of CSI on ASEP based opportunistic DF relaying systems," *IEEE Transactions on Vehicular Technology*, vol. 60, no. 4, pp. 1898–1904, May 2011.

[82] A. Agrawal and R. S. Kshetrimayum, "Analysis of UWB communication over IEEE 802.15.3a channel by superseding lognormal shadowing by mixture of gamma distributions," *International Journal of Electronics and Communications*, pp. 1795–1799, 2015.

[83] R. Y. Mesleh, H. Haas, S. Sinanovic, C. W. Ahn, and S. Yun, "Spatial modulation," *IEEE Transactions on Vehicular Technology*, vol. 57, no. 4, pp. 2228–2241, July 2008.

[84] M. D. Renzo, H. Haas, and P. M. Grant, "Spatial modulation for multiple-antenna wireless systems: a survey," *IEEE Communications Magazine*, vol. 49, no. 12, pp. 182–191, December 2011.

[85] C. C. Cheng, H. Sari, S. Sezginer, and Y. T. Su, "Enhanced spatial modulation with multiple signal constellations," *IEEE Transactions on Communications*, vol. 63, no. 6, pp. 2237–2248, June 2015.

[86] B. S. Adejumobi, N. Pillay, and S. H. Mneney, "A study of spatial media-based modulation using RF mirrors," in *2017 IEEE AFRICON*, Sep. 2017, pp. 336–341.

[87] Y. Naresh and A. Chockalingam, "On media-based modulation using RF mirrors," *IEEE Transactions on Vehicular Technology*, vol. 66, no. 6, pp. 4967–4983, June 2017.

[88] Y. Naresh and A. Chockalingam, "On media-based modulation using RF mirrors," in *2016 Information Theory and Applications Workshop (ITA)*, Jan 2016, pp. 1–10.

[89] A. K. Khandani, "Media-based modulation: A new approach to wireless transmission," in *2013 IEEE International Symposium on Information Theory*, July 2013, pp. 3050–3054.

[90] A. K. Khandani, "Media-based modulation: Converting static rayleigh fading to AWGN," in *2014 IEEE International Symposium on Information Theory*, June 2014, pp. 1549–1553.

[91] E. Seifi, M. Atamanesh, and A. K. Khandani, "Media-based MIMO: A new frontier in wireless communications," *CoRR*, vol. abs/1507.07516, 2015. [Online]. Available: http://arxiv.org/abs/1507.07516

[92] A. Bhowal, A. S. Sapre, R. Lalani, and R. S. Kshetrimayum, "Advanced spatial modulation for efficient MIMO-based B2B communications in sporting activities," *IET Communications*, vol. 13, no. 20, pp. 3529–3536, 2019.

[93] A. Bhowal and R. S. Kshetrimayum, "Performance analysis of B2B communication for different sporting activities," *IEEE Sensor Letters*, vol. 3, no. 7, 2019.

[94] W. Popoola, *Subcarrier intensity modulated free space optical communication systems*. PhD thesis, 2009.

[95] S. Arnon, "Effects of atmospheric turbulence and building sway on optical wireless-communication systems," *Opt. Lett.*, vol. 28, no. 2, pp. 129–131, Jan 2003. [Online]. Available: http://ol.osa.org/abstract.cfm?URI=ol-28-2-129

[96] W. O. Popoola and Z. Ghassemlooy, "BPSK subcarrier intensity modulated free-space optical communications in atmospheric turbulence," *Journal of Lightwave Technology*, vol. 27, no. 8, pp. 967–973, April 2009.

[97] I. S. Ansari, F. Yilmaz, and M. S. Alouini, "Performance analysis of free-space optical links over Malaga ($\mathcal{M}$) turbulence channels with pointing errors," *IEEE Transactions on Wireless Communications*, vol. 15, no. 1, pp. 91–102, Jan 2016.

[98] L. C. Andrews, R. L. Phillips, and C. Y. Hopen, *Laser Beam Scintillation With Applications*. Bellingham, WA: SPIE, 2001.

[99] M. R. Bhatnagar, "A one bit feedback based beamforming scheme for FSO MISO system over gamma-gamma fading," *IEEE Transactions on Communications*, vol. 63, no. 4, pp. 1306–1318, April 2015.

[100] A. Jaiswal, M. R. Bhatnagar, and V. K. Jain, "Performance evaluation of space shift keying in free-space optical communication," *IEEE/OSA Journal of Optical Communications and Networking*, vol. 9, no. 2, pp. 149–160, Feb 2017.

[101] A. Jaiswal, M. R. Bhatnagar, and V. K. Jain, "BER analysis of optical space shift keying in atmospheric turbulence environment," in *2016 10th International Symposium on Communication Systems, Networks and Digital Signal Processing (CSNDSP)*, July 2016, pp. 1–6.

[102] V. S. Adamchik and O. I. Marichev, "The algorithm for calculating integrals of hypergeometric type functions and its realization in reduce system," in *Proc. Int. Conf. Symbolic Algebraic Comput., Tokyo, Japan*, July 1990, pp. 212–214.

[103] Y. Tang, X. Zhou, Z. Zhang, and Q. Tian, "Performance analysis of a two-way network-coded free space optical relay scheme over strong turbulence channels," in *2011 IEEE Vehicular Technology Conference (VTC Fall)*, Sept 2011, pp. 1–5.

[104] M. Kim, M. Medard, and U. M. O'Reilly, "Network coding and its implications on optical networking," in *2009 Conference on Optical Fiber Communication - incudes post deadline papers*, March 2009, pp. 1–3.

[105] M. Uysal, J. Li, and M. Yu, "Error rate performance analysis of coded free-space optical links over gamma-gamma atmospheric turbulence channels," *IEEE Transactions on Wireless Communications*, vol. 5, no. 6, pp. 1229–1233, June 2006.

[106] E. Bayaki, R. Schober, and R. K. Mallik, "Performance analysis of MIMO free-space optical systems in gamma-gamma fading," *IEEE Transactions on Communications*, vol. 57, no. 11, pp. 3415–3424, Nov 2009.

[107] M. Karimi and M. Nasiri-Kenari, "BER analysis of cooperative systems in free-space optical networks," *Journal of Lightwave Technology*, vol. 27, no. 24, pp. 5639–5647, Dec 2009.

[108] M. Karim and I. M. Nasiri-kenari, "Outage analysis of relay-assisted free-space optical communications," *IET Communications*, vol. 4, no. 12, pp. 1423–1432, August 2010.

[109] C. Abou-Rjeily and A. Slim, "Cooperative diversity for free-space optical communications: Transceiver design and performance analysis," *IEEE Transactions on Communications*, vol. 59, no. 3, pp. 658–663, March 2011.

[110] M. Razavi and J. H. Shapiro, "Wireless optical communications via diversity reception and optical preamplification," *IEEE Transactions on Wireless Communications*, vol. 4, no. 3, pp. 975–983, May 2005.

[111] S. G. Wilson, M. Brandt-Pearce, Q. Cao, and J. H. Leveque, "Free-space optical MIMO transmission with Q-ary PPM," *IEEE Transactions on Communications*, vol. 53, no. 8, pp. 1402–1412, Aug 2005.

[112] P. Puri, P. Garg, and M. Aggarwal, "Asymptotic analysis of TWR assisted FSO links with partial dual-relay selection," *IEEE Communications Letters*, vol. 19, no. 5, pp. 879–882, 2015.

[113] P. Puri, N. D. Chatzidiamantis, P. Garg, M. Aggarwal, and G. K. Karagiannidis, "Two-way relay selection in multiple relayed FSO networks," *IEEE Wireless Communications Letters*, vol. 4, no. 5, pp. 485–488, 2015.

[114] R. Mesleh, H. Haas, C. W. Ahn, and S. Yun, "Spatial modulation - a new low complexity spectral efficiency enhancing technique," in *2006 First International Conference on Communications and Networking in China*, Oct 2006, pp. 1–5.

[115] R. Mesleh, H. Elgala, and H. Haas, "Optical spatial modulation," *IEEE/OSA Journal of Optical Communications and Networking*, vol. 3, no. 3, pp. 234–244, March 2011.

[116] R. Mesleh, R. Mehmood, H. Elgala, and H. Haas, "Indoor MIMO optical wireless communication using spatial modulation," in *2010 IEEE International Conference on Communications*, 2010, pp. 1–5.

[117] W. O. Popoola, E. Poves, and H. Haas, "Spatial pulse position modulation for optical communications," *Journal of Lightwave Technology*, vol. 30, no. 18, pp. 2948–2954, 2012.

[118] T. Fath, H. Haas, M. Di Renzo, and R. Mesleh, "Spatial modulation applied to optical wireless communications in indoor LOS environments," in *2011 IEEE Global Telecommunications Conference - GLOBECOM 2011*, 2011, pp. 1–5.

[119] T. Fath and H. Haas, "Performance comparison of mimo techniques for optical wireless communications in indoor environments," *IEEE Transactions on Communications*, vol. 61, no. 2, pp. 733–742, 2013.

[120] T. Ozbilgin and M. Koca, "Optical spatial modulation over atmospheric turbulence channels," *Journal of Lightwave Technology*, vol. 33, no. 11, pp. 2313–2323, June 2015.

[121] K. P. Peppas and P. T. Mathiopoulos, "Free-space optical communication with spatial modulation and coherent detection over H-K atmospheric turbulence channels," *Journal of Lightwave Technology*, vol. 33, no. 20, pp. 4221–4232, Oct 2015.

[122] M. Abaza, R. Mesleh, A. Mansour, and E. H. M. Aggoune, "The performance of space shift keying for free-space optical communications over turbulent channels," *Proc. SPIE*, vol. 9387, p. p. 93870V, 2015.

[123] P. Puri, P. Garg, and M. Aggarwal, "Outage and error rate analysis of network-coded coherent TWR-FSO systems," *IEEE Photonics Technology Letters*, vol. 26, no. 18, pp. 1797–1800, Sept 2014.

[124] P. Puri, P. Garg, M. Aggarwal, and P. K. Sharma, "Outage analysis of two-way relay assisted FSO systems over weak turbulence region," in *2013 Annual IEEE India Conference (INDICON)*, Dec 2013, pp. 1–5.

[125] Z. Abu-Almaalie, Z. Ghassemlooy, H. Le-Minh, and N. Aslam, "Physical layer network coding with two-way relay free space optical communication link," in *2015 Internet Technologies and Applications (ITA)*, Sept 2015, pp. 292–297.

[126] M. Zhang, Y. Zhao, L. Wang, J. Wang, and P. Ye, "Design and analysis of all optical XOR gate using SOA based Mach-Zehnder interferometer," *Optics Communications*, vol. 223, no. 4, pp. 301–308, 2003.

[127] A. Jaiswal, M. R. Bhatnagar, P. Soni, and V. K. Jain, "Differential optical spatial modulation over atmospheric turbulence," *IEEE Journal of Selected Topics in Signal Processing*, vol. 13, no. 6, pp. 1417–1432, Oct 2019.

[128] A. Bhowal and R. S. Kshetrimayum, "Outage probability bound of decode and forward two-way relay employing optical spatial modulation over gamma-gamma channels," *IET Optoelectronics*, vol. 13, no. 4, pp. 183–190, 2019.

[129] A. Bhowal and R. S. Kshetrimayum, "Transmit laser selection for two hop decode and forward FSO communication with pointing errors," *IEEE Communications Letters*, vol. 23, no. 12, pp. 2301–2305, Dec 2019.

[130] A. A. Farid and S. Hranilovic, "Outage capacity optimization for free-space optical links with pointing errors," *Journal of Lightwave Technology*, vol. 25, no. 7, pp. 1702–1710, July 2007.

[131] J. Wang, J. Wang, M. Chen, Y. Tang, and Y. Zhang, "Outage analysis for relay-aided free-space optical communications over turbulence channels with nonzero boresight pointing errors," *IEEE Photonics Journal*, vol. 6, no. 4, pp. 1–15, Aug 2014.

[132] J. Wang, J. Zhu, S. Lin, and J. Wang, "Adaptive spatial modulation based visible light communications: Ser analysis and optimization," *IEEE Photonics Journal*, vol. 10, no. 3, pp. 1–14, June 2018.

[133] J. Wang, H. Ge, J. Zhu, J. Wang, J. Dai, and M. Lin, "Adaptive spatial modulation for visible light communications with an arbitrary number of transmitters," *IEEE Access*, vol. 6, pp. 37 108–37 123, 2018.

[134] B. Kumbhani and R. S. Kshetrimayum, "Source and relay transmit antenna selection in two hop cooperative communication systems over κ-μ fading channels," in *2016 Twenty Second National Conference on Communication (NCC)*, March 2016, pp. 1–5.

[135] B. Kumbhani and R. S. Kshetrimayum, "Error performance of two-hop decode and forward relaying systems with source and relay transmit antenna selection," *Electronics Letters*, vol. 51, no. 6, pp. 530–532, 2015.

[136] A. Jaiswal, M. R. Bhatnagar, and V. K. Jain, "Performance of optical space shift keying over Gamma-Gamma fading with pointing error," *IEEE Photonics Journal*, vol. 9, no. 2, pp. 1–16, April 2017.

[137] A. Jaiswal, M. R. "Bhatnagar", and V. K. "Jain", "BER analysis of optical space shift keying with Gamma-Gamma fading and pointing error," in *2016 International Conference on Advanced Technologies for Communications (ATC)*, 2016, pp. 369–374.

[138] J. Park, E. Lee, C. Chae, and G. Yoon, "Impact of pointing errors on the performance of coherent free-space optical systems," *IEEE Photonics Technology Letters*, vol. 28, no. 2, pp. 181–184, 2016.

[139] P. L. Yeoh, M. Elkashlan, and I. B. Collings, "Exact and asymptotic SER of distributed TAS/MRC in MIMO relay networks," *IEEE Transactions on Wireless Communications*, vol. 10, no. 3, pp. 751–756, March 2011.

[140] P. L. Yeoh, M. Elkashlan, and I. B. Collings, "MIMO relaying: Distributed TAS/MRC in Nakagami-m fading," *IEEE Transactions on Communications*, vol. 59, no. 10, pp. 2678–2682, October 2011.

[141] A. Garcia-Zambrana, C. Castillo-Vazquez, B. Castillo-Vazquez, and A. Hiniesta-Gomez, "Selection transmit diversity for FSO links over strong atmospheric turbulence channels," *IEEE Photonics Technology Letters*, vol. 21, no. 14, pp. 1017–1019, 2009.

[142] H. Samimi, "Performance analysis of free-space optical links with transmit laser selection diversity over strong turbulence channels," *IET Communications*, vol. 5, no. 8, pp. 1039–1043, 2011.

[143] H. Moradi, H. H. Refai, and P. G. LoPresti, "Circular MIMO FSO nodes with transmit selection and receive generalized selection diversity," *IEEE Transactions on Vehicular Technology*, vol. 61, no. 3, pp. 1174–1181, 2012.

[144] M. Elamassie, M. Al-Nahhal, R. C. Kizilirmak, and M. Uysal, "Transmit laser selection for underwater visible light communication systems," in *2019 IEEE 30th Annual International Symposium on Personal, Indoor and Mobile Radio Communications (PIMRC)*, 2019, pp. 1–6.

[145] A. García-Zambrana, B. Castillo-Vázquez, and C. Castillo-Vázquez, "Asymptotic error-rate analysis of FSO links using transmit laser selection over gamma-gamma atmospheric turbulence channels with pointing errors," *Opt. Express*, vol. 20, no. 3, pp. 2096–2109, Jan 2012. [Online]. Available: http://www.opticsexpress.org/abstract.cfm?URI=oe-20-3-2096

[146] A. García-Zambrana, C. Castillo-Vázquez, and B. Castillo-Vázquez, "Space-time trellis coding with transmit laser selection for FSO links over strong atmospheric turbulence channels," *Opt. Express*, vol. 18, no. 6, pp. 5356–5366, Mar 2010. [Online]. Available: http://www.opticsexpress.org/abstract.cfm?URI=oe-18-6-5356

[147] A. García-Zambrana, R. Boluda-Ruiz, C. Castillo-Vázquez, and B. Castillo-Vázquez, "Novel space-time trellis codes for free-space optical communications using transmit laser selection," *Opt. Express*, vol. 23, no. 19, pp. 24 195–24 211, Sep 2015. [Online]. Available: http://www.opticsexpress.org/abstract.cfm?URI=oe-23-19-24195

[148] W. Gappmair and M. Flohberger, "Error performance of coded FSO links in turbulent atmosphere modeled by gamma-gamma distributions," *IEEE Transactions on Wireless Communications*, vol. 8, no. 5, pp. 2209–2213, May 2009.

[149] R. S. Kshetrimayum, *Fundamentals of MIMO Wireless Communications*. Cambridge University Press, 2017.

[150] C. Abou-Rjeily, "On the optimality of the selection transmit diversity for mimo-fso links with feedback," *IEEE Communications Letters*, vol. 15, no. 6, pp. 641–643, June 2011.

[151] R. Mesleh and A. Alhassi, *Space Modulation Techniques*. New Jersey, USA: Wiley, 2018.

[152] G. Auer, V. Giannini, C. Desset, I. Godor, P. Skillermark, M. Olsson, M. A. Imran, D. Sabella, M. J. Gonzalez, O. Blume, and A. Fehske, "How much energy is needed to run a wireless network?" *IEEE Wireless Communications*, vol. 18, no. 5, pp. 40–49, 2011.

[153] Minicircuits(2017). Rf transciver ics. [Online]. Available: http://www.digikey.com/product-detail/en/analog-devices-inc/AD9364BBCZ/AD9364BBCZ-ND/4747823

[154] Microchip(2017). 16-bit microcontrollers. [Online]. Available: http://eu.mouser.com/ProductDetail/Microchip-Technology/PIC24FJ64GB406-I-PT/?qs=w3MdF6xSSP5O%2Fs8hl8VR2A%3D%3D

[155] Mouser(2017). Serial to parallel logic converters. [Online]. Available: http://eu.mouser.com/ProductDetail/Texas-Instruments/SN74LV8153PWR

[156] oeMarket. Fiber optical switch. [Online]. Available: http://www.oemarket.com/catalog/product_info.php/1x11x2-fiber-optical-switch-p-81

[157] B. Majlesein, A. Gholami, and Z. Ghassemlooy, "A complete model for underwater optical wireless communications system," in *2018 11th International Symposium on Communication Systems, Networks Digital Signal Processing (CSNDSP)*, July 2018, pp. 1–5.

[158] H. Guo, J. Ge, and M. Gao, "Transmit antenna selection for two-hop decode-and-forward relaying," *Electronics Letters*, vol. 47, no. 18, pp. 1050–1052, September 2011.

[159] J. Wang, M. Sheng, X. Song, Y. Jiao, and M. Chen, "Comments on 'BER performance of FSO links over strong atmospheric turbulence channels with pointing errors'," *IEEE Communication Letters*, vol. 16, no. 1, pp. 22–23, Jan. 2012.

[160] B. Vo and H. H. Nguyen, "Improved quadrature spatial modulation," in *2017 IEEE 86th Vehicular Technology Conference (VTC-Fall)*, Sept 2017, pp. 1–5.

[161] T. Datta and A. Chockalingam, "On generalized spatial modulation," in *2013 IEEE Wireless Communications and Networking Conference (WCNC)*, April 2013, pp. 2716–2721.

[162] J. M. Luna-Rivera and M. G. Gonzalez-Perez, "An improved spatial modulation scheme for MIMO channels," in *2012 6th European Conference on Antennas and Propagation (EUCAP)*, March 2012, pp. 1–5.

[163] R. Mesleh, S. Althunibat, and A. Younis, "Differential quadrature spatial modulation," *IEEE Transactions on Communications*, vol. 65, no. 9, pp. 3810–3817, 2017.

[164] C. Rajesh Kumar and R. K. Jeyachitra, "Power efficient generalized spatial modulation MIMO for indoor visible light communications," *IEEE Photonics Technology Letters*, vol. 29, no. 11, pp. 921–924, 2017.

[165] S. P. Alaka, T. L. Narasimhan, and A. Chockalingam, "Generalized spatial modulation in indoor wireless visible light communication," in *2015 IEEE Global Communications Conference (GLOBECOM)*, 2015, pp. 1–7.

[166] D. W. Dawoud, F. HÃľliot, M. A. Imran, and R. Tafazolli, "Spatial quadrature modulation for visible light communication in indoor environment," in *2017 IEEE International Conference on Communications (ICC)*, 2017, pp. 1–6.

[167] B. Zhuang, C. Li, and Z. Xu, "Enhanced performance of spatial modulation with angular diversity receiver for indoor visible light communication," in *2016 IEEE/CIC International Conference on Communications in China (ICCC)*, 2016, pp. 1–6.

[168] M. A. Kashani, M. Uysal, and M. Kavehrad, "On the performance of MIMO FSO communications over double generalized gamma fading channels," in *2015 IEEE International Conference on Communications (ICC)*, June 2015, pp. 5144–5149.

[169] M. Sahu, K. V. Kiran, and S. K. Das, "FSO link performance analysis with different modulation techniques under atmospheric turbulence," in *2018 Second International Conference on Electronics, Communication and Aerospace Technology (ICECA)*, March 2018, pp. 619–623.

[170] Z. Zeng, S. Fu, H. Zhang, Y. Dong, and J. Cheng, "A survey of underwater optical wireless communications," *IEEE Communications Surveys Tutorials*, vol. 19, no. 1, pp. 204–238, Firstquarter 2017.

[171] W. Cox, *Simulation, modeling, and design of underwater optical communication systems.* North Carolina State University, Raleigh: Ph.D. dissertation, 2012.

[172] M. A. Khalighi, C. Gabriel, T. Hamza, S. Bourennane, P. LÃĺon, and V. Rigaud, "Underwater wireless optical communication; recent advances and remaining challenges," in *2014 16th International Conference on Transparent Optical Networks (ICTON)*, July 2014, pp. 1–4.

[173] D. Pompili and I. F. Akyildiz, "Overview of networking protocols for underwater wireless communications," *IEEE Communications Magazine*, vol. 47, no. 1, pp. 97–102, January 2009.

[174] L. J. Johnson, F. Jasman, R. J. Green, and M. S. Leeson, "Recent advances in underwater optical wireless communications," *Underwater Technol.*, vol. 32, no. 3, pp. 167–175, 2014.

[175] M. V. Jamali, J. A. Salehi, and F. Akhoundi, "Performance studies of underwater wireless optical communication systems with spatial diversity: MIMO scheme," *IEEE Transactions on Communications*, vol. 65, no. 3, pp. 1176–1192, March 2017.

[176] A. C. Boucouvalas, K. P. Peppas, K. Yiannopoulos, and Z. Ghassemlooy, "Underwater optical wireless communications with optical amplification and spatial diversity," *IEEE Photonics Technology Letters*, vol. 28, no. 22, pp. 2613–2616, Nov 2016.

[177] J. Liu and Y. Dong, "On capacity of underwater optical wireless links under weak oceanic turbulence," in *OCEANS 2016 - Shanghai*, April 2016, pp. 1–4.

[178] A. Huang, L. Tao, and Q. Jiang, "BER performance of underwater optical wireless MIMO communications with spatial modulation under weak turbulence," in *2018 OCEANS - MTS/IEEE Kobe Techno-Oceans (OTO)*, May 2018, pp. 1–5.

[179] D. W. Dawoud, F. Heliot, M. A. Imran, and R. Tafazolli, "Spatial quadrature modulation for visible light communication in indoor environment," in *2017 IEEE International Conference on Communications (ICC)*, May 2017, pp. 1–6.

[180] B. Cochenour, L. Mullen, and A. Laux, "Phase coherent digital communications for wireless optical links in turbid underwater environments," in *OCEANS 2007*, Sep. 2007, pp. 1–5.

[181] M. Usman, H. Yang, and M. Alouini, "Practical switching-based hybrid FSO/RF transmission and its performance analysis," *IEEE Photonics Journal*, vol. 6, no. 5, pp. 1–13, 2014.

[182] K. A. N. Alhamawi and E. S. Altubaishi, "Capacity analysis of amplify-and-forward based dual-hop free space optical communication system with backup RF link," in *2016 12th International Conference on Innovations in Information Technology (IIT)*, Nov 2016, pp. 1–5.

[183] B. Majlesein, A. Gholami, and Z. Ghassemlooy, "A complete model for underwater optical wireless communications system," in *2018 11th International Symposium on Communication Systems, Networks Digital Signal Processing (CSNDSP)*, July 2018, pp. 1–5.

[184] Y. Dong, S. Tang, and X. Zhang, "Effect of random sea surface on downlink underwater wireless optical communications," *IEEE Communications Letters*, vol. 17, no. 11, pp. 2164–2167, November 2013.

[185] A. Celik, N. Saeed, T. Y. Al-Naffouri, and M. Alouini, "Modeling and performance analysis of multihop underwater optical wireless sensor networks," in *2018 IEEE Wireless Communications and Networking Conference (WCNC)*, 2018, pp. 1–6.

[186] K. W. S. Palitharathna, R. I. Godaliyadda, V. R. Herath, and H. A. Suraweera, "Relay-assisted optical wireless communications in turbid water," in *Proceedings of the Thirteenth ACM International Conference on Underwater Networks and Systems*, 2018, pp. 1–5.

[187] K. M. Rabie, B. Adebisi, and M.-S. surname, "Half-duplex and full-duplex AF and DF relaying with energy-harvesting in log-normal fading," *IEEE Transactions on Green Communications and Networking*, vol. 1, no. 4, p. 468âĂŞ480, Dec 2017. [Online]. Available: http://dx.doi.org/10.1109/TGCN.2017.2740258

[188] J. Yang, P. Fan, T. Q. Duong, and X. Lei, "Exact performance of two-way AF relaying in nakagami-m fading environment," *IEEE Transactions on Wireless Communications*, vol. 10, no. 3, pp. 980–987, March 2011.

[189] M. T. Dabiri and S. M. S. Sadough, "Performance analysis of all-optical amplify and forward relaying over log-normal FSO channels," *IEEE/OSA Journal of Optical Communications and Networking*, vol. 10, no. 2, pp. 79–89, 2018.

[190] Y. Kono, A. Pandey, and A. Sahu, "Ber analysis of lognormal and gamma-gamma turbulence channel under different modulation techniques for fso system," in *2019 3rd International Conference on Trends in Electronics and Informatics (ICOEI)*, 2019, pp. 1385–1388.

[191] S. Lim and K. Ko, "Approximation of multi-hop relay to dual-hop relay and its error performance analysis," *IEEE Communications Letters*, vol. 21, no. 2, pp. 342–345, Feb 2017.

[192] L. Xu, H. Zhang, J. Wang, W. Shi, and T. A. Gulliver, "End-to-end performance analysis of AF relaying M2M cooperative system," *International Journal of Multimedia and Ubiquitous Engineering*, vol. 10, no. 9, pp. 211–224, September 2015.

[193] M. O. Hasna and M. S. Alouini, "End-to-end performance of transmission systems with relays over rayleigh-fading channels," *IEEE Transactions on Wireless Communications*, vol. 2, no. 6, pp. 1126–1131, Nov 2003.

[194] S. J. Grant and J. K. Cavers, "Multiuser channel estimation for detection of cochannel signals," in *1999 IEEE International Conference on Communications (Cat. No. 99CH36311)*, vol. 1, 1999, pp. 63–67 vol.1.

[195] L. W. Xu, H. Zhang, T. T. Lu, and T. A. Gulliver, "Performance analysis of the IAF relaying M2M cooperative networks over N-nakagami fading channels," *Journal of Communications*, vol. 10, no. 3, pp. 185–191, October 2015.

[196] A. P. Prudnikov, Y. A. Brychkov, and O. I. Marichev, *Integrals and Series, vol. 3: More Special Functions : Special Functions, Additional Chapters.* N. Y. London, Tokyo (First ed. in Moscow): Gordon and Breach Sci. Publ., 1989.

[197] O. Korotkova, N. Farwell, and E. Shchepakina, "Light scintillation in oceanic turbulence," *Waves in Random and Complex Media, Taylor and Francis*, vol. 22, no. 2, pp. 260–266, 2012.

[198] M. V. Jamali, F. Akhoundi, and J. A. Salehi, "Performance characterization of relay-assisted wireless optical CDMA networks in turbulent underwater channel," *IEEE Transactions on Wireless Communications*, vol. 15, no. 6, pp. 4104–4116, June 2016.

[199] K. P. Peppas, A. C. Boucouvalas, and Z. Ghassemloy, "Performance of underwater optical wireless communication with multi-pulse pulse-position modulation receivers and spatial diversity," *IET Optoelectronics*, vol. 11, no. 5, pp. 180–185, 2017.

[200] A. Huang, L. Tao, C. Wang, and L. Zhang, "Error performance of underwater wireless optical communications with spatial diversity under turbulence channels," *Appl. Opt.*, vol. 57, no. 26, pp. 7600–7608, Sep 2018. [Online]. Available: http://ao.osa.org/abstract.cfm?URI=ao-57-26-7600

[201] O. V. Sinkin, A. V. Turukhin, Y. Sun, H. G. Batshon, M. V. Mazurczyk, C. R. Davidson, J. Cai, W. W. Patterson, M. A. Bolshtyansky, D. G. Foursa, and A. N. Pilipetskii, "SDM for power-efficient undersea transmission," *Journal of Lightwave Technology*, vol. 36, no. 2, pp. 361–371, Jan 2018.

[202] A. Huang, L. Tao, and Q. Jiang, "Ber performance of underwater optical wireless mimo communications with spatial modulation under weak turbulence," *2018 OCEANS - MTS/IEEE Kobe Techno-Oceans (OTO)*, pp. 1–5, 2018.

[203] M. Wen, B. Zheng, K. J. Kim, M. Di Renzo, T. A. Tsiftsis, K. Chen, and N. Al-Dhahir, "A survey on spatial modulation in emerging wireless systems: Research progresses and applications," *IEEE Journal on Selected Areas in Communications*, vol. 37, no. 9, pp. 1949–1972, Sep. 2019.

[204] R. Mesleh, S. S. Ikki, and H. M. Aggoune, "Quadrature spatial modulation," *IEEE Transactions on Vehicular Technology*, vol. 64, no. 6, pp. 2738–2742, June 2015.

[205] J. Li, M. Wen, X. Cheng, Y. Yan, S. Song, and M. H. Lee, "Generalized precoding-aided quadrature spatial modulation," *IEEE Transactions on Vehicular Technology*, vol. 66, no. 2, pp. 1881–1886, Feb 2017.

[206] M. Safari and M. Uysal, "Cooperative diversity over log-normal fading channels: performance analysis and optimization," *IEEE Transactions on Wireless Communications*, vol. 7, no. 5, pp. 1963–1972, May 2008.

[207] S. J. Halme, B. K. Levitt, and R. S. Orr., "Bounds and approximations for some integral expression involving lognormal statistics," *MIT Res. Lab. Electron. Quart. Prog. Rept.*, 1969.

[208] W. Wang, P. Wang, T. Cao, H. Tian, Y. Zhang, and L. Guo, "Performance investigation of underwater wireless optical communication system using M -ary OAMSK modulation over oceanic turbulence," *IEEE Photonics Journal*, vol. 9, no. 5, pp. 1–15, Oct 2017.

[209] A. García-Zambrana, R. Boluda-Ruiz, C. Castillo-Vázquez, and B. Castillo-Vázquez, "Transmit alternate laser selection with time diversity for fso communications," *Opt. Express*, vol. 22, no. 20, pp. 23 861–23 874, Oct 2014. [Online]. Available: http://www.opticsexpress.org/abstract.cfm?URI=oe-22-20-23861

[210] S. Anees and M. R. Bhatnagar, "Performance of an amplify-and-forward dual-hop asymmetric RF-FSO communication system," *IEEE/OSA Journal of Optical Communications and Networking*, vol. 7, no. 2, pp. 124–135, February 2015.

[211] N. D. Chatzidiamantis, G. K. Karagiannidis, E. E. Kriezis, and M. Matthaiou, "Diversity combining in hybrid RF/FSO systems with PSK modulation," in *2011 IEEE International Conference on Communications (ICC)*, 2011, pp. 1–6.

[212] B. He and R. Schober, "Bit-interleaved coded modulation for hybrid RF/FSO systems," *IEEE Transactions on Communications*, vol. 57, no. 12, pp. 3753–3763, 2009.

[213] H. Dahrouj, A. Douik, F. Rayal, T. Y. Al-Naffouri, and M. Alouini, "Cost-effective hybrid RF/FSO backhaul solution for next generation wireless systems," *IEEE Wireless Communications*, vol. 22, no. 5, pp. 98–104, October 2015.

[214] T. Rakia, H. Yang, M. Alouini, and F. Gebali, "Outage analysis of practical FSO/RF hybrid system with adaptive combining," *IEEE Communications Letters*, vol. 19, no. 8, pp. 1366–1369, Aug 2015.

[215] Y. F. Al-Eryani, A. M. Salhab, S. A. Zummo, and M. Alouini, "Protocol design and performance analysis of multiuser mixed RF and hybrid FSO/RF relaying with buffers," *IEEE/OSA Journal of Optical Communications and Networking*, vol. 10, no. 4, pp. 309–321, April 2018.

[216] V. Jamali, D. S. Michalopoulos, M. Uysal, and R. Schober, "Link allocation for multiuser systems with hybrid RF/FSO backhaul: Delay-limited and delay-tolerant designs," *IEEE Transactions on Wireless Communications*, vol. 15, no. 5, pp. 3281–3295, 2016.

[217] L. Kong, W. Xu, L. Hanzo, H. Zhang, and C. Zhao, "Performance of a free-space-optical relay-assisted hybrid RF/FSO system in generalized m-distributed channels," *IEEE Photonics Journal*, vol. 7, no. 5, pp. 1–19, Oct 2015.

[218] A. Touati, A. Abdaoui, F. Touati, M. Uysal, and A. Bouallegue, "On the effects of combined atmospheric fading and misalignment on the hybrid FSO/RF transmission," *IEEE/OSA Journal of Optical Communications and Networking*, vol. 8, no. 10, pp. 715–725, Oct 2016.

[219] L. Chen, W. Wang, and C. Zhang, "Multiuser diversity over parallel and hybrid FSO/RF links and its performance analysis," *IEEE Photonics Journal*, vol. 8, no. 3, pp. 1–9, June 2016.

[220] R. Hui and M. O. Sullivan, *Fiber optic measurement techniques*. Academic Press, 2009.

[221] M. O. Hasna and M. S. Alouini, "End-to-end performance of transmission systems with relays over rayleigh-fading channels," *IEEE Transactions on Wireless Communications*, vol. 2, no. 6, pp. 1126–1131, Nov 2003.

[222] Minicircuits(2017). Sw spdt. [Online]. Available: https://www.minicircuits.com/WebStore/dashboard.html?model=HSWA2-30DR%2B

[223] A. P. Prudnikov, Y. A. Brychkov, and O. I. Marichev, *Integrals and Series*. New York, NY, USA: Gordon and Breach, 1990.

[224] A. P. Prudnikov, Y. A. Brychkov, and O. I. Marichev, *Integral and Series: Inverse Laplace Transforms, 5th Ed.* London, UK: Gordon and Breach, 1992.

भारतीय प्रौद्योगिकी संस्थान गुवाहाटी
Indian Institute of Technology Guwahati

A. Appendix

The PEP for spatial domain part (where laser index j is estimated as i) is given by:

$$PEP(j \to i) = \int_0^\infty Q\left(\frac{1}{N_D}\sqrt{\frac{\gamma_{eff}}{2}\sum_{l=1}^{N_D}|h_{lj} - h_{li}|^2}\right) f_{\gamma_z}(\gamma_z) d\gamma_z \ . \tag{A.1}$$

To calculate the PEP for spatial domain part, the PDF of the absolute value of the difference between two G-G random variables needs to be calculated. Let $Y_l = |h_{lj} - h_{li}|$, $X_l = h_{lj} - h_{li}$ and γ_l be a new random variable such that $\gamma_l = Y_l^2 \gamma_{eff}$ and $\gamma_z = \sum \gamma_l$. Thus to find out the PDF of γ_z, PDF of γ_l is required which in turn needs the value of PDF of Y_l. The PDF of the difference of random variables is the challenging part. h_{li} and h_{lj} are two independent random variables following non-negative G-G distribution (as in Eq. (4.36)). Hence the PDF of X_l is given by [136]:

$$f_{X_l}(x) = \begin{cases} \int_0^\infty f_{h_l}(x + h_i) f_{h_i}(h_i) dh_i, x \geq 0 \\ \int_{-x}^\infty f_{h_l}(x + h_i) f_{h_i}(h_i) dh_i, x < 0 \ . \end{cases} \tag{A.2}$$

Now the PDF of Y_l using the PDF of X_l, can be written as:

$$f_{Y_l}(y) = f_{X_l}(y) + f_{X_l}(-y) \ , \tag{A.3}$$

where $f_{X_l}(y) = f_{X_l}(x)$ for $x > 0$ and $f_{X_l}(-y) = f_{X_l}(x)$ for $x < 0$. Since Y_l is a random variable formed by the modulus of of X_l, hence both the positive and negative value of X_l should be considered. Using the PDF of G-G distribution with pointing error, the PDF of $f_{X_l}(x)$ can be written as:

$$f_{X_l}(x) = \frac{(\alpha_G \beta_G \zeta^2)^2}{(A_0 h_l \Gamma(\alpha_G)\Gamma(\beta_G))^2} \int_0^\infty G_{1,3}^{3,0}\left(\begin{matrix}\zeta^2 \\ \zeta^2 - 1, \alpha_G - 1, \beta_G - 1\end{matrix}\middle| \frac{\alpha_G \beta_G (x + h_i)}{A_0 h_l}\right) \times G_{1,3}^{3,0}\left(\begin{matrix}\zeta^2 \\ \zeta^2 - 1, \alpha_G - 1, \beta_G - 1\end{matrix}\middle| \frac{\alpha_G \beta_G h_i}{A_0 h_l}\right) dh_i \ . \tag{A.4}$$

We can evaluate $f_{X_l}(x)$ for $x \geq 0$ (using [223] Eq. (2.24.1.3)), [136]:

$$f_{X_l}(x) = f_{X_l}(y) = \frac{\alpha_G \beta_G \xi^4}{A_0 h_l (\Gamma(\alpha_G)\Gamma(\beta_G))^2} \sum_{k=0}^{\infty} \frac{(-\alpha_G \beta_G y/(A_0 h_l))^k}{k!} G_{5,5}^{3,4}\left(\begin{matrix} 0, k+1-\zeta^2, k+1-\alpha_G, k+1-\beta_G, \zeta^2 \\ \zeta^2-1, \alpha_G-1, \beta_G-1, k-\zeta^2, k \end{matrix} \middle| 1 \right) . \tag{A.5}$$

Similarly PDF of $f_{X_l}(-y)$ can be calculated. Finally, the PDF of Y_l (from Eq. (A.3)) can be written as:

$$f_{Y_l}(y) = \frac{2\alpha_G \beta_G \xi^4}{A_0 h_l (\Gamma(\alpha_G)\Gamma(\beta_G))^2} \left[\sum_{k=0}^{\infty} \frac{(-\alpha_G \beta_G y/(A_0 h_l))^k}{k!} G_{5,5}^{3,4}\left(\begin{matrix} 0, k+1-\zeta^2, k+1-\alpha_G, k+1-\beta_G, \zeta^2 \\ \zeta^2-1, \alpha_G-1, \beta_G-1, k-\zeta^2, k \end{matrix} \middle| 1 \right) \right] . \tag{A.6}$$

The PDF of γ_l (considering change in random variables) is computed as:

$$f_{\gamma_l}(\gamma_l) = \frac{\alpha_G \beta_G \xi^4}{A_0 h_l (\Gamma(\alpha_G)\Gamma(\beta_G))^2 \sqrt{\gamma_l}} \sum_{k=0}^{\infty} \frac{(-\alpha_G \beta_G \sqrt{\gamma_l}/(A_0 h_l))^k}{\gamma_{eff}^{(k+1)/2} k!} G_{5,5}^{3,4}\left(\begin{matrix} 0, k+1-\zeta^2, k+1-\alpha_G, k+1-\beta_G, \zeta^2 \\ \zeta^2-1, \alpha_G-1, \beta_G-1, k-\zeta^2, k \end{matrix} \middle| 1 \right). \tag{A.7}$$

The PDF of γ_z cannot be solved directly as the PDF of summation of multiple Meijer G terms is not known. This is another challenging task. It is considered that the channels are independent of each other. Hence if we can obtain the moment generating function (MGF) of each γ_l variables, then the product of these MGFs can give the MGF of γ_z. MGF is basically the Laplace transform of a signal to represent a signal in s domain and the inverse Laplace transform can be used to retrieve the original signal in time domain. Therefore, the product of MGF of independent random variables can give the MGF of a new random variable which is basically the sum of multiple independent random variables. This MGF technique is used to obtain the PDF of γ_z. Hence the MGF of γ_l is computed by Laplace transform and written as:

$$M_{\gamma_l}(s) = \int_0^{\infty} e^{-sx} f_{\gamma_l}(x) dx . \tag{A.8}$$

The MGF of γ_l can be obtained with a few mathematical computations and can be written as (Eq. (3.38.1) in [224]):

$$M_{\gamma_l}(s) = \frac{\alpha_G \beta_G \xi^4}{A_0 h_l (\Gamma(\alpha_G)\Gamma(\beta_G))^2 s^{(k+1)/2}} \sum_{k=0}^{\infty} \frac{(-\alpha_G \beta_G/(A_0 h_l))^k}{\gamma_{eff}^{(k+1)/2} k!} G_{5,5}^{3,4}\left(\begin{matrix} 0, k+1-\zeta^2, k+1-\alpha_G, k+1-\beta_G, \zeta^2 \\ \zeta^2-1, \alpha_G-1, \beta_G-1, k-\zeta^2, k \end{matrix} \middle| 1 \right). \tag{A.9}$$

The channels are independent of each other and since there are N_D photodetectors, hence there will be N_D number of channels. The MGF of $\gamma_z = \sum \gamma_l$ can be evaluated as:

$$M_{\gamma_z}(s) = C^{N_D} s^{-\frac{k+N_D}{2}} \left(\sum_{k=0}^{\infty} \frac{(-\alpha_G \beta_G/(A_0 h_l))^k}{\gamma_{eff}^{(k+1)/2} k!} G_{5,5}^{3,4}\left(\begin{matrix} 0, k+1-\zeta^2, k+1-\alpha_G, k+1-\beta_G, \zeta^2 \\ \zeta^2-1, \alpha_G-1, \beta_G-1, k-\zeta^2, k \end{matrix} \middle| 1 \right) \right)^{N_D} , \tag{A.10}$$

where $C = \frac{\alpha_G \beta_G \xi^4}{A_0 h_l (\Gamma(\alpha_G)\Gamma(\beta_G))^2}$. The PDF of $f_{\gamma_z}(\gamma_z)$ is now evaluated by computing the inverse Laplace transform of MGF and is written as:

$$f_{\gamma_z}(\gamma_z) = \left(C \sum_{k=0}^{\infty} \frac{(-\alpha_G \beta_G/(A_0 h_l))^k}{\gamma_{eff}^{(k+1)/2} k!} G_{5,5}^{3,4}\left(\begin{matrix} 0, k+1-\zeta^2, k+1-\alpha_G, k+1-\beta_G, \zeta^2 \\ \zeta^2-1, \alpha_G-1, \beta_G-1, k-\zeta^2, k \end{matrix} \middle| 1 \right) \right)^{N_D} \frac{\gamma_z^{\frac{k+N_D-2}{2}}}{(\frac{k+N_D-2}{2})!} . \tag{A.11}$$

Now by using Eq. (A.11), the PEP of Eq. (A.1) can be evaluated as:

$$\begin{aligned} PEP(j \to i) &= \int_0^{\infty} Q\left(\frac{1}{N_D} \sqrt{\frac{\gamma_z \gamma_{eff}}{2}} \right) f_{\gamma_z}(\gamma_z) d\gamma_z \\ &= \left(C \sum_{k=0}^{\infty} \frac{(-\alpha_G \beta_G/(A_0 h_l))^k}{\gamma_{eff}^{(k+1)/2} k!} G_{5,5}^{3,4}\left(\begin{matrix} 0, k+1-\zeta^2, k+1-\alpha_G, k+1-\beta_G, \zeta^2 \\ \zeta^2-1, \alpha_G-1, \beta_G-1, k-\zeta^2, k \end{matrix} \middle| 1 \right) \right)^{N_D} \frac{1}{2(\frac{k+N_D-2}{2})!} \\ &\times \int_0^{\infty} \gamma_z^{\frac{k+N_D-2}{2}} erfc\left(\frac{1}{2N_D} \sqrt{\gamma_z \gamma_{eff}} \right) d\gamma_z. \end{aligned} \tag{A.12}$$

By using the relation, $\int_0^{\infty} x^{\frac{a-1}{2}} erfc(b\sqrt{x}) dx = 2\frac{\Gamma(\frac{a+2}{2})}{(a+1)b^{a+1}\sqrt{\pi}}$, the PEP of the spatial domain part is obtained as:

$$\begin{aligned} PEP(j \to i) = \sum_{k=0}^{\infty} & \frac{(2N_D)^{k+N_D} \Gamma(\frac{k+N_D+1}{2})}{\gamma_{eff}^{(k+N_D)/2} \sqrt{\pi}(k+N_D)\Gamma((k+N_D)/2)} \\ & \times \left(C \frac{(-\alpha_G \beta_G/(A_0 h_l))^k}{\gamma_{eff}^{(k+1)/2} k!} G_{5,5}^{3,4}\left(\begin{matrix} 0, k+1-\zeta^2, k+1-\alpha_G, k+1-\beta_G, \zeta^2 \\ \zeta^2-1, \alpha_G-1, \beta_G-1, k-\zeta^2, k \end{matrix} \middle| 1 \right) \right)^{N_D} . \end{aligned} \tag{A.13}$$

The above equation is used in Eq. (4.69). The equation is in closed form which gives us the flexibility to study the system performance with SNR variation. Asymptotic analysis for spatial domain part can be easily performed. Future optimization techniques can be easily done because of closed form expressions, to optimize the values of N_D to get a particular error probability.

भारतीय प्रौद्योगिकी संस्थान गुवाहाटी
Indian Institute of Technology Guwahati

Publications

Published papers

Journal papers

- A. Bhowal and R. S. Kshetrimayum, "Relay based Hybrid FSO/RF Communication with Hybrid Spatial Modulation and Transmit Source Selection", IEEE Transactions on Communications, doi: 10.1109/TCOMM.2020.2991054, April 2020. (Related to chapter 6)

- A. Bhowal, A. S. Sapre, R. Lalani, and R. S. Kshetrimayum, "Enhanced Spatial Modulation and Spatial Media Based Modulation for efficient B2B communications in sporting activities", IET Communications, vol. 13, no. 20, pp. 3529-3536, December 2019. (Related to chapter 3)

- A. Bhowal and R. S. Kshetrimayum, "Transmit laser selection for two hop decode and forward FSO communication with pointing errors", IEEE Communications Letters, vol. 23, no. 12, pp. 2301-2305, December 2019. (Related to chapter 4)

- A. Bhowal and R. S. Kshetrimayum, "Performance analysis of B2B communication for different sporting activities", IEEE Sensors Letters, vol. 3, no. 7, July 2019. (Related to chapter 3)

- A. Bhowal and R. S. Kshetrimayum, "Outage Probability Bound of Decode and Forward Two Way Relay employing Spatial Modulation over Cascaded α-μ Channels", Wiley International Journal of Communication Systems, vol. 32, no. 3, e3876, February 2019. (Related to chapter 2)

- A. Bhowal and R. S. Kshetrimayum, "Performance Analysis of One-way and Two-way Relay for Underwater Optical Wireless Communications", OSA Continuum, vol. 1, no. 4, pp. 1400-1413, November 2018. (Related to chapter 5)

- A. Bhowal and R. S. Kshetrimayum, "Outage Probability Bound of Decode and Forward Two Way Relay employing Optical Spatial Modulation over Gamma-Gamma Channels", IET Optoelectronics, vol. 13, no. 4, pp. 183-190, July 2019. (Related to chapter 4)

Conference papers

- A. Bhowal and R. S. Kshetrimayum, "Transmit laser selection for dual hop decode and forward UOWC cooperative communication", in Proc. IEEE Wireless Communications and Networking Conference (WCNC), Seoul, South Korea, pp. 1-6, May 2020. (Related to chapter 5)

- A. Bhowal and R. S. Kshetrimayum, "End to End Performance Analysis of M2M Cooperative Communication over Cascaded α-μ Channels", in Proc. COMSNETS, Bangalore, India, pp. 116-122, 2017. (Related to Chapter 2)

Book

- A. Bhowal and R. S. Kshetrimayum, "Advanced Spatial Modulation Systems", Book proposal accepted for publication in Springer, June 2020 (Related to Chapter 3, 4, 5, 6).

Papers under review

- A. Bhowal and R. S. Kshetrimayum, "Advanced Optical Spatial Modulation techniques for FSO communication", Under review for IEEE Transactions on Communications. (Related to chapter 4)

- A. Bhowal and R. S. Kshetrimayum, "Optical Improved Quadrature Spatial Modulation for Cooperative Underwater Wireless Communication under Weak Oceanic Turbulence Conditions", Revision submitted in IET Optoelectronics. (Related to chapter 5)

Author's Biography

Anirban Bhowal was born on 25 Jaunary 1990 in Kolkata, West Bengal. He obtained Bachelor of Technology degree in Electronics and Communication Engineering from Heritage Institute of Technology, Kolkata in 2012. He received Master of Technology degree in Communication Engineering from Indian Institute of Information Technology, Allahabad in 2015. He joined the PhD program in the Department of Electronics and Electrical Engineering, Indian Institute of Technology, Guwahati in 2015. His research interests include spatial modulation in RF and FSO systems, UOWC and FSO cooperative systems, hybrid FSO/RF communication and BAN communication.